THE PRODUCTION OF HOLLOW-WARE

BY

DEEP-DRAWING AND BULGE FORMING

by

Mohammad M. Al-Makky, B.Sc.

A thesis presented to the University of Sheffield for the Degree of Doctor of Philosophy

Department of Mechanical Engineering
University of Sheffield
December 1980

TEXT BOUND CLOSE TO THE SPINE IN THE ORIGINAL THESIS

TO MY WIFE, SON AND PARENTS ...

ACKNOWLEDGEMENTS

The author wishes to express his gratitude to Dr. D. M. Woo for his supervision, fruitful guidance and constant inspiration during the course of this research.

Thanks are due to the Syrian government for their research grant and to Mr. E. Redfern for his help in manufacturing some of the specimens and test apparatus.

SUMMARY

Results of a study of the production of hollow-ware by deep-drawing and bulge forming are presented. Axisymmetrical and asymmetrical shapes were successfully produced from soft aluminium flat blanks in one stroke of a punch. The process consists of drawing, ironing and bulging inside a closed die cavity. The constituent operations are studied individually.

In deep drawing without a blank-holder, an approach to convex type die design is presented. The investigation evaluates the effect of die profile geometry on the drawing performance. Three dies of the second degree spiral type,one near to the tractrix shape and the other two with larger radius of curvature, are considered. The materials tested include mild steel, stainless steel, soft aluminium and brass. The drawing process through tractrix, exponential spiral, second degree spiral and conical type dies is analysed using a numerical solution formulated earlier and the theoretical results on the punch load and the strain development are compared with the experimental results. Good correlation is obtained on the development of strains. The theoretical prediction of the punch load is reasonably good except for mild steel which is highly anisotropic. It is shown that by modifying the die profile, the punch load can be significantly reduced. The reductions predicted by theory are in good agreement with experiment which means that optimum die design for minimum load is possible.

In ironing of cups, using soft aluminium blanks, it was found that punch speeds in the range 7-45 mm/sec have negligible effect on the drawing load. The ironing load decreases slightly as the speed increases in this range. The reduction is more significant with higher degrees of ironing. Measurement of ironed cup wall thickness showed that thickness variations are attributed to planar anisotropy of the blank and geometrical errors in tooling.

Free bulge forming is used as a simplified approach to closed die forming. The bulge profile modes under different loading conditions of internal pressure and axial force, the effect of the unsupported cup length and the effect of the cup wall thickness on the bulge ratio were investigated using a specially designed test rig. For bulging of as deep-drawn cups, the bulge ratio increases with increase of cup wall thickness, and it decreases with increase of length. For bulging of annealed cups the length effect is negligible and the bulge ratio increases slightly with increase of cup wall thickness.

The procedure used in producing different hollow-ware shapes is described together with typical failure examples. The thickness reduction and bulge ratio distributions are shown and comparison is made between annealed and as deep-drawn cups.

CONTENTS

NOMENCLATURE

a, a_1, a_2	Die profile constants
c_r	Radial clearance between punch and die
F	External axial compressive force
f	Single variable function
f'	Derived function of the function f
H	Die height
h	Cup height
i	Current element of material
j	Current stage of deformation
P	Punch load
p	Internal pressure
R	Initial radius of an element of material
R_1	Blank radius
R_o	Initial mean radius of cup
R_p	Punch stem radius
r	Current radius
r_1	Die lip radius
r_2	Die throat radius
r_a	Current rim radius of the partly drawn cup
r_b	Current contact radius between die profile and material
r_c	Current contact radius between punch profile radius and material
r_d	Punch flat base radius
r_e	Radius at the bulge crown centre
r_o	Initial radius of the polar zone
S	Punch stroke

t	Current thickness of material
t'	New value of thickness in successive approximation of t
t_o	Initial thickness of material
α	Reduction in the cup wall thickness during ironing
γ	Ratio of width strain to thickness strain in simple tension test
ΔA	Surface area of an element of material
Δh	Current height of the polar zone dome.
Δh_c	Current height of the crown zone
ΔL	Initial length of an element of material
ΔX	Half width of the crown zone
ε_θ, ε_ϕ, ε_t	Principal strains
$\bar{\varepsilon}$	Equivalent strain
μ_d	Coefficient of friction between material and die
μ_p	Coefficient of friction between material and punch
ρ	Radius of curvature of die profile
ρ_1 and ρ_2	Principal radii of curvature
ρ_c	Radius of curvature of the polar zone
ρ_p	Punch profile radius
σ_θ, σ_ϕ, σ_t	Principal stresses
$\bar{\sigma}$	Equivalent stress

$(\sigma_\phi t)$	Unit-tangential force according to plasticity relations
$(\sigma_\phi t)'$	Unit-tangential force according to equilibrium equation
ϕ	Profile angle
ϕ'	New value of angle in successive approximation of ϕ
Superfix, ',	Denotes parameter referred to the inner plane of material
Superfix, ",	Denotes parameter referred to the outer plane of material
Suffix, n,	Denotes number of iterations

CHAPTER 1

INTRODUCTION

The production of hollow-ware from sheet metal by means of spinning has been well established in industry. The process is simple and efficient especially in the production of large and deep cylindrical or conical vessels. But for spinning components of more complicated shapes such as spherical or barrel shaped articles, a segmented mandrel has to be used and several separate stages of forming are required. This reduces considerably the productivity of the process. However, when asymmetric and non-rotational components are to be made, other forming techniques and hydraulic bulge forming in particular are of great interest.

A new forming process was suggested by Turner and Woo [1]* in which vessels or containers of required shape are produced from flat blanks. The process involves deep drawing without a blank-holder, ironing and bulging in one continuous operation. Recently, Woo [2], described a bulge forming machine which is under development. This prototype production machine incorporates drawing, ironing and hydraulic bulging in one stroke of a punch. He reported that spherical and conical vessels were successfully formed from aluminium and pewter blanks and the process appeared to be promising. The work was entirely experimental. Further investigation of the new forming process is desirable in order to have a

---

* Number in brackets means source is given in reference list.

better knowledge of its individual stages. This knowledge may be applied to improve the performance of the forming process and the tooling design and to widen the range of application. Also, this may help to define its advantages and limitations. It is believed that by examining each of the constituent processes separately, the benefit of this research work may be identified.

Although deep-drawing without a blank-holder and ironing are simple forming processes, they have received little scientific study and the published work is mostly presented in the form of empirical rules. This may be due to their physical complexities. A great deal of research work has been carried out on the hydraulic bulging of a circular diaphragm. Small proportion of this work deals with hydraulic bulging of cups inside a closed die cavity under the effect of internal pressure and axial force.

The present work is presented in four parts. Part One deals with the process of deep drawing without a blank-holder. An approach to die geometry and design is outlined. A general analysis of the deep drawing process without a blank-holder was developed. It was based on a numerical solution using the plasticity theory and the work-hardening characteristic of the material together with the equations of equilibrium of forces and the strain relationship according to the volume constancy condition. The analysis was applied mainly for the prediction of the punch load, and for examining the effectiveness of reducing the punch load by modifying the die profile. Three die profiles including

the tractrix were considered, and the materials used were mild steel, stainless steel, soft aluminium and brass. To compare theory with experiment, comprehensive tests were performed. The punch loads, thickness and circumferential strains were measured. In particular, the effect of die profile on the punch load was noted.

In Part Two, the prospect of the new process productivity is investigated. Experiments were carried out to study the effect of the punch speed on the drawing and ironing loads for different reductions in the cup wall thickness. The distribution of hardness and thickness in the cup wall was also measured.

Since the analysis of bulge forming inside a closed die cavity is complicated and because of the dependence of the instability conditions on the geometry of the die cavity and on the frictional condition between the material and the die cavity, it was decided to use the free bulging tests as a simplified approach to the problem.

Part Three of this work is concerned with the free bulging of cups. The instability conditions, bulge ratio and bulging profile modes which occur in the cup under different loading conditions of internal pressure and axial force were investigated. The effect of the cup wall thickness and length on instability and the limiting bulge ratio were also examined. A theoretical analysis of cup bulging under internal pressure and axial force was made and verified by experiments.

In Part Four the capabilities of the new forming process is demonstrated. Axisymmetric articles of basic shapes as spherical, conical, cylindrical and others, as well as the more difficult asymmetric hollow-ware of square and elliptical sections were studied and produced from flat blanks of aluminium of 172 mm diameter and 2.5 mm thickness. The blanks were drawn, ironed and then bulged to the required shape under the effect of internal pressure and axial force, in one stroke of the punch. In some cases annealing was necessary after ironing. The art of controlling the internal pressure, axial force and axial compression of the cup is described, and typical failures are given. The distribution of thickness reduction and bulge ratio of different articles was measured.

CHAPTER 2

SURVEY OF PREVIOUS WORK

2.1 Deep Drawing

Deep drawing of circular flat blanks for producing cylindrical cups is a simple and well known process. As far as its essential tooling is concerned, the process may be divided into two categories:

1. Deep drawing with a blank-holder or conventional deep drawing. As shown in Figure (2.1), the essential tooling in this case consists of a die of constant profile radius, cylindrical punch and a blank-holder.
2. Deep drawing without a blank-holder. Its essential tooling is shown in Figure (2.2). It consists of a convex type die and a cylindrical punch. The die profile may take the form of a tractrix curve or any other suitable curve. It is been known that for a certain die profile and blank material, the ratio of the blank diameter to its thickness determines whether a blank-holder is needed or not.

The limiting drawing ratio is defined as the ratio of the diameter of the largest blank which can be drawn successfully to the diameter of the punch. The maximum limiting drawing ratio that can be achieved in conventional drawing, on a single draw basis, is approximately 2.2, in drawing without a blank-holder this ratio can be increased to 2.7 or even more when a relatively thick blank and a

convex type die such as a tractrix type die is used. The mechanism of drawing and the theory of deformation in both categories are similar. A special reference is made in the present survey to deep drawing without a blank-holder.

Conventional deep-drawing, according to Smith (1908)* was invented in Rhenish in Prussia in the early nineteenth century. Since then the process has been studied many times. The early work of research on conventional deep-drawing can be thought of as starting with the work of Sommer (1926) and culminating in the work of Chung and Swift (1951). In this period several attempts have been made to formulate theories for radial drawing. Sommer (1926), Siebel and Pomp (1929), Crane (1932), Asimow (1936), Fukui (1938), and Voce (1948) were concerned with stresses and punch loads. Sachs (1931), Swift (1943), Jackson (1949) and Hill [3] have attempted also to predict the strains involved during plane radial drawing of a non-hardening material, but the effect of friction over the die profile, the blank-holding force and bending were neglected. The early experimental work was on a limited scale to provide a reliable standard for comparison with theory, and frequently omitted essential measurements, such as strain distribution measurements. Eksergian (1926), Siebel and Pomp (1929), Crane (1931), Sachs (1930,1934), Herrmann and Sachs (1934), Mijon (1938) and Bartholomew (1943) were concerned with punch load measurement. Oehler (1937),

---

* Date in brackets means source is listed in bibliography in alphabetical order.

Fukui (1938), Swift (1939) and Jackson (1949) attempted also to measure thickness changes. The first comprehensive and successful investigation in both theory and experiment is due to Chung and Swift (1951). This work led to a good understanding of radial drawing and to an appreciation of the thinning of the material as it passes over the die profile. The following assumptions were made in the theoretical solution:

1. The blank-holding force is exerted at the cup rim only;
2. The equivalent strain is numerically equal to the circumferential strain;
3. The material is subjected to bending and unbending on reaching and leaving the die profile respectively; and
4. The variation of the material thickness can be neglected in the equilibrium equation.

These assumptions were shown to be justified in a detailed comparison between the theoretical and experimental results. In the first assumption, it is apparant that the blank-holding force must be distributed over a certain area near the rim. The second assumption may introduce significant errors in the die profile region. In their comparison of the theoretical and experimental strain distribution only the final strains were compared and an adjustment of 7 per cent was made in the flow stress for mild steel to allow for different straining rates between cup drawing and the tensile test. They were not able to extend the solution to analyse the stretch forming over the punch head and they did not attempt to predict the

limiting drawing ratio. They were however able to predict the punch load/punch stroke relation with reasonable accuracy by assuming that the contribution of the punch stretching to the total load was negligible.

It is believed that deep drawing without a blank-holder was first used in Germany in 1934, when May (1934) introduced the tractrix type die. It was proposed that considerably larger values of drawing ratio are obtainable by drawing the blank through a die having a wide entry section in the form of tractrix. The used tractrix has the following equation:

$$y = -(a^2-x^2)^{\frac{1}{2}} + a \ln \left(\frac{a + (a^2-x^2)^{\frac{1}{2}}}{x}\right) \text{ , see Figure (3.1),}$$

where a is a constant and y is the axis parallel to the die centre line. The same result was confirmed later by Bauder (1951).A Similar conclusion was reached by Beisswänger (1950, 1950a) when using conical dies.

Although the above theoretical work assumed that the material was isotropic, it was well known that all materials exhibit anisotropy to a certain degree and sheet metal in particular could be strongly anisotropic. Lankford, Snyder and Bauscher (1950) recognized the importance of planar anisotropy in unsymmetrical operations.

Various theories of anisotropic yielding were developed during the second world war and they were released for publication after the war. The theories which have proved most useful in engineering applications are based on modifications of the von Mises yield criterion and its associated rule.

The theories developed independently by Jackson, Smith and Lankford (1948), Hill (1948) and Dorn (1949) have several points in common. The theory of Hill has the advantage of rigor within the basic assumptions adopted and it is perhaps the simplest to understand. Consequently it is most generally quoted today.

Fukui, Yuri and Yoshida (1958) analysed the deep drawing process using plane and conical dies. The total strain theory combined with shearing strain energy theory has been used. The authors revealed that they were able to predict the punch load with good accuracy and that the strain distributions over the flange region are nearly independent of the mechanical properties of the sheet material. In their formability investigations they suggested that the conical dies can be used in comparing the formability qualities of materials.

A numerical solution of conventional deep drawing was suggested by Yamada (1961). The theory assumes Mises yield condition and adopts the Hencky's total strain theory or Lévy-Mises equation in incremental theory. Solutions of radial drawing and drawing over the die and punch profile radii were presented. The punch load predicted by the total strain theory and the incremental strain theory showed no essential difference in radial drawing of non-hardening material.

Whiteley [4] showed that preferred orientation is the most important material variable influencing the performance of ordinary ductile metals in cylindrical cup-drawing with a

flat headed punch. He reported that the limiting drawing ratio increased as the average γ-value of the material increased. Other investigators, Fukui, Yoshida and Abe (1960) and Warwick and Alexander (1962-1963), found low correlation between limiting drawing ratio and material properties. Experiments by Lilet and Wybo (1964) provided results in good agreement with those of Whitely.

In 1963, Oehler [5] discussed the results of previous investigations by Haverbeck [6] and Shawki (1961) in connection with the advantages of deep drawing without a blank-holder and die design using tractrix and conical die profiles. He proposed that conventional deep-drawing tools can be operated without a blank-holder for small drawing ratios, and that the pressing depth h attainable without a blank-holder depends on nominal sheet thickness t_o and punch diameter d_p in accordance with the empirical relationship:

$$h \leq 0.3 \, (d_p)^{\frac{2}{3}} \, (t_o)^{\frac{1}{2}}.$$

Comparative tests by Shawki (1961) on deep drawing with tractrix shaped dies and conical dies (in most cases with a die angle of 30 degrees) have shown that the amount of work required is the same in both cases, but that the punch load for a conical die is about 1.4 times greater than that for a tractrix shaped die. It was reported that the limiting curve separating the wrinkle-free region from the region with a tendency to wrinkle, when a tractrix or conical die is used, can be approximated as a straight line with a negative slope.

Thus, for sheet of good deep-drawing quality, the limiting drawing ratio β is given by the equation:

$$\beta = 3.4 - 0.024\ (d_p/t_o).$$

For sheet of moderately good deep-drawing quality,

$$\beta = 3.4 - 0.06\ (d_p/t_o).$$

Although it has been mentioned in this work that the tractrix entry section is better from the point of view of any tendency to wrinkle than the conical entry, no allowance has been made in the above relations for the die type. The following relation was given for the determination of the cup depth h,

$$h = (D^2 - d_p^{\,2})/4d_p,$$

where D is the blank diameter.

It is clear that the above relation has disregarded the effect of anisotropy and the effect of the radial clearance between punch and die throat. Haverbeck [6] found that even better results can be obtained by using a modified tractrix curve, situated between two particular tractrix curves, the first curve being drawn with a die breadth of h equal to $(D-d_p)/2$, and the second being drawn with a die breadth of h as determined from the above equation. The modified tractrix is drawn between the top point of the first curve and the bottom point of the second curve. It can be seen that the modified tractrix is arbitrarily determined and that

no consideration has been made for the radial clearance between punch and die throat and for the effective die height.

A general solution has been suggested by Woo [7] for the study of the axisymmetric forming processes of sheet metal such as cup-drawing and hydroforming. The method involves the application of the plasticity theory together with the work-hardening characteristic of the material, equations of equilibrium of forces and the strain relation which can be deduced from the volume constancy of an element. Successive approximations are used to determine the stresses and strains at each element boundary. Woo [8] applied this general solution by developing a numerical analysis for the study of the conventional drawing process with a pressure blank-holder which included radial drawing over a die and stretch-forming over a punch. Agreement was good between the theoretical and experimental circumferential strains and punch load, but the correlation of the thickness strains in the stretch-forming region was unsatisfactory. This was due to the simplifying assumption of the material being in full contact with the punch profile radius at early stages of drawing. The solution was recommended for moderate die and punch profile radii. It was found that there is not much difference between assuming that the blank-holding force is concentrated on the rim or uniformly distributed in a certain area near the rim. In a further investigation by Woo [9] the above analysis was modified to include material anisotropy and the boundary conditions in the drawing and stretch-forming

region were determined for different stages of drawing. The punch load/punch travel diagram was constructed and the general correlation between the theoretical and experimental results was satisfactory.

There have been several theoretical studies of the dependence of the limiting drawing ratio on the work-hardening exponent n (as in the empirical equation $\bar{\sigma} = K \bar{\varepsilon}^{n}$) and the average strain ratio γ. In most cases failure was assumed to occur by necking under plane strain tension in the region where the punch profile radius joins the straight punch stem. The maximum loads in pure radial drawing were calculated for various n and γ values and various drawing ratios. At the limiting drawing ratio the maximum radial drawing load is equal to the load necessary to cause necking in plane strain tension in the material on the punch stem. This criterion was used by Yamada (1964) and Moore and Wallace (1964). Chiang and Kobayashi (1966) gave more details about stress and strain distribution due to drawing using an incremental method. Budiansky and Wang (1966) employed a finite deformation theory of rigid-plastic orthotropic sheet that is isotropic in its plane to study the Swift cup test. El-Sebaie and Mellor (1972) presented both theoretical and experimental investigations. Their theory predicted higher limiting drawing ratios compared with experiment. In all these solutions, any possible weakening effect due to stretching over the punch head and the presence of a blank-holder and its effect on the deformation are ignored. Nevertheless, the

theoretical results give a useful guide to the important effect of n and γ on the limiting drawing ratio in deep drawing with a flat headed punch.

Among others, the problems of failure by wrinkling in the flange or puckering of unsupported material between punch and die have been investigated. Senior (1956) has suggested theoretical relations for wrinkling in the flange. He concluded that the critical diameter is affected to a far greater extent by the geometry of the drawing tools and material thickness. Naziri and Pearce (1970) concluded from experiments that a high average strain ratio was beneficial for resisting wrinkling.

In recent years, with the progress of computers, there have been more advanced and comprehensive studies to analyse the deep drawing process. Wifi (1976) has used an incremental variational method to analyse axisymmetric elastic plastic solids at large strains including deep drawing with a hemispherical headed punch. He formulated the contact problem at different zones and used the finite element method. The material was assumed to be isotropic. He stated that such problems are computationally time consuming. Lee and Kobayashi (1975) have used a matrix method of analysis for rigid-plastic materials to solve the problmes of plane-stress bore expanding and flange drawing. The analysis was performed for two materials, one having normal anisotropy and the other possessing planar anisotropy. The results for planar anisotropy showed that in the bore expanding, the bore remained

closely round even after considerable expansion but the thickness strains near the bore varied with orientation. In flange drawing, the method enabled an analysis of ear formation to be made. The authors concluded that the nonuniform thickness distribution, caused by planar anisotropy, appears to have important implications for the occurrance of instability, such as necking in bore expanding and wrinkling in flange drawing. Gotoh (1980) analysed the deformation of the flange in the cylindrical cup drawing process by the newly-designed hybrid rigid plastic finite element method on the basis of a fourth-degree yield function t of orthotropy and the results were compared with those based on traditional quadratic function g and the experiments. He concluded that irrespective of ear-configuration, deformation of the flange which produces at most 8 ears can be numerically simulated very well up to the end of drawing by this method, including the distribution of drawing force along the inner periphery. Kobayashi and Kim (1978) described the development of a finite element model for analysing the sheet-metal forming processes. Materials were assumed to be rigid-plastic with the view that the usefullness of an analytical method depends largely on solution accuracy and computation efficiency. First, the variational formulation applicable to sheet metal forming was described by considering solution uniqueness and the effect of geometry change involved in the forming processes. From this variational formulation, a finite element process model based on the membrane theory is developed. Then, three basic sheet metal forming processes including deep drawing of

a sheet with a hemispherical head punch, were solved. When comparing the strain distribution predicted by this theory with the experimental data, the agreement was excellent over the flange of the sheet. However, over the punch head, the agreement was not as good. Wang and Budiansky (1978) developed a general finite element procedure on the basis of the nonlinear theory of membrane shells for calculating the deformations in the stamping of sheet metal by arbitrary shaped punches and dies. The sheet material was assumed to be elastic-plastic and to satisfy a rate-insensitive, Mises-type flow rule taking into account finite deformation, work-hardening and normal anisotropy. Theoretical results were compared with existing solutions and experimental data of the stretch forming process using a hemispherical punch.

Zienkiewicz, Onate and Heinrich (1978) have made a study of both the deep drawing and stretch forming of a circular blank with a hemispherical punch. Constitutive relations for a von Mises type flow were developed using the viscous shell formulation. The finite element method was applied for discretizing the equilibrium equations using a linear element. The effects of friction and work-hardening were conidered and the material was assumed to be rigid-plastic. The authors showed that their theoretical results on the punch load, thickness and circumferential strains agreed well with the existing results by Woo [9]. It may be noted, however, that in this work, the anisotropy of the material was neglected. In stretch forming a great discrepancy was noticed in the zone near the punch centre line. This was attributed by the authors to the prestrain imposed in the experiment which had not been taken into account in the analysis.

Mellor and Parmer (1978) presented a paper in which they surveyed the application of plasticity theory to sheet metal forming problems including deep drawing. The authors discussed the current position of the plasticity theory and concluded that it is necessary to check the validity of any theory by careful experiments, paying particular attention to the correlation between the theoretical and experimental strain distributions.

The only available analysis of deep-drawing without a blank-holder is due to Woo [10]. He used previous solutions, Woo [8] and Woo [9], to develop an analysis of the deep drawing of a circular blank into a cylindrical shell through a tractrix type die. Because of the difficulty in deducing the strain relationship when the material is in contact with the die profile, he used a modified tractrix of the following polar equation:

$$\rho = a_1\phi + a_2\phi^2 .$$

The constants a_1 and a_2 were determined by considering two points on the curve so that the resultant curve fits well with the tractrix curve. An expression for the strain relationship using the modified tractrix was given. Experiments were performed using aluminium blanks. Comparison between the theoretical and experimental thickness and circumferential strain distribution was made for the die contact zone, as shown in Figure (2.3) and Figure (2.4). The punch load was compared at three stages of drawing using total and incremental strain solutions. The author concluded that the comparison between the theoretical and experimental results

showed reasonable correlation. It may be said therefore that the solution could be applied for the design of die profile for minimizing the load required for deep-drawing.

2.2 Ironing

Ironing is applied principally for reducing the wall thickness of a cup by restricting the clearance between punch and die. Ironing process has received little scientific study. The first systematic investigation can be traced is the work of Lowe and Swift [11]. This work was extended by Knowles and Swift [12]. In these two works experiments were carried out on a standardized form of cup ironed in a small hydraulic subpress fitted with an autographic indicator. They found that a linear relationship exists between the ironing load and the reduction for cup wall thickness. They concluded that for general use over a fairly wide range of reductions in common practice, a die angle of 10 degrees to 15 degrees is apparently a highly satisfactory compromise. Leeming and Freeman (1952), Freeman and Leeming (1954) and Loxely and Freeman (1954) made an attempt to determine the constituents of the ironing load, namely the direct load on punch head and the tractional or frictional load transmitted to the punch through the cup wall. The ironing load and its constituents were measured independently by means of strain gauges mounted on a special hemispherical headed punch. The punch load is, in fact, a measure of tension in the ironed cup wall, and is consequently a prime factor in determining maximum reduction.

Shawki [13] presented an experimental investigation into the ironing of cylindrical cartridge brass cups under various

conditions of operation including die geometry and severity of cup wall reduction. He showed that the ironing load is fairly constant during ironing and that it increases with the degree of ironing in a manner not quite linear. He found that the ironing operation leads to increased hardness in a manner quite similar to the true stress/strain characteristic of the material. Increasing the die land gives rise to higher punch loads on account of increased frictional resistance at the die throat and that the efficiency of ironing operation is found to attain a maximum value at an optimum value of cup wall reduction of some 58 per cent. A theoretical study of ironing considering work-hardening was made by Fukui and Hansson (1970).

When ironing is combined with deep drawing without a blank-holder using a tractrix die profile, the operation seems to have special advantages. Shaw [14] illustrated this method. He claimed that the products of a press can exhibit qualities of predictable and consistant accuracy. Excellent surface finish and mechanical properties can be obtained when producing cylindrical deep-drawn pressings.

2.3 Hydraulic Bulge Forming

The deformation of a clamped sheet metal diaphragm by applying hydraulic pressure on one side of the diaphragm has been studied many times in the past. The importance of this method of deformation has been in the field of sheet metal forming research where the bulge test (balanced biaxial tension test) has been extensively employed to study the behaviour of sheet metal without the complications arising from friction

between tool and specimen. Hydraulic bulging of tubes by means of internal pressure is a useful industrial process, but its application has been limited due to thinning in the expanded wall of the tube and to the relatively small bulge ratios which can be obtained before instability and fracture take place. The bulge ratio obtained is usually quoted as 25-30%. The process can be improved by the application of an indipendent axial force. In 1965, Wallick (1965) reported that hydraulic tube bulging combined with axial pressure upsetting enables expansions of more than 60 per cent to be obtained in one operation. According to Wallick (1965), Fuchs (1965), Ogura, Ueda and Takagi (1966), Ogura (1969) and Limb, Chakrabarty, Garber and Mellor (1973) axisymmetric and asymmetric shapes can be produced by this method. Woo and Hawkes (1968) adopted this technique to develop a method for determining the stress/strain characteristic of tubular materials. They showed that the bulging process can be greatly extended by applying an axial compressive force to the tube subjected to internal pressure. The manner in which the internal pressure and axial load must be varied during the process, has been theoretically worked out by Limb, Chakrabarty, Garber (1974) for minimum thickness change in the formed tube. They found reasonably well agreement between theory and experiment for radial expansion up to 50%. Deep-drawing and hydraulic bulge forming in one continuous operation was introduced in 1975 by Turner and Woo [1]. They suggested a forming process for producing vessels or containers of required shape from sheet metal by drawing, ironing and bulging under internal pressure and axial com-

pressive force in one continuous operation. Soft aluminium speherical and conical vessels were produced by this method. They concluded that the continuity of the process gives an advantage over other forming methods such as spinning and forming with a rubber punch and that the success of the process is much dependent on the axial force which in turn has to be closely controlled relating to bulging pressure. Woo [2] described a prototype production machine for manufacturing a wide range of vessels. The machine incorporates drawing, ironing and hydraulic bulge forming in one stroke of a punch. Aluminium and pewter vessels were successfully formed. Measurement of thickness strain distribution in a certain axisymmetric and asymmetric components was made by Limb, Chakrabarty, Garber and Roberts (1976). In asymmetric forming of a tee-piece, they investigated the effect of using different lubricants on the bulged height of the tee dome.

A numerical solution for analysis of the bulging process of a thin-walled tube under internal pressure and axial force was proposed by Woo [15]. The solution is applied to a case in which the longitudinal stress resulted from the internal pressure and axial force is tensile along the whole length of the bulged tube. The material was considered to be isotropic. He concluded that total strains may be used in the theory, thus the computation is much simplified. Recently, Woo and Lua [16] extended the analysis by taking into consideration the anisotropy effect. The comparison of the theoretical and experimental results was shown to be satisfactory.

PART ONE

DEEP DRAWING

WITHOUT A BLANK-HOLDER

CHAPTER 3

GEOMETRY AND DESIGN OF CONVEX TYPE DIES

The success of the deep drawing of cups without a blank-holder depends largely on the correct choice of die geometry. For a certain material, blank size, die and punch geometries are the decisive factors for a successful draw.

3.1 Theoretical Geometry of Convex Type Dies

The favourite general features of a good die geometry can be summarized in the following:

1. An increasing radius of curvature towards the die throat to give the lowest possible drawing load. The lower the drawing load the higher is the drawing ratio which can be obtained.
2. A smooth continuous curve to ensure a homogeneous flow of material during drawing. This may reduce the tendancy of the material to wrinkle or buckle.
3. A flexible mathematical curve which can be easily fitted with any overall dimensions of the die, and which can be adjusted to alter its steepness during the design stage. The latter may be necessary so that the die profile thus designed will not cause buckling of the cup during drawing.
4. A die geometry which has a relatively flat entry to avoid slipping of the blank during the initial stage of drawing.
5. A die geometry which results in a simple deep drawing die assembly and a low production cost.

6. A profile which enables a theoretical strain relationship to be deduced. This is essential if a theoretical analysis of the drawing process is required, for instance, the prediction of the punch load.

In the present investigation, the theoretical die profile geometry is assumed:

3.1.1 The Tractrix Curve

The Tractrix Curve is perhaps the most widely used in the actual workshop practice. Figure (3.1) shows the geometry of this curve. The formation of the tractrix can be physically illustrated by assuming a man standing at, O, holding a rope of length, a, to which a weight is attached, initially at w_o. The man walks along the Y-axis dragging the weight after him, when the man is at m, the weight is at w. The path of the weight (the tractrix) will at least resemble the curve shown, where

$$-\frac{dy}{dx} = \tan\phi = \frac{\sqrt{a^2 - x^2}}{x}, \qquad (3.1)$$

which can be integrated to give

$$y = -\sqrt{a^2 - x^2} + a \ln \left(\frac{a + \sqrt{a^2 - x^2}}{x}\right). \qquad (3.2)$$

From the mathematical definition of the radius of curvature,

$$\rho = \left[1 + \left(\frac{dy}{dx}\right)^2\right]^{3/2} / \left(\frac{d^2y}{dx^2}\right).$$

It can be shown that the tractrix radius of curvature at any point is

$$\rho = \frac{a\sqrt{a^2 - x^2}}{x} .$$

Using equation (3.1) we get

$$\rho = a \tan\phi . \qquad (3.3)$$

The radius of curvature increases from $\rho = 0$ at the die rim to relatively high values depending on the die height to be used. Theoretically, $\rho = \infty$, when $\phi = \pi/2$.

From the practical point of view, only the upper part of the tractrix is used in the workshop applications, so that the die height is not excessive.

From the overall dimensions r_1, r_2 and H of the die, the tractrix parameter a can be determined from equation (3.2) with

$$x = a - (r_1 - r_2) \text{ and } y = H .$$

Let $b = r_1 - r_2$ and $c = \sqrt{2ab - b^2}$.

From equation (3.2)

$$H = a \ln \left(\frac{a+c}{a-b}\right) - c .$$

Using Newton's method of successive approximations [17], the value of a can be determined as follows:

$$f(a) = a \ln \left(\frac{a+c}{a-b}\right) - c - H ,$$

$$f'(a) = \ln \left(\frac{a+c}{a-b}\right) + \frac{a}{a+c}\left(1 + \frac{b}{c}\right) - \frac{a}{a-b} - \frac{b}{c} , \qquad (3.4)$$

$$(a)_{n+1} = (a)_n - \frac{f(a)_n}{f'(a)_n} .$$

For the first approximation, a_o may be chosen slightly higher than the value of b. The tractrix curve is traced from

$$r = r_1 - a\,(1 - \cos\phi) , \qquad (3.5)$$

$$y = - a \sin\phi + a \ln \left(\frac{1+\sin\phi}{\cos\phi}\right) . \qquad (3.6)$$

The tracing is terminated at ϕ_2 where

$$\phi_2 = \cos^{-1}\left(1 - \frac{b}{a}\right) ,$$

which corresponds to die throat radius.

3.1.2 The Second Degree Spiral Curve

The second degree spiral curve shown in Figure (3.2), was suggested by Woo [10], in analysis of the deep drawing problem over a tractrix die. The radius of curvature of this curve is given by the polar equation

$$\rho = a_1\phi + a_2\phi^2 .$$

The curve can be traced from

$$r = r_1 - a_1\,(\cos\phi + \phi\sin\phi - 1) - a_2[2\,\phi\cos\phi + (\phi^2 - 2)\,\sin\phi] , \qquad (3.7)$$

$$y = a_1 (\sin\phi - \phi\cos\phi) + a_2[2\,\phi\sin\phi - (\phi^2 - 2)\cos\phi - 2]. \tag{3.8}$$

It has been shown by Woo [10] that this curve fits with the tractrix for certain values of a_1 and a_2 and it has the property over the tractrix that at the die throat radius the curve terminates at $\phi_2 = \pi/2$.

To fit this curve to a certain die with known parameters, we put $\phi = \pi/2$ in equations (3.7) and (3.8), taking into account that at this point: $r = r_2$ and $y = H$. Thus,

$$a_2 = 3.0989\,[H - 1.7519\,(r_1 - r_2)]\,, \tag{3.9}$$

$$a_1 = 1.7519\,(r_1 - r_2) - 0.8189\,a_2\,,$$

when chosing $\rho = a_1\,\phi + a_2\phi^2$, the constants a_1 and a_2 are supposed to have positive values so that ρ of the die profile is positive.

The die height H is a consequence of a_2 value, chosen to give increasing radius of curvature ρ,

$$H = 0.3227\,a_2 + 1.7519\,(r_1 - r_2)\,. \tag{3.10}$$

If a_1 is negative, ρ is negative for the values of ϕ given by

$$\phi < -\left(\frac{a_1}{a_2}\right).$$

A special case of the second degree spiral curve is obtained when $a_1 = 0$. In this case the curve polar equation becomes

$$\rho = a\phi^2.$$

To get the tracing equations we substitute, $a_1 = 0$, into equation (3.7) and (3.8)

$$r = r_1 - a[2\ \phi\cos\phi + (\phi^2 - 2)\ \sin\phi], \tag{3.11}$$

$$y = a[\,2\ \phi\sin\phi - (\phi^2 - 2)\ \cos\phi - 2]. \tag{3.12}$$

Taking into account that $\phi_2 = \pi/2$ at the die throat radius, and $y = H$, the constant a can be obtained from

$$a = 0.876H, \tag{3.13}$$

where

$$H = 2.4423\ (r_1 - r_2), \tag{3.14}$$

H in the last equation is restricted to the value of $(r_1 - r_2)$ and cannot be chosen independently from that value.

3.1.3 The Exponential Spiral Curve

The idea for introducing this new curve comes from the need for a die geometry which satisfies the features described earlier for a good die profile. It was reported by Haverbeck [6] and Oehler [5] that to produce cups from sheet of good deep-drawing quality, it has been proved to be

more suitable to use a modified tractrix instead of the usual tractrix for maximum attainable values of drawing ratio. The modified tractrix described by Oehler [5] is steeper towards the lower part of the die, and it is drawn between two tractrices and approximated by the designer.

The exponential spiral curve is given by the polar equation

$$\rho = a_1 \, (e^{a_2 \phi} - 1). \tag{3.15}$$

The tracing equations are:

$$\begin{aligned} r &= r_1 - \frac{a_1 e^{a_2 \phi}}{1 + a_2^2} (\sin\phi + a_2 \cos\phi) + a_1 \sin\phi + \frac{a_1 a_2}{1 + a_2^2}, \\ y &= \frac{a_1 e^{a_2 \phi}}{1 + a_2^2} (a_2 \sin\phi - \cos\phi) + a_1 \cos\phi + \frac{a_1}{1 + a_2^2} - a_1 . \end{aligned} \tag{3.16}$$

The two constants a_1 and a_2 can be determined by substituting $\phi = \pi/2$ into the last two equations, and noting that at this point,

$$y = H \text{ and } r = r_2 ,$$

hence,

$$r_1 - r_2 = a_1 \left(\frac{e^{\pi/2a_2}}{1 + a_2^2} - \frac{a_2}{1 + a_2^2} - 1\right),$$

$$H = a_1 \left(\frac{a_2 e^{\pi/2a_2}}{1 + a_2^2} + \frac{1}{1 + a_2^2} - 1\right).$$

By dividing the first expression by the second one, and denoting $d = (r_1 - r_2)/H$, we get the equation

$$(a_2 d - 1)e^{\pi/2a_2} + (1 - d)\, a_2^{\,2} + a_2 + 1 = 0.$$

This equation can be solved, using Newton's method of successive approximations, to determine the value of a_2 as follows:

$$f(a_2) = (a_2 d - 1)e^{\pi/2a_2} + (1 - d)\, a_2^{\,2} + a_2 + 1,$$

$$f'(a_2) = (\tfrac{\pi}{2} a_2 d + d - \tfrac{\pi}{2})e^{\pi/2a_2} + 2(1 - d)\, a_2 + 1, \qquad (3.17)$$

$$(a_2)_{n+1} = (a_2)_n - \frac{f(a_2)_n}{f'(a_2)_n}.$$

The first value $(a_2)_o$ can be chosen as $H/(r_1 - r_2)$ and the other constant a_1 can be obtained from

$$a_1 = \frac{H(1 + a_2^{\,2})}{a_2 e^{\pi/2a_2} - a_2^{\,2}}. \qquad (3.18)$$

Figure (3.3) demonstrates the flexibility of this curve and its ability to increase its steepness and radius of curvature by increasing the die height.

3.1.4 The Conical Die

The conical die is a special case of the convex curves when $\rho = \infty$. Figure (3.4) shows the geometry of this die. The die is usually characterized by its cone angle ϕ_c,

$$\phi_c = 2 \tan^{-1} \left(\frac{r_1 - r_2}{H}\right).$$

The current radius at any point is

$$r = r_1 - y \tan (\phi c/2).$$

3.2 Design of Convex Type Dies

Die design when a convex type die is used, may be considered as an easy task to perform when the following information is available:

1. Dimensions of the cup to be produced.
2. The average strain ratio γ of the blank material.
3. The maximum drawing ratio, which is defined as the ratio of the maximum blank diameter which can be drawn successfully to the punch diameter. This ratio should not be exceeded in the die design.

From the plasticity conditions at the cup rim,

$$\varepsilon_t = - \frac{\varepsilon_\theta}{1 + \gamma}.$$

The derivation of the above expression will be shown later in section (4.8). Using this expression, the maximum thickness t_{max} when the cup rim approaches the die throat can be written as

$$t_{max} = t_o \left(\frac{R_1}{r_2 - \frac{t_{max}}{2}}\right)^{\frac{1}{1+\gamma}}. \qquad (3.19)$$

As far as the lower part of the die is concerned, the radial clearance, c_r between the punch and die throat diameter is very important and may be expressed as

$$c_r = r_2 - R_p \tag{3.20}$$

or, in terms of the cup maximum thickness as

$$c_r = X.t_{max}\,, \tag{3.21}$$

where X is a constant which determines the maximum amount of ironing between punch and die as follows:

1. When $X > 1$, no ironing and the final interior shape of the cup is not fully cylindrical.
2. When $X < 1$, ironing will take place.
3. When $X = 1$, the material is just filling the clearance between punch and die throat.

It would be better for the designer to chose the value of X so that the maximum load due to ironing does not exceed the maximum drawing load. However, excessive ironing between punch and die should be avoided because it would result in high loads and localized wear on the die throat zone.

The following expression can be deduced using equations (3.19), (3.20) and (3.21):

$$\left(\frac{r_2 - R_p}{Xt_o}\right)^{1+\gamma} (2r_2X - r_2 + R_p) = 2R_1X.$$

This equation can be used to determine the die throat radius, Newton's method of successive approximation is used as follows:

$$f(r_2) = \left(\frac{r_2 - R_p}{Xt_o}\right)^{1+\gamma} [r_2(2X - 1) + R_p] - 2R_1X,$$

$$f'(r_2) = \left(\frac{r_2 - R_p}{Xt_o}\right)^{1+\gamma} \left[\frac{(1 + \gamma)(2r_2X - r_2 + R_p)}{(r_2 - R_p)} + (2X - 1)\right],$$

$$(r_2)_{n+1} = (r_2)_n - \frac{f(r_2)_n}{f'(r_2)_n}. \qquad (3.22)$$

The first value $(r_2)_o$ in the approximation may be taken slightly higher than R_p.

The cup height may be approximated by assuming that $\varepsilon_\theta = 0$ at the punch radius, the cup wall thickness is linearly increased from t_o at the cup base to t_{max} at the cup top and allowing for partial ironing between punch and die throat. Using the above assumptions, the following relationship can be obtained:

$$h = \frac{(R_1^2 - R_p^2)\, t_o}{2R_p\, c_r(t_{max}^2 - t_o^2)}[t_{max}^2 + c_r^2 - 2c_r\, t_o] + t_o, \qquad (3.23)$$

where $t_o < c_r < t_{max}$.

For full ironing of cup walls, by assuming that $\varepsilon_\theta = 0$ at the punch radius. The cup height for fully ironed cup walls may be approximated as

$$h = \frac{(R_1^2 - R_p^2)\, t_o}{2R_p\, c_r}. \qquad (3.24)$$

The maximum reduction ratio in ironing α_{max} at the cup rim may be approximated as,

$$\alpha_{max} = 1 - X. \qquad (3.25)$$

Once the required cup size is obtained, the die curve can be selected, the die height is assumed and the die curve constants can be determined so that the die profile can be traced as it was described earlier.

3.3 Selection of Die Profiles for Theoretical and Experimental Investigations

Five different die profiles were selected for the theoretical and experimental investigations of the deep drawing problem through a convex type die without a blank-holder.

Die profiles 1-4 were designed to produce experimental cups of 50 mm internal diameter from circular flat blanks of 120 mm diameter and 1.6 mm nominal thickness. The punch profile radius is 10 mm. Die profile 5 is fitted on the bulge forming machine to produce cups for ironing and hydraulic bulge forming tests. This die is an exact tractrix type die and its details and results are given in Part Two.

Die profiles 1-3 were chosen from existing dies used in the department research laboratory in some preliminary experiments on the effect of die geometry on punch load. The die curves were corrected slightly to suite the purpose of this work. These dies are used mainly to investigate the effect of the die radius of curvature on the punch load, and therefore, their profiles have been given the same second degree spiral curve. It can be seen in Figure (3.6) that the radius of curvature has been increased from die profile 1 to die

profile 3. Since the radius of curvature varies along the die profile and is not constant as in the conventional deep drawing die with a blank-holder, therefore, it was thought that in order to get a marked reduction in the punch load the radius of curvature should be increased greatly, i.e. more steep dies should be used.

The reason for selecting the second degree spiral curve was to examine further possibility of reducing the punch load in deep drawing.

The die design procedure given in Section (3.2) was not followed here because of the variety of material under cosiderations. In order to reduce the number of dies required to a minimum, a radial clearance of 1.75 mm was assumed for die profiles 1-4.

The die throat diameter for die profiles 1-4 is calculated from equation (3.20), hence

$$r_2 = 25 + 1.75,$$

$$r_2 = 26.75 \text{ mm}.$$

1. Die Profile 1:

The die curve is given by the polar equation

$$\rho = 21\phi + 45.3\phi^2,$$

where the two constants of this equation have been chosen to obtain a close fit with a tractrix curve of a = 37.11 mm.

The die lip radius is equal to the blank radius,

$$r_1 = 60 \text{ mm}.$$

The die height is calculated from equation (3.10),

$$H = 72.72 \text{ mm}.$$

Die profile 1 and the tractrix which fits closely with it are shown in Figure (3.5). The tractrix is shown for comparison. Both curves were traced using equations (3.7), (3.8) and (3.5), (3.6) respectively.

2. Die Profile 2:

The die curve is given by the following polar equation:

$$\rho = 150\phi^2.$$

The theoretical die height is deduced from equation (3.13),

$$H_t = 171.24 \text{ mm}.$$

The theoretical die lip radius is determined according to equation (3.14) as

$$r_1 = 96.86 \text{ mm}.$$

Since the blank radius is 60 mm, therefore only the latter part of the curve is used, which corresponds to

ϕ_1 = 1.012 radians and ϕ_2 = $\pi/2$ radians

The working die height is found from equation (3.12) as follows

$H_w = y(\pi/2) - y(1.012)$

$= 136.21$ mm.

The die curve shown in Figure (3.5) was traced using equations(3.11) and (3.12).

3. Die Profile 3:

The die curve is expressed by its polar equation as

$\rho = 214\phi^2$.

r_1, H_t, ϕ_1, ϕ_2 and H_w are found in the same way as is used for die profile 2, hence,

$r_1 = 126.77$ mm, $H_t = 244$ mm,

$\phi_1 = 1.132$ radians, $\phi_2 = \pi/2$ radians, and

$H_w = 167.76$ mm.

The die curve shown in Figure (3.5) was traced using equations (3.11) and (3.12).

4. Die Profile 4:

This die profile was designed after experiments on die profiles 1, 2 and 3 were completed, in an attempt to reduce the punch load for aluminium blanks which showed a tendency to buckle during drawing when die profiles 2 and 3 were used. It was also an opportunity to examine the performance of the new exponential spiral curve as a profile for deep drawing die.

For the purpose of comparison,die profile 4 was given the same working dimensions as die profile 3, hence,

$$r_1 = 60 \text{ mm}, \; r_2 = 26.75 \text{ mm and } H = 167.76 \text{ mm}.$$

The die constants a_2 and a_1 were determined from equations (3.17) and (3.18) respectively, giving the following polar equation:

$$\rho = 0.341 \, (e^{5.0\phi} - 1).$$

The die curve was traced using equations(3.16), and it is shown in Figure (3.5).

The radius of curvature versus the current radius relation for die profiles 1-4 is given in Figure (3.6) for comparison.

CHAPTER 4

THEORETICAL ANALYSIS OF DEEP DRAWING THROUGH A CONVEX TYPE DIE

4.1 General Description

The deep-drawing operation, through a convex type die without a blank-holder, is used to produce cylindrical cups from flat circular blanks of sheet metal.

The success of the process depends on the drawing ratio, blank thickness, material drawability and the frictional conditions at the interface between the drawn material and each of the punch and the die profiles.

The essentials of the tools are shown diagrammatically in Figure (4.1), where the blank is shown in two positions. The first position is before the operation and the second position shows the partly drawn cup as a result of the punch movement.

The main advantages of this operation over the conventional deep drawing with a blank-holder are:

1. Higher drawing ratios can be achieved in a single draw, Oehler [5].
2. Simpler tooling design and hence lower tooling cost.
3. Lower drawing load which means that lower press capacity is needed to produce a certain component.
4. Quicker setting-up times and hence higher production rate.

5. The operation can be easily followed by ironing, to achieve even higher drawing ratios, Shaw [14].
6. The operation can be followed by ironing and hydraulic bulging to produce vessels or containers from flat blanks, Turner and Woo [1] and Woo [2].

Regarding the final cup shape, the conventional operation has the advantage of being capable of producing cups with a flange on their top end.

With reference to Figure (4.1), the deep drawing operation without a blank-holder may be considered as consisting of the following parts:

1. Drawing through the die profile.
2. Stretching between die and punch.
3. Stretching over the punch profile radius.
4. Plane-stretching over the flat base of punch.

1. Drawing Through the Die Profile

Drawing takes place in the annular zone between r_a and r_b. The material in this zone is drawn progressively inwards towards the die throat under an applied tangential tensile stress and the effect of continuously decreasing the radii in this zone is to induce a compressive circumferential stress which causes a considerable increase in material thickness. The maximum increase in thickness occurs at r_a; the value of the maximum thickness for a certain blank is a function of the current outer radius and the strain ratio. As the draw

proceeds, more material from the stretch forming zone comes into contact with the die profile and becomes thicker. This material has been previously thined under tension in the zone between die and punch. The net effect for the outer parts of this zone is an increase in the thickness of the material.

As far as the punch load is concerned, die profile geometry and the frictional conditions at the interface between material and die play a major role in determining the punch load behaviour for a given blank.

While the material is being drawn through the die, it is also subjected to bending. This bending effect lasts until the moment when the material comes into contact with the die profile. After that moment the material undergoes unbending over the convex shape of the die profile. Under the effect of unbending the material is gradually straightend-up over an increasing radii of curvature until it finally forms the cylindrical shape of the cup wall. In the present analysis, the effects of bending and unbending are neglected. This assumption will be justified later when comparing the theoretical results with those done by experiment.

2. Stretching Between Die and Punch

Stretching takes place in the annular zone between r_b and r_c, where r_b lies on the die profile and r_c lies on the punch profile radius. The material in this zone is stretched under the effect of the punch load which causes a decrease in the material thickness. As the operation proceeds the

material in this zone moves gradually to zones 1 and 3, where it will be caused to increase in thickness in zone 1, and a further decrease in thickness in zone 3.

3. Stretching Over the Punch Profile Radius

This process occurs in the annular zone between r_c and r_d over the punch profile radius. The material in this zone is stretched progressively outwards under an applied tangential tensile stress and the effect of continuously increasing the radii in this zone is to induce a tensile circumferential stress which causes decrease in the material thickness. By moving from r_c towards r_d, the tensile tangential stress decreases and the tensile circumferential stress increases in a way which depends on the punch profile radius and the frictional conditions in this zone, until they become equal at r_d. The effect of bending of material in the punch profile region is neglected in the present analysis.

4. Plane-Stretching Over the Flat Base of the Punch

The process of plane-stretching occurs in the circular zone of radius r_d. According to Woo [8], in this zone, $\sigma_t = 0$, the material is therefore stretched under biaxial stress conditions. The stress and strain state is identical to that in pure uniaxial compression plus the addition of a uniform hydrostatic state of tensile stress equal to the uniaxial yield stress. It follows, therefore, that the state of stress and strain is uniform in the flat base of the cup.

Under the effect of the biaxial tensile stress the material thickness in this zone is uniformly decreased and part of the material slides outwards from this zone to zone 3.

4.2 Effect of Anisotropy in Sheet Metals

All metals exhibit anisotropy to a greater or lesser degree when deformed at room temperature, that is the mechanical properties of the metal vary in different directions. The amount and type of anisotropy is characteristic of its mechanical and heat treatment history. In sheet metals it is convenient to define two types of anisotropy:

1. Planar Anisotropy:

Planar anisotropy describes the variations of mechanical properties in the plane of the sheet and is characterized by the amount of earing that occurs when drawing a cylindrical cup from a flat circular blank. As such, planar anisotropy is usually considered objectionable in drawing quality sheet metals, because it represents a waste of material. In the drawing of a cylindrical cup, ears would be expected to develop from the rim of the blank at positions where the uniaxial yield strength has a minimum value in the circumferential direction. The number and form of ears vary from material to another.

2. Normal Anisotropy:

Normal anisotropy describes the strength of the metal through the thickness of the sheet relative to its strength in the plane of the sheet. Whiteley [4] mentioned, that its practical importance lies in the fact that the resistance of sheet metal to thinning, which is advantageous for deep drawing operations, is a function of its normal anisotropy, and that normal anisotropy indicated by a high average strain ratio is desirable for good drawability.

The tensile strain ratio, γ, is commonly accepted as a measure of anisotropic plasticity and has been widely employed as a parameter for the measurement of plastic normal anisotropy in subsequent investigations. The tensile strain ratio is defined as the ratio of the natural strains in width and thickness measured in simple tension test,

$$\gamma = \frac{\ell n(W_o/W)}{\ell n(t_o/t)} , \qquad (4.1)$$

where W_o and W are the initial and current width of the specimen respectively.

4.3 Anisotropic Plasticity Relations

The theory of plasticity for anisotropic materials is applied in the present analysis to describe the mechanics of plastic deformation of the material during the deep drawing operation. Since the material in deep drawing undergoes large plastic deformations, it follows that the relatively small elastic strains can be ignored. That means that the

total strain increment is equal to the plastic strain increment, and the material is considered to be rigid plastic.

Hill's theory of plastic anisotropy (see Appendix A) will be applied for its simplicity.

Figure (4.2) shows an element of the drawn material over the die profile, when the material is in contact with either the punch or the die, and whenever a relative slide between tool and material exists, there is frictional force at the interface opposite to the sliding direction. If ordinary Coulomb friction is assumed to be valid in this case, the frictional shear stress is proportional to the contact pressure and the proportionality factor is the coefficient of friction. In deep drawing practice, lubricant is usually used, which means that the coefficient of friction is relatively small, and therefore, the frictional shear stress is small if compared with other stress components and can be neglected. Furthermore, the stress in the thickness direction due to the contact force N is comparatively small and can be ignored. Therefore, the stress state is reduced to a plane stress condition.

Rotational symmetry of the sheet metal about the z-axis is assumed. Following Bramely and Mellor [18], the average of planar anisotropic properties of the material is considered, and according to Woo [10] the average planar properties can be represented by the average strain ratio γ from the following equation:

$$\gamma = \frac{\gamma_o + \gamma_{45} + \gamma_{90} + \gamma_{-45}}{4} . \tag{4.2}$$

For sheet material subjected to plane stress, with rotational symmetry about the z-axis, it is known from Hill's theory that,

$$\gamma = \frac{H}{G} = \frac{H}{F} . \tag{4.3}$$

From the above equation and equation (A.13), see Appendix A, it can be seen that the equivalent strain increment is,

$$d\bar{\varepsilon} = \{\frac{2(2 + \gamma)}{3(1 + 2\gamma)} [2d\varepsilon_\theta^2 + (1 + \gamma)\, d\varepsilon_t^2 + 2d\varepsilon_\theta\, d\varepsilon_t]\}^{\frac{1}{2}} . \tag{4.4}$$

Assuming, $\sigma_t = 0$, it can be shown using equation (4.3) and equations (A.12), see Appendix A, that the principal stresses are given by the following equations:

$$\sigma_\phi = - \frac{2(2 + \gamma)}{3(1 + 2\gamma)} \frac{\bar{\sigma}}{d\bar{\varepsilon}} [d\varepsilon_\theta + (1 + \gamma)\, d\varepsilon_t] , \tag{4.5}$$

$$\sigma_\theta - \sigma_\phi = \frac{2(2 + \gamma)}{3(1 + 2\gamma)} \frac{\bar{\sigma}}{d\bar{\varepsilon}} (2d\varepsilon_\theta + d\varepsilon_t) . \tag{4.6}$$

From equation (4.5), the following equation is used for successive approximations of t in the numerical solution,

$$d\varepsilon'_t = - \frac{1}{(1 + \gamma)} [\frac{3(1 + 2\gamma)}{2(2 + \gamma)} (\frac{d\bar{\varepsilon}}{\bar{\sigma}}) \frac{(\sigma_\phi t)'}{t} + d\varepsilon_\theta] , \tag{4.7}$$

where $(\sigma_\phi t)'$ is the unit tangential force determined from the equilibrium equation.

The relationship between the equivalent stress $\bar{\sigma}$ and the equivalent strain $\bar{\varepsilon}$ for a given material is determined experimentally as described in the following section (4.4).

Because of the variety of materials considered in this investigation, it is more conventient to represent the stress/strain relationship as:

$$\bar{\sigma} = A + B\ (\bar{\varepsilon} - c)^n, \tag{4.8}$$

which may take any of the following forms:

When $A = c = 0$,

$$\bar{\sigma} = B\ (\bar{\varepsilon})^n, \tag{4.9}$$

when $c = 0$ and $n = 1$,

$$\bar{\sigma} = A + B\ \bar{\varepsilon}, \tag{4.10}$$

When $c = 0$,

$$\bar{\sigma} = A + B\ \bar{\varepsilon}^n, \tag{4.11}$$

where A, B, c and n are constants, and $\bar{\varepsilon}$ is equal to $\int d\bar{\varepsilon}$, $d\bar{\varepsilon}$ being the incremental equivalent strain calculated from equation (4.4).

4.4 Determination of the Equivalent Stress/Strain Relationship

The equivalent stress/strain relationship is experimentally determined in this investigation using two methods; balanced biaxial tension and simple tension tests. This is used as a means to check the validity of Hill's anisotropic

theory of plasticity for individual materials under consideration. The results of the balanced biaxial tension test are used in the theoretical analysis of the deep drawing operation for two reasons:

1. The strain range which can be obtained by biaxial tension test is usually wider than that obtained by tension test.
2. The biaxial tension test simulates the stress conditions in the deep drawing operation.

The simple tension test results are used for comparison and for determining the strain ratios which are needed in the biaxial tension test and the theoretical analysis.

4.4.1 Simple Tension Test

Simple tension is the most widely used test for determining the mechanical properties of materials.

According to Hill's theory, Taghvaipour and Mellor [19] showed that, the equivalent stress, $\bar{\sigma}$, and the equivalent strain, $\bar{\varepsilon}$, can be written in terms of the longitudinal stress or strain in simple tension as follows:

From a simple tension test in the direction of rolling,

$$\bar{\sigma} = \left[\frac{3}{2}\left(\frac{1 + \gamma_o}{1 + \gamma_o + \frac{\gamma_o}{\gamma_{90}}}\right)\right]^{\frac{1}{2}} \sigma_o \,, \qquad \bar{\varepsilon} = \left[\frac{2}{3}\left(\frac{1 + \gamma_o + \frac{\gamma_o}{\gamma_{90}}}{1 + \gamma_o}\right)\right]^{\frac{1}{2}} \varepsilon_o \tag{4.12}$$

From simple tension test perpendicular to the rolling direction,

$$\bar{\sigma} = \left[\frac{3}{2}\left(\frac{1 + \gamma_{90}}{1 + \gamma_{90} + \gamma_{90}/\gamma_o}\right)\right]^{\frac{1}{2}} \sigma_{90} ,$$

$$\bar{\varepsilon} = \left[\frac{2}{3}\left(\frac{1 + \gamma_o + \gamma_{90}/\gamma_o}{1 + \gamma_{90}}\right)\right]^{\frac{1}{2}} \varepsilon_{90} \qquad (4.13)$$

According to the theory, γ-values between 0^o and 90^o do not affect the results.

4.4.2 Balanced Biaxial Tension Test

The tensile conditions are achieved by clamping a circular diaphragm at its periphery and applying oil pressure on one side. Since the materials under consideration are relatively thick, it is more accurate to determine the equivalent strain in terms of r in the middle section of the specimen. From the measured r" and Δh" in the experiment, the value of r is determined as follows:

With reference to Figure (4.3a), the radius of curvature ρ_c" can be found from the geometry of the bulged diaphragm at the outer surface of the polar zone as,

$$\rho_c" = \frac{r"^2 + (\Delta h")^2}{2\ \Delta h"} . \qquad (4.14)$$

With reference to Figure (4.3b),

$$r = r" - \frac{tr"}{2\ \rho_c"} . \qquad (4.15)$$

From the incompressibility condition,

$$\varepsilon_t = -2\,\varepsilon_\theta$$

$$\text{or}, \quad \left(\frac{r}{r_o}\right)^2 = \frac{t_o}{t}\,. \tag{4.16}$$

Using equations (4.15) and (4.16), it can be shown that the radius at the middle section of the diaphragm is given by the following equation,

$$r^3 - r''\,r^2 + c = 0\,,$$

where

$$c = \frac{t_o\,r''\,r_o^{\,2}}{2\,\rho_c''}\,. \tag{4.17}$$

The third degree equation in r can be solved* using Newton's method of successive approximations as in the following:

$$f(r) = r^3 - r''\,r^2 + c\,,$$

$$f'(r) = 3r^2 - 2\,r''\,r\,, \tag{4.18}$$

$$(r)_{n+1} = (r)_n - \frac{f(r)_n}{f'(r)_n}\,.$$

The first value in the approximations can be chosen as, $(r)_o = r''$. Similar equation can be obtained in terms of t, using the same equations (4.15) and (4.16)

$$t^3 - 4\,\rho_c''\,t^2 + 4\,\rho_c''^2\,t - \frac{4\,t_o\,r_o^{\,2}\,\rho_c''^2}{r''^2} = 0$$

---

* An exact solution can be obtained using the goniometric method, see Reference [24] , p. 47.

and can be solved to find the value of t in the same way described above.

After r is found, the hoop strain and the thickness can be calculated from

$$\varepsilon_\theta = \ell n \left(\frac{r}{r_o}\right) , \quad \text{and}$$

$$t = t_o e^{-2\varepsilon_\theta}$$

The equilibrium equation of forces along the vertical direction at the pole gives,

$$\sigma_\phi = \frac{p\ (\rho_c" - t)^2}{2t\ (\rho_c" - t/2)} . \tag{4.19}$$

By applying Hill's theory of plastic anisotropy (see Appendix A), assuming a rotational symmetry about the z-axis and considering the biaxial tension condition at the pole, it can be shown that the equivalent strain is given by the equation

$$\bar{\varepsilon} = \left(\frac{2 + \gamma}{3}\right)^{\frac{1}{2}} 2\varepsilon_\theta \tag{4.20}$$

and the equivalent stress is

$$\bar{\sigma} = \left(\frac{3}{2 + \gamma}\right)^{\frac{1}{2}} \sigma_\phi . \tag{4.21}$$

4.5 The Volume Constancy Relations

The volume constancy relation is used in the present analysis as a relationship between the geometrical variables of the deformation process of an element of material. It will be applied specifically to deduce the relationship between ε_t and ε_θ in the theoretical analysis. The volume constancy relation is obtained from the condition of incompressibility of an element, that is, for each element of the material, the volume before and after deformation remains constant. Let us consider the circular blank of uniform thickness t_o, in Figure (4.4). Each element has the shape of a circular ring. The volume constancy relation may be approximated as,

$$\pi\ (R_i^{\,2} - R_{i+1}^{\,2})\ t_o = \Delta A\ \left(\frac{t_i + t_{i+1}}{2}\right),$$

where ΔA is the surface area at the middle section of that particular element after deformation. From the above equation, the surface area at the middle section is,

$$\Delta A = \frac{2\pi\ (R_i^{\,2} - R_{i+1}^{\,2})t_o}{(t_i + t_{i+1})} \quad . \tag{4.22}$$

When the material is in contact with a tool of known geometry, then the surface area can be determined from the following integration:

$$\Delta A = \int_{\phi_i}^{\phi_{i+1}} 2\pi\ (r'' - t/2\ \sin\phi)(\rho'' + t/2)\ d\phi\,, \tag{4.23}$$

where r" and ρ" are functions of ϕ.

(a) The volume constancy equation when the material is drawn through the die profile:

1. Tractrix die curve

Referring to Figure (3.1), the surface area of an element of material in contact with a tractrix type die can be found using equation (4.23) where r" and ρ" for a tractrix curve are given by equations (3.5) and (3.3) respectively:

$$\Delta A = \int_{\phi_i}^{\phi_{i+1}} 2\pi\,(r_1 - a + a\cos\phi - t/2\,\sin\phi)(a\tan\phi + t/2)\,d\phi .$$

By integrating this equation, we get

$$\Delta A = 2\pi\{(r_1 - a)\,t/2\phi + a\,t\,\sin\phi + (t^2/4 - a^2)\,\cos\phi - \frac{a\,t}{4}\left[\ell n\left(\frac{1+\sin\phi}{1-\sin\phi}\right)\right] + (a - r_1)\,a\,\ell n\cos\phi\}_{\phi_i}^{\phi_{i+1}} .$$

By substituting the above expression into equation (4.22), we obtain,

$$\left(\frac{R_i^2 - R_{i+1}^2}{t_i + t_{i+1}}\right) t_o = \{(r_1 - a)\,t/2\phi + a\,t\,\sin\phi + (t^2/4 - a^2)\,\cos\phi - \frac{a\,t}{4}\left[\ell n\left(\frac{1+\sin\phi}{1-\sin\phi}\right)\right] + (a - r_1)\,a\,\ell n\cos\phi\}_{\phi_i}^{\phi_{i+1}} . \qquad (4.24)$$

In the present analysis of the deep drawing problem, ϕ_i and t_i are known from previous step. If t_{i+1} of the next step is assumed, ϕ_{i+1} can be determined from the above

equation and hence r_{i+1} can be found from, $r_{i+1} = r_1 - a(1 - \cos\phi_{i+1}) - t_{i+1/2} \sin\phi_{i+1}$. This shows how the strains ε_t and ε_θ are related to each other using the volume constancy principle.

To determine ϕ_{i+1} from equation (4.24), Newton's method of successive approximation is used as follows:

$$f(\phi_{i+1}) = \{(r_1 - a)\, t/2\phi + a\, t \sin\phi + (t^2/4 - a^2)\cos\phi - \frac{a\, t}{4}\left[\ln\left(\frac{1 + \sin\phi}{1 - \sin\phi}\right) + (a - r_1)\, a \ln\cos\phi\right]_{\phi_i}^{\phi_{i+1}} - \left(\frac{R_i^2 - R_{i+1}^2}{t_i + t_{i+1}}\right) t_o,$$

$$f'(\phi_{i+1}) = (r_1 - a + a\cos\phi_{i+1} - t/2 \sin\phi_{i+1})(a \tan\phi_{i+1} + t/2),$$

$$(\phi_{i+1})_{n+1} = (\phi_{i+1})_n - \frac{f(\phi_{i+1})_n}{f'(\phi_{i+1})_n}, \tag{4.25}$$

where $t = \dfrac{t_i + t_{i+1}}{2}$. (4.26)

The first value, $(\phi_{i+1})_o$, in the approximation may be found by considering the volume constancy of an element and assuming that $\rho_{i+1} = \rho_i$ and $r_{i+1} = r_i$ according to the following equation,

$$\phi_{i+1} = \phi_i + \frac{(R_i^2 - R_{i+1}^2)}{(t_i + t_{i+1})} \frac{t_o}{\rho_i\, r_i}. \tag{4.27}$$

2. Second degree spiral curve

The volume constancy relation corresponding to this curve, see Figure (3.2), was shown by Woo [10] as,

$$\left(\frac{R_i^2 - R_{i+1}^2}{t_i + t_{i+1}}\right) t_o = \left[\left(\frac{r_1 + a_1}{2}\right) t\phi + \left(\frac{r_1 + a_1}{2}\right) a_1\phi^2 \right.$$

$$+ \left(\frac{r_1 + a_1}{3}\right) a_2\phi^3 + (20\, a_1\, a_2 - \tfrac{3}{2}\, a_1 t) \sin\phi$$

$$- (3\, a_1^2 + 4\, a_2 t - 40\, a_2^2 - t^2/4) \cos\phi$$

$$- (3\, a_1^2 + 3\, a_2 t - 40\, a_2^2)\, \phi\sin\phi -$$

$$- (20\, a_1\, a_2 - a_1 t)\, \phi\cos\phi - 9\, a_1\, a_2\phi^2 \sin\phi$$

$$+ (a_1^2 + a_2 t - 20\, a_2^2)\phi^2 \cos\phi - 6\, a_2^2\phi^3 \sin\phi$$

$$\left. + 2\, a_1\, a_2\phi^3 \cos\phi + a_2^2\phi^4 \cos\right]_{\phi_i}^{\phi_{i+1}}.$$

Newton's method is used to determine ϕ_{i+1},

$$f(\phi_{i+1}) = \left[\left(\frac{r_1 + a_1}{2}\right) t\phi + \left(\frac{r_1 + a_1}{2}\right) a_1\phi^2 + \ldots\right]_{\phi_i}^{\phi_{i+1}}$$

$$- \frac{(R_1^2 - R_{i+1}^2)}{(t_i - t_{i+1})}\, t_o\,,$$

$$f'(\phi_{i+1}) = \{r_1 - a_1\, (\cos\phi_{i+1} + \phi_{i+1} \sin\phi_{i+1} - 1)$$

$$- a_2\, [2\phi_{i+1} \cos\phi_{i+1} + (\phi_{i+1}^2 - 2) \sin\phi_{i+1}],$$

$$- t/2 \sin\phi_{i+1}\}(a_1\phi_{i+1} + a_2\phi_{i+1}^2 + t/2),$$

equation cont.

$$(\phi_{i+1})_{n+1} = (\phi_{i+1})_n - \frac{f(\phi_{i+1})_n}{f'(\phi_{i+1})_n}, \tag{4.28}$$

where t and $(\phi_{i+1})_o$ are given by equations (4.26) and (4.27) respectively.

3. Exponential spiral curve

From the geometry of the exponential spiral curve, r" and ρ" are given by equations (3.16) and (3.15). Using these two equations and equation (4.23), the surface area of an element is given by the expression,

$$\Delta A = 2\pi \int_{\phi_i}^{\phi_{i+1}} \{r_1 - \frac{a_1 e^{a_2\phi}}{1 + a_2^2} (\sin\phi + a_2 \cos\phi) + a \sin\phi + \frac{a_1 a_2}{1 + a_2^2} - t/2 \sin\phi\}[a_1 (e^{a_2\phi} - 1) + t/2] \, d\phi .$$

By integrating this equation, and using equation (4.22), the volume constancy relation of the exponential spiral curve is,

$$\begin{aligned}(\frac{R_i^2 - R_{i+1}^2}{t_i + t_{i+1}}) \, t_o = \{&(-r_1 a - \frac{a_1^2 a_2}{1 + a_2^2} + r_1 \, t/2 + \frac{a_1 a_2 \, t/2}{1 + a_2^2})\phi \\ &+ (a_1^2 - a_1 t + t^2/4) \cos\phi + e^{a_2\phi}(r_1 \frac{a_1}{a_2} \\ &+ \frac{a_1^2}{1 + a_2^2}) + \frac{e^{a_2\phi}}{(1 + a_2^2)^2} (a_2 \sin\phi - \cos\phi) \\ &[a_1^2 (1 + a_2^2) + a_1^2 - a_1 \, t/2 \\ &- \frac{a_1 t}{2} (1 + a_2^2)] + \frac{a_1 a_2 e^{a_2\phi}}{(1 + a_2^2)^2} (\sin\phi + a_2 \cos\phi) \\ &(a_1 - t/2) - \frac{a_1^2 e^{a_2\phi}}{(1 + a_2^2)(1 + 4a_2^2)} [3a_2^2 \sin\phi \\ &+ (2a_2^2 - 1) \cos\phi]\}_{\phi_i}^{\phi_{i+1}} .\end{aligned}$$

Newton's method is used for approximating ϕ_{i+1},

$$f(\phi_{i+1}) = \{(- r_1 a - \frac{a_1^2 a_2}{1 + a_2^2} + r_1 t/2 + \frac{a_1 a_2 t/2}{1 + a_2^2})\phi + ..\}_{\phi_i}^{\phi_{i+1}} - \frac{(R_i^2 + R_{i+1}^2)}{(t_i + t_{i+1})} t_o ,$$

$$f'(\phi_{i+1}) = [r_1 - \frac{a_1 e^{a_2\phi}}{1 + a_2^2} (\sin\phi + a_2 \cos\phi) + a_1 \sin\phi + \frac{a_1 a_2}{1 + a_2^2} - t/2 \sin\phi] [a_1 (e^{a_2\phi} - 1) + t/2],$$

$$(\phi_{i+1})_{n+1} = (\phi_{i+1})_n - \frac{f(\phi_{i+1})_n}{f'(\phi_{i+1})_n} . \qquad (4.29)$$

where t and $(\phi_{i+1})_o$ are given by equations (4.26) and (4.27) respectively.

4. Conical die

The deformed element over the die has the shape of a conical frustum of a cone angle equal to ϕ_c. It can be shown using equation (4.22) that the volume constancy relation of a conical die may be approximated as

$$r_{i+1} = [r_i^2 + 2(\frac{R_{i+1}^2 - R_i^2}{t_i + t_{i+1}}) t_o \sin (\phi_c/2)]^{\frac{1}{2}} .$$

From the above expression, the following relationship between ε_θ and ε_t can be obtained:

$$\varepsilon_{\theta_{i+1}} = \tfrac{1}{2} \ln [\frac{r_i^2}{R_{i+1}^2} + 2 (1 - \frac{R_i^2}{R_{i+1}^2}) \frac{\sin (\phi_c/2)}{e^{\varepsilon_{t_i}} + e^{\varepsilon_{t_{i+1}}}}] . \qquad (4.30)$$

(b) The volume constancy relation when the material is stretched between die and punch:

The idea of approximating the shape of the deformed element in this zone to the frustum of a cone was adopted by Woo [15] in his work on tube bulging under internal pressure and axial force. The derived volume constancy relation proved to be simple and effective. By applying this method of approximation and using equation (4.22), the volume constancy relation, when the material is stretched between die and punch, may be written as,

$$r_{i+1} = \left[r_i^2 + 2\left(\frac{R_{i+1}^2 - R_i^2}{t_i + t_{i+1}}\right) t_o \cos\left(\frac{\phi_i + \phi_{i+1}}{2}\right)\right]^{\frac{1}{2}} \qquad (4.31)$$

or, in terms of ε_θ and ε_t as

$$\varepsilon_{\theta_{i+1}} = \tfrac{1}{2} \ell n \left[\frac{r_i^2}{R_{i+1}^2} + 2\left(1 - \frac{R_i^2}{R_{i+1}^2}\right)\right]\left[\frac{\cos\left(\frac{\phi_i + \phi_{i+1}}{2}\right)}{e^{\varepsilon_{t_i}} + e^{\varepsilon_{t_{i+1}}}}\right],$$

where t_{i+1}, $\varepsilon_{t_{i+1}}$ and ϕ_{i+1} are to be assumed before it becomes possible to deduce r_{i+1} and $\varepsilon_{\theta_{i+1}}$.

(c) The volume constancy relation when the material is stretched over the punch profile radius:

The volume constancy relation for this zone is derived in a similar way to that of the die zone, see Woo [8].

With reference to Figure (4.5), the current radius r' is given by,

$$r' = r_d + (\rho_p + t/2) \sin\phi . \qquad (4.32)$$

The surface area of an element at the middle section, may be approximated using equation (4.32) from the following integration:

$$\Delta A = \int_{\phi_i}^{\phi_{i+1}} 2\pi \, [r_d + (\rho_p + t/2) \sin\phi] \, (\rho_p + t/2) \, d\phi .$$

By integrating this equation and using equation (4.22), the volume constancy relation over the punch profile radius can be shown as

$$\left(\frac{R_i^2 - R_{i+1}^2}{t_i + t_{i+1}}\right) t_o = [r_d \, (\rho_p + t/2)\phi - (\rho_p + t/2)^2 \cos\phi]_{\phi_i}^{\phi_{i+1}} .$$

To determine ϕ_{i+1} from the above equation, Newton's method is used as follows:

$$f(\phi_{i+1}) = [r_d \, (\rho_p + t/2)\phi - (\rho_p + t/2)^2 \cos\phi]_{\phi_i}^{\phi_{i+1}} - \left(\frac{R_i^2 - R_{i+1}^2}{t_i + t_{i+1}}\right) t_o ,$$

$$f'(\phi_{i+1}) = [r_d + (\rho_p + t/2) \sin\phi_{i+1}] \, (\rho_p + t/2),$$

$$(\phi_{i+1})_{n+1} = (\phi_{i+1})_n - \frac{f(\phi_{i+1})_n}{f'(\phi_{i+1})_n} , \qquad (4.32$$

where $t = \dfrac{t_i + t_{i+1}}{2}$.

The first value in the approximation, $(\phi_{i+1})_o$, may be found by considering the volume constancy of an element and assuming that $r_{i+1} = r_i$ from the following equation:

$$\phi_{i+1} = \phi_i - \frac{t_o \, (R_i^2 - R_{i+1}^2)}{(t_i + t_{i+1})[\rho_p + 0.25 \, (t_i + t_{i+1})] \, r_i} . \qquad (4.33)$$

4.6 Equilibrium Equations

Equilibrium equations are used in the present theoretical analysis of the deep drawing problem to determine the value of the unit-tangential force, $(\sigma_\phi t)'$, to be compared with the unit tangential force, $(\sigma_\phi t)$, which is found from the plasticity relations, and to be used as a new value in the process of successive approximations of t.

At the tool-material interface the frictional force is assumed, on the basis of ordinary Coulomb friction, to be proportional to the normal force whenever relative sliding occurs.

(a) The equilibrium equation when the material is drawn over the die profile:

From the condition of static equilibrium of forces in the directions parallel and perpendicular to σ_ϕ, two equations can be obtained. By eliminating N from these equations, an expression for $(\sigma_\phi t)$ can be found.

1. The equilibrium equation when a convex-type die is used:

With reference to Figure (4.2), this equation was shown by Woo [10] as

$$(\sigma_\phi t)'_{i+1} = (\sigma_\phi t)_i - \int_{\phi_i}^{\phi_{i+1}} [\sigma_\theta t\ (\cos\phi + \mu_d \sin\phi) - \sigma_\phi t \cos\phi] \frac{(\rho + t/2)}{r}\, d\phi + \int_{\phi_i}^{\phi_{i+1}} \mu_d\, \sigma_\phi t\, d\phi \,.$$

The above equation can be numerically integrated using the trapezoidal rule [17], thus

$$(\sigma_\phi t)'_{i+1} = \frac{(\sigma_\phi t)_i [2 + (\phi_{i+1} - \phi_i)(B_i + \mu_d)] - (\phi_{i+1} - \phi_i)(A_i + A_{i+1})}{2 - (\phi_{i+1} - \phi_i)(B_{i+1} + \mu_d)}, \tag{4.34}$$

where

$$A = \sigma_\phi t \ (\cos\phi + \mu_d \sin\phi) \ \frac{(\rho + t/2)}{r},$$

$$B = (\frac{\rho + t/2}{r}) \cos\phi \cdot$$

2. The equilibrium equation when a conical die is used:

With reference to Figure (4.6), it can be shown that the equilibrium equation is,

$$(\sigma_\phi t)'_{i+1} = (\sigma_\phi t)_i + \int_{r_i}^{r_{i+1}} \{\sigma_\theta t \ [1 + \mu_d \ \text{cotg} \ (\phi_c/2)] - \phi_\phi t\} \ \frac{dr}{r} \cdot \tag{4.35}$$

By numerical integration, using the trapezoidal rule, we get,

$$(\sigma_\phi t)'_{i+1} = \frac{2 \ (\sigma_\phi t)_i + \{A[(\frac{\sigma_\theta t}{r})_i + (\frac{\sigma_\theta t}{r})_{i+1}] - (\frac{\sigma_\phi t}{r})_i\} \ (r_{i+1} - r_i)}{2 + (r_{i+1} - r_i)/r_{i+1}}, \tag{4.36}$$

where

$$A = 1 + \mu_d \ \text{cotg} \ (\phi_c/2) \cdot$$

(b) The equilibrium equation when the material is stretched between die and punch:

Since the deformation process in this zone is not bounded by the tool surface as in the previous case. The

values of t and ϕ have to be assumed in every step and two equilibrium equations are required.

1. Equilibrium equation to determine $(\sigma_\phi t)'$.

Referring to Figure (4.7), the equilibrium equation is obtained by putting $\mu_d = 0$ in equation (4.35), hence

$$(\sigma_\phi t)'_{i+1} = (\sigma_\phi t)_i + \int_{r_i}^{r_{i+1}} \frac{(\sigma_\theta - \sigma_\phi)}{r}\, dr.$$

By numerical integration, using the trapezoidal rule, we get,

$$(\sigma_\phi t)'_{i+1} = \frac{2(\sigma_\phi t)_i + [(\frac{\sigma_\theta t - \sigma_\phi t}{r})_i + (\frac{\sigma_\theta t}{r})_{i+1}](r_{i+1} - r_i)}{2 + (r_{i+1} - r_i)/r_{i+1}}. \qquad (4.37)$$

2. Equilibrium equation to determine ϕ'.

The equilibrium of forces in the vertical direction gives,

$$P = 2\pi\, r_i (\sigma_\phi t)_i \sin\phi_i = 2\pi\, r_{i+1}\, (\sigma_\phi t)_{i+1} \sin\phi_{i+1}$$

hence,

$$\phi'_{i+1} = \sin^{-1} [\frac{P}{2\pi\, r_{i+1}\, (\sigma_\phi t)_{i+1}}], \qquad (4.38)$$

where P is the punch load.

(c) The equilibrium equation when the material is stretched over the punch profile radius.

Referring to Figure (4.8), this equation can be obtained in a similar way to that mentioned above for the die. Woo [8] showed that this equation has the following form:

$$(\sigma_\phi t)'_{i+1} = (\sigma_\phi t)_i - \int_{\phi_i}^{\phi_{i+1}} [\sigma_\theta t\ (\cos\phi + \mu_p \sin\phi) - \sigma_\phi t \cos\phi] \frac{(\rho_p + t/2)}{r_d + (\rho_p + t/2)\sin\phi}\, d\phi + \int_{\phi_i}^{\phi_{i+1}} \mu_p\, \sigma_\phi t\, d\phi .$$

The above equation may be numerically integrated using the trapezoidal rule,

$$(\sigma_\phi t)'_{i+1} = \frac{(\sigma_\phi t)_i [2 + (\phi_{i+1} - \phi_i)(B_i + \mu_p)] - (\phi_{i+1} - \phi_i)(A_i + A_{i+1})}{2 - (\phi_{i+1} - \phi_i)(B_{i+1} + \mu_p)}, \qquad (4.39)$$

where

$$A = \sigma_\theta t\ (\cos\phi + \rho_p \sin\phi)\left(\frac{\rho_p + t/2}{r}\right),$$

$$B = \left(\frac{\rho_p + t/2}{r}\right).$$

4.7 Punch Stroke and Cup Height

Figure (4.9) shows the deep drawing operation through a convex-type die without the use of a blank-holder, in two positions. Position I shows the beginning of the drawing operation and position II shows an intermediate stage of

drawing corresponding to a punch movement S_j and cup height h_j.

The current cup height, which corresponds to a certain stage of drawing, j, may be approximated using the following equation:

$$h_j = [y''(\phi)]_{\phi_a}^{\phi_b} + \sum_{i=i_b}^{i=i_c} (r''_i - r''_{i+1}) \tan\left(\frac{\phi_i + \phi_{i+1}}{2}\right) + \rho_p - (\rho_p + t_c)\cos\phi_c + t_d , \qquad (4.40)$$

where $y''(\phi)$ depends on the type of the die curve to be considered. For example, $y''(\phi)$ is given by equation (3.8) when the second order spiral is considered as the die curve.

The stroke which corresponds to this stage of drawing, j, may be approximated in a similar way from the equation,

$$S_j = t_o + [y''(\phi)]_{\phi_o}^{\phi_b} + \sum_{i=i_b}^{i=i_c} (r''_i - r''_{i+1}) \tan\left(\frac{\phi_i + \phi_{i+1}}{2}\right) + \rho_p - (\rho_p + t_c)\cos\phi_c . \qquad (4.41)$$

4.8 Boundary Conditions

The boundary conditions in this theoretical analysis are divided into two categories, edge boundaries and intermediate boundaries.

(a) Edge Boundaries

Edge boundaries describe the conditions of the partly draw cup at the cup rim radius and at the flat base of the cup.

1. Edge boundary condition at the rim radius, r_a, of the partly drawn cup, can be obtained from the fact that the tangential stress at this radius is equal to zero, hence

$$(\sigma_\phi)_a = 0 \cdot \tag{4.42}$$

By substituting this value into equation (4.5), it can be shown that

$$(d\varepsilon_t)_a = - \frac{(d\varepsilon_\theta)_a}{1 + \gamma} \cdot$$

Since the ratio of $d\varepsilon_t$ to $d\varepsilon_\theta$ remains constant, as it is shown in the above equation, therefore, total strains can be used,

$$(\varepsilon_t)_a = - \frac{(\varepsilon_\theta)_a}{1 + \gamma}$$

$$\text{or,} \quad t_a = t_o \left(\frac{R_1}{r_a}\right)^{\frac{1}{1+\gamma}} \cdot \tag{4.43}$$

It can be shown using the above equation and the second degree spiral curve as an example that it is possible to adjust the inner rim radius, r_a', to a predetermined value required in the theoretical analysis as follows:

From the geometry of the second degree spiral curve,

$$r_a'' = r_1 - a_1 (\cos\phi + \phi\sin\phi - 1) - a_2[2\phi\cos\phi + (\phi^2 - 2) \sin\phi] . \tag{4.44}$$

The current radius, r_a, is given by

$$r_a = r_a'' - \frac{t_a}{2} \sin\phi \cdot$$

By substituting t_a from equation (4.43), we get

$$r_a = r''_a - \frac{t_o}{2} \left(\frac{R_1}{r_a}\right)^{\frac{1}{1+\gamma}} \sin\phi \, .$$

It can be seen from this equation that for a certain value of ϕ the outer radius, r''_a, is determined from equation (4.44), and r_a can be calculated using Newton's method of successive approximation according to the following equations:

$$f(r_a) = - r_a - r''_a - \frac{t_o}{2} \left(\frac{R_1}{r_a}\right)^{\frac{1}{1+\gamma}} \sin\phi \, ,$$

$$f'(r_a) = - 1 + \frac{t_o}{2\,(1+\gamma)} R_1^{\frac{1}{1+\gamma}} r_a^{-\left(\frac{2+\gamma}{1+\gamma}\right)} \, , \qquad (4.45)$$

$$(r_a)_{n+1} = (r_a)_n - \frac{f(r_a)_n}{f'(r_a)_n} \, .$$

t_a can be found from equation (4.43), and the inner rim radius, r'_a, is given by

$$r'_a = r''_a - t_a \sin\phi \, . \qquad (4.46)$$

It is clear from the above procedure that it is possible by adjusting ϕ in a particular manner, to set r'_a to a predetermined value within the required accuracy. The way in which, ϕ, is adjusted will be explained in the next section (4.9).

It is obvious that setting r''_a to a predetermined value would be easier to perform when required.

2. Edge boundary condition at the flat base of the partly drawn cup. Due to the balanced biaxial stress condition in the punch flat base zone,

$$\sigma_\phi = \sigma_\theta \cdot \tag{4.47}$$

By substituting the above equation into equation (4.6), we get

$$d\varepsilon_t = -2\, d\varepsilon_\theta \cdot \tag{4.48}$$

The first edge boundary condition is automatically verified during computation, while the above condition is to be checked. Computations start from the rim radius of the partly drawn cup. The theoretical analysis of any stage of drawing is considered to be valid only when the above boundary conditions are satisfied.

(b) Intermediate boundaries

Intermediate boundaries represent the conditions at the shared sections between different zones of the partly drawn cup. At each section the stresses and strains should have the same values at either side of the section.

1. Intermediate boundary condition at the die contact radius, r_b, between the drawing zone and the stretching zone. Since r_b is unknown, therefore, it will be given a rough estimate and then adjusted until the edge boundary conditions are satisfied.

2. Intermediate boundary condition at the punch profile contact radius, r_c, between the stretching zones 2 and 3: from the punch geometry, this condition is satisfied when

$$r \simeq r_d + (\rho_p + t/2) \sin\phi \ . \qquad (4.49)$$

This equation can be used to check the intermediate boundary condition at r_c when computations are carried out from the outer zone towards the inner zone. If the process of computation is reversed then r_c is assumed and the boundary condition at r_b is satisfied when $r \simeq r'' - t/2 \sin\phi$, where r'' is a function of the die curve under consideration.

3. Intermediate boundary condition at the punch flat base radius, r_d, between stretching zone 3 and punch flat base zone 4. This boundary condition is satisfied when the punch profile contact angle approaches zero, thus

$$\phi \simeq 0 \qquad (4.50)$$

4.9 The Computer Programme

The present numerical solution of the deep drawing problem through a convex type die, without the use of a blank-holder, is based on the general solution suggested by Woo [7] for the analysis of axisymmetric forming of sheet metal and hydrostatic bulging process and on another work by Woo [10] for the analysis of deep drawing over a tractrix die.

The solution is formulated as follows:

The initial conditions of the material are represented by the blank which is divided into small elementary rings of known initial radii and constant thickness.

The current conditions of the partly drawn cup at any stage of drawing, such as stresses, strains and punch load, can be determined by the application of the plasticity theories together with the work-hardening characteristic of the material. Equilibrium equations in one or two directions are used in the solution depending on the number of unknowns. The volume constancy relation is also employed in the solution to determine the relation between ε_t and ε_θ. The computations for a certain stage of drawing start at the rim radius of the partly drawn cup. The die contact radius, r_b, is assumed, and computations are then carried out from point to point towards the centre of the partly drawn cup. The die contact radius, r_b, is changed in a logical order, as will be described later, until the boundary condition at the punch flat base radius is satisfied. As an illustration of this general solution, the main procedure for deep drawing through a second degree-spiral type die is given below.

The procedures for other convex type dies can be obtained by conveniently replacing the relevant equations in the given solution with those of the die type required. These replacements are to be done in the die contact zone only; other zones remain unchanged. All necessary equations

for other common convex type dies have been given in previous sections.

The procedure of the numerical solution for a second degree-spiral type die may be outlined as follows:

(a) The die contact zone:

Let us consider a certain stage of drawing, j, corresponding to a certain inner rim radius of the partly drawn cup.

1. Rim radius:

Computation starts at this radius, r_a, which is considered as the step, i = 1. In this particular stage, j, the rim radius, r_a, which corresponds to a certain value of the die contact angle, ϕ_a, is found from the set of equations (4.45), using Newton's method, and t_a is given by equation (4.43). The method of adjusting r''_a to a predetermined value r''_{ap} is as follows: ϕ_a is assumed equal to that in the previous stage, and is then increased by a suitable increment, Δ, until r''_a is less than, r''_{ap}. Then the increment is halved and ϕ_a is decreased by $\Delta/2$ until r''_a is greater than r''_{ap}. After that ϕ_a is increased or decreased by ($\Delta/4$, $\Delta/8$, $\Delta/16$ ..) depending on whether r''_a is smaller or greater than r''_{ap}. The cycle is repeated until, $r''_a \simeq r''_{ap}$, within a specified accuracy. The values of thickness and circumferential strains are deduced from the following equations:

$$\varepsilon_{t_{i,j}} = \ell n\ (t_{i,j}/t_o)\ , \tag{4.51}$$

$$\varepsilon_{\theta_{i,j}} = \ell n\ (r_{i,j}/R_{i,j})\ . \tag{4.52}$$

If finite strain increments are assumed, then, the strain increments are

$$d\varepsilon_{t_{i,j}} = \varepsilon_{t_{i,j}} - \varepsilon_{t_{i,j-1}} \tag{4.53}$$

and $$d\varepsilon_{\theta_{i,j}} = \varepsilon_{\theta_{i,j}} - \varepsilon_{\theta_{i,j-1}}\ . \tag{4.54}$$

The equivalent strain increment, $d\bar{\varepsilon}_{i,j}$, is computed from the plasticity relation (4.4), and the equivalent strain is given by

$$\bar{\varepsilon}_{i,j} = d\bar{\varepsilon}_{i,j} + \bar{\varepsilon}_{i,j-1}\ . \tag{4.55}$$

The equivalent stress, $\bar{\sigma}$, is deduced from the work-hardening characteristic of the material, equation (4.8).

From the edge boundary conditions at the rim radius, the tangential stress, σ_ϕ, is equal to zero, and the circumferential stress, σ_θ, is deduced form the plasticity relation (4.6).

At this point, control is tranferred to the next part of the programme.

2. Other steps in the die contact zone:

In this part of the programme, computations start with the second step, i = 2, in the die contact zone. As a first

approximation, the value of t is assumed to be equal to that in the previous step, hence ε_t and $d\varepsilon_t$ can be calculated. The value of the die contact angle is given its first approximation from equation (4.27), and then the value of ϕ which corresponds to the assumed value of t is computed from the set of equations (4.28) using Newtons's method. The current radius, r, is determined from the following equation:

$$r = r'' - t/2 \sin\phi ,$$

where r'' in this case is given by equation (3.7).

The values of ε_θ, $d\varepsilon$, $d\varepsilon$, $\bar{\varepsilon}$, $\bar{\sigma}$ and σ_θ are computed from the same expressions given in the previous step, and σ_ϕ is determined from equation (4.5). Hence the plasticity relation-value of the unit-tangential force, $(\sigma_\phi t)$, can be found. The equilibrium equation-value of the unit-tangential force, $(\sigma_\phi t)'$, is calculated from equation (4.34). The two values of the unit-tangential force are compared using the following inequality:

$$\left|\frac{(\sigma_\phi t)}{(\sigma_\phi t)'} - 1\right| \leq \text{Accuracy} . \qquad (4.56)$$

If the above inequality is correct, this means that the assumed value of t is correct and the control is tranferred to the next step in the die contact zone. If the inequality is not satisfied, a new value of the thickness, t', is assumed from equation (4.7), and the procedure of this step is repeated. If the value of t' during the process of

successive approximation reaches a very small value, then necking is assumed and the control is tranferred to part (d) in the programme.

Computations are carried out for the remaining steps in the die contact zone,in the same way as is described above for step, i = 2, until the die contact radius, r_b, is reached. After that, the control is transferred to the next zone.

(b) The stretching zone between die and punch:

In the first step of this zone, both ϕ and t are given the same values of ϕ and t in the previous step as a first approximation. The current radius, r, is found from equation (4.31), hence the values of ε_t, $d\varepsilon_t$, ε_θ, $d\varepsilon_\theta$, $d\bar{\varepsilon}$, $\bar{\varepsilon}$, $\bar{\sigma}$, σ_θ, σ_ϕ and $(\sigma_\phi t)$ are computed in the same way as described above for step, i = 2, of the die contact zone. The value of $(\sigma_\phi t)'$ is determined from equation (4.37). The two values of the unit-tangential force are compared in the same way as described earlier.

When t is found to be correct, then ϕ' is determined from equation (4.38), and the two values of the angle are compared using the following inequality,

$$\left|\left(\frac{\phi}{\phi'}\right) - 1\right| \leq \text{Accuracy} . \qquad (4.57)$$

When the above inequality is satisfied, it means that the assumed value of ϕ is correct, and the control is traferred to the next step in the stretching zone between die and punch.

If the inequality is not satisfied, a new value of the angle, ϕ, may be assumed from the following equation

$$\phi' = \frac{\phi + \phi'}{2} \tag{4.58}$$

and the procedure of this step is repeated.

Computations are carried out for the following steps in this zone in the same way described above, until the condition given by the following inequality is reached

$$r < r_d + (\rho_p + t/2) \sin\phi , \tag{4.59}$$

which means that the control has just passed the intermediate boundary between this zone and the stretch forming zone over the punch profile radius. The position of the boundary is checked by the following inequality:

$$\left| \left[\frac{r_d + (\rho_p + t/2) \sin\phi}{r} \right] - 1 \right| \leq \text{Accuracy} .$$

If the above inequality is found to be valid, then the current radius, r, is considered as the punch profile contact radius, r_c, and control is transferred to the next zone. If the inequality is not valid, then the initial radius, R, which corresponds to this step, is increased by adding an increment, Δl, equal to half the distance between this step and the step before, i.e. $\Delta l = \frac{R_i - R_{i-1}}{2}$. The procedure of computation for this step is repeated with the new value of R and the above inequality is checked. If it is not correct, then the increment, Δl, is halved in the sequence, $\Delta l/2$, $\Delta l/4$, $\Delta l/8$ ... The manner in which the resulting

increment is added or substracted from R depends on the sign of the inequality. When the above inequality is satisfied, the control is transferred to the next zone.

(c) The stretch-forming zone over the punch profile radius.

In the first step of this zone t is assumed and the value of the punch contact angle is given its first approximation from equation (4.33), then the value of ϕ which corresponds to the assumed value of t is found from the set of equations (4.32) using Newton's method. The current radius, r, is determined from the following equation:

$$r = r_d + (\rho_p + t/2) \sin\phi .$$

Hence the values of ε_t, $d\varepsilon_t$, ε_θ, $d\varepsilon_\theta$, $d\bar{\varepsilon}$, $\bar{\varepsilon}$, $\bar{\sigma}$, σ_θ, σ_ϕ and $(\sigma_\phi t)$ are computed from the same equations used in step, i = 2, of the die contact zone. The value of $(\sigma_\phi t)'$ is determined from equation (4.39), and the two values of the unit tangential force are compared in the same way described for step, i = 2, at the die contact zone.

Computations for this zone are carried out from step to step following the same procedure for the previous step until the condition given by the following inequality is reached,

$$\phi < 0 .$$

Which means that computations has gone beyond the intermediate boundary between this zone and the punch flat base zone. The

accuracy of this boundary is checked using the following inequality:

$$| \phi | \leq \text{Accuracy}.$$

The procedure of adjusting the initial radius, R, which corresponds to this step, is similar to that given in the previous zone for finding the punch profile contact radius, r_c.

As the punch profile contact angle approaches zero, the punch flat base zone is reached. Since the stress and strain conditions in this zone are uniform, therefore, no computations need to be carried out for this zone and control is transferred to the next part of the programme.

(d) Boundary condition at the flat base.

At the flat base, ε_t must be equal to $- 2\varepsilon_\theta$.

The following observations were made during the initial testing of the programme:

1. $\varepsilon_t > - 2 \varepsilon_\theta$, when the assumed die contact radius, r_b, is less than the actual one.
2. $\varepsilon_t < - 2 \varepsilon_\theta$, when r_b is greater than the actual die contact radius.
3. $\varepsilon_t \simeq -2 \varepsilon_\theta$, when r_b is approximately equal to the actual die contact radius.

This behaviour can be explained by considering a certain stage of drawing, when the assumed die contact radius is less than the actual one (case 1). As a result of that, the die contact zone with the material is larger and the punch load is higher than the actual value. Consequently, the material in the zones following the die contact radius undergoes extra thinning, and the thickness strain becomes more pronounced than the circumferential strain.

It was found very useful to apply this logical relation between the boundary conditions at the punch flat base contact radius and the die contact radius. The relation can be used to control the assumed die contact radius in order to obtain the correct boundary condition. If the adjustment was done manually, the computation would be very tedious, and the application of this solution would be very limited and impracticable.

For economical reasons, the adjustment of the die contact radius is performed in two modes. In the first mode a rough adjustment is made by shifting the step number, i, which corresponds to the assumed die contact radius, by adding one or subtracting one for as many times as required until the inequalities in 2 or 1 respectively are reversed. This means that the actual die contact radius lies somewhere between this step and the step before. Then the second mode of fine adjustment is applied in which a technique of halving the distance between two consecutive steps is used in the same way as is described previously for finding the punch profile contact radius. After each adjustment of the die contact radius,

the control is transferred back to the die contact zone. Since the steps before r_b are not affected by its adjustment, therefore, the control is transferred to the step, i, which corresponds to, r_b.

The assumed value of the die contact radius is considered correct when the following inequality is valid:

$$\left|\frac{2\varepsilon_\theta}{\varepsilon_t} + 1\right| \leq \text{Accuracy}.$$

However, it should be pointed out that in order to get a rigourously traced strain history, any change to be carried out in a certain initial radius of a particular stage of deformation must be preceded by doing a similar change in all previous stages starting with the first stage. At the same time the appropriate corrections in the values of strains should be made. These changes proved to be vital whenever incremental strains are used, especially in those stages near to the maximum punch load, when, the strain increments become very small. Also, care has to be taken so that after each unsuccessful adjustment of the die contact radius, every change carried out in previous stages must be recovered to its original value before the adjustment. Otherwise the initial element distribution will be severely disturbed, which may lead to inaccuracies or even failure of the program. Therefore, the programme is provided with separate memory locations, reserved for some of the variables, especially strains. These variables are stored in this separate memory after each successful stage, so that they keep the up-to-date values for future reference during computations.

The following equations are used to extrapolate the first approximate values of t and ϕ, as applicable:

$$t_{i,j} = 2\, t_{i-1,j} - t_{i-2,j}, \text{ when } i = 3$$

$$t_{i,j} = 3\, t_{i-1,j} - 3t_{i-2,j} + t_{i-3,j}, \text{ when } 3 < i < i_b \text{ and } i_c < i < i_d$$

$$\phi_{i,j} = \phi_{i-1,i} + (\phi_{i-1,j} - \phi_{i-2,j}) \left(\frac{R_{i,j} - R_{i-1,j}}{R_{i-1,j} - R_{i-2,j}}\right) \quad \text{when } i = i_c, \; i = i_d, \text{ and}$$

$$t_{i,j} = t_{i-1,j} + (t_{i-1,j} - t_{i-2,j}) \left(\frac{R_{i,j} - R_{i-1,j}}{R_{i-1,j} - R_{i-2,j}}\right) \quad i_b < i < i_c.$$

This programme is capable of analysing stresses, strains, punch load, etc., for a given case, up to the point of maximum punch load which is considered sufficient for the purpose of the present investigation.

Figure (4.10) shows a general flow chart of the programme.

CHAPTER 5

EXPERIMENTAL APPARATUS AND METHOD

5.1 Deep Drawing Test Rig

The deep drawing test rig used in the present work is an existing one used in the department for investigating the deep-drawing process without a blank-holder. Figure (5.1) shows a sectional view of the test rig. It can be seen that the tooling design is simple as a blank-holder is not required in the case of the deep-drawing through a convex type die. The test rig is designed so that it can accommodate different dies with the same outside diameter but different die geometry or different height. This is done by adjusting the height of the spacer under the die housing.

The drawing tests have been carried out using an Avery self indicating universal testing machine available in the department research laboratory. The maximum capacity of the machine is 50 tons. It has a load indicating unit consisting of four capacity charts and two load indicators,one is a live load pointer and the other is a maximum load pointer. Plate (5.1) shows a photographic view of the deep-drawing test rig in position on the universal testing machine.

5.2 Measurement of Punch Load/Reduction of Blank Diameter

Several measurements of punch load/reduction of blank diameter have to be taken at successive stages of drawing. For each measurement during the test, the punch was stopped

and the corresponding punch load was read from the load indicating unit at the point of the maximum load pointer. The corresponding rim diameter of the partly drawn cup was measured in four directions, corresponding to 0^{o}, $\pm 45^{o}$ and 90^{o} to the rolling direction, the average rim diameter was determined and the reduction of blank diameter was determined from the following equation,

$$\text{Reduction of blank diameter} = \frac{R_1 - r_a'}{R_1} .$$

The measurements for different stages were taken in the same way until the punch load reached its maximum and started to decrease.

5.3 Measurement of Circumferential and Thickness Strains

The initial conditions are represented by a grid of circles of 2.5 mm intervals and four lines passing through the circles centre, indicating the direction 0^{o}, $\pm 45^{o}$ and 90^{o} to the rolling direction. The grid was scribed lightly on the flat blank, see Plate (5.2). The initial diamters of these circles were measured in the four directions, using X-Y travelling microscope. The travelling microscope provides an accuracy of measurement better than 0.01 mm in both directions. The initial thickness was measured using a dial gauge (Figure (5.2)), at 8 points of 45 degree intervals, starting with 0^{o} which corresponds to the rolling direction. The dial gauge provides an accuracy of measurement better than 0.0025 mm. The current diamters of a

particular stage of drawing were measured at four directions using the travelling microscope. The current thickness at each circle was measured at 8 points, 45^{o} intervals, starting with the rolling direction. The dial guage arrangement described above was used. The average values of thickness and diameter were considered in the determination of the strain distribution.

5.4 Strain Ratio and Simple Tension Test Apparatus

Since there was no standard method or device which could be used to determine the strain ratio in simple tension, it was necessary to design a special device for this purpose.

The design criteria were adopted following recommendations by Atkinson [20] for accurate strain ratio determinations which include:

1. A sample large enough to accommodate variations in plastic anisotropy.
2. A large extension to minimize measurement errors and strain sensitive variations in anisotropic plasticity.
3. Precise measurement since the calculated strain ratio value is hypersensitive to small errors.
4. Co-ordination of measurements to compare accurately related strains.

The direct method of measuring the change in width and thickness was adopted for the following reasons:

1. Materials under investigation are of 1.6 and 2.5 mm nominal thickness and may be considered as relatively thick materials. Therefore the sensitivity to measurement error in thickness is less than those encountered in thin materials.

2. The variety of materials to be tested and hence the large number of tests to be carried out necessitate a quick method of measurement. The strain ratio measurement is only a small part of this investigation.

Plate (5.3) shows a general view of the strain ratio and simple tension test apparatus. The strain ratio and the stress/strain values are measured using the same specimen. The tensile specimen is gripped on a Hounsfield tensile testing machine. The changes which occur in the width and thickness directions of the specimen, under tensile loading, are detected by two displacement transducers(L.V.D.T.), while fixed on a specially designed attachment.

Figure (5.3) shows two sectional views of the transducer attachment. The tensile specimen is maintained in line contact with two reference pins 1 and 2 by means of spring loaded discs 3 and 4. Each disc is fitted around the transducer's stylus which slides freely inside a hole at the middle of the disc, for detecting the change in thickness or width. The transducers have the main specifications given in Table (5.1).

Table (5.1). The main specifications of the displacement transducers (L.V.D.T.)

	Thickness Transducer	Width Transducer
Rated stroke, mm	2.5	5.0
Sensitivity, mv/v/mm	88.7	75.2
Max. permitted error, % total stroke	0.1	0.3

The transducers are connected to a twin channel digital a.c. carrier amplifier with the following main specifications:

1. Linearity at constant temperature: 0.1% $\pm$ 1 digit.
2. Digital indicator reads up to $\pm$ 1999 digits.
3. Sensitivity: From 2.3 mv (maximum gain of 500) to 5V (minimum gain of 2) for 1000 digit on D.V.M.

The system was calibrated by removing the transducers from their attachment and applying a known displacement to each transducer individually. A dial gauge stand with standard block gauges of different sizes was used in the calibration. The gains given in Table (5.2) were adjusted on the amplifier.

Table (5.2). Adjusted values of amplifier gains

	Width Transducer (Channel A)	Thickness Transducer (Channel B)
Coarse gain value	5.0	5.0
Fine gain value	0.3255	0.7145

Input/output diagrams are given in Figure (5.4). The sensitivity of measurement is defined as output/input, hence

Width measurement sensitivity is, 0.5 digit/μm, and

Thickness measurement sensitivity is, 1 digit/μm

5.5 Balanced Biaxial Tension Test Apparatus and Method

Plate (5.4) shows a general view of the balanced biaxial test apparatus. An existing clamping die of 100 mm is used. The hydraulic oil pressure is obtained from a two-speed hand pump, which is capable of producing pressure from 0 to 675 bars. A hydraulic accumulator of 1.15 litre capacity and 340 bars maximum working pressure is fitted on the delivery line of the hand pump. The pressure is measured by a pressure measuring system which consists of a pressure transducer, and the twin channel carrier amplifier described earlier. The pressure transducer has the following main specifications:

1. Range: 0-270 bars.
2. Full range output: 1.521 mv/v.
3. Maximum input voltage: 30V.
4. Accuracy (linearity and hysteresis): ± 0.26%.

The pressure measuring system was calibrated on a dual range dead weight tester. The error of this tester when used at standard room temperature of 20°C does not exceed 0.03% of the pressure being measured.

The following gain values were adjusted on the amplifier (Channel A):

Coarse gain: 500

Fine gain: 1.195

The calibration curve of the pressure measuring system is shown in Figure (5.5) as a straight line. The sensitivity of measurement is 3 digits/bar.

The method of testing may be summarized as follows:

A circle of 25 mm and four lines, corresponding to 0°, ± 45° and 90° to the rolling direction were lightly scribed on the outer surface of the specimen. The four lines cross the centre of the circle which coincides with the clamping die centre. The specimen was clamped firmly on the die. In the first stage of the test, the pressure was gradually increased until a movement of 2.5 mm was approximately achieved at the centre point of the polar zone. This movement was detected by using an electrical circuit. The arrangement consists of the specimen, a vertical micrometer with its point end stylus, an electrical power supply (batteries) and an indicating lamp. The lamp was on when the micrometer stylus came into contact with the centre point of the polar zone. Once the lamp was on, pumping was stopped and the

pressure was slightly released to avoid creeping and the danger of bursting. The pressure value before releasing was recorded from the D.V.M. of the amplifier. The current radius „r" was measured using X-Z travelling micrometer placed over the bulging die as shown in Plate (5.4), along four lines corresponding to 0^{o}, $\pm 45^{o}$ and 90^{o} to the rolling direction. The accuracy of the travelling micrometer in the X-direction is better than 0.0025 mm. The current radius of curvature ρ_c" at the pole, was determined indirectly using a depth micrometer which has a span between its two legs of 25 mm, the current depth Δh" was measured at the four lines. The accuracy of the depth micrometer is better than 0.025 mm.

The average results of the current radius r" and the depth Δh" were considered for deducing the stress/strain curve. The following stages in the experiment were performed in the same way as is given above until bursting occurred.

CHAPTER 6

MECHANICAL PROPERTIES OF MATERIAL

6.1 General Description

For comprehensive study of deep-drawing through a convex type die without a blank-holder, four different materials were used in the present investigation. The materials are mild steel, stainless steel, aluminium and brass. Some general description of the materials is given in Table (6.1).

Table (6.1). General description of materials

Material	Nominal thickness mm
Mild steel	1.6
Stainless steel B.S. 304	1.6
99.5% pure, soft aluminium	1.6 2.5
½ hard brass	1.6

All materials were commercially supplied.

6.2 Strain Ratio Measurement

A standard tensile specimen of a relatively large size was selected for all sheet materials under consideration according to B.S.18, part 1, 1970 and part 3, 1971. The tensile specimen dimensions are given in Figure (6.1). The

specimens were cut to the required size on a milling machine using an existing special fixture. Care was taken to avoid scratches and overheating. The same specimen was used to determine the strain ratio and the stress/strain curve.

The changes in width and thickness were recorded with the corresponding load value. The test was stopped at the point when necking started to take place and the condition of the test was not uniaxial any more. Figures (6.2) to (6.13) show the width/thickness strain relationship for mild steel, soft aluminium, stainless steel, and brass respectively. In the case of mild steel and soft aluminium, three specimens were tested in each direction corresponding to 0^{o}, $\pm 45^{o}$ and 90^{o} to the rolling direction. In the case of stainless steel and brass, it was decided, due to material shortage, to do one test in each of the four directions for stainless steel and one test in each direction corresponding to 0^{o} and 90^{o} for brass which had shown a fair amount of rotational anisotropy in preliminary tests.

It can be seen from the width/thickness strain curves, that the strain relation can be very well approximated as a straight line which passes through the origin of co-ordinates. The slope of this line represents the strain ratio. A computer programme was used to fit the experimental points to a straight line which passes through the origin of co-ordinates, using the least square method. The resultant strain ratio values of different materials are given in Table (6.2).

Table (6.2). Values of strain ratio

Material	γ_{0°	γ_{45°	γ_{90°	γ_{-45°	γ_{AV}
Mild steel	2.061	1.619	2.363	1.403	1.862
Stainless steel	0.993	1.123	1.091	1.079	1.072
Soft aluminium 1.6 mm thick	0.618	0.750	0.635	0.664	0.667
Soft aluminium 2.5 mm thick	0.663	0.775	0.775	0.710	0.731
Brass	0.846	-	0.856	-	0.855

6.3 Simple Tension and Balanced Biaxial Tension Results and Their Correlation

To avoid any possible effect of the strain rate on the experimental results, the strain rate in both types of test was maintained approximately within the same low range values by observing the loading speed in simple tension and the speed of raising the pressure in biaxial tension. The simple tension results for mild steel, stainless steel, soft aluminium and brass are given in Figures (6.14) to (6.18) respectively. The anisotropic $\bar{\sigma}/\bar{\varepsilon}$ curves, of 0° and 90° to the rolling direction, were deduced using equations (4.12) and (4.13). In the case of balanced biaxial tension, three specimens of each material were tested, except stainless steel where one specimen was carefully tested due to material shortage.

A special computer programme was prepared for determining the stress/strain curve from the experimental data. The programme follows the theoretical procedure given in (4.4.2).

An investigation was made to study the difference between the suggested method which calculates $\bar{\sigma}$ and $\bar{\varepsilon}$ in relation to the stresses and strains in the middle-section of the specimen thickness and considers the pressure to be applied underneath the specimen, and the conventional method which calculates $\bar{\sigma}/\bar{\varepsilon}$ curve assuming that the material thickness is negligible. Typical results of this investigation are shown in Figure (6.19) and Figure (6.22). It can be seen that the suggested method gives lower stress/strain curve in general, the difference being under 5% for materials of 1.6 mm nominal thickness. This difference is increased to about 7.5% for soft aluminium of 2.5 mm nominal thickness. The results of the suggested method are used throughout the following investigation.

For the purpose of comparison, the biaxial test $\bar{\sigma}/\bar{\varepsilon}$ curves for different materials are included with the relevant simple tension results in Figures (6.14) to (6.18). It can be seen that when anisotropy is considered, there is a difference generally under 10% between the biaxial and simple tension $\bar{\sigma}/\bar{\varepsilon}$ curves. A difference slightly higher is observed in the case of mild steel at low strain values. The biaxial test curves fall below the simple tension curves at low strain values and the correlation is generally better at high

strain values. This may be attributed to underestimating the radius of curvature of the polar zone at the initial stages of bulging. When anisotropy is neglected, the correlation is poor especially in the case of mild steel which is highly anisotropic as indicated by its high average strain ratio. The correlation for stainless steel is approximately the same as before and the correlation for brass and soft aluminium* of 2.5 mm thickness is slightly better, in general, than the correlation when anisotropy is considered.

Since the balanced biaxial $\bar{\sigma}/\bar{\varepsilon}$ relationships for different materials are to be used in the theoretical analysis, they have been fitted to empirical equations as appropriate. The experimental and empirical curves of the materials are shown in Figures (6.19) to (6.23). It is clear that the strain ranges obtained from the biaxial tests are higher than those obtained from simple tension, from about 40% higher in the case of stainless steel to more than 250% higher in the case of mild steel. However, it should be mentioned that the biaxial tension results showed a very good degree of consistancy and repeatability. The experimental points have been omitted from the $\bar{\sigma}/\bar{\varepsilon}$ curves for clarity.

---

* Hill has proposed a new yield criterion, which might accomodate the results for balanced biaxial tension, and which is particularly applicable for those materials having γ-values less than unity, see Appendix (C).

CHAPTER 7

THEORETICAL RESULTS AND THEIR INTERPRETATIONS

The theoretical solution of the deep drawing problem through a convex type die using the computer programme described earlier was tested and verified for different die profiles including the tractrix, exponential spiral, second degree spiral and conical type dies. A complete list of the programme using a second degree spiral type die is given in Appendix (B). Comment statements are provided to explain the main steps in the programme and a typical stage input/output is also given to illustrate the data requirements and the results obtained. Mild steel and die profile 1 were used in this typical example. The programme is written in Fortran and it was run and tested using the University ICL 1906S computer.

The element width and the number of stages required in the solution were investigated. It was found that an element width less than 0.6 mm and number of stages more than six do not give any appreciable change in the results within the used accuracies. Therefore, an element width of 0.6 mm and six stages have been used to obtain the theoretical results with the exception of using an element width of 0.3 mm for the punch profile radius zone where the radius is small compared with the die profile. The accuracy used for elements and edge boundaries is of the order of 0.0001. Typical computation time using the above figures is between 250-300 seconds. Higher accuracies give more exact results of strains

and stresses in the punch profile zone, especially in the latter stages of drawing. The punch load remains practically unaffected.

In the cup drawing experiments, the die profile was lubricated using graphited grease while the punch was kept dry. Therefore, in the analysis the values of the coefficient of friction between the material and each of the punch and die profile were assumed with reference to the work by Swift [21]. The coefficient of friction for stainless steel is assumed to be similar to that of mild steel. The values of the coefficient of friction for different materials are given in Table (7.1).

It was noted that the theoretical punch load determined by assuming total strains in the theoretical analysis or according to the approximate boundary condition, $\varepsilon_\theta = 0$ at

Table (7.1). Values of coefficient of friction

Material	μ_d, on die profile	μ_p, on punch profile
Mild steel	0.06	0.13
Stainless steel	0.06	0.13
Aluminium	0.028	0.1
Brass	0.04	0.13

the punch radius, do not differ significantly from the result based on the more exact solution. Figure (7.1) gives a comparison of the punch load as determined by the three methods with mild steel and die profile 1.

7.1 Stress and Strain Distribution

Figures (7.2) to (7.5) show the strain and stress distribution for a typical case, using mild steel and die profile 1. The circumferential and thickness strain development is illustrated by showing the strain path of particular elements, the contact boundary on the die and the contact boundary on the punch. It can be seen from the thickness distribution curves that due to the thinning effect over the punch profile radius, one neck on either side of the punch profile zone has been initiated in the last two stages of drawing. It can also be seen from the stress distribution that the stress level at the neck near the flat base radius is higher. Great resistance to thinning is noticed for mild steel as indicated by the small thickness strains at the lower parts of the partly drawn cup, this is attributed to the high material anisotropy.

7.2 Effect of Friction Between Material and Die Profile

There was uncertainty regarding the values of the coefficient of friction assumed in the theoretical solution particularly in the case of stainless steel. Figures (7.6) and (7.7) demonstrate the effect of friction on the stress and strain distribution in a stage of drawing near to the

maximum punch load. Aluminium and die profile 1 are used in this example. The coefficient of friction between the material and the punch was kept constant. It can be seen that the increase in the thickness strain, when the coefficient of friction μ_d is increased from 0.028 to 0.1, is more pronounced than the increase in the circumferential strain. This is because the thickness strain is more sensitive to small changes in thickness, caused by the increase in friction and hence the punch load, than the circumferential strain which is mostly determined by the geometry of tooling. Accordingly, it was noted that the frictional conditions between the die profile and material have a small effect on the die contact radius.

Figures (7.8) and (7.9) illustrate the significant effect of the chosen value of μ_d on the theoretical punch load for different materials.

7.3 Effect of Punch Profile Radius

The importance of investigating the effect of punch profile radius arises from the fact that instability and fracture usually occur over the punch profile radius. Four values of the punch profile radius, 5, 10, 15 and 20 mm, were investigated. It was found that the maximum punch load does not change significantly with the change of the punch profile radius ρ_p. The more generous the ρ_p, the longer is the punch stroke and the more gradual is the punch load/stroke relation. The stress and strain distribution curves for a typical stage of drawing using aluminium and

die profile 1 are shown in Figures (7.10) and (7.11), where a comparison is also made between the results for values of punch profile radius of 5 and 20 mm. The strains, stresses and the die contact radius in the die zone remained practically unchanged, which explains the reason for the punch load being unaffected by the change of ρ_p. The present theory predicts that stresses and particularly strains in the punch profile radius zone increase with increase of the punch profile radius. This may be interpreted as instability and fracture are more likely to occur in a spherical headed punch than in a flat headed one. These results are not in agreement with the experimental evidence shown by Swift [22]. However, inaccuracies in predicting the strains and stresses over the punch profile head are inevitable in the present analysis because of neglecting the bending effect over the punch profile radius. Bending effect decreases with increase of the punch profile radius. It is expected that the present solution would give better results with a spherical headed punch rather than a flat headed one.

7.4 Optimum Die Design

An attempt is made here using the present theoretical solution, to show that for a given material, die lip diameter, die throat diameter and die curve, there is an optimum die height at which the load becomes approximately minimum and any further increase in the die height beyond a certain limit is not of any practical use.

Stainless steel with tractrix and exponential spiral curves are used in this investigation together with die heights of 60, 100, 140, 180 and 220 mm. The punch load/ blank reduction ratio relations are shown in Figure (7.12), and the maximum punch load versus the die height relations are shown in Figure (7.13). In the case of a tractrix type die, the maximum punch load is reduced by 37% when the die height is increased from 60-150 mm. Further increase in the die height over 150 mm has no effect on the maximum punch load. In the case of an exponential spiral type die, the maximum punch load is reduced by 59% when the die height is increased from 60-220 mm. It can be seen from the results that the tractrix curve has a better performance at die height between 60-120 mm while the exponential spiral has a better performance for die height exceeding 120 mm. Of course, the application of these results in the workshop depends mainly on the material deep drawability and the available stroke of the press to be used.

CHAPTER 8

EFFECT OF DIE GEOMETRY

One of the main objectives of the present work is to examine both experimentally and theoretically the effect of die geometry on the punch load and to suggest the required modification in die geometry to achieve the least punch load in a certain deep drawing operation.

Comprehensive deep-drawing tests were carried out using the universal testing machine and the deep drawing test rig described previously. The materials investigated include mild steel, stainless steel, soft aluminium and brass blanks of 120 mm diameter and 1.6 mm nominal thickness. Die profiles 1, 2 and 3 were used. In order to eliminate any material strain rate sensitivity, when comparing theoretical and experimental results, a drawing speed of 0.5×10^{-4} m/sec was maintained throughout the course of the tests. This speed was chosen to be comparable with those speeds of simple tension and balanced biaxial tension tests so that the resulting strain rates in different tests are approximately of the same order.

It was noted that the aluminium and brass blanks tended to wrinkle during drawing on the die profiles 2 and 3, hence results on die profile 1 only could be obtained. This difficulty did not arise when drawing mild steel and stainless steel blanks. Unfortunately, there was no sufficient stainless steel material for the tests to be carried out on die profile 3. Die profiles 2 and 3 showed some tendency of the

blank to slip during early stages of drawing near the steep die entrance. The problem was solved in the experiments by manually pressing the blank against the punch flat base.

8.1 Comparison of Theoretical and Experimental Strains*

As the investigation concerns primarily the effect of die profile on the drawing process, comparison of the theoretical and experimental strain distributions is made mainly for the drawing region as shown in Figures (8.1) to (8.6), although in the case of aluminium the comparison extends also to the punch region as shown in Figure (8.7). From the results it can be seen that the correlation in the drawing region is generally good for stainless steel, aluminium and brass. The agreement is less accurate in the second stage of drawing for brass. This may be attributed to a slight variation in the material properties of this particular specimen. For mild steel, the comparison is fairly close for the circumferential strain but significant difference exists for the thickness strain near the punch region particularly at latter stages of drawing. Regarding the punch profile region in the case of aluminium, the correlation is generally poor especially over the neck and in the latter stages of drawing. It is believed that this poor agreement is mostly due to neglecting the bending effect over the punch profile radius in the theoretical analysis.

---

* Some of the results obtained have appeared in an article in Int. J. Mech. Sci., see reference [23].

The experimental value of the die contact radius which represent the contact boundary between the partly drawn cup and the die profile was estimated from the marking left on the surface of the cup, as the zone in contact with the die has smooth surface finish. Comparison between the theoretical and experimental values of the die contact radius indicated good agreement as given in Table (8.1) where a typical example is presented using mild steel and die profile 1.

Table (8.1). Die contact radius

Stage	r_b, mm (Theoretical)	r_b, mm (Experimental)
1	44.4	45.7
2	37.8	38.5
3	32.5	33.2

It was noted that only a small change occurred in the die contact radius of a certain stage when different materials were drawn through the same die, this shows that the material work-hardening characteristic and the strain ratio have a minor effect on the die contact radius. It may be seen that the correlation between the theoretical and experimental strains at the rim of the partly drawn cup is excellent in all cases as shown in Figures (8.1) to (8.7). This suggests that the average strain ratio values determined in simple tension are quite accurate.

8.2 Theoretical and Experimental Punch Loads

Three blanks were drawn to determine the punch load/ reduction of blank diameter relation. Comparison between the theoretical and experimental punch loads for mild steel, when die profiles 1, 2 and 3 are used, indicates generally the same poor agreement as shown in Figure (7.8b). This may be due to the fact that the mild steel tested has high planar and normal anisotropy as indicated by the high values and variation of the strain ratio values as given in Table (6.2). However, when the stress/strain relation determined from simple tension test at zero degree to the rolling direction is used in the theory, the punch load is higher and the correlation is improved as shown in Figure (7.8a). For stainless steel and aluminium the comparison is better as shown in Figures (7.9) and (8.8) because the anisotropy of these two materials is nearer to the rotationally symmetric condition. A very good correlation is obtained, as shown in Figure (8.9), in the case of brass which is very close to the rotationally symmetric condition assumed in the theory.

8.3 Effect of Die Geometry on Punch Load

Figures (7.8b) and (7.9) show the effect of die geometry on the punch load for mild steel and stainless steel respectively. It can be seen that the maximum punch load is significantly reduced when die profile 1 is replaced by die profile 2. In the case of mild steel it is clear

that another reduction lower than before was obtained when die profile 2 is replaced by die profile 3.

Table (8.2) gives the reductions in the maximum punch load. It is shown that reductions of 35% and perhaps more may be achieved by using die profiles with higher radius of curvature. This offers a good advantage when drawing tough materials especially when high punch loads are involved. In spite of the difference between theory and experiment in determining the punch load, the reduction in maximum punch load predicted by theory shows generally a fair agreement with the reduction determined by experiment.

Table (8.2). Reduction in maximum punch load

Dies replacement order	Mild steel		Stainless steel	
	Theo.	Exp.	Theo.	Exp.
1 - 2	29%	25%	26%	21%
2 - 3	14%	13%	-	-
1 - 3	39%	35%	-	-

In an attempt to explain the reason behind this reduction in the punch load, the theoretical unit tangential force distribution for mild steel, when drawn through die profiles 1, 2 and 3, is shown in Figure (8.10) at a stage near the maximum punch load. The following observations were made for the same stage of drawing on the three die profiles.

1. From the theoretical and experimental results, the die contact radius is increased from die 1 to 3, hence the die contact zone between the material and the die profile is decreased . The difference between the die contact radii of the three dies decreases until near the point of maximum load when they become very close, but with decreased contact area from die 1 to 3.

2. The unit tangential force at the die contact radius is significantly reduced from die 1 to 3.

3. The die profile contact angle at the point of maximum load increases slightly, and is generally in the range 1.38 to 1.43 radians. Since the punch load is given by the equation:

$$P = 2\pi r\ (\sigma_{\phi} t)\ \sin\phi,$$

therefore, the reduction in the maximum punch load is mainly due to the reduction in the unit tangential force when different dies of higher radius of curvature and greater depth are used.

In an attempt to reduce the punch load for aluminium and to overcome its tendency to buckle, an exponential spiral type die (die profile 4) was designed with more flat entrance than die profiles 2 and 3. When aluminium blanks were drawn using the die profile 4, they tended to buckle again, but at later stages than before which indicated that an even flatter entrance is required. However, mild steel blanks were successfully drawn using this die. The punch load/reduction

in blank diameter relation is shown in Figure (8.11). By comparing the maximum punch load of this die with that of die profile 3, see Figure (7.8b), it is found that they are almost the same. It is expected that exponential spiral type dies may offer a good alternative to the experimental die profiles 2 and 3 for actual production application, since they give the same maximum punch load, and reduce the tendency of buckling and slipping of the blank near the die entrance and also they are relatively easier to design.

The author regrets that due to time limitations it was not possible to carry out more experiments on the effect of die geometry using exponential spiral and tractrix type dies.

CHAPTER 9

CONCLUSIONS

A numerical solution for the deep-drawing problem through a convex type die without the use of a blank-holder is formulated. The solution is general in nature and any suitable die profile curve may be analysed provided that its mathematical expression can be used to obtain a relationship between ε_θ and ε_t using the volume constancy condition. A computer programme is presented and the performance of deep drawing through different die types could be studied. The die types treated include tractrix, exponential spiral, second degree spiral and conical type dies. Computation time for a typical case of complete analysis is about 300 seconds. If only the punch load/stroke relation is to be predicted, total strains may be used in the numerical solution and the computation time is reduced by about 3 times. If the maximum punch load is the main interest, the approximate solution considering the drawing region only may be used and the computation time is reduced by about 10 times.

According to the theoretical investigations given in Chapter 7, the following conclusions may be drawn:

1. Increasing the coefficient of friction between the drawn material and die profile increases the punch load significantly.
2. The punch profile radius has no appreciable effect on the maximum punch load, but the punch stroke increases with increase of punch profile radius.

3. The maximum punch load is greatly reduced by increasing the tractrix die height (depth) and the radius of curvature of the die profile up to a certain limit. Heights beyond this limit give no appreciable reduction in the maximum punch load. Further reduction in the maximum punch load is possible by drawing through an exponential spiral type die of greater height. The tractrix is superior when relatively short die heights are to be used while the exponential spiral is superior when greater die heights may be used.
4. The present theoretical solution may be applied in optimum die design, for finding the optimum die height which gives the least drawing load.

From the theoretical and experimental results given in Chapter 8 the following conclusions may be made:

1. The correlation between the theoretical and experimental thickness and circumferential strain distribution in the drawing region is generally good when using different die geometries and materials.
2. The correlation is not satisfactory when comparing the theoretical and experimental thickness strain distribution in the punch region, especially over the punch profile radius. Only soft aluminium was used in the comparison. The discrepancy is mainly due to disregarding the bending effect over the punch profile radius.
3. The punch load/reduction of blank diameter relation for any die geometry may be very well predicated from the theory provided that the material anisotropic properties are nearly

rotationally symmetric in the plane of the sheet material, as assumed in the theory. The accuracy of prediction decreases with increase of the planar anisotropy of the material.

4. The die profile geometry has a great influence on deep drawing without a blank-holder and on the maximum punch load in particular. Significant reductions in the maximum punch load of 35% and more may be achieved by using die profiles of more depth and steepness with increased radius of curvature. Less unit-tangential force and die contact area are the most influencing factors behind the load reduction.

5. Using dies of steep entrence may cause buckling for some materials, at early stage of drawing. It seems therefore that for some materials, a die of flat entrance , such as the tractrix type die entrance , is necessary. Flat die entrance prevents the tendency of the blank to slip at the on-set of the drawing process.

6. The reduction in the maximum punch load predicted by the theory when using two different dies, is in reasonable agreement with the reduction determined by experiment. This suggests that the present theoretical solution may be reasonably used in optimum die design to find the theoretical die profile required for drawing a particular cup under minimum load requirements.

PART TWO

IRONING

OF CUPS

CHAPTER 10

EXPERIMENTAL APPARATUS AND METHOD

The testing machine used for carrying out the planned experimental investigation on ironing is the experimental bulge forming machine described by Woo [2], see section (20.1). The machine has a capacity of 250 kN and a working stroke of about 500 mm. The arrangement of the drawing and ironing dies is shown in Figure (10.1). In this arrangement the cup is first drawn from a flat blank and is followed by the ironing process.

Since the machine has no facilities for measuring the punch load and the punch travel, it was decided to provide the machine with a measuring system before carrying out the experiments.

10.1 Deep Drawing Tools

The deep drawing die is a tractrix type die designed empirically and fitted on the bulge forming machine. The die has the following main dimensions:

Die lip diameter = 172.72 mm,

Die throat diameter = 71.61 mm,

Die height = 115.57 mm.

The tractrix curve constant, a, is found from equation (3.4), hence

$a = 55.70$ mm.

The die curve is given by the polar equation

$$\rho = 55.70 \tan\phi .$$

The die profile is shown in Figure (10.1).

The punch diameter is 65.9 mm, and the punch profile radius is 10 mm.

The radial clearance between the punch and the die is

$$C_r = 2.86 \text{ mm} .$$

The maximum thickness of the cup at its rim when the cup approaches the die throat is calculated from equation (3.19) as

$$t_{max} = 4.32 \text{ mm} .$$

The maximum reduction of cup wall thickness in ironing is obtained from equation (3.25), and hence

$$\alpha_{max} = 33\% .$$

10.2 Ironing Dies

In order to get different reductions in ironing, it was found easier to use different die throat diameters rather than different punch diameters. Four ironing dies were selected from an existing set of dies designed previously for the bulge forming machine. All dies have the same ironing die semi-angle of 15^{o} which is in the range of ironing die semi-angle recommended by Knowles and Swift [12]

for general use. The dimensions of the four dies were chosen to be the same with the exception of the die throat diameter which has to be changed for getting different reductions in the cup wall thickness. The die shape and dimensions are shown in Figure (10.1), and the planned reductions of different dies are given in Table (10.1).

Table (10.1). Reductions in ironing

Ironing die no.	Die throat dia., mm	Max. reduction, per cent		Variation in reduction, per cent
		theo.	exp.	
1	69.19	42.6	41.1	3
2	68.86	48.3	47.8	1
3	68.68	51.5	50.9	1
4	68.4	56.4	56.6	-0.3

10.3 Measurement of Punch Load/Travel

It was intended to carry out an autographic measurement of the punch load/travel relation. The arrangement is shown in Figure (10.2). A load cell is used to detect the changes in the punch load and the displacement transducer is used to detect the punch travel. A special attachment for the load cell had to be designed, so that it could be fitted on the punch any time a punch load measurement is required. The designed attachment is shown in Figure (10.3). The load and displacement signals are transferred to a twin channel amplifier, and the amplified signals are taken to the X-Y plotter. Once the system is calibrated, an autographic

representation of the punch load/travel relation can be obtained.

The load cell used has the following principal specifications:

1. Capacity, 30 ton.
2. Sensitivity, 100 x 10^{-6}/TON (G.F. 200).
3. Non-linearity, 0.2% F.S.

The long stroke displacement transducer has the following principal specifications:

1. Rated stroke, 300 mm.
2. Sensitivity, 1.73 mv/v/mm.
3. Linearity, 0.3% of full stroke.

The twin channel A.C. carrier amplifier described in section (5.4) was used. The load cell was connected to channel B of the amplifier and calibrated on an universal testing machine. The calibration curve is shown in Figure (10.4) as a straight line,and hence the sensitivity of punch load measurement is

50 digits/ton.

The displacement transducer was connected to channel A of the amplifier and was calibrated to the nearest 0.5 mm using a long metal ruler. The following gains have been adjusted on the amplifier:

	Course Gain	Fine Gain
Load cell	500	6.215
Displacement transducer	2	3.250

The X-Y plotter was then connected and adjusted to obtain the required scales.

10.4 Test Procedure

Soft aluminium blanks of 172 mm diameter and 2.5 mm nominal thickness were carefully turned from the supplied discs of 215 mm diameter, using an existing fixture. The blanks were lubricated on one side only, the blank side facing the punch was kept dry. The lubrication process was performed by brushing a layer of colloidal-graphite in alcohol on one side of the flat blank and allowing it to dry. Graphited oil was then spread over the graphited side of the blank and the die profile surface just before the onset of the drawing/ironing operation. This procedure proved to be satisfactory for the purpose of the present work.

For each punch speed and reduction in the ironing process, two specimens were tested and an autographic plotting of the punch load/travel in deep drawing and ironing was obtained. The average speed of the punch was assessed by determining the total stroke of the punch and measuring the time taken, using a stop watch. A photographic view of the full apparatus used for carrying out the experiments is shown in Plate (10.1).

The hardness measurements were taken using a Vickers hardness testing machine with 5 kg load. A punch of a similar size to that of the cup internal diameter was inserted inside the cup and a V-block was used to stop the cup from rolling during measurement. The cup wall thickness was measured using the dial gauge arrangement described earlier in section (5.3). To measure the hardness and thickness distributions, three longitudinal lines at 120^{o} interval were marked on the outside surface of the cup and measurements were taken at 10 mm intervals along these lines starting from a point 20 mm from the cup base.

CHAPTER 11

EXPERIMENTAL RESULTS AND THEIR DISCUSSION

The material used in this investigation is soft aluminium sheets of 2.5 mm nominal thickness. The material strain ratio and its work-hardening characteristic have been determined in part one, see section (6.3). The average strain ratio of the material is 0.731 and its stress/strain characteristic is given in Figure (6.22).

11.1 Distribution of Thickness and Hardness Along and Across the Cup Walls

In the present experimental investigation of the ironing process, ironing takes place after deep drawing and the two processes are performed in one stroke of the punch. It follows as a result of the drawing process that the cup specimen to be ironed has a variable thickness along its walls due to thickening in the upper part and thinning in the lower part of the drawn cup.

Although some amount of ironing of about 33% maximum reduction occurred between the punch and the drawing die in the top part of the drawn cup, this ironing was not sufficient to make the cup walls fully cylindrical, as it is shown in Figure (11.1).

A photograph of the drawn cup and the ironed cups with different reductions is given in Plate (11.1). It can be seen that the ironed cups have got a brighter and smoother surface finish than the drawn cup on the left of the picture.

The number and type of ears showed that the supplied material has variable anisotropic properties. Three types of ears were observed in the tests: cups with four, six and eight ears. The lengths of the ironed cups are given in Table (11.1). One cup specimen was used for measuring both thickness and hardness distributions for reduction in the ironing process. The punch speed used in the tests was 6.7 mm/sec.

As shown in Figure (11.1), the distribution of the drawn cup wall thickness has two modes of variations, the first mode being at the lower part of the cup with a relatively small and consistant variations, the second mode being at the top part of the drawn cup with relatively larger and inconsistant variations. It should be noted that some amount of ironing occurred between the punch and the die in the top part of the cup during drawing. Accordingly, it is clear that the first mode of variation is due to the planar anisotropic properties of the blank material. The second mode is mostly caused by the superposition of the planar anisotropy variation and other variations due to one or more of the following factors; ovality of the die throat, misalignment between punch and die centre lines and stiffness of the tooling system.

The distributions of the cup wall thicknesses for different degrees of ironing using ironing dies 1, 2, 3 and 4 are shown in Figures (11.3), (11.5), (11.7) and (11.9). It can be seen that in all ironing dies, larger thickness

Table (11.1). Thickness and length of ironed cups

Ironing die. no.	Cup total length, mm	Radial clearance, mm	Wall thickness, mm	Variation of thickness %
1	148	1.64	1.71	4
2	164	1.48	1.52	3
3	177	1.39	1.43	3
4	204	1.25	1.26	1
Drawing die	96	2.86	2.91	2

variations in the top part of the ironed cup are possibly reproduced from the drawing stage. The distributions of the cup wall thickness in the lower part have generally the same amount of small variations reflected from the drawing stage.

From the results, it may be concluded that to improve the uniformity of the cup wall thickness, the following points should be observed.

1. Geometrical errors such as ovality have to be minimized.
2. Concentric alignment between punch and die.
3. Higher stiffness of the tooling system.

The average cup wall thickness distributions in the ironed cups are quite uniform along the cup as is shown in Figure (11.12). It was noted that the average wall thickness of the ironed cup was greater than the nominal radial

clearance between the punch and the die throat, see Table (11.1). This can only be explained in terms of elastic deformation under high radial pressure between die throat, material and punch during the ironing process. The same feature occurred in ironing between punch and deep drawing die in the upper part of the drawn cup. The thickness deviation is not consistent as shown in Table (11.1). This is possibly due to differences in material and heat treatment history between the ironing dies. This feature was first reported by Lowe and Swift [11].

For the drawn and ironed cup using ironing dies 1, 2, 3 and 4, the distributions of the hardness which have been measured at the same points of thickness measurements are shown in Figures (11.2), (11.4), (11.6), (11.8) and (11.10). It was observed that the hardness distribution is generally similar to that of the pattern of thickness distribution and the reduction in the cup wall thickness. The distributions of the average hardness are shown in Figure (11.11). The maximum hardness versus the maximum reduction in ironing is included in Figure (11.16). It can be seen that the hardness increases with the degree of ironing and the distribution curves become flat at higher reductions. This is analogous to the material work-hardening characteristic.

11.2 Effect of Punch Speed on Punch Load in Deep Drawing and Ironing

Three different punch speeds of averagely 6.7, 33 and 44 mm/sec were investigated. Higher speeds have not been attempted due to safety precautions when using the manual mode of operation. Two cups were tested for each speed and reduction of wall thickness, giving a total of 24 tests. A typical punch load/travel autographic output for continuous deep drawing and ironing is reproduced in Figure (11.13). It can be seen that this typical punch load/travel relation has three separate and consecutive humps. These humps correspond to deep drawing, ironing between punch and drawing die and the ironing stage respectively. The punch load/travel relation in drawing is similar to that shown in the previous experiments described in part one. The sharp and narrow hump of the punch load in ironing between the punch and the drawing die indicates that only the top part of the cup was ironed. The punch load in the ironing stage rises sharply at the start of the process due to the sudden application of a certain degree of ironing. It then increases gradually with increase of wall thickness reduction towards the top of cup until it reaches approximately a constant level with a little hump near the end. This constant load part of the curve corresponds to the fully ironed part at the top of the drawn cup which has approximately a constant thickness.

The effect of speed on the punch load in deep drawing is studied by considering the average of 8 test results. The average maximum loads for different speeds in the deep drawing stage are given in Table (11.2).

Table (11.2). Effect of speed in deep drawing

Punch speed, mm/sec.	Max. punch load in drawing, KN	Max. punch load in drawing die ironing, KN
6.7	35.7	42.4
33	35.9	41.8
44	35.9	40.6

The results indicate that the punch load in deep drawing remained practically unaffected by the increase in the punch speed within the present range. The situation for ironing between punch and drawing die is different. The punch load values showed a tendency to decrease as the punch speed was increased as indicated in Table (11.2). This was more evident when the reduction of wall thickness was higher, see Table (11.3).

Table (11.3). Effect of speed in ironing

Punch speed, mm/sec.	Max. punch load, KN			
	Die 1	Die 2	Die 3	Die 4
6.7	42.5	46.5	49.5	52.5
33	42.0	45.5	48.0	50.5
44	42.0	45.5	47.0	51.0

The approximately constant punch load in deep drawing may be understood as the material has a negligible sensitivity to strain rate within the present range of speed. The reason for the decrease in punch load with increase of punch speed in ironing is probably due to change in the frictional and lubricating conditions at the interface between material and ironing die, where the contact pressure is very much higher compared with the pressure involved in deep drawing. For identical cups, the contact area between material and ironing die depends on the die semi-angle and the reduction in the cup walls thickness. Since the die semi-angle is the same in the four ironing dies, the contact area A is a function of the reduction α. The relationship between A and α is derived from the geometry of the ironing zone as

$$A = \frac{\pi t_o^2}{\cos\phi_s} \left[2 \left(\frac{R_p}{t_o} + 1\right) \alpha - \alpha^2\right],$$

where ϕ_s is the ironing die semi-angle, t_o, the thickness of cup and R_p, the punch radius.

For relatively large values of (R_p/t_o) in the above equation, the relationship between A and α may be assumed proportional. The reduction in the ironing load with increase of speed is probably due to the fact that the lubricant is less likely to be squeezed out during ironing at high speed, and that the increase in the contact area between material and ironing die at higher reduction reduces further this possibility which is indicated by the

more significant reductions in the punch load at higher reductions. It can also be seen that the speed effect becomes less evident as the speed gets higher.

Although the reduction in the cup walls thickness in ironing between the punch and the deep drawing die is about 33%, the punch load is similar to that in ironing using ironing die 1 which gives a reduction of 41.2%. This is due to the small ironing angles near the throat of the drawing die. It may be recommended that the drawing die curve be terminated at a die profile angle of about 80^{o} so that the zone near the die throat may act as an ironing die of die semi-angle of about 10^{o}, thus insuring a minimum ironing load. This is more important if higher reductions are to be carried out. According to previous experience, it is unlikely that this termination would have any significant effect on the maximum punch load during drawing.

11.3 Effect of the Degree of Ironing on the Punch Load

Typical punch load/travel autographic measurement for different reductions in ironing using dies 1 to 4 respectively are reproduced in Figure (11.15). The maximum punch load values versus the maximum reduction in ironing is shown in Figure (11.16). The results for each punch speed gives a relation close to a straight line. It was found difficult to fit the experimental points to an exponential curve similar to the findings by Shawki [13] who used copper

in his experiments. Since the suggested exponential curve is very flat and close to a straight line, it seems that a high number of tests should be carried out to assess the shape of the relation correctly.

11.4 Prediction of the Punch Load/Travel in Deep Drawing from Theory

Since an accurate autographic measurement of the punch load/travel was made for deep drawing as well as ironing, it was thought that the prediction of this relation in the drawing part using the theoretical solution developed in Part One could be made. This would give an opportunity to examine the correlation between theory and experiment, when a cup of a relatively large size is drawn through an exact tractrix type die, as in the present case. The average strain ratio and the stress/strain relationship of the material have already been determined in Part One, see Chapter 6. The coefficients of friction between material and die and between material and punch are assumed to be the same as those assumed for soft aluminium of 1.6 mm thickness in the previous part thus,

$$\mu_d = 0.028, \quad \mu_p = 0.1 .$$

The theoretical and experimental results are compared in Figure (11.14).

It can be seen that good agreement exists between theory and experiment, and by comparing this result with

that given for aluminium of 1.6 mm thickness in Part One, see Figure (8.8), it is clear that the maximum load predicted in this case is slightly more accurate. The general correlation of the whole punch load/travel relation presented here is better than the punch load/reduction in blank diameter given previously in Figure (8.8). It may be said that because of its continuity, the autographic method of measurement is generally more accurate than the other method which involves measuring the punch load and the rim diameter of the partly drawn cup at certain stages of drawing, although the latter is necessary when strain comparison is to be made.

CHAPTER 12

CONCLUSIONS

According to the experimental results presented in Chapter 11 the following conclusions may be drawn:

1. The punch speed within the range tested has no significant effect on the maximum punch load in deep drawing.
2. The maximum punch load in ironing decreases slightly as the punch speed increases up to a speed of about 35-45 mm/sec. The reduction in maximum punch load is more significant with higher degrees of ironing.
3. According to conclusions 1 and 2, the punch speed and hence the process productivity may be increased with confidence to about 45 mm/sec or more without increase in the punch load.
4. The ironing load increases approximately in a linear manner as the reduction in the cup wall thickness increases.
5. Variations in the cup wall thickness in the ironed cup are caused by planar anisotropy of the cup material and the geometrical errors in tooling. These variations are reproduced in subsequent ironing. Rotational anisotropy in sheet metal and accuracy in tooling are necessary to reduce these variations and hence give more uniform cup wall thickness.
6. The hardness of the wall of the ironed cup increases with increase of reduction in the cup wall thickness in a

manner similar to the work-hardening characteristic of the material.

7. The average wall thickness of ironed cup is slightly greater than the nominal radial clearance between punch and die throat. This increase is mainly due to elastic deformation of die.

PART THREE

FREE
BULGE FORMING

CHAPTER 13

THEORETICAL ANALYSIS OF FREE HYDRAULIC BULGE FORMING OF CUPS

A theoretical analysis of free hydraulic bulge forming of cups under internal pressure and axial compressive force is presented. The analysis is based on a general solution suggested by Woo [7] for the analysis of axisymmetric forming of sheet metal and hydrostatic bulging processes. The present work is also related to two other works, Woo [15] and Woo and Lua [16], on tube bulging. The analysis is based on a numerical solution using the plasticity relations and the work-hardening characteristic of the cup material together with the equilibrium equations and the strain relationship according to the volume constancy condition. The material is assumed to be rigid plastic and anisotropy is taken into account in the analysis. Annealed cups are considered in the investigation and the deformation of the cup base is neglected.

13.1 Plasticity Relations

The material is deformed plastically under the effect of internal pressure p and axial compressive force F. The stresses induced in an element of the cup wall after deformation are shown in Figure (13.1). The stress σ_t in the present case is relatively small and may be neglected, and therefore, the stress condition is reduced to one of plane stress . Accordingly, when rotational anisotropy

about the Z-axis is assumed, the principal stresses σ_ϕ and σ_θ, the equivalent strain increment $d\bar{\varepsilon}$ and the new value of the thickness t' used in the successive approximation of t in the numerical solution, are determined from the same expressions as are used for deep drawing, see Section (4.3).

The stress/strain relationship is determined experimentally as will be described later. The following relationship is used as an empirical representation of the stress/strain curve:

$$\bar{\sigma} = A\bar{\varepsilon}^n , \qquad (13.1)$$

where A and n are constants.

It is known that this empirical relation fits well with soft aluminium.

13.2 Equilibrium Equations

The first equilibrium equation used in the analysis is to determine $(\sigma_\phi t)'$. The equation is similar to that given previously for stretch forming of material between the punch and the drawing die. It may be numerically integrated in the same way, see Section (4.6).

With reference to Figure (13.2), the second equilibrium equation for forces in the vertical direction is:

$$\pi P(r')^2 - F = 2\pi r\ (\sigma_\phi t)\ \sin\phi . \qquad (13.2)$$

Depending on the values of P and F, the following cases of the tangential stress σ_ϕ may be obtained:

1. σ_ϕ is tensile, when $r' > \sqrt{F/\pi P}$.
2. σ_ϕ is zero, when $r' = \sqrt{F/\pi P}$.
3. σ_ϕ is compressive, when $r' < \sqrt{F/\pi P}$.

The following equation is obtained from the equilibrium equation (13.2),

$$\phi' = \sin^{-1} \left[\frac{P(r')^2}{2r(\sigma_\phi t)} - \frac{F}{2\pi r(\sigma_\phi t)}\right]. \qquad (13.3)$$

This equation is used for the successive approximations of ϕ in the numerical solution.

The following equation is obtained from the equilibrium equation (13.2). When substituting $\phi = \pi/2$, at the crown centre of the bulge:

$$(\sigma_\phi t)' = \frac{P(r')^2}{2r} - \frac{F}{2\pi r}. \qquad (13.4)$$

This equation is used to find the unit tangential force at the crown centre of the bulge for the successive approximations of t.

13.3 Determination of the Stress/Strain Relationship of the Cup Material

The cup thickness is usually small and it is difficult to obtain a tensile test specimen of a reasonable size out of the cup wall. It should be noted that the axes of

anisotropy in the original sheet blank have been distorted due to the plastic deformation in deep drawing and ironing.

The cup bulge test is used to assess the stress/strain relationship of the cup material as follows:

From the conditions at the crown centre of the bulge ($\phi = \pi/2$):

$$\rho_2 = r_e'' - t/2 \,. \tag{13.5}$$

The average value of ρ_1 is found from the geometry at the crown of the bulge. With reference to Figure (13.3) the following equation is obtained,

$$\rho_1 = \frac{\Delta X^2}{2\Delta h_c} + \frac{\Delta h_c}{2} - \frac{t}{2} \,. \tag{13.6}$$

The strains are determined from the following equations:

$$\varepsilon_\theta = \ell n \, (\frac{\rho_2}{R_o}) \,, \tag{13.7}$$

$$\varepsilon_t = \ell n \, (\frac{t}{t_o}) \,, \tag{13.8}$$

$$\varepsilon_\phi = - (\varepsilon_\theta + \varepsilon_t) \,. \tag{13.9}$$

The equilibrium equation of forces in the direction of p, see Figure (13.1), is:

$$P \, [(\rho_1 - t/2) \, d\phi][(r - t/2 \, \sin\phi) \, d\theta]$$

$$= 2\sigma_\theta \, (t.\rho_1.d_\phi) \, \sin \frac{d\theta}{2} \sin\phi + 2\sigma_\phi \, (t.r.d\theta) \, \sin \frac{d\phi}{2} \,.$$

In the above equation, the values of ρ_1, ρ_2, r, σ_θ and σ_ϕ are related to the middle plane of the element.

From this equation, it can be shown that

$$\sigma_\theta = \frac{P.\rho_1'.\rho_2'}{t.\rho_1} - \sigma_\phi \frac{\rho_2}{\rho_1} . \qquad (13.10)$$

When the thickness t is small in comparison with ρ_1 and ρ_2, the above equation can be reduced to the well known equation for a thin membrane,

$$\frac{P}{t} = \frac{\sigma_\theta}{\rho_2} + \frac{\sigma_\phi}{\rho_1} .$$

The following equation is deduced from equilibrium equation (13.2), by substituting $\phi = \pi/2$ at the crown centre of the bulge:

$$\sigma_\phi = \frac{P(\rho_2')^2}{2\rho_2 t} - \frac{F}{2\pi\rho_2 t} . \qquad (13.11)$$

The stress σ_t is assumed negligible,

$$\sigma_t = 0 . \qquad (13.12)$$

Assuming rotational symmetry about the Z-axis, it follows from Hill's theory that:

$$\gamma = \frac{H}{G} = \frac{H}{F} . \qquad (13.13)$$

By substituting equations (13.9), (13.12) and (13.13) into equation (A.12), see Appendix A, the following equation may be obtained:

$$\frac{\sigma_\theta - \sigma_\phi}{\sigma_\phi} = - \frac{2d\varepsilon_\theta + d\varepsilon_t}{(1+\gamma)\ d\varepsilon_t + d\varepsilon_\theta} \ . \qquad (13.14)$$

Putting

$$X = \frac{d\varepsilon_t}{d\varepsilon_\theta} \text{ and } m = \frac{\sigma_\theta}{\sigma_\phi} \ ,$$

it can be shown that the average strain ratio γ may be determined from the equation,

$$\gamma = \frac{(1+X)m + 1}{(1-m)X} \ . \qquad (13.15)$$

The equivalent stress may be obtained from equation (A.9) by substituting equations (13.12) and (13.13) into the above equation, hence,

$$\bar{\sigma} = \{\frac{3}{2} \ [\frac{(1+\gamma)(\sigma_\phi{}^2+\sigma_\theta)^2 - 2\gamma\sigma_\phi\sigma_\theta}{2 + \gamma}]\}^{\frac{1}{2}} \ . \qquad (13.16)$$

The equivalent strain increment is determined from equation (4.4).

The procedure for calculating the $\bar{\sigma}/\bar{\varepsilon}$ relation is as follows:

r_e", t, P, F, X and Δh_c are measured in the experiment. Then ρ_2, ρ_1, ε_θ, ε_t, ε_ϕ, σ_θ are deduced from equations (13.5), (13.6), (13.7), (13.8), (13.11) and (13.10) respectively. The average strain ratio γ is determined from equation (13.15) preferably by considering several experimental points. The equivalent stress $\bar{\sigma}$ and the equivalent strain increment $d\bar{\varepsilon}$ are deduced from equations (13.16) and (4.4) respectively.

13.4 Volume Constancy Relation

According to Woo [15], the volume constancy relation for tube bulging may be obtained by approximating the profile to the frustum of a cone. Similarly, the volume constancy relation for cup bulging is

$$r_{i+1}=[r_i^2 - 4\, R_c\, \Delta L\, (\frac{t_o}{t_i + t_{i+1}})\, \cos\, (\frac{\phi_i + \phi_{i+1}}{2})]^{\frac{1}{2}} . \quad (13.17)$$

In the first approximation t_{i+1} and ϕ_{i+1} have to be assumed.

13.5 Boundary Condition

The boundary condition is obtained from the condition at the clamping ring of the cup, that is, radial outward deformation at the clamp is assumed to be restricted, hence

$$\varepsilon_\theta = 0 . \quad (13.18)$$

By substituting the above value into equation (13.14),

$$\frac{\sigma_\theta - \sigma_\phi}{\sigma_\phi} = - \frac{1}{1 + \gamma}$$

or, $\sigma_\theta = \sigma_\phi\, (\frac{\gamma}{1 + \gamma})$.

13.6 Computer Programme

The present numerical solution for analysing the cup bulging process under the effect of internal pressure and axial force is formulated as follows:

The stresses and strains in the cup due to a certain internal pressure P and axial force F are determined in the following way:

The computation for a particular stage of bulging starts at the crown centre of the bulge. The radius r_e at the crown centre of the bulge is assumed, and computation is carried out from point to point towards the clamped radius of the cup. The radius r_e is changed in a logical order, as will be described later, until the boundary condition at the clamped radius is satisfied. Due to bulge symmetry about the crown centre, only one half of the cup is considered in the analysis.

The procedure of the numerical solution for the case when the tangential stress σ_ϕ is tensile along the whole profile of the bulge may be outlined as follows:

(a) The step at the crown centre of the bulge

Let us consider a certain stage of bulging j which corresponds to internal pressure value of P_j and axial force value of F_j. Computation starts at the crown radius r_e which is considered as the step i = 1 in this particular stage j. As a first approximation, the values of r_e and t at the crown centre of the bulge are assumed. The values of thickness and circumferential strains $\varepsilon_{t_{i,j}}$ and $\varepsilon_{\theta_{i,j}}$, are deduced from equation (4.51) and (4.52) respectively. The strain increments, $d\varepsilon_{t_{i,j}}$ and $d\varepsilon_{\theta_{i,j}}$, are obtained from

equations (4.53) and (4.54). The equivalent strain increment $d\bar{\varepsilon}_{i,j}$ is computed from the plasticity relation (4.4) and the equivalent strain $\bar{\varepsilon}_{i,j}$ is given by equation (4.55). The equivalent stress $\bar{\sigma}$ is deduced from the work-hardening characteristic of the material represented by the empirical relation (13.1). The tangential and circumferential stresses σ_ϕ and σ_θ are computed from the plasticity relations (4.5) and (4.6). The value of the unit-tangential force $(\sigma_\phi t)'$, according to the equilibrium condition is determined from equation (13.4) and is compared with the plasticity relation value $(\sigma_\phi t)$ using the inequality (4.56). If the inequality is correct, it implies that the assumed value of t is correct and control is transferred to the next step in the bulge profile. If the inequality is not satisfied, a new value of thickness t' is assumed from equation (4.7) and the procedure of this step is repeated.

(b) Other steps along the bulge profile

In the first step of this part, which corresponds to $i = 2$, ϕ is assumed slightly lower and t is assumed slightly higher than the values of ϕ and t in the previous step as a first approximation.

The current radius is found from equation (13.17), hence the values of ε_t, $d\varepsilon_t$, ε_θ, $d\varepsilon_\theta$, $d\bar{\varepsilon}$, $\bar{\varepsilon}$, $\bar{\sigma}$, σ_ϕ, σ_θ and $(\sigma_\phi t)$ are computed in the same way as described above for step $i = 1$, at the crown centre of the bulge. The value of $(\sigma_\phi t)'$ is determined from equation (4.37), and the two values

of the unit tangential force are compared in the same way as described above. When t is found to be correct, then ϕ' is determined from equation (13.3) and the two values of the angle are compared using the inequality (4.57). Once the inequality is correct,so also is the assumed value of ϕ correct and control is then transferred to the next step in the bulge profile. If the inequality is not satisfied, a new value of the angle ϕ' is assumed from equation (4.58) and the procedure of this step is repeated.

When the value of t' during the process of successive approximation reaches a very small value, then necking is assumed to be occuring and control is transferred to part (c) in the programme.

Similar computation is carried out step by step along the bulge profile until the following condition is reached: $i = m$, where m is the total number of initial elements of the cup. This means that the stresses and strains have been computed for all the cup initial elements. At this point, control is transferred to part (c) in order to check the boundary condition at the clamping end and to make the right adjustment of r_e if necessary.

The following equations are used to extrapolate the first approximate values of t and ϕ, as applicable:

When $i = 3$,

$$t_{i,j} = 2\, t_{i-1,j} - t_{i-2,j}$$

and $$\phi_{i,j} = 2\, \phi_{i-1,j} - \phi_{i-2,j}\,.$$

When $i > 3$,

$$t_{i,j} = 3t_{i-1,j} - 3t_{i-2,j} + t_{i-3,j}$$

and $$\phi_{i,j} = 3\phi_{i-1,j} - 3\phi_{i-2,j} + \phi_{i-3,j} \cdot$$

(c) Boundary condition at the clamping end

At the clamping end of the cup, ε_θ must be equal to zero.

The following observations were made during the initial testing of the programme:

1. $\varepsilon_\theta > 0$, when the assumed crown radius r_e was greater than the actual one.
2. $\varepsilon_\theta < 0$, when r_e was less than the actual crown radius.
3. $\varepsilon_\theta \simeq 0$, when r_e was approximately equal to the actual crown radius.

This logical relation between the boundary condition at the clamping end and the crown radius is used to drive the programme towards the right boundary condition within a specified accuracy. The same technique used in deep drawing for adjusting the die contact radius, see section (4.9), may be used here.

A general flow chart of the programme is given in Figure (13.4).

CHAPTER 14

EXPERIMENTAL APPARATUS AND METHOD

14.1 Design of a Test Rig for Free Bulge Forming

A special test rig was designed for free bulge forming tests. The test rig is shown in Figure (14.1). It can be seen that the hydraulic oil which provides the internal pressure is admitted through the feed tube 1 and it then passes through a hole in the punch 2 until it reaches the cavity of the cup specimen 3. Good sealing is ensured between the punch 2 and the clamping ring 4 by using two O-ring seals. The clamping ring is so designed that its surface which is in contact with the outer surface of the cup can be machined again to a bigger diameter to suit cups of greater thickness. The hydraulic oil which provides the axial compressive force is admitted through the union5 to push the piston 6 upwards. The resultant axial force is transmitted through the cup walls to the punch 2 until it reaches the load cell 7 which is firmly supported from the top by the cup-height adjusting screw 8. This screw can be adjusted to suit the required height of the cup.

14.2 Free Bulge Forming Apparatus

A photographic view of the free bulge forming apparatus is shown in Plate (14.1). The hydraulic pressure required is supplied by two high pressure hand pumps, described earlier in Section (5.5). A hydraulic accumulator

of 1.15 litre capacity is connected on the delivery line of each pump. The first pump is connected to joint 1 of the test rig, shown in Figure (14.1), to supply internal hydraulic pressure inside the cup. Another hydraulic accumulator of 4.5 litre capacity is connected on the delivery line of this pump, and a relief valve is fitted on the same line. A pressure transducer is fitted on joint 1 of the test rig for measuring the internal pressure. The pressure transducer and the load cell are connected to the twin channel amplifier.

14.3 Measurement of Internal Pressure and Axial Force

To ensure accurate measurements of the internal pressure and the axial compressive force, the same measuring system which was calibrated and used in the balanced biaxial tension test, was used for measuring the internal pressure, see Section (5.5). The load measuring system which was calibrated and used for measuring the drawing/ironing load, was used for measuring the axial compressive force, see Section (10.3).

14.4 Preparation of Specimens

About 110 blanks of 2.5 mm thickness and 172 mm diameter, were machined carefully from the supplied material. They were drawn/ironed using the drawing die described in Section (10.1) and the ironing dies described in Section (10.2). The bulge forming machine which is

described in Section (20.1) was used as the drawing press. The cup sizes and quantities are given in Table (14.1).

Table (14.1). Cup specimens

Ironing die	Cup length, mm	Thickness mm	Quantity of specimens
1	148	1.71	12
2	164	1.52	12
3	177	1.43	12
4	204	1.26	72

The quantity of each cup size was devided into two halves; one half is to be tested as in the drawn/ironed condition and the second half is to be tested in the annealed condition.

For the purpose of studying the effect of length on the bulge ratio, the cup size obtained by ironing die 4 was used. Five different lengths were carefully cut, using a hard-wood mandrel in order not to damage the specimens, to the heights of 115, 125, 135, 145 and 155 mm. For the purpose of studying the effect of thickness on the bulge ratio, a unified cup height of 135 mm was used.

The specimens to be annealed were first cleaned using a degreasing agent and an air circulating electrical furnace was used in the heat treatment. The cup specimens were kept in the furnace at a temperature of about 400^{o}C for about 30

minutes. To ensure that the material was well annealed, the hardness of the cup after annealing was compared with the hardness of the original flat blanks. The following results were obtained:

The average V.D.P. hardness (5 kg) of the original flat blank = 20.8.

The average V.D.P. hardness (5 kg) of the annealed cup = 21.

The results were considered satisfactory.

14.5 Test Procedure

The free bulge forming apparatus was used in all the experiments described below.

1. The procedure of the bulge test for the determination of the stress/strain relation is summarized as follows:

Four longitudinal lines at 90^{o} intervals were lightly scribed on the outer surface of the cup wall. A small mark was scribed across each line to mark the position of the crown centre of the bulge. The cup specimen was fitted in position on the free bulge forming test rig and internal pressure and axial force were increased conveniently until an increase of about 2.5 mm in the crown diameter was obtained. The internal pressure and axial force values were recorded from the D.V.M. of the twin channel amplifier. The pressure was released and the cup was removed from its position. The crown diameter and thickness were measured. To find the radius of curvature ρ_1", the specimen was

fitted on a punch and two V-blocks. The depth Δh_c at equal distance ΔX of the crown centre of the bulge was measured using the travelling micrometer described earlier in Section (5.5). ΔX being taken as 2.5 mm. The specimen was fitted again and the same procedure was repeated until fructure.

2. The following procedure was used in bulging specimens with the aim of comparing their strain distribution with that obtained by theory:

Four longitudinal lines of 90^{o} intervals were lightly scribed on the outer surface of the cup wall. A small mark was scribed across each line to mark the position of the crown centre of the bulge, and then small marks of 5 mm intervals were scribed along the cup length for identifying the initial elements. Internal pressure and axial force were applied and recorded. The current radius and thickness for each initial element were measured. The specimen was then fitted on a punch and two V-blocks. The current positions of elements along the cup were measured using the X-Z travelling micrometer described in Section (5.5).

3. The experimental procedure used for investigating the effect of the cup initial length and thickness on the bulge ratio was the same for both annealed and as drawn/ironed cups. The procedure is summarized as follows:

A certain value of the internal pressure was chosen by adjusting the relief valve and then the specimen was fitted in position on the free bulge forming test rig. Oil was

pumped simultaneously from the two high pressure hand pumps. Because of the existance of the relief valve on the internal pressure line, only the axial force was allowed to vary during the test and the internal pressure remained practically constant. The axial compression was increased until splitting or buckling occurred. The values of internal pressure, maximum axial force, total compression and the maximum bulge radius were recorded.

A simple technique was used to obtain the maximum bulge ratio in a single stage of internal pressure. In this technique the internal pressure was given a certain value. If the cup after bulging was split, the next specimen was tested under lower internal pressure; if the cup after bulging was buckled, the next specimen was tested under higher internal pressure. The process was repeated until a stage was reached when a slight increase or decrease resulted in splitting or buckling. The pressure was increased or decreased in steps. The step was halved every time the result was changed from splitting to buckling or vice versa.

CHAPTER 15

MECHANICAL PROPERTIES OF THE MATERIAL

15.1 General Description

The material is a commercially supplied 99.5% pure soft aluminium of 2.5 mm nominal thickness. The strain ratios of the material were determined in simple tension, see Section (6.2). The stress/strain characteristic of the sheet material was determined in both simple tension and balanaced biaxial tension tests, see Section (6.3).

15.2 Results of the Cup Bulge Test

Two annealed cups of 66 mm internal diameter, 1.26 mm thickness and 93 mm unsupported height were tested. The results of the average strain ratio as determined from equation (13.15) are given in Table (15.1).

Table (15.1). Strain ratios determined in cup bulge test

Bulge stage	1	2	3	4	5	6	7	Average
specimen 1	0.817	0.899	0.689	0.721	0.660	0.742	0.855	0.769
specimen 2	0.837	0.778	0.651	0.708	0.665	0.791	0.934	0.766

The average strain ratio from the results of the two tests is $\gamma = 0.767$. As compared with 0.731 determined in

simple tension, the difference may be caused by the deformation process during drawing/ironing of the cup. The stress/strain relation obtained from specimens 1 and 2 showed a good degree of consistancy. The average curve is compared in Figure (6.22) with the stress/strain curve determined in the balanced biaxial tension test using a flat blank of the same material. It can be seen that the bulge test curve is lower than the balanced biaxial tension curve by about 10%. However, the bulge test curve is much closer to the tension test curves, measured at 0^{o} and 90^{o} to the rolling direction, than the balanced biaxial tension test curve, see Figure (6.16).

CHAPTER 16

COMPARISON BETWEEN EXPERIMENTAL AND THEORETICAL STRAIN DISTRIBUTIONS

Experimental and theoretical results were obtained for annealed cups with five different unsupported lengths of 83, 93, 103, 113 and 123 mm. The cups were bulge-formed under the same internal pressure of 2.77 MN/m^2 and the same axial force of 9.2 KN. The cup wall thickness was 1.26 mm.

In the experiments, the circumferential strains were measured for the five specimens, while only one typical thickness strain distribution of the cup with 93 mm unsupported length was measured.

In the theory, the computer programme described in Section (13.6) was written in Fortran, tested and run on the departmental ICL 1906S computer. The effect of the number of elements and accuracy used in the successive approximation were investigated. It was found that an element step less than 1 mm and an accuracy less than 0.0001 did not result in a significant difference in the result. A typical computation time for one stage of bulging is about 20 seconds. The average strain ratio of 0.767 and the cup bulge test stress/strain curve shown in Figure (6.22) were used in the analysis.

The theoretical and experimental strain distributions are shown in Figures (16.1) to (16.6). It can be seen that

the correlation of the circumferential strains is good in the top half of the bulged cup but not as good in the lower part. This is due to the effect of the cup profile radius near the cup base which was left unsupported in the experiments. The thickness strain distribution of a typical case is shown in Figure (16.3). Again the agreement between theory and experiment in the top half is satisfactory, while a significant difference exists in the lower part of the cup due to the sinking of the cup profile radius under the effect of the axial compressive force.

CHAPTER 17

EXPERIMENTAL RESULTS AND THEIR DISCUSSION

Numerous tests have been carried out in this part of the investigation. Figure (17.1) shows the typical test results for two specimens, the first specimen being annealed and the second being as drawn/ironed specimen. Two typical test sets are given. The first set of the experimental results is shown in Plate (17.1), where as drawn/ironed cups of the same size were bulged under the effect of increasing internal pressure from specimen A to F. It can be seen that in all cups the bulge took place near the cup base. This is due to the relatively lower work-hardening in the cup wall near its base which was caused by the drawing/ironing process. When the internal pressure was relatively low as in specimens A and B, severe buckling occurred. When the internal pressure was relatively high as in specimen F, an early split occurred. The bulge was at its maximum near the boundary between splitting and buckling as in specimen D. However, the mode of bulging in both cases is similar, but different in size. The second typical set of experimental results is shown in Plate (17.2), where annealed cups of the same size were bulged under the effect of increasing internal pressure from specimen G to L. Two distinguishable modes of bulging were observed. The first mode occurred at relatively high internal pressure as in specimens J, K and L, where one large bulge occurred in the unsupported part of the cup. In the second mode twin similar bulges occurred under relatively low internal

pressure as in specimens G, H and I. The twin bulges were formed under relatively high axial force. The formation of the twin bulges is attributed to the symmetry of the bulging process about the crown centre and to the homogenous material properties as well as the relatively low internal pressure and high axial force. The maximum bulge occurred near the boundary between the two modes of bulging.

These modes of bulging may be exploited in closed die bulge forming according to the die profile shape. This investigation has produced some practical results about the effect of internal pressure and axial force on the bulge forming process.

17.1 Investigating the Effect of the Unsupported Length of Cup on the Bulge Limit

The maximum bulge ratio* for each cup length was investigated as described above. The specimens which gave the maximum bulge ratio for each length are shown in Plate (17.3) and Plate (17.4) for annealed and as drawn/ironed cups respectively. The maximum bulge ratio versus the unsupported initial cup length relation is shown in Figure (17.2). It can be seen that, within the range of the cup length tested, there is no noticable effect of the unsupported length of cup on the maximum bulge ratio for annealed cups. In the case of as drawn/ironed cups, the maximum bulge ratio was generally increased with decrease of cup length from 123 to 93 mm. This is due to the fact that

---

* The bulge ratio = $\frac{\text{Current diameter of vessel}}{\text{Initial diameter of cup}}$.

the cup wall is less work-hardened near the cup base. Therefore, for shorter cups, greater part of the cup length can be severely bulged resulting in greater bulge ratio. No noticable change occurred in the bulge ratio for cup lengths between 83-93 mm.

17.2 Investigating the Effect of the Cup Wall Thickness on the Bulge Limit

The maximum bulge ratio for each cup wall thickness was investigated as described earlier. The specimens which gave the maximum bulge ratio for each cup wall thickness are shown in Plate (17.5) and Plate (17.6) for annealed and as drawn/ironed cups respectively. The maximum bulge ratio/ cup wall thickness relation is shown in Figure (17.3). It can be seen that within the investigated range of thickness, the bulge ratio is increased slightly with increase of cup wall thickness.

In the case of as drawn/ironed cups, the maximum bulge ratio increased significantly with increase of cup wall thickness. For cups of 1.71 mm wall thickness, the bulge ratio was nearly equal to that for annealed cup. This increase in the bulge ratio is due to the lower degree of work-hardening obtained when lower reductions in ironing are used. The result indicates that for the soft aluminium used in this investigation, a reasonably low reduction in ironing may give a bulge ratio comparable to that obtained when annealed cups are used. The results of the present work may be considered of special importance for the continuous bulge forming process required for producing hollow-ware from flat blanks which will be described later in Part Four.

CHAPTER 18

CONCLUSIONS

According to the theoretical and experimental results given in Chapter 16, the following conclusions may be drawn:

1. The average strain ratio for the wall material of an annealed cup may be reasonably determined from the cup bulge test using the theoretical relations given in Section (13.3).

2. The stress/strain relationship for the wall material of an annealed cup may be determined satisfactorily using the cup bulge test method. The method simulates the deformation occurred in a bulge forming process and gives results more representative of the material behaviour in such a process.

3. The stresses and strains induced in free bulge forming, when the tangential stress σ_ϕ is tensile along the unsupported length of the cup may be well predicted from the suggested numerical solution.

Within the scope of the experimental work presented in Chapter 17 the following conclusions may be made:

1. Only one mode of bulging occurs for as deep-drawn/ironed cups under different loading conditions of internal pressure and axial force. The bulge zone is usually shifted from the centre of the unsupported cup length towards the cup base. The bulge size is relatively small when buckling occurs.

In the case of annealed cups, two modes of bulging are possible. The first mode occurs at relatively high internal pressure and low axial force values. The bulge shape is a full bulge of the unsupported length of the cup. The second mode has two similar bulges at the ends symmetrical about the centre of the unsupported cup length. This mode occurs at relatively low internal pressure and high axial force.

2. The effect of varying the unsupported cup length on the bulge limit of annealed cups is negligible.

3. The effect of varying the unsupported cup length on the bulge limit of as deep-drawn/ironed cups is significant for cup lengths between 93 and 123 mm. The effect is small for cup lengths between 83 and 93 mm.

4. The bulge limit is slightly increased with increase of cup wall thickness for annealed cups.

5. The bulge limit is greatly increased with increase of cup wall thickness for as deep-drawn/ironed cups by applying smaller reductions in ironing.

PART FOUR

BULGE FORMING INSIDE A CLOSED DIE CAVITY

CHAPTER 19

BULGE FORMING OF HOLLOW-WARE FROM FLAT BLANKS

Bulge forming of hollow-ware from flat blanks is a process in which hollow-ware articles of required shape are produced from circular blanks of sheet metal in one continuous stroke of a punch. The process consists of the following three consecutive operations:

1. Deep-drawing without a blank-holder, in which a relatively thick blank of sheet metal is deep-drawn, through a convex type die such as tractrix type die, into a cylindrical cup of a certain height. This method of deep drawing has several advantages over conventional deep drawing including simpler tooling, higher cup height/diameter ratio and lower punch load. The drawn cup has generally a variable wall thickness due to thickening in the upper part and thinning in the lower part of the cup. Also it has inconsistent and poor surface finish, and therefore, ironing of the cup wall is necessary before hydraulic bulging can be carried out.

2. Ironing of the drawn cup, where single or multi-stage ironing dies may be used depending on the total reduction required in the cup wall thickness. Ironing may be performed when one or more of the following requirements are necessary: extra cup height, good surface finish and uniform wall thickness. The acceptable limit of total reduction is determined

by the effect of work-hardening on the bulging process that follows. The cup height for a fully ironed cup may be approximated using equation (3.24).

3. Hydraulic bulging under internal pressure and axial compressive force, in which the cylindrical cup is deformed plastically inside a closed die cavity. The die is in two halves to allow the formed article to be removed. The split die has to be clamped with a sufficient force to ensure good sealing of the pressurized oil inside the cup and to prevent the split die from outward movement during forming. The values of internal pressure, axial force and axial compression must be closely controlled and related to each other during the bulge forming of a certain shape.

Assuming that the formed article has a uniform thickness the same as that of the original cup, the axial compression Δh_b required may be deduced on the basis of surface redistribution of the cylindrical cup wall over the die cavity, thus

$$\Delta h_b = \frac{S_d}{\pi D} - h_b , \qquad (19.1)$$

where S_d is the surface area of the die cavity, D the cup outside diameter and h_b the height of the die cavity.

The value of Δh_b may be used for rough assessment of during the stage of experimental production of a particular component. Values of Δh_b in excess to the above value means

that thickening will occur, while values less than the above means that thinning will occur which is mostly the case.

The actual success of the process depends on the values of the internal pressure and axial force, the shape of the component and the frictional conditions between material and die cavity.

Assuming that the time required to bulge form a particular component is T, the flow rate required to supply the internal fluid for bulging is:

$$\text{Flow rate} = (V_2 - V_1)/T \quad ,$$

where V_1 and V_2 are the initial and final volumes of the bulged part of the component.

The corresponding speed of axial compression is given by

$$v = \Delta h_b/T \quad .$$

CHAPTER 20

EXPERIMENTAL APPARATUS AND PROCEDURE

20.1 The Bulge Forming Machine

The experimental investigation of this part was carried out on the bulge forming machine shown in Plate (20.1). The electro-hydraulic control unit is on the left of the view and the machine proper is on the right of the view. The main part of the machine shown in Figure (20.1) has been described by Woo [2]. The sequence of operation is as follows: (a) At the start of the forming operation, the punch 1 and the compression plate 6 are moved to their top positions. The compression plate is in two halves and is attached to the annular piston 5. When moving up with the piston, the plate opens out as its two rollers, one at either side, comes into contact with the cam 4. This is necessary so as to allow the cup to pass through during the drawing and ironing stage. (b) A blank is placed on the tractrix type die 2. The punch which is connected to the piston rod of a hydraulic cylinder is driven downwards drawing the blank through the tractrix type die 2 and the ironing die 3 until it reaches a suitable position inside the split die cavity 8. (c) Oil under pressure is admitted through the top of the punch and pushes the cup away until it reaches the bottom position, thus leaving a space for oil to bulge the cup. (d) The split forming die 8 which is connected to the piston rods of two cylinders, driven by hydraulic pressure, one at either side, is closed in and the

two halves of the ring 7 are pressed firmly on to the cup to prevent any leakage of oil, thereby maintaining the oil pressure necessary for bulging. (e) While the oil pressure inside the cup is building up, the pressure plate is moved downwards compressing the cup. (f) At the end of the bulge forming operation the punch lifts up and the forming die opens out allowing the formed vessel to be removed from the press. For more accurate measurement of the internal pressure, the pressure gauge fitted on the machine was replaced by the calibrated pressure measuring system described earlier in Section (5.5).

The machine has the following main specification:

1. Drawing/ironing capcity: 200 KN.
2. Total punch stroke: 500 mm.
3. Maximum punch speed: 50 mm/sec.
4. Maximum internal pressure: 210 bars.
5. Maximum axial compression: 40 mm.

20.2 Design and Selection of Forming Dies

To investigate the hydraulic bulge forming of axisymmetric hollow-ware, five different dies were selected. Three of them were of basic shapes including cylindrical, conical and spherical. The other two were of more complex shapes including the double bulge and barrel shapes. Conical and spherical dies have been successfully used by Woo [2]. The other three dies were chosen from an existing set of dies provided with the machine for testing. All dies

are of split die design. The shapes of axisymmetric die cavities are shown in Figures (20.2) to (20.6).

Three forming die cavities were specially designed to investigate the hydraulic bulge forming of asymmetric hollow-ware. One square and two elliptical die cavities of different sizes were designed. The shapes of the asymmetric die profile cavities are shown in Figure (20.7) and Figure (20.8).

The above shapes were chosen to demonstrate the capability of the process. The shapes were carefully selected so that they cover a number of basic shapes encountered in the actual production of a typical component in industry.

20.3 Test Procedure

The flat circular blanks were prepared and lubricated as mentioned in Section (10.4). The tractrix type die described in Section (10.1) was used for deep drawing, and ironing die 3 described in Section (10.2) was used for the ironing of cups. This was followed by hydraulic bulge forming. The experimental procedure for determining the optimum values of internal pressure, axial force and axial compression for each shape is based on the previously gained experience in the experimental investigation of free bulge forming described in Part Three.

The procedure is summarized as follows:

1. The internal pressure was adjusted to a certain value P_1 which was the optimum value determined in the free bulging experiments described previously. The cup was compressed by a small amount. The split die was opened and the forming process was observed. The die was closed again and further small steps of axial compression were applied and observations were followed closely until one of the following situations was reached: (a) The cup buckled. In this case, the internal pressure was slightly increased and the above procedure was repeated using a new specimen. (b) The cup split. In this case, the internal pressure was slightly reduced and the above procedure was repeated using a new specimen. (c) The deformation of a cup was estimated to be close enough to the shape of the die cavity under consideration. In this case, stage 2 described below was attempted. (d)A Small decrease or increase of P_1 led to the splitting or buckling of a cup and the obtained shape was not close to the required shape. In this case, no further attempts were made and the production of this particular article was considered not possible.

2. The internal pressure was considerably increased to a level of P_2 which was estimated to be sufficient to give the deformed cup its final shape. No axial compression was applied at this stage. One of the following results was obtained after the application of P_2: (a) the required shape was obtained.

A second test was carried out to ensure that the results are repeatable. (b) Splitting of the cup occurred. A new specimen was used as stage 1b described above. (c) The required shape was fully formed but a local wrinkle appeared somewhere in the final shape. This indicated excessive axial compression. Therefore, the test was repeated and P_1 and P_2 were kept the same. The axial compression was slightly reduced.

The same procedure was used for the bulge forming of annealed cups. The annealing process was performed in the same way described in Section (14.4). The stress/strain relationship of the material is similar to that given in Figure (6.22).

CHAPTER 21

EXPERIMENTAL RESULTS AND THEIR DISCUSSION

The cups produced by deep drawing/ironing have an internal diameter of 66 mm and an average wall thickness of 1.43 mm. The resultant cup height varied according to the type of earing which occurred in drawing. Three types of earing were observed in the tests due to variation of the supplied material. They include four, six and eight ears, see specimens 1, 2 and 4 in Plate (21.1). This variation presented great difficulty in obtaining the optimum values of internal pressure and axial compression for a particular shape. However, the average cup height may be considered as 175 mm. The produced articles of axisymmetric and asymmetric shapes are presented in the form of vases for illustration. 10-15 tests or more were made for each shape before a successful result was obtained.

21.1 Axisymmetric Hollow-Ware

1. Axisymmetric hollow-ware produced from flat blanks in one continuous operation: Four different shapes were produced successfully from flat blanks in one continuous operation including deep drawing, ironing and hydraulic bulge forming. The produced shapes are: cylindrical, conical, spherical and double bulge. They are shown as specimens 5, 1, 3 and 2 respectively in Plate (21.2). It was not possible to produce the barrel shaped article due to the large expansion in volume involved. More axial

compression was needed, but this was not possible due to the insufficient height of the cup produced with the present tooling. The problem of the buckling of the ears made the cup height more critical. The optimum values of P_1, P_2 and Δh_b used in producing the above shapes are given in Table (21.1).

Different techniques were essential to produce different shapes. These techniques are mostly dictated by the shape to be made and by the fact that the cup wall material has been work-hardened particularly towards the top of the cup. This means that the material starts to flow, if the die shape allows it, from the part near the cup base. The technique used for each of the above shapes together with typical examples of failure and defects are given briefly in the following:

1. Conical shape: It was found necessary to allow the cup to buckle, see specimen 1 in Plate (21.1), near the top where the bulge ratio is maximum. This enabled the material at the top part to thicken. The next stage was to increase the internal pressure to a fairly high value, thus allowing the shape to expand and fill the die cavity.

2. Double bulge shape: No difficulty was experienced in this case when a small buckle was allowed at the top bulge as shown in specimen 2 in Plate (21.1). If the buckling was severe, it was difficult to rectify it , see specimen 2 in Plate (21.1).

3. Spherical shape: This shape was difficult to form. It was vulnerable to splitting and buckling. The best results were obtained by bulging the lower half of the shape in the first stage as shown in Plate (21.1) specimen 4. In the second stage, the shape was pressed out to give the required profile inside the die cavity. Specimen 5 shows a severe buckling situation when the internal pressure is lower than the optimum value. Specimen 6 shows the case in which the internal pressure is higher than the optimum value. Specimen 7 in Plate (21.3) shows a buckled ring at the middle of the spherical shape. This is due to excessive axial compression.

4. Cylindrical shape: This was a straight forward job. The available maximum pressure was not sufficient to force the cup to fill the small radii at the corners of the die cavity.

The thickness reduction and bulge ratio distribution of axisymmetric shapes including cylindrical, conical, spherical and double bulge shapes are given in Figures (21.1) to (21.4).

As an example, the ideal axial compression of the spherical shape, deduced from equation (19.1), is about 26 mm. By comparing this value with the actual value of 19.5 mm given in Table (21.1), it indicates that a fair amount of compression was possible and not much thinning effect is expected as shown in Figure (21.3).

Table (21.1). Values of P_1, P_2 and Δh_b used in bulge forming of as drawn/ironed cups

Shape	P_1 (bars)	P_2 (bars)	Δh_b (mm)
Conical	60.0	125.0	20.0
Double bulge	58.3	125.0	18.0
Spherical	59.3	125.0	19.5
Cylindrical	63.3	116.7	7.5

2. Axisymmetric hollow-ware produced with intermediate annealing before bulge forming:

The forming process in this case was found to be easier than that in the previous case. Providing that the internal pressure is high enough in relation to the axial force, bulging starts to take place gradually with the maximum bulge at the middle point of the unsupported zone. The process in this case is less sensitive to the magnitude of the internal pressure. Since the material is annealed, the first and second stage pressures are much lower than those required in the previous case. This is considered to be particularly important in reducing the sealing problems when materials of high strength, such as stainless steel, are to be used in bulge forming. Three shapes were produced. The first one is the barrel shape which was not possible to form previously. This shape is shown as specimen 4 in Plate (21.2). The other two shapes, the spherical and cylindrical

ones, were formed especially to make a comparison of the thickness reduction distribution between annealed and non-annealed cups in bulge forming. The values of P_1, P_2 and Δh_b used in producing the above mentioned shapes from annealed cups are given in Table (21.2).

Table (21.2). Values of P_1, P_2 and Δh_b in bulge forming of annealed cups

Shape	P_1 (bars)	P_2 (bars)	Δh_b (mm)
Barrel shaped	31.7	70.3	20.0
Spherical	26.7	68.0	12.5
Cylindrical	31.7	80.0	5.0

Typical sections of the produced axisymmetric shapes are shown in Plate (21.4). Quarter sections were made from the formed shapes to show their thickness, profile and interior surface.

3. Comparison of thickness reduction and bulge ratio when annealed and non-annealed cups are used in the production of axisymmetric hollow-ware:

The results for cylindrical and spherical shapes are given in Figures (21.1) and (21.3) respectively. It can be seen that the thickness reduction distribution for the spherical shape is fairly uniform over the spherical zone when both annealed and non-annealed cups are used. This indicates the

favourable effect of the axial compressive force in overcoming the thinning effect especially at the part of maximum bulge ratio, and in smoothing the thinning effect in the forming zone. It also indicates that there is no special advantage in using annealed cups. Similar results may be noted for the cylindrical shape. In addition to that, a small difference can be seen in the bulge ratio distribution near to the corners of the cylindrical bulge zone. This shows the difficulty of filling small radii at dead corners even when the material is softer.

21.2 Asymmetric Hollow-Ware

Three different asymmetric shapes were produced successfully. The produced shapes are square and two elliptical shapes of different sizes. They are shown in Plate (21.5). The production of these shapes were more sensitive to the frictional conditions between material and die cavity surface. Unlike the dies for axisymmetric shapes, good surface finish was necessary before successful results could be obtained. Due to the asymmetric shape, the material is forced to slide later in the deformation process along the narrower zones in order to fill the larger parts of the die cavity. Although no additional lubricant was used between the material and the die cavity in the present experiments, it is believed that adding a special lubricant to the bulge forming process may improve the material flow and thickness distribution particularly when high internal pressure is used.

1. Asymmetric hollow-ware produced from flat blanks in one continuous operation:

Square and elliptical shapes were produced. The square shape tended to buckle easily in its flat walls. The amount of axial compression must be closely adjusted. The forming of an elliptical shape, using elliptical die 1, showed that the die shape at the parts of the ellipse which have a smaller radius of curvature offered high resistance to material flow. Slight increase or decrease in the internal pressure resulted in splitting or buckling as seen in specimens 8 and 9 in Plate (21.3). The final shape was formed with the part around the major axis of the ellipse not fully formed. Similar behaviour was observed when using elliptical die 2, see specimens 10 and 11 in Plate (21.3). The values of P_1, P_2 and Δh_b used in the successful tests are given in Table (21.3).

Table (21.3). Values of P_1, P_2 and Δh_b used in bulge forming of as drawn/ironed cups

Shape	P_1 (bars)	P_2 (bars)	Δh_b (mm)
Square	60.0	116.6	20
Elliptical 1	59.3	66.0	12

2. Asymmetric hollow-ware produced with intermediate annealing before bulge forming:

Square, elliptical 1 and elliptical 2 shapes were produced successfully. The forming techniques of the

process were easier than those in the previous case. More effort was needed to obtain the optimum axial compression. It was found that the success of the process is less sensitive to internal pressure but more sensitive to axial compression.A typical example of buckling due to excessive axial compression is shown in specimen 10A in Plate (21.3). The values of P_1, P_2 and Δh_b used in the successful tests are given in Table (21.4).

Table (21.4). Values of P_1, P_2 and Δh_b used in bulge forming of annealed cups

Shape	P_1 (bars)	P_2 (bars)	Δh_b (mm)
Square	29.7	70	14.0
Elliptical 1	31.7	70	11.5
Elliptical 2	30.0	72	7.5

Typical sections of asymmetric shapes are given in Plate (21.6). Thickness reduction and bulge ratio distributions are given in Figures (21.5) and (21.6).

3. Comparison of thickness reduction and bulge ratio when annealed and non-annealed cups are used in the production of asymmetric hollow-ware:

The comparison is made for the square and elliptical 1 shapes. It can be seen from the results for the square shape, shown in Figure (21.5), that the thickness reduction

distribution across the specimen is more uniform in the case of an annealed cup. This may be attributed to the difference in frictional conditions and mechanical properties. Two clear necks were found in the case of as drawn/ironed cups near to the point where the two sides of the square meet the radius of the corner. This indicates that high frictional forces along the sides of the square restricted the material flow in this direction. It can also be seen that the bulge ratio at the radius of the corner across the specimen is short of the maximum theoretical value for the as drawn/ ironed cups. The results for elliptical shape 1 showed that the full bulge ratio was obtained along the major axis of the ellipse of annealed cups. For as drawn/ironed cups, a considerably lower bulge ratio was obtained along this axis. The results are shown in Figure (21.6). A high thickness reduction of more than 50% was obtained for annealed cups. The thickness reduction near the minor axis of the ellipse is small in both cases.

CHAPTER 22

CONCLUSIONS

With reference to the experimental results given in Chapter 21, the following conclusions may be drawn:

1. It is possible to produce axisymmetric and asymmetric hollow-ware of conical, spherical, cylindrical, double bulge, square and elliptical shapes from flat blanks in one continuous operation which includes deep drawing, ironing and hydraulic bulge forming in one stroke of a punch.

2. Providing that the blank material has consistent mechanical properties, the success of the process is repeatable.

3. Bulge ratios of 1.45 or more could be obtained.

4. High friction between material and bulge forming die cavity is undesirable especially when asymmetric shapes are to be produced.

5. Corners of small radius are not recommended in any position, because they require relatively high internal pressure for forming, thus introducing sealing problems. In this case, bulge forming of annealed cups is generally more effective.

6. Blank material having rotationally symmetric anisotropic properties in the plane of the sheet metal is desirable. This is important in the forming process to ensure uniform

application of the axial compressive force, thereby preventing buckling of the cup ears. This also helps to reduce material wastage.

7. The tooling used in the process is fairly simple and the same set of deep drawing/ironing dies may be used to produce different shapes by changing the bulge forming die. This gives an economical advantage in the production of small and medium batches.

8. Not much difference in the forming capability was observed when bulge forming a particular shape from as drawn/ ironed cup or from annealed cup. Greater axial compression is usually needed in the forming of a particular shape from as drawn/ironed cup. Higher thickness reductions can be obtained when bulge forming annealed cups. The process in the latter case is less sensitive to internal pressure but more sensitive to axial compression.

9. The internal pressure required for the bulge forming of annealed cups is considerably lower than that required for as drawn/ironed cups. This will be advantageous when forming strong materials such as stainless steel.

REFERENCES

1. Turner, G. M. and Woo, D. M. "Bulge Forming of Vessels from Flat Blanks". Int. J. Mech. Sci., Vol. 17, p. 53 (1975).

2. Woo, D. M. "Development of a Bulge Forming Process". Sheet Metal Industries, Vol. 55, p. 623 (1978).

3. Hill, R. "The Mathematical Theory of Plasticity". Oxford University Press (1950).

4. Whiteley, R. L. "The Importance of Directionality in Drawing Quality Sheet Steel". Trans. A.S.M., Vol. 52, p. 154 (1960).

5. Oehler, G. "Deep-Drawing Without a Blank-Holder by Bending Around Convex-Shaped Dies". Engineers Digest, Vol. 24, p. 81 (1963).

6. Haverbeck, K. "Von AuBenborden an Blechteilen zwischen Stempel und Ringen". Dissertation TH Hannover 1961, Auszug heirvon Mitt. Forschungsges. Blechverabeitung, No. 12 und 13, p. 150-156 (1961).

7. Woo, D. M. "The Analysis of Axisymmetric Forming of Sheet Metal and the Hydrostatic Bulging Process". Int. J. Mech. Sci., Vol. 6, p. 303 (1964).

8. Woo, D. M. "Analysis of the Cup-Drawing Process". J. Mech. Engng. Sci., Vol. 6, p. 116 (1964).

9. Woo, D. M. "On the Complete Solution of the Deep-Drawing Problem". Int. J. Mech. Sci., Vol. 10, p. 83 (1968).

10. Woo, D. M. "Analysis of Deep-Drawing Over a Tractrix Die". J. Engng. Mat. Tech., Trans. A.S.M.E., No. 76-Mat-B (1976).

11. Lowe, R. N. F. and Swift, H. W. "Ironing of Mild Steel Cups". Instn. Auto Engrs., Rep. No. 1945/R/3 (1945).

12. Knowles, W. S. and Swift, H. W. "Ironing of Metal Cups: Effect of Die Angle and Wall Thickness". The Motor Ind. Res. Association, Rep. No. 1946/R/3 (1946).

13. Shawki, G. S. A. "Optimum Design of Ironing Dies". Sheet Metal Industries, Vol. 47, p. 885 (1970).

14. Shaw, F. J. D. "Precision Low-Pressure Deep-Drawing". Sheet Metal Industries, Vol. 47, p. 81 (1970).

15. Woo, D. M. "Tube-Bulging Under Internal Pressure and Axial Force". J. Engng. Mat. Tech., Trans. A.S.M.E., No. 73-Mat-V (1973).

16. Woo, D. M. and Lua, A. C. "Plastic Deformation of Anisotropic Tubes in Hydraulic Bulging". J. Engng. Mat. Tech., Trans. A.S.M.E., Vol. 100, p. 421 (1978).

17. Hamming, R. W. "Numerical Methods for Scientists and Engineers". McGraw Hill (1973).

18. Bramley, A. N. and Mellor, P. B. "Plastic Flow in Stabilized Sheet Metal". Int. J. Mech. Sci., Vol. 8, p. 101 (1966).

19. Taghvaipour, M. and Mellor, P. B. "Plane Strain Compression of Anisotropic Sheet Metal". Proc. Instn. Mech. Engrs; London, Vol. 185, p. 593 (1970).

20. Atkinson, M. "Assessing Normal Anisotropy of Sheet Metals". Sheet Metal Industries, Vol. 44, p. 167 (1967).

21. Swift, H. W. "Plastic Bending Under Tension". Engineering, Vol. 166, p. 357 (1948).

22. Swift, H. W. "The Mechanism of a Simple Drawing Operation: A Study of Stretch-Forming". Engineering, Vol. 178, p. 431 (1954).

23. Al-Makky, M. M. and Woo, D. M. "Deep-Drawing Through Tractrix Type Dies". Int. J. Mech. Sci., Vol. 22, p. 467 (1980).

24. Johnson, W. and Mellor, P. B. "Engineering Plasticity". Van Nostrand Reinhold Company Ltd. (1975).

25. Parmar, A. and Mellor, P. B. "Predictions of Limit Strains in Sheet Metal Using a More General Yield Criterion". Int. J. Mech. Sci., Vol. 20, p. 385 (1978).

BIBLIOGRAPHY

Asimow, W. 1936 "An Investigation of the Plastic Flow Process Involved in Drawing Cylindrical Shells from Flat Circular Blanks". Publication in Engineering, University of California, Vol. 3, p. 235.

Bartholomew, E. L. Jnr. 1943 "Stress-Strain Measurements in the Drawing of Cylindrical Cups". Trans. ASM, Vol. 31, p. 582.

Bauder, U. 1951 "Tiefzichen von Hohlkörpen aus dicken Stahlblechen". Stahl u. Eisen, No. 10, p. 500.

Beisswänger, H. 1950 "Tiefzichen dünner Bleche mit konischen Ziehringen und mit Doppelzugwerkzeugen" Mitt. Forschungsges. Blechverabeitung, No. 30, p. 1-5.

Beisswänger, H. 1950a "Halterfreies Zichn mitkonischen Ringen". Mitt. Forschungsges. Blechverabeitung, No. 33, p. 1-3.

Budiansky, B. and Wang, N. M. 1966 "On the Swift Cup Test". J. Mech. Phys. Solids, Vol. 14, p. 357.

Chiang, D. C. and Kobayashi, S. 1966 "The Effect of Anisotropy and Work-Hardening Characteristics on the Stress and Strain Distribution in Deep Drawing". J. Engng. Ind. (Trans. ASME, B), Vol. 88, p. 443.

Crane, E. V. 1931 "Plastic Working of Metals". John Wiley and Sons, New York.

Crane, E. V. 1932 "Plastic Working of Metals". John Wiley and Sons, New York.

Chung, S. Y. and Swift, H. W. 1951 "Cup Drawing from a Flat Blank". Proc. Instn. Mech. Engrs., Vol. 165, p. 199.

Dorn, J. E. 1949 "Stress Strain Relations for Anisotropic Plastic Flow". J. Appl. Phys., Vol. 20, p. 15.

Eksergian, G. L. 1926 "The Plastic Behaviour of Metals in Drawing". Trans. ASME, Vol. 48, p. 609.

El-Sebaie, M. G. and Mellor, P. B. 1972 "Plastic Instability Conditions in the Deep-Drawing of a Circular Blank of Sheet Metal". Int. J. Mech. Sci., Vol. 14, p. 535.

Freeman, P. and Leeming, H. 1954 "Ironing of Thin-Walled Metal Cups: The Distribution of the PUnch Load". B.I.S.R.A. Report No. MW/E/46/53.

Fuchs, F. J. 1965 "Production Metal Forming With Hydrostatic Pressures". ASME Paper 65 - Prod. 17.

Fukui, S. 1938 "Researches on the Deep-Drawing Process". Science Papers of the Inst. Phys. and Chemical Research, Tokyo, No. 849, p. 1422; and 1939 No. 885, p. 373.

Fukui, S., Yuri, H. and Yoshida, K. 1958 "Analysis for Deep-Drawing of Cylindrical Shell Based on Total Strain History and Some Formability Tests". Aero. Res. Inst., University of Tokyo, Rep. No. 332, p. 43.

Fukui, S., Yoshida, K. and Abe, K. 1960 "Researches on the Deep-Drawing Process". Science Papers of the Inst. Phys. and Chemical Research, Tokyo, No. 54, p. 199.

Fukui, S. and Hansson, A. 1970 "Analytical Study of Wall Ironing, Considering Work-Hardening". Annals of C.I.R.P., Vol. 18, p. 593.

Gotoh, M. 1980 "A Finite Element Analysis of the Rigid-Plastic Deformation of the Flange in a Deep-Drawing Process Based on a Fourth Degree Yield Function" - II. Int. J. Mech. Sci., Vol. 22, p. 367.

Herrmann, L. and Sachs, G. 1934 "Untersuchungen Über das Tiefziehn". Metallwirtschaft, Vol. 13, p. 687.

Hill, R. 1948 "A Theory of the Yielding and Plastic Flow of Anisotropic Metals". Proc. Roy. Soc. A., Vol. 193, p. 281.

Jackson, K. L. 1949 "Determination of Plastic Strains in Sheet Metal". Sheet Metal Industries, Vol. 26, p. 1447.

Jackson, L. R., Smith, K. F. and Lankford, W. T. 1948 "Plastic Flow in Anisotropic Sheet Metal". Metals Technology Tech. Pub., p. 2440.

Kobayashi, S. and Kim, J. H. 1978 "Deformation Analysis of Axisymmetric Sheet Metal Forming Processes by the Rigid-Plastic Finite Element Method". Mechanics of Sheet Metal Forming, General Motors Res. Lab., p. 341.

Lankford, W. T., Snyder, S. C. and Bauscher, J. A. 1950 "New Criteria for Predicting the Press Performance of Deep-Drawing Sheets". Trans. ASM, Vol. 42, p. 1197.

Lee, S. H. and Kobayashi, Shiro. 1975 "Rigid-Plastic Analysis of Bore Expanding and Flange Drawing with Anisotropic Sheet Metals by the Matrix Method". Proc. 15th Int. Mach. Tool Design and Res. Conf., Birmingham, p. 561.

Leeming, H. and Freeman, P. 1952 "An Autographic Recorder for Drawing and Ironing". B.I.S.R.A., Rep. No. MW/E/58/51, 13 pages.

Lilet, L. and Wybo, M. 1964 "Effect of Plastic Anisotropy and Rate of Work-Hardening in Deep Drawing". Sheet Metal Industries, Vol. 41, p. 783.

Limb, M. E., Chakrabarty, J. and Garber, S. 1974 "The Axisymmetric Tube Forming Process". Int. Inst. for Prod. Eng. Research Conf., Tokyo.

Limb, M. E., Chakrabarty, J., Garber, S. and Mellor, P. B. 1973 "The Forming of Axisymmetric and Asymmetric Components from Tubes". 14th Int. MTDR Conf., p. 799.

Limb, M. E., Chakrabarty, J. Garber, S. and Roberts, W. T. 1976 "Hydraulic Forming of Tubes". Sheet Metal Ind., Vol. 43, p. 418.

Loxley, E. M. and Freeman, P. 1954 "Some Lubrication Effects in Deep Drawing Operations". J. Inst. Petro., Vol. 40, p. 299.

May, O. 1934 Unpublished Report and German Patent No. 685, 898.

Mellor, P. B. and Parmar, A. 1978 "Plasticity Analysis of Sheet Metal Forming". Mechanics of Sheet Metal Forming, General Motors Res. Lab., p. 53.

Mijon, M. 1938 "Résultats de Quelques Essais Démontessage et de ses Applications". Revue de l'Aluminium, Vol. 15, p. 1481.

Moore, G. G. and Wallace, J. F. 1964 "The Effect of Anisotropy of Instability in Sheet-Metal Forming". J. Inst. Met., Vol. 93, p. 33.

Naziri, H. and Pearce, R. 1970 "The Effect of Plastic Anisotropy on Flange Wrinkling Behaviour During Sheet-Metal Forming". Metal. Ital., Vol. 62, p. 727.

Oehler, G. 1937 "Die Tiefzichgute von Messingblechen nach AEG - Prafverfahren". Metallwirtschaft, Vol. 16, p. 1059.

Ogura, T. 1969 "Liquid Bulge Forming". Proc. 1st Int. Conf. on Prod. Develop. and Manuf. Tech., Univ. of Strathcylde, p. 253.

Ogura, T., Ueda, T. and Takagi, R. 1966 "The Hydraulic Bulging Process". Industrie-Anzeiger, 88, 770, p. 1001.

Sachs, G. 1930 "Spanlose Formug der Metalle". Akademische verlagogessellschaft M.B.H., Leipzig.

Sachs, G. 1931 "Spanlose Formung" (Springer, Berlin).

Sachs, G. 1934 "New Researches on the Drawing of Cylindrical Shells". Proc. Inst. Automobile Engrs., Vol. 29, p. 588.

Senior, B. W. 1956 "Flange Wrinkling in Deep-Drawing Operations". J. Mech. Phys. Solids, Vol. 4, p. 235.

Shawki, G. 1961 "Niederhalterloses Tiefziehen". Mitt. Forschungsges Blechverarbetung, No. 18, p. 229.

Siebel, E. and Pomp, A. 1929 "Under den Kraftverlauf beim Tiefzichen und bei der Tiefungsprüfung". Mitt. K. Wilh. Inst. Eisenforsch, Vol. 11, p. 139.

Smith, O. 1908 "Press Working of Metals". John Wiley and Sons, New York.

Sommer, M. H. 1926 "Versuche uber das Zieben von Hahlkorpern". Forsch-Arb., No. 286.

Swift, H. W. 1939 "Drawing Tests for Sheet Metal". Proc. Inst. Automobile Engrs., Vol. 34, p. 361.

Swift, H. W. 1943 "Two-Stage Drawing of Cylindrical Cups". Trans. Inst. Eng. and Shipbuilders in Scotland, Vol. 86, p. 195.

Voce, E. 1948 "True Stress-Strain Curves and Their Applications to Cold-Working Processes". Metal Treatment and Drop Forging, Vol. 15, p. 53.

Wallick, C. R. 1965 "Tube Bulging with Axial Pressure". Metalworking Production, July, p. 52.

Wang, N. M. and Budiansky, B. 1978 "Analysis of Sheet Metal Stamping by a Finite Element Method". J. Appl. Mech., Vol. 45, p. 73.

Warwick, J. O. and Alexander, J. M. 1962 "Prediction of the Limiting Drawing Ratio from the Stress/Strain Curve". J. Inst. Met., Vol. 91, p. 1.

Wifi, A. S. 1976 "An incremental Complete Solution of the Stretch-Forming and Deep-Drawing of a Circular Blank Using a Hemispherical Punch". Int. J. Mech. Sci., Vol. 18, p. 23.

Woo, D. M. and Hawkes, P. J. 1968 "Determination of Stress/Strain Characteristics of Tubular Materials". J. Inst. Met., Vol. 96, p. 357.

Yamada, Y. 1961 "Studies on Formability of Sheet Metals". Rep. Inst. Ind. Sci., University of Tokyo, Vol. 11, No. 5.

Yamada, Y. 1964 "Effects of R-Value on the Deep-Drawing of Sheet Metals". J. Japan Soc. Tech. of Plasticity, Vol. 5, No. 5., p. 183.

Zienkiewicz, D. C.,Onate, E. and Heinrich, J. C. 1978 "Plastic Flow in Metal Forming, II Thin Sheet Metal". ASME, ADM-Vol. 28, p. 107.

APPENDIX A

HILL'S THEORY OF PLASTIC ANISOTROPY

The theory of plasticity was described by Hill [3] and Johnson and Mellor [24]. The following account of Hill's theory of plastic anisotropy is based on the latter reference.

A.1 The Yield Criterion

The theory of Hill [3] describes a state of a simple orthotropic anisotropy, that is, there are three mutually orthogonal planes of symmetry at every point. The intersections of these planes are known as the principal axes of anisotropy. The yield criterion proposed by Hill when referred to these axes has the form

$$2f(\sigma_{ij}) \equiv F(\sigma_y - \sigma_z)^2 + G(\sigma_z - \sigma_x)^2 + H(\sigma_x - \sigma_y)^2 + 2L\tau_{yz}^2 + 2M\tau_{zx}^2 + 2N\tau_{xy}^2 = 1 , \qquad (A.1)$$

where $f(\sigma_{ij})$ is the plastic potential,

σ_x, σ_y and σ_z are normal stresses,

τ_{yz}, τ_{zx} and τ_{xy} are shear stresses, and

F, G, H, L, M and N are parameters characteristic of the current state of anisotropy. It is assumed that there is no Bauschinger effect and that a hydrostatic stress does not influence yielding. Hence, linear terms are not included and only differences between normal stress components appear in the yield criterion.

If X, Y and Z are the tensile stresses in the principal directions of anisotropy, it is easily shown that

$$\frac{1}{X^2} = G + H, \quad 2F = \frac{1}{Y^2} + \frac{1}{Z^2} - \frac{1}{X^2}$$

$$\frac{1}{Y^2} = H + F, \quad 2G = \frac{1}{Z^2} + \frac{1}{X^2} - \frac{1}{Y^2}$$

$$\frac{1}{Z^2} = F + G, \quad 2H = \frac{1}{X^2} + \frac{1}{Y^2} - \frac{1}{Z^2} .$$

If R, S and T are the yield stresses in shear with respect to the principal axes of anisotropy, then

$$2L = \frac{1}{R^2}, \quad 2M = \frac{1}{S^2} \quad \text{and} \quad 2N = \frac{1}{T^2} .$$

The condition of planar isotropy (rotational symmetry about the Z-axis) are determined by noting that equation (A.1) must remain invariant for arbitrary (x,y) axes of reference, it can be shown that

$$N = F + 2H = G + 2H, \; L = M . \tag{A.2}$$

For complete isotropy

$$L = M = N = 3F = 3G = 3H . \tag{A.3}$$

When anisotropy is vanishingly small the expression (A.1) reduces to the von Mises criterion. Substituting from (A.3) into (A.1) the yield criterion then becomes

$$(\sigma_y - \sigma_z)^2 + (\sigma_z - \sigma_x)^2 + (\sigma_x - \sigma_y)^2 + 6\tau_{yz}^2 + 6\tau_{zx}^2 + 6\tau_{xy}^2 = \frac{1}{F} = 6k^2,$$

Since for pure shear

$$\sigma_x = -\sigma_y = k, \quad \sigma_z = 0$$

and $\tau_{yz} = \tau_{zx} = \tau_{xy} = 0$

giving

$$\frac{1}{F} = 6k^2,$$

where k is the yield shear stress.

A.2 The Flow Rule

By analogy with the Lévy-Mises equation for isotropic material it is supposed that $f(\sigma_{ij})$, in equation (A.1), is the plastic potential. The incremental strains are thus derived by partially differentiating $f(\sigma_{ij})$ with respect to σ_{ij}.

$$\frac{\partial f}{\partial \sigma_x} = G(\sigma_x - \sigma_z) + H(\sigma_x - \sigma_y)$$

and hence

$$\frac{d\varepsilon_x^p}{G(\sigma_x - \sigma_z) + H(\sigma_x - \sigma_y)} = d\lambda .$$

Assuming a rigid-plastic material the superfix 'p' in the above equation can be dropped. Similar expressions are obtained for the other components of the strain increment and can be written down as

$$d\varepsilon_x = d\lambda[H(\sigma_x - \sigma_y) + G(\sigma_x - \sigma_z)], \quad d\gamma_{yz} = d\lambda L\tau_{yz},$$

$$d\varepsilon_y = d\lambda[F(\sigma_y - \sigma_z) + H(\sigma_y - \sigma_x)], \quad d\gamma_{zx} = d\lambda M\tau_{zx}, \qquad (A.4)$$

$$d\varepsilon_z = d\lambda[G(\sigma_z - \sigma_x) + F(\sigma_z - \sigma_y)], \quad d\gamma_{xy} = d\lambda N\tau_{xy}.$$

The above equations give the relation between stress and strain increment.

If a simple tension is applied to a strip lying in the (x,y) plane and cut parallel to the X-axis of anisotropy the incremental strain ratios are obtained from equation (A.4).

$$d\varepsilon_x : d\varepsilon_y : d\varepsilon_z = G + H : -H : -G.$$

The ratio of thickness to width strain is known as the r-value and therefore

$$r_x = \frac{d\varepsilon_y}{d\varepsilon_z} = \frac{H}{G},$$

where the suffix 'x' denotes that the specimen is oriented along the 'x'-direction. For a strip cut in the y-direction.

$$d\varepsilon_x : d\varepsilon_y : d\varepsilon_z = -H : F + H : -F$$

and $r_y = \frac{d\varepsilon_x}{d\varepsilon_z} = \frac{H}{F}$.

In order to derive the required anisotropic parameters for plane-stress deformation of sheet it is ncessary to carry

out a tensile test in at least one other direction in the plane of the sheet. If anisotropic sheet is subjected to forces in the plane of the sheet, the (x,y) plane, then τ_{yz} and τ_{zy} will be zero. Suppose a strip tensile specimen is cut at an angle to the x-direction then from consideration of equilibrium

$$\sigma_x = \sigma\cos^2\alpha,\ \sigma_y = \sigma\sin^2\alpha,\ \tau_{xy} = \sigma\sin\alpha\ \cos\alpha\ ,$$

where σ is the applied tensile yield stress. Substitution of these values in equation (A.4) gives

$$d\varepsilon_x = [(G + H)\ \cos^2\alpha - H\ \sin^2\alpha]\sigma\ d\lambda\ ,$$

$$d\varepsilon_y = [(F + H)\ \sin^2\alpha - H\ \cos^2\alpha]\sigma\ d\lambda\ ,$$

$$d\varepsilon_z = -[F\ \sin^2\alpha + G\ \cos^2\alpha]\sigma\ d\lambda\ .$$

From considerations of the geometry of small strain, the width strain increment $d\varepsilon_{\alpha + (\pi/2)}$ is given by

$$d\varepsilon_{\alpha + (\pi/2)} = d\varepsilon_x\ \sin^2\alpha + d\varepsilon_y\ \cos^2\alpha - 2\ d\gamma_{xy}\ \sin\alpha\ \cos\alpha$$

and therefore

$$r_\alpha = \frac{d\varepsilon_{\alpha + (\pi/2)}}{d\varepsilon_z} = \frac{d\varepsilon_x\ \sin^2\alpha + d\varepsilon_y\ \cos^2\alpha - 2\ d\gamma_{xy}\ \sin\alpha\ \cos\alpha}{d\varepsilon_z}\ ,$$

$$r_\alpha = \frac{H + (2N - F - G - 4H)\ \sin^2\alpha\ \cos^2\alpha}{F\ \sin^2\alpha + G\ \cos^2\alpha}\ .$$

In sheet metal the rolling direction is usually an axis of anisotropy and the x-direction is then taken to coincide with the rolling direction. The above equation yields

$$r_x = r_o = \frac{H}{G},$$

$$r_y = r_{90} = \frac{H}{F},$$

$$r_{45} = \frac{2N - (F + G)}{F + G} \quad \text{or} \quad \frac{N}{G} = (r_{45} + 1/2)(1 + \frac{r_o}{r_{90}}).$$

r_o, r_{45} and r_{90} indicate r-values along, at forty-five degrees and ninty degrees to the rolling direction.

A.3 Stress and Strain Relations

When a material is deformed plastically the state of anisotropy changes. However, it will be assumed here that this change in anisotropy is negligible compared with the anisotropy existed in the material at the start of the test.

If the state of anisotropy remains constant the yield stresses must increase in strict proportion as the material work-hardens and it follows that the anisotropic parameters must decrease in strict proportion. The ratios of the parameters will therefore remain constant and it is the ratios not the absolute values of the individual parameters that are determined by experiment.

Hill [3] has proposed that the equivalent stress should be defined as

$$\bar{\sigma} = \sqrt{3/2}\left[\frac{F(\sigma_y-\sigma_z)^2+G(\sigma_z-\sigma_x)^2+H(\sigma_x-\sigma_y)^2+2L\tau_{yz}^2+2M\tau_{zx}^2+2N\tau_{xy}^2}{F+G+H}\right]^{\frac{1}{2}}. \tag{A.5}$$

When it is understood that only ratios of the anisotropic parameters, not the absolute values, will be considered. When anisotropy is negligible the expression reduces to

$$\bar{\sigma} = \{\tfrac{1}{2}[(\sigma_y-\sigma_z)^2+(\sigma_z-\sigma_x)^2+(\sigma_x-\sigma_y)^2+6\tau_{yz}^2+6\tau_{zx}^2+6\tau_{xy}^2]\}^{\frac{1}{2}},$$

which is the equivalent stress for isotropic material based on the von Mises criterion.

Following Jackson, Smith and Lankford (1948), Hill [3] assumed by analogy with isotropic theory that $\bar{\sigma}$ is a function of the plastic work. The increment of plastic work per unit volume, for an assumed rigid-plastic material, is

$$d\omega = \sigma_{ij}\ d\varepsilon_{ij} = \sigma_{ij}\ \frac{\partial f}{\partial \sigma_{ij}}\ d\lambda,$$

where σ_{ij} and $d\varepsilon_{ij}$ are stress and strain increment tensors respectively.

From equations (A.4) we obtain

$$\begin{aligned} G\,d\varepsilon_y - H\,d\varepsilon_z &= (FG+GH+HF)(\sigma_y-\sigma_z)\,d\lambda, \\ H\,d\varepsilon_z - F\,d\varepsilon_x &= (FG+GH+HF)(\sigma_z-\sigma_x)\,d\lambda, \\ F\,d\varepsilon_x - G\,d\varepsilon_y &= (FG+GH+HF)(\sigma_x-\sigma_y)\,d\lambda. \end{aligned} \tag{A.6}$$

Assuming that loading is along the principal axes, the increment of plastic work per unit volume can be expressed as

$$d\omega = \bar{\sigma}\, d\bar{\varepsilon} = \sigma_x\, d\varepsilon_x + \sigma_y\, d\varepsilon_y + \sigma_z\, d\varepsilon_z \,. \tag{A.7}$$

Substituting the strain increment from equations (A.4) gives

$$d\omega = d\lambda\, [F(\sigma_y - \sigma_z)^2 + G(\sigma_z - \sigma_x)^2 + H(\sigma_x - \sigma_y)^2] \,. \tag{A.8}$$

From equation (A.5) we get

$$\bar{\sigma} = \sqrt{3/2}\, \left[\frac{F(\sigma_y - \sigma_z)^2 + G(\sigma_z - \sigma_x)^2 + H(\sigma_x - \sigma_y)^2}{F + G + H}\right]^{\frac{1}{2}} \tag{A.9}$$

$$\text{or,}\quad \frac{2}{3}\,\bar{\sigma}^2 (F + G + H) = F(\sigma_y - \sigma_z)^2 + G(\sigma_z - \sigma_x)^2 + H(\sigma_x - \sigma_y)^2 \,. \tag{A.10}$$

From equations (A.7), (A.8) and (A.9) we obtain

$$d\lambda = \frac{3}{2}\, \frac{1}{(F + G + H)}\, \frac{d\bar{\varepsilon}}{\bar{\sigma}} \tag{A.11}$$

By substituting equation (A.11) into equations (A.6) we get

$$\begin{aligned}
\sigma_x - \sigma_y &= \frac{2}{3}\, \frac{\bar{\sigma}}{d\bar{\varepsilon}}\, \left(\frac{F + G + H}{FG + GH + FH}\right) (F\, d\varepsilon_x - G\, d\varepsilon_y) \,, \\
\sigma_y - \sigma_z &= \frac{2}{3}\, \frac{\bar{\sigma}}{d\bar{\varepsilon}}\, \left(\frac{F + G + H}{FG + GH + FH}\right) (G\, d\varepsilon_y - H\, d\varepsilon_z) \,, \\
\sigma_z - \sigma_x &= \frac{2}{3}\, \frac{\bar{\sigma}}{d\bar{\varepsilon}}\, \left(\frac{F + G + H}{FG + GH + FH}\right) (H\, d\varepsilon_z - F\, d\varepsilon_x) \,.
\end{aligned} \tag{A.12}$$

An expression for the equivalent strain increment $d\bar{\varepsilon}$ may be derived as follows:

From equations (A.7) and (A.8),

$$d\bar{\varepsilon} = \frac{d\lambda\,[F(\sigma_y - \sigma_z)^2 + G(\sigma_z - \sigma_x)^2 + H(\sigma_x - \sigma_y)^2]}{\bar{\sigma}}.$$

By substituting equations (A.6) and (A.9) into the above, it can be shown that

$$d\bar{\varepsilon} = \sqrt{2/3}\,\frac{(F + G + H)^{\frac{1}{2}}}{(FG + GH + FH)}\,[F(G\,d\varepsilon_y - H\,d\varepsilon_z)^2 + G(H\,d\varepsilon_z - F\,d\varepsilon_x)^2 + H(F\,d\varepsilon_x - G\,d\varepsilon_y)^2]^{\frac{1}{2}}. \qquad (A.13)$$

APPENDIX B

DEEP DRAWING COMPUTER PROGRAMME

```
      MASTER STRSTR
      COMMON C1,C2,C3,C4,C5,C6,C7,C8,C9,G,TA
      DIMENSION T(100,12),R2(100,12),E1(100,12),E2(100,12),S3(100,12),S4
     1(100,12),R(100,12),S5(100,12),E3(100,12),FI(100,12),D1(100,12),D2(
     2100,12),D3(100,12),S2(100,12),RO(100,12),TS(100,12),RC(12),AB(100,
     312),Y1(100,12),Y2(100,12),YS(100,12),CH(100,12),PC(12),FBC(12),WS(
     4100,12),TOS(100,12),R7(100,12),ER(100,12),STG(12),RA(12)
C     THIS IS A NUMERICAL SOLUTION OF THE DEEP DRAWING PROBLEM THROUGH
C     A CONVEX TYPE DIE WITHOUT A BLANK-HOLDER.
C     THIS PROGRAM EVALUATES THE STRESSES ,STRAINS ,PUNCH LOAD ,ETC....
```

```
C       WHICH OCCUR IN THE CUP DURING THE DEEP DRAWING PROCESS.
C       NUMB: NO. OF CASES TO BE STUDIED.
        READ(1,981)NUMB
        NF=0
  982   NF=NF+1
        WRITE(2,700)
C       M: NO. OF STEPS .
C       N: NO. OF STAGES .
C       R1: THEORETICAL DIE LIP RADIUS,MEASURED AT Y=0. ,(MM) .
C       R3: PUNCH RADIUS,(MM).
C       R6: BLANK RADIUS,(MM).
C       A3 AND A4: CONSTANTS OF DIE PROFILE CURVE,(MM) .
C       ACC,PRE,AC1 AND PR1:ACCURACIES FOR APPROXIMATING STEPS BOUNDARIES.
        READ(1,29)M,N,R1,R6,R3,A3,A4,ACC,PRE,AC1,PR1
        WRITE(2,701)M,N,R1,R6,R3,A3,A4
        WRITE(2,702)ACC,PRE,AC1,PR1
C       PR: PUNCH PROFIE RADIUS, IN(MM).
C       PBR;PUNCH FLAT BASE RADIUS, (MM).
C       AC4: ACCURACY FOR APPROXIMATING EDGE BOUNDARY CONDITIONS.
C       W: COEFFICIENT OF FRICTION BETWEEN MATERIAL AND PUNCH.
        READ(1,345)PR,PBR,AC4,W
        WRITE(2,703)PR,PBR,AC4,W
C       ME: CONSTANT, IF EQUAL ZERO TOTAL STRAINS ARE USED . IF GREATER
C       THAN ONE INCREMENTAL STRAINS ARE ASSUMED.
C       KN: MAXIMUM NO. OF ITERATIONS ALLOWED FOR CONVERGANCE.
C       NN: MAXIMUM NO. OF ITERATIONS ALLOWED FOR APPROXIMATING THE
C       INTERMEDIATE BOUNDARIES.
C       DD2: INCREMENT USED FOR HALVING THE STEP WIDTH WHEN CHANGING
C       INITIAL RADII AT DIFFERENT BOUNDARIES,(MM).
        READ(1,900)ME,KN,NN,DD2
        WRITE(2,704)ME,KN,NN,DD2
C       R2: INITIAL RADII OF ELEMENTS,(MM).
        READ(1,17)(R2(I,1),I=1,M)
        WRITE(2,705)(R2(I,1),I=1,M)
C       G: AVERAGE STRAIN RATIO.
C       U: COEFFICIENT OF FRICTION BETWEEN MATERIAL AND DIE.
C       C1-C9: CONSTANTS OF MATERIAL WORKHARDENING RELATIONS DEFINED AS
C       FOLLOWS:
C         1.  S=C3*(E**C4)  FOR E LESS OR EQUAL C1 .
C         2.  S=C5+C6*E   FOR E BETWEEN C1 AND C2 .
C         3.  S=C7+C8*((E-C2)**C9)   FOR E GREATER THAN C2 .
C       WHERE S IS MEASURED IN(MN PER METRE SQUARED) .
C       TA: INITIAL THICKNESS OF MATERIAL,(MM).
        READ(1,10)G,U,C1,C2,C3,C4,C5,C6,C7,C8,C9,TA
        WRITE(2,706)G,U,C1,C2,C3,C4
        WRITE(2,707)C5,C6,C7,C8,C9,TA
C       RA: CUP INNER LIP RADIUS OF A PREDETERMINED STAGE OF DRAWING,(MM).
        READ(1,39)(RA(J),J=2,N)
        WRITE(2,708)(RA(J),J=2,N)
C       RC: ROUGH ESTIMATE OF THE INITIAL ELEMENT NO. WHICH CORRESPONDS TO
C       THE CONTACT BOUNDARY BETWEEN MATERIAL AND DIE FOR A CERTAIN STAGE
C       OF DRAWING.
        READ(1,39)(RC(J),J=2,N)
        WRITE(2,709)(RC(J),J=2,N)
C       STG:CONSTANT, IF GREATER THAN ONE IT CAUSES NO CHANGES IN THE DIE
C       CONTACT RADIUS TO BE CARRIED OUT .
        READ(1,39)(STG(J),J=2,N)
        WRITE(2,710)(STG(J),J=2,N)
        WRITE(2,25)NF
        JO=1
```

```
C       START A NEW STAGE.
 101    J=JO+1
        WRITE(2,79)JO
C       SET CONSTANTS OF MONITORING BOUNDARY CONDITIONS TO THIER INITIAL
C       VALUES.
        DD1=DD2
        DD3=0.1
        IS=0
        IT=0
        NB=0
        NC=0
        N9=0
        M9=0
        CALL CONS(JA,JZ,JJ,JN,JOK,JOD,JS,DD2,AC3,DD4,N5,N6,N7,N8)
C       SELECT INCREMENTAL OR TOTAL STRAINS MODE.
        IF(ME.GT.1)GO TO 621
        DO 19 I=1,M
        R2(I,J)=R2(I,1)
        E1(I,(J-1))=0.
        E2(I,(J-1))=0.
        E3(I,(J-1))=0.
   19   CONTINUE
        GO TO 643
  621   DO 622 I=1,M
        R2(I,J)=R2(I,(J-1))
  622   CONTINUE
C       START THE DIE CONTACT ZONE.
C       START AT THE CUP EDGE RADIUS.
  643   I=0
C       SET THE INNER RADIUS OF CUP EDGE TO ITS GIVEN VALUE.
        FI((I+1),J)=FI((I+1),(J-1))
  605   NO=0
        E=R1-A3*(COS(FI((I+1),J))+FI((I+1),J)*SIN(FI((I+1),J))-1.)-A4*(2.*
       1FI((I+1),J)*COS(FI((I+1),J))+(FI((I+1),J)**2.-2.)*SIN(FI((I+1),J))
       2)
        R((I+1),J)=E
  600   NO=NO+1
        X=E-R((I+1),J)-0.5*TA*SIN(FI((I+1),J))*((R6/R((I+1),J))**(1./(1.+G
       1)))
        Z=-1.+0.5*TA*SIN(FI((I+1),J))*(R6**(1./(1.+G)))*(R((I+1),J)**((-2.
       1-G)/(1.+G)))/(1.+G)
        R((I+1),J)=R((I+1),J)-X/Z
        IF(NO.GT.KN)STOP
        X=ABS(X/Z)
        IF(X.GT.AC4)GO TO 600
        T((I+1),J)=TA*((R6/R((I+1),J))**(1./(1.+G)))
        IF(ABS(((R((I+1),J)-0.5*T((I+1),J)*SIN(FI((I+1),J)))/RA(J))-1.).LT
       1.ACC)GO TO 243
        IF((R((I+1),J)-0.5*T((I+1),J)*SIN(FI((I+1),J))).GT.RA(J))GO TO 244
        GO TO 245
  244   M8=1
        IF(M9.GE.1)GO TO 246
        FI((I+1),J)=FI((I+1),J)+DD3
        N9=N9+1
        GO TO 605
  245   M8=-1
        IF(N9.GE.1)GO TO 246
        FI((I+1),J)=FI((I+1),J)-DD3
        M9=M9+1
        GO TO 605
```

```
 246  DD3=DD3/2.
      FI((I+1),J)=FI((I+1),J)+DD3*M8
      GO TO 605
C     CALCULATE STRESSES AND STRAINS FROM PLASTICITY RELATIONS.
 243  CALL STR(I,J,R,R2,E1,E2,E3,S2,S3,S4,D1,D2,D3,T)
      RO((I+1),J)=A3*FI((I+1),J)+A4*(FI((I+1),J)**2.)
C     START THE SECOND STEP IN THE DIE CONTACT ZONE.
      I=1
C     ASSUME THE VALUE OF THICKNESS.
      T((I+1),J)=T(I,J)
  75  K=0
C     APPROXIMATE THE VALUE OF THE DIE CONTACT ANGLE.
  70  K=K+1
      ID=I
      IF(K.GT.KN)GO TO 500
  50  V=4.*ASIN(1.)*TA*(R2(I,J)**2.-R2((I+1),J)**2.)/(T((I+1),J)+T(I,J))
      F1=FI(I,J)+V/(4.*ASIN(1.)*R(I,J)*RO(I,J))
      NO=0
  91  NO=NO+1
      Y=4.*ASIN(1.0)*((R1+A3)*(T((I+1),J)+T(I,J))*(F1-FI(I,J))/4.+0.5*(R
     11+A3)*A3*(F1**2.-FI(I,J)**2.)+(R1+A3)*A4*(F1**3.-FI(I,J)**3.)/3.+(
     220.*A3*A4-0.75*A3*(T((I+1),J)+T(I,J)))*(SIN(F1)-SIN(FI(I,J)))-(3.*
     3(A3**2.)+2.0*A4*(T((I+1),J)+T(I,J))-40.*(A4**2.)-0.0625*((T((I+1),
     4J)+T(I,J))**2.))*(COS(F1)-COS(FI(I,J)))-(3.*(A3**2.)+1.5*A4*(T((I+
     51),J)+T(I,J))-40.*(A4**2.))*(F1*SIN(F1)-FI(I,J)*SIN(FI(I,J)))-(20.
     6*A3*A4-A3*0.5*(T((I+1),J)+T(I,J)))*(F1*COS(F1)-FI(I,J)*COS(FI(I,J)
     7))-9.*A3*A4*((F1**2.)*SIN(F1)-(FI(I,J)**2.)*SIN(FI(I,J))))
      X=Y+4.*ASIN(1.0)*((A3**2.+A4*0.5*(T((I+1),J)+T(I,J))-20.*(A4**2.))
     1*((F1**2.)*COS(F1)-(FI(I,J)**2.)*COS(FI(I,J)))-6.*(A4**2.)*((F1**3
     2.)*SIN(F1)-(FI(I,J)**3.)*SIN(FI(I,J)))+2.*A3*A4*((F1**3.)*COS(F1)-
     3(FI(I,J)**3.)*COS(FI(I,J)))+(A4**2.)*((F1**4.)*COS(F1)-(FI(I,J)**4
     4.)*COS(FI(I,J))))-V
      Z=4.*ASIN(1.0)*(R1-A3*(COS(F1)+F1*SIN(F1)-1.)-A4*(2.*F1*COS(F1)+(F
     11**2.-2.)*SIN(F1))-(T((I+1),J)+T(I,J))*SIN(F1)/4.)*(A3*F1+A4*(F1**
     22.)+(T((I+1),J)+T(I,J))/4.)
      FI((I+1),J)=F1-X/Z
      X=ABS(X/Z)
      IF(X.LT.ACC)GO TO 90
      F1=FI((I+1),J)
      IF(NO.GT.KN)GO TO 500
      GO TO 91
C     CHECK WHETHER THE VALUE OF THE DIE CONTACT ANGLE IS IN THE
C     WORKING RANGE OR NOT.
  90  IF(FI((I+1),J).GE.ASIN(1.))GO TO 1000
      R((I+1),J)=R1-A3*(COS(FI((I+1),J))+FI((I+1),J)*SIN(FI((I+1),J))-1.
     1)-A4*(2.*FI((I+1),J)*COS(FI((I+1),J))+(FI((I+1),J)**2.-2.)*SIN(FI(
     2(I+1),J)))-T((I+1),J)*SIN(FI((I+1),J))/2.
C     CALCULATE STRESSES AND STRAINS FROM PLASTICITY RELATIONS.
      CALL STR(I,J,R,R2,E1,E2,E3,S2,S3,S4,D1,D2,D3,T)
      RO((I+1),J)=A3*FI((I+1),J)+A4*(FI((I+1),J)**2.)
C     FIND THE VALUE OF THE UNIT-TANGENTIAL FORCE FROM EQUILIBRIUM
C     EQUATION.
      S5((I+1),J)=(S5(I,J)*(2.0+(FI((I+1),J)-FI(I,J))*(COS(FI(I,J))*((RO
     1(I,J)+0.5*T(I,J))/R(I,J))+U))-(FI((I+1),J)-FI(I,J))*(S3(I,J)*T(I,J
     2)*(COS(FI(I,J))+U*SIN(FI(I,J)))*((RO(I,J)+0.5*T(I,J))/R(I,J))+S3((
     3I+1),J)*T((I+1),J)*(COS(FI((I+1),J))+U*SIN(FI((I+1),J)))*((RO((I+1
     4),J)+0.5*T((I+1),J))/R((I+1),J))))/(2.-(FI((I+1),J)-FI(I,J))*(COS(
     5FI((I+1),J))*((RO((I+1),J)+0.5*T((I+1),J))/R((I+1),J))+U))
      IF(S4((I+1),J).LT.0.)GO TO 80
      IF(S3((I+1),J).GT.0.)GO TO 80
```

```
      E=ABS((S4((I+1),J)*T((I+1),J)/S5((I+1),J))-1.)
C     COMPARE THE VALUE OF THE UNIT-TANGENTIAL FORCE OBTAINED FROM
C     EQUILIBRIUM EQUATION WITH THAT OBTAINED FROM PLASTICITY RELATION.
      IF(E.GT.PRE)GO TO 83
      IF(JZ.GE.1)GO TO 190
      IC=I
C     CHECK THE END OF THE DIE CONTACT ZONE.
      IF(I.GE.RC(J))GO TO 154
C     START A NEW STEP IN THE DIE CONTACT ZONE.
      I=I+1
      IF(I.EQ.2)GO TO 82
      IF(I.GE.M)GO TO 84
C     ASSUME THE VALUE THICKNESS.
      T((I+1),J)=3.*T(I,J)-3.*T((I-1),J)+T((I-2),J)
      GO TO 75
   82 T((I+1),J)=2.*T(I,J)-T((I-1),J)
      GO TO 75
C     ASSUME A NEW VALUE OF THICKNESS.
   80 CALL APP(I,J,D1,D3,E2,S2,S5,T)
      IF(T((I+1),J).LT.(TA/20.))GO TO 500
      GO TO 70
C     START THE STRETCHING ZONE BETWEEN PUNCH AND DIE.
  154 ID=I
      K=0
  142 NU=0
      NU=0
  143 NU=NU+1
      IF((R(I,J)**2.).LT.(2.*(R2(I,J)**2.-R2((I+1),J)**2.)*TA*COS((FI((I
     1+1),J)+FI(I,J))/2.)/(T(I,J)+T((I+1),J))))GO TO 500
      R((I+1),J)=SQRT(R(I,J)**2.-2.*(R2(I,J)**2.-R2((I+1),J)**2.)*TA*COS
     1((FI((I+1),J)+FI(I,J))/2.)/(T(I,J)+T((I+1),J)))
C     COMPUTE STRESSES AND STRAINS FROM PLASTICITY RELATIONS.
      CALL STR(I,J,R,R2,E1,E2,E3,S2,S3,S4,D1,D2,D3,T)
C     FIND THE VALUE OF THE UNIT-TANGENTIAL FORCE FROM EQUILIBRIUM
C     EQUATION.
      S5((I+1),J)=(2.*S5(I,J)+(R((I+1),J)-R(I,J))*(((S3(I,J)-S4(I,J))*T(
     1I,J)/R(I,J))+(S3((I+1),J)*T((I+1),J)/R((I+1),J))))/(2.+((R((I+1),J
     2)-R(I,J))/R((I+1),J)))
      IF(S4((I+1),J).LT.0.)GO TO 144
      E=ABS((S4((I+1),J)*T((I+1),J)/S5((I+1),J))-1.)
C     COMPARE THE VALUE OF UNIT-TANGENTIAL FORCE OBTAINED FROM EQUILIBR-
C     IUM EQUATION WITH THAT OBTAINED FROM PLASTICITY RELATION.
      IF(E.LT.AC1)GO TO 754
  144 NO=NO+1
      IF(NU.GT.15)GO TO 754
C     ASSUME A NEW VALUE OF THE THICKNESS.
  151 CALL APP(I,J,D1,D3,E2,S2,S5,T)
      IF(T((I+1),J).LT.(TA/20.))GO TO 500
      IF(K.GT.KN)GO TO 500
      GO TO 143
  754 KK=RC(J)
C     CHECK WHETHER THE ASSUMED VALUE OF THE ANGLE IS CORRECT OR NOT.
      IF(ABS(S5(KK,J)*R(KK,J)*SIN(FI(KK,J))/(S5((I+1),J)*R((I+1),J))).GT
     1.(1.0))GO TO 1002
      F=ASIN(R(KK,J)*S5(KK,J)*SIN(FI(KK,J))/(R((I+1),J)*S5((I+1),J)))
      X=ABS((FI((I+1),J)/F)-1.)
      IF(X.LT.PR1)GO TO 170
C     ASSUME A NEW VALUE OF THE ANGLE.
      FI((I+1),J)=(FI((I+1),J)+F)/2.
      K=K+1
```

```
      IF(K.GT.KN)GO TO 500
      GO TO 142
 1002  K=K+1
C     ASSUME A NEW VALUE OF THE ANGLE.
      FI((I+1),J)=ATAN(R(KK,J)*S5(KK,J)*SIN(FI(KK,J))/(R((I+1),J)*S5((I+
     11),J)*COS(FI((I+1),J))))
      IF(K.LT.KN)GO TO 142
      WRITE(2,1003)
      GO TO 500
 170  IF(E.GT.AC1)GO TO 151
      IF(JS.GE.1)GO TO 190
      IF(JOK.GE.1)GO TO 191
      IF(JJ.GE.1)GO TO 192
C     CHECK THE END OF THE ZONE BETWEEN DIE AND PUNCH.
      IF((R3-R((I+1),J)+0.5*T((I+1),J)*SIN(FI((I+1),J))).GT.(PR*(1.-SIN(
     1FI((I+1),J))))))GO TO 105
      IF(JN.GE.1)GO TO 523
      I=I+1
 145  IF(I.GE.M)GO TO 84
      CALL EXT(I,J,FI,T,R2)
      GO TO 154
 105  IS=I
C     CHANGE THE INITIAL RADIUS WHICH CORRESPONDS TO THE PUNCH PROFILE
C     CONTACT RADIUS,AND ALL PREVIOUS STAGES AS APROPRIATE.
      IF(ABS(((R3-R((I+1),J)+0.5*T((I+1),J)*SIN(FI((I+1),J)))/(PR*(1.-SI
     1N(FI((I+1),J)))))-1.).LT.AC1)GO TO 106
      IF(N6.GT.NN)GO TO 366
      IF((R2(I,J)-R2((I+1),J)).LE.AC3)GO TO 527
      IF(N7.LT.1)GO TO 528
      AC3=AC3/2.
      N6=N6+1
 528  JA=JA+1
      R2((I+1),J)=R2((I+1),J)+AC3
      JJ=JJ+1
      JN=JN+1
      GO TO 127
 523  N7=N7+1
      IF(N6.GT.NN)GO TO 366
      R2((IS+1),J)=R2((IS+1),J)-AC3
      GO TO 105
 527  AC3=AC3/2.
      N6=N6+1
      GO TO 105
 127  JUN=J
      IF(ME.LT.1)GO TO 128
      J=1
 192  J=J+1
      IF(J.GE.JUN)GO TO 128
      R2((I+1),J)=R2((I+1),JUN)
      KK=FBC(J)
      IF(R2((IS+1),JUN).LE.R7(KK,J))GO TO 192
      T((I+1),J)=(R2((I+1),J)-R2(I,J))*(T(I,J)-T((I-1),J))/(R2(I,J)-R2((
     1I-1),J))+T(I,J)
      KK=PC(J)
      IF(R2((IS+1),JUN).LT.R7(KK,J))GO TO 107
      FI((I+1),J)=FI(I,J)+(FI(I,J)-FI((I-1),J))*(R2((I+1),J)-R2(I,J))/(R
     12(I,J)-R2((I-1),J))
      GO TO 154
 128  JA=3
```

```
      CALL EXT(I,J,FI,T,R2)
      GO TO 154
C     START A NEW STEP IN THE PUNCH PROFILE CONTACT ZONE.
 106  I=I+1
      IF(I.GE.M)GO TO 84
      ID=I
C     EXTRAPOLATE THE VALUE OF THICKNESS.
      T((I+1),J)=(R2((I+1),J)-R2(I,J))*(T(I,J)-T((I-1),J))/(R2(I,J)-R2((
     1I-1),J))+T(I,J)
 107  K=0
C     APPROXIMATE THE VALUE OF THE PUNCH PROFILE CONTACT ANGLE.
 111  K=K+1
      F1=FI(I,J)-TA*(R2(I,J)**2.-R2((I+1),J)**2.)/((PR+0.25*(T(I,J)+T((I
     1+1),J)))*(R(I,J)*(T((I+1),J)+T(I,J))))
      NO=0
 108  NO=NO+1
      X=(R2((I+1),J)**2.-R2(I,J)**2.)*TA+((PR+0.25*(T((I+1),J)+T(I,J)))*
     1*2.)*((PBR*(FI(I,J)-F1)/(PR+0.25*(T((I+1),J)+T(I,J))))-(COS(FI(I,J
     2))-COS(F1)))*(T((I+1),J)+T(I,J))
      Z=-((PR+0.25*(T((I+1),J)+T(I,J)))**2.)*((PBR/(PR+0.25*(T((I+1),J)+
     1T(I,J))))+SIN(F1))*(T((I+1),J)+T(I,J))
      FI((I+1),J)=F1-X/Z
      X=ABS(X/Z)
      IF(X.LT.ACC)GO TO 109
      F1=FI((I+1),J)
      IF(NO.GT.KN)GO TO 500
      GO TO 108
 109  R((I+1),J)=R3-PR+(PR+0.5*T((I+1),J))*SIN(FI((I+1),J))
C     CALCULATE STRESSES AND STRAINS FROM PLASTICITY RELATIONS.
      CALL STR(I,J,R,R2,E1,E2,E3,S2,S3,S4,D1,D2,D3,T)
C     FIND THE VALUE OF THE UNIT-TANGENTIAL FORCE FROM EQUILIBRIUM
C     EQUATION.
      S5((I+1),J)=(S5(I,J)*(2.+(FI((I+1),J)-FI(I,J))*(COS(FI(I,J))*((PR+
     10.5*T(I,J))/R(I,J))+W))-(FI((I+1),J)-FI(I,J))*(S3(I,J)*T(I,J)*(COS
     2(FI(I,J))+W*SIN(FI(I,J)))*((PR+0.5*T(I,J))/R(I,J))+S3((I+1),J)*T((
     3I+1),J)*(COS(FI((I+1),J))+W*SIN(FI((I+1),J)))*((PR+0.5*T((I+1),J))
     4/R((I+1),J))))/(2.-(FI((I+1),J)-FI(I,J))*(COS(FI((I+1),J))*((PR+0.
     55*T((I+1),J))/R((I+1),J))+W))
      E=ABS((S4((I+1),J)*T((I+1),J)/S5((I+1),J))-1.)
C     COMPARE THE VALUE OF THE UNIT-TANGENTIAL FORCE OBTAINED FROM EQUI-
C     LIBRIUM EQUATION WITH THAT OBTAINED FROM PLASTICITY RELATION.
      IF(E.LT.PRE)GO TO 116
C     ASSUME A NEW VALUE OF THE THICKNESS.
 115  CALL APP(I,J,D1,D3,E2,S2,S5,T)
      IF(T((I+1),J).LT.(TA/20.))GO TO 500
      IF(K.GT.KN)GO TO 500
      GO TO 111
 116  IF(JOD.GE.1)GO TO 191
      IF(JA.GE.1)GO TO 192
C     CHECK THE END OF THE PUNCH PROFILE CONTACT ZONE.
      IF(FI((I+1),J).LT.0.)GO TO 135
      IF(FI((I+1),J).LT.ACC)GO TO 118
      IF(JOK.GE.1)GO TO 520
      IF(S4((I+1),J).LT.0.)GO TO 84
      GO TO 106
 135  IT=I
C     CHANGE THE INITIAL RADIUS WHICH CORRESPONDS TO THE PUNCH FLAT
C     BASE RADIUS,AND ALL PREVIOUS STAGES AS APROPRIATE.
      IF(N5.GT.NN)GO TO 366
      IF((R2(I,J)-R2((I+1),J)).LE.DD4)GO TO 526
```

```
      IF(N8.LT.1)GO TO 529
      DD4=DD4/2.
      N5=N5+1
  529 JOK=JOK+1
      R2((I+1),J)=R2((I+1),J)+DD4
      JOD=JOD+1
      JUN=J
      IF(ME.LT.1)GO TO 137
      J=1
  191 J=J+1
      IF(J.GE.JUN)GO TO 137
      R2((I+1),J)=R2((I+1),JUN)
      KK=FBC(J)
      IF(R2((IT+1),JUN).LE.R7(KK,J))GO TO 191
      T((I+1),J)=(R2((I+1),J)-R2(I,J))*(T(I,J)-T((I-1),J))/(R2(I,J)-R2((
     1I-1),J))+T(I,J)
      KK=PC(J)
      IF(R2((IT+1),JUN).LT.R7(KK,J))GO TO 107
      FI((I+1),J)=FI(I,J)+(FI(I,J)-FI((I-1),J))*(R2((I+1),J)-R2(I,J))/(R
     12(I,J)-R2((I-1),J))
      GO TO 104
  137 JOD=0
      CALL EXT(I,J,FI,T,R2)
      GO TO 107
  520 N8=N8+1
      IF(N5.GT.NN)GO TO 366
      R2((IT+1),J)=R2((IT+1),J)-DD4
      GO TO 135
  526 DD4=DD4/2.
      N5=N5+1
      GO TO 135
  118 I=I+1
      IF(I.GE.M)GO TO 84
      ID=I
      E1((I+1),J)=E1(I,J)
      E2((I+1),J)=E2(I,J)
      E3((I+1),J)=E3(I,J)
      GO TO 118
C     CONVERGENCE IS NOT OBTAINED.
C     ASSIGN STRESSES AND STRAINS TO ZERO AND MAKE ONE STEP BACKWARD.
  500 E1((I+1),J)=0.
      E2((I+1),J)=0.
      E3((I+1),J)=0.
      S3((I+1),J)=0.
      S4((I+1),J)=0.
      ID=ID-1
C     CHECK WHETHER THE BOUNDARY CONDITION AT THE PUNCH FLAT BASE RADIUS
C     IS VERIFIED OR NOT.
   84 IF(STG(J).GT.1.)GO TO 83
      CALL CONS(JA,JZ,JJ,JN,JOK,JOD,JS,DD2,AC3,DD4,N5,N6,N7,N8)
C     CHANGE THE INITIAL RADIUS WHICH CORRESPONDS TO THE DIE CONTACT
C     RADIUS, AND ALL PREVIOUS STAGES AS APROPRIATE.
      IF(2.*E1((ID+1),J).LT.(-E2((ID+1),J)))GO TO 153
      IF(ABS((2.*E1((ID+1),J)/E2((ID+1),J))+1.).LT.AC4)GO TO 83
      IF(NC.GE.1)GO TO 850
      NB=NB+1
      RC(J)=RC(J)-1.
      GO TO 193
  153 IF(ABS((2.*E1((ID+1),J)/E2((ID+1),J))+1.).LT.AC4)GO TO 83
      IF(NB.GE.1)GO TO 800
```

```
      RC(J)=RC(J)+1.
      GO TO 193
  195 IS=0
      IT=0
      I=IC-2
      GO TO 75
  193 IF(ME.GT.1)GO TO 620
  623 R2((IT+1),J)=R2((IT+1),1)
      R2((IS+1),J)=R2((IS+1),1)
      GO TO 195
  620 IF(J.GT.2)GO TO 788
      R2((IT+1),J)=R2((IT+1),(J-1))
      R2((IS+1),J)=R2((IS+1),(J-1))
      GO TO 195
  788 R2((IS+1),J)=R7((IS+1),(J-1))
      R2((IT+1),J)=R7((IT+1),(J-1))
      JUN=J
      J=1
  194 J=J+1
      IF(J.GE.JUN)GO TO 195
      CALL REVA(IS,IT,J,R2,E1,E2,E3,R,T,FI,S3,S4,S5,R7,WS,TS,TOS,ER,AB,Y
     1S,CH,Y1,Y2)
      GO TO 194
  800 IF(NC.GT.NN)GO TO 83
      IF((R2(IC,J)-R2((IC+1),J)).LE.DD1)GO TO 860
      R2(IC,J)=R2(IC,J)-DD1
  870 DD1=DD1/2.
      NC=NC+1
      GO TO 103
  850 IF(NC.GT.NN)GO TO 83
      IF((R2((IC-1),J)-R2(IC,J)).LE.DD1)GO TO 875
      R2(IC,J)=R2(IC,J)+DD1
      GO TO 870
  860 DD1=DD1/2.
      NC=NC+1
      GO TO 800
  875 DD1=DD1/2.
      NC=NC+1
      GO TO 850
  103 IF(ME.LT.1)GO TO 623
      IF(J.GT.2)GO TO 787
      R2((IS+1),J)=R2((IS+1),(J-1))
      R2((IT+1),J)=R2((IT+1),(J-1))
      GO TO 100
  787 R2((IS+1),J)=R7((IS+1),(J-1))
      R2((IT+1),J)=R7((IT+1),(J-1))
      JUN=J
      J=1
  190 J=J+1
      IF(J.GE.JUN)GO TO 100
      CALL REVA(IS,IT,J,R2,E1,E2,E3,R,T,FI,S3,S4,S5,R7,WS,TS,TOS,ER,AB,Y
     1S,CH,Y1,Y2)
      I=IC-1
      R2(IC,J)=R2(IC,JUN)
      JS=JS+1
      JZ=JZ+1
      KK=RC(J)
      IF(R2(IC,JUN).GT.R7(KK,J))GO TO 75
      JZ=0
      GO TO 154
```

```
 100  I=IC-2
      JZ=0
      JS=0
      IT=0
      IS=0
      GO TO 75
  83  JO=JO+1
C     COMPUTE THE PUNCH STROKE AND THE CUP HEIGHT.
      FBC(J)=IT+1
      PC(J)=IS+1
      DO 356 I=1,ID+1
      AB(I,J)=R(I,J)-T(I,J)*SIN(FI(I,J))/2.
 356  CONTINUE
      DO 555 I=IC,(IS+1)
      Y2((I+1),J)=Y2(I,J)+(AB(I,J)-AB((I+1),J))*TAN((FI(I,J)+FI((I+1),J)
     1)/2.)
 555  CONTINUE
      Y1(1,J)=A3*(SIN(FI(IC,J))-FI(IC,J)*COS(FI(IC,J)))+A4*(2.*FI(IC,J)*
     1SIN(FI(IC,J))+(2.-FI(IC,J)**2.)*COS(FI(IC,J))-2.)-A3*(SIN(FI(1,1))
     2-FI(1,1)*COS(FI(1,1)))-A4*(2.*FI(1,1)*SIN(FI(1,1))+(2.-FI(1,1)**2.
     3)*COS(FI(1,1))-2.)
      Y1(IC,J)=A3*(SIN(FI(IC,J))-FI(IC,J)*COS(FI(IC,J)))+A4*(2.*FI(IC,J)
     1*SIN(FI(IC,J))+(2.-FI(IC,J)**2.)*COS(FI(IC,J))-2.)-A3*(SIN(FI(1,J)
     2)-FI(1,J)*COS(FI(1,J)))-A4*(2.*FI(1,J)*SIN(FI(1,J))+(2.-FI(1,J)**2
     3.)*COS(FI(1,J))-2.)
      YS((IT+1),J)=Y1(1,J)+Y2((IS+1),J)-(PR+T((IS+1),J))*COS(FI((IS+1),J
     1))+PR+TA
      CH((IT+1),J)=Y1(IC,J)+Y2((IS+1),J)-(PR+T((IS+1),J))*COS(FI((IS+1),
     1J))+PR+T((IT+1),J)
C     WRITE THE RESULTS.
      WRITE(2,333)YS((IT+1),J),CH((IT+1),J)
      WRITE(2,18)
      WRITE(2,712)
      DO 666 I=1,IT+1
      ER(I,J)=R(I,J)+T(I,J)*SIN(FI(I,J))/2.
      TOS(I,J)=ALOG(AB(I,J)/R2(I,J))
      TS(I,J)=0.004*ASIN(1.)*R(I,J)*S5(I,J)*SIN(FI(I,J))
      WRITE(2,99)I,AB(I,J),TOS(I,J),E2(I,J),S3(I,J),S4(I,J),S5(I,J),FI(I
     1,J),R2(I,J),TS(I,J),ER(I,J)
      IF(I.EQ.IC)WRITE(2,713)
      IF(I.EQ.IS)WRITE(2,714)
 666  CONTINUE
      IF(ME.LT.1)GO TO 257
C     STORE THE UP TO DATE RESULTS IN A SEPERATE MEMORY FOR FUTURE
C     REFERENCE.
      DO 256 J=2,JO
      DO 256 I=1,ID+1
      R7(I,J)=R2(I,J)
      WS(I,J)=E1(I,J)
      TS(I,J)=E2(I,J)
      TOS(I,J)=E3(I,J)
      ER(I,J)=R(I,J)
      AB(I,J)=T(I,J)
      YS(I,J)=FI(I,J)
      CH(I,J)=S3(I,J)
      Y1(I,J)=S4(I,J)
      Y2(I,J)=S5(I,J)
 256  CONTINUE
 257  J=JO+1
C     CHECK THE NUMBER OF STAGES.
```

```
      IF(J.LE.N)GO TO 101
C     CHECK THE NUMBER OF CASES.
      IF(NF.LT.NUMB)GO TO 982
      STOP
  366 WRITE(2,715)
      STOP
 1000 WRITE(2,880)
      STOP
   10 FORMAT(8F9.4/4F9.4)
   17 FORMAT(10F7.4)
   25 FORMAT(//30X,10HTEST  NO.=,I3)
   29 FORMAT(2I3,2X,5F9.4,2F9.6/2F9.6)
   39 FORMAT(12F6.3)
   69 FORMAT(12F6.2)
   18 FORMAT(1H ,3X,103HI  INNER-RAD  C-STRAIN  T-STRAIN  CIR-STR  TAN-S
     1TR    U-T-FORCE      ANGLE  ELE-RAD      LOAD   OUTER-RAD/8X,4H(MM),
     28X,13H(MN/SQ.METRE),1X,16H(MN.MM/SQ.METRE),2X,5H(RAD),3X,4H(MM),7
     3X,4H(KN),6X,4H(MM))
   99 FORMAT(1H ,2X,I3,2X,F6.2,5X,F7.5,3X,F7.5,2X,F7.2,2X,F7.2,4X,F7.2,6
     1X,F6.4,2X,F8.4,2X,F7.2,4X,F6.2)
  900 FORMAT(3I3,2X,F7.5)
  345 FORMAT(2F6.3,4F9.6)
  981 FORMAT(3I3)
   79 FORMAT(1H ,5X,10HSTAGE NO =,I3)
  777 FORMAT(1H ,5X,3HK =,I3)
  333 FORMAT(//4X,14HPUNCH TRAVEL =,F7.2,1X,4H(MM)/4X,12HCUP HEIGHT =,F7
     1.2,1X,4H(MM))
  883 FORMAT(//4X,17HLARGE STAGE ANGLE)
  504 FORMAT(1H ,4X,2HJ=,I3,2X,3HID=,I3,2X,2HK=,I3,2X,3HNO=,I3)
  611 FORMAT(1H ,4X,3HIS=,I3,2X,3HIT=,I3)
 1003 FORMAT(//4X,15HFI OUT OF RANGE)
  700 FORMAT(//4X,20HTHE GIVEN DATA ARE :)
  701 FORMAT(//4X,3HM =,I3,2X,3HN =,I3,2X,4HR1 =,F9.4,2X,4HR6 =,F9.4,2X,
     14HR3 =,F9.4,2X,4HA3 =,F9.4,2X,4HA4 =,F9.4)
  702 FORMAT(/4X,5HACC =,F9.6,2X,5HPRE =,F9.6,2X,5HAC1 =,F9.6,2X,5HPR1 =
     1,F9.6)
  703 FORMAT(/4X,4HPR =,F9.3,2X,5HPBR =,F6.3,2X,5HAC4 =,F9.6,2X,3HW =,F9
     1.6)
  704 FORMAT(/4X,4HME =,I3,2X,4HKN =,I3,2X,4HNN =,I3,2X,5HDD2 =,F7.5)
  705 FORMAT(/4X,4HR2 =,/(4X,8F9.4))
  706 FORMAT(/4X,3HG =,F9.4,2X,3HU =,F9.4,2X,4HC1 =,F9.4,2X,4HC2 =,F9.4,
     12X,4HC3 =,F9.4,2X,4HC4 =,F9.4)
  707 FORMAT(/4X,4HC5 =,F9.4,2X,4HC6 =,F9.4,2X,4HC7 =,F9.4,2X,4HC8 =,F9.
     14,2X,4HC9 =,F9.4,2X,4HTA =,F9.4)
  708 FORMAT(/4X,4HRA =,(8F8.3))
  709 FORMAT(/4X,4HRC =,(8F8.3))
  710 FORMAT(/4X,5HSTG =,(8F8.3))
  712 FORMAT(/4X,18HDIE CONTACT ZONE :,/)
  713 FORMAT(/4X,28HZONE BETWEEN DIE AND PUNCH :,/)
  714 FORMAT(/4X,28HPUNCH PROFILE CONTACT ZONE :,/)
  715 FORMAT(/4X,18HPLEASE INCREASE NN)
      END

GMENT, LENGTH  3878, NAME  STRSTR

      SUBROUTINE STR(I,J,R,R2,E1,E2,E3,S2,S3,S4,D1,D2,D3,T)
      COMMON C1,C2,C3,C4,C5,C6,C7,C8,C9,G,TA
      DIMENSION R(100,12),E1(100,12),R2(100,12),E3(100,12),S2(100,12),S3
```

```
     1(100,12),S4(100,12),D1(100,12),D2(100,12),D3(100,12),E2(100,12),T(
     2100,12)
C      THIS SUBROUTINE COMPUTES THE STRESSES AND STRAINS ACCORDING TO THE
C      PLASTICITY RELATIONS.
       E2((I+1),J)=ALOG(T((I+1),J)/TA)
       D2((I+1),J)=E2((I+1),J)-E2((I+1),(J-1))
       E1((I+1),J)=ALOG(R((I+1),J)/R2((I+1),J))
       D1((I+1),J)=E1((I+1),J)-E1((I+1),(J-1))
       D3((I+1),J)=SQRT((2.*(2.+G)/(3.*(1.+2.*G)))*(2.*(D1((I+1),J)**2.)+
     1((1.+G)*(D2((I+1),J)**2.))+2.*D1((I+1),J)*D2((I+1),J)))
       E3((I+1),J)=D3((I+1),J)+E3((I+1),(J-1))
       IF(E3((I+1),J).LE.C1)GO TO 204
       IF(E3((I+1),J).LE.C2)GO TO 205
       GO TO 206
 204   S2((I+1),J)=C3*(E3((I+1),J)**C4)
       GO TO 207
 205   S2((I+1),J)=C5+C6*E3((I+1),J)
       GO TO 207
 206   S2((I+1),J)=C7+C8*((E3((I+1),J)-C2)**C9)
 207   S4((I+1),J)=-(2.*(2.+G)*S2((I+1),J)*(D1((I+1),J)+(1.+G)*D2((I+1),J
     1))/(3.*(1.+2.*G)*D3((I+1),J))
       S3((I+1),J)=S4((I+1),J)+((2.*(2.+G)*S2((I+1),J)*(2.*D1((I+1),J)+D2
     1((I+1),J)))/(3.*(1.+2.*G)*D3((I+1),J)))
       RETURN
       END

GMENT, LENGTH    391, NAME  STR


       SUBROUTINE EXT(I,J,FI,T,R2)
       DIMENSION FI(100,12),T(100,12),R2(100,12)
C      THIS SUBROUTINE EXTRAPOLATES NEW VALUES OF THE ANGLE AND THE
C      THICKNESS FROM PREVIOUS STEPS.
       FI((I+1),J)=FI(I,J)+(FI(I,J)-FI((I-1),J))*(R2((I+1),J)-R2(I,J))/(R
     12(I,J)-R2((I-1),J))
       T((I+1),J)=(R2((I+1),J)-R2(I,J))*(T(I,J)-T((I-1),J))/(R2(I,J)-R2((
     1I-1),J))+T(I,J)
       RETURN
       END

GMENT, LENGTH    115, NAME  EXT


       SUBROUTINE APP(I,J,D1,D3,E2,S2,S5,T)
       COMMON C1,C2,C3,C4,C5,C6,C7,C8,C9,G,TA
       DIMENSION D1(100,12),D3(100,12),E2(100,12),S2(100,12),S5(100,12),T
     1(100,12)
C      THIS SUBROUTINE COMPUTES NEW VALUE OF THE THICKNESS FROM THE
C      PLASTICITY RELATIONS.
       T((I+1),J)=TA*EXP(-((((3.*(1.+2.*G)*D3((I+1),J)*S5((I+1),J))/(2.*(
     12.+G)*S2((I+1),J)*T((I+1),J)))+D1((I+1),J))/(1.+G))+E2((I+1),(J-1)
     2))
       RETURN
       END

GMENT, LENGTH    118, NAME  APP
```

```
      SUBROUTINE CONS(JA,JZ,JJ,JN,JOK,JOD,JS,DD2,AC3,DD4,N5,N6,N7,N8)
C     THIS SUBROUTINE SETS THE VALUES OF THE VARIABLES USED TO CONTROL
C     DIFFERENT SEGMENTS OF THE PROGRAM TO THIER INITIAL VALUES.
      DD4=DD2
      AC3=DD2
      JA=0
      JZ=0
      JJ=0
      JN=0
      JOK=0
      JOD=0
      JS=0
      N5=0
      N6=0
      N7=0
      N8=0
      RETURN
      END
```

GMENT, LENGTH 104, NAME CONS

```
      SUBROUTINE REVA(IS,IT,J,R2,E1,E2,E3,R,T,FI,S3,S4,S5,R7,WS,TS,TOS,E
     1R,AB,YS,CH,Y1,Y2)
      COMMON C1,C2,C3,C4,C5,C6,C7,C8,C9,G,TA
      DIMENSION R2(100,12),E1(100,12),E2(100,12),E3(100,12),R(100,12),T(
     1100,12),FI(100,12),S3(100,12),S4(100,12),S5(100,12),R7(100,12),WS(
     2100,12),TS(100,12),TOS(100,12),ER(100,12),AB(100,12),YS(100,12),CH
     3(100,12),Y1(100,12),Y2(100,12)
C     THIS SUBROUTINE ASSIGNS THE VALUES OF STRESSES,STRAINS,,ETC, OF
C     PREVIOUS STAGES TO THEIR MATCHING VARIABLES STORED IN THE
C     REFERENCE MEMORY,WHENEVER A FUTURE CHANGE IN THE DIE CONTACT
C     RADIUS IS CARRIED OUT.
      R2((IS+1),J)=R7((IS+1),J)
      R2((IT+1),J)=R7((IT+1),J)
      E1((IS+1),J)=WS((IS+1),J)
      E2((IS+1),J)=TS((IS+1),J)
      E3((IS+1),J)=TOS((IS+1),J)
      E1((IT+1),J)=WS((IT+1),J)
      E2((IT+1),J)=TS((IT+1),J)
      E3((IT+1),J)=TOS((IT+1),J)
      R((IS+1),J)=ER((IS+1),J)
      R((IT+1),J)=ER((IT+1),J)
      T((IS+1),J)=AB((IS+1),J)
      T((IT+1),J)=AB((IT+1),J)
      FI((IS+1),J)=YS((IS+1),J)
      FI((IT+1),J)=YS((IT+1),J)
      S3((IS+1),J)=CH((IS+1),J)
      S3((IT+1),J)=CH((IT+1),J)
      S4((IS+1),J)=Y1((IS+1),J)
      S4((IT+1),J)=Y1((IT+1),J)
      S5((IS+1),J)=Y2((IS+1),J)
      S5((IT+1),J)=Y2((IT+1),J)
      RETURN
      END
```

GMENT, LENGTH 343, NAME REVA

THE GIVEN DATA ARE :

M = 95 N = 2 R1 = 60.0000 R6 = 60.0000 R3 = 25.0000 A3 = 21.0000 A4 = 45.3000

ACC = 0.000010 PRE = 0.000010 AC1 = 0.000010 PR1 = 0.000010

PR = 10.000 PBR =15.000 AC4 = 0.000010 W = 0.130000

ME = 50 KN =250 NN = 16 DD2 =0.30300

R2 =

60.0000	59.4000	58.8000	58.2000	57.6000	57.0000	56.4000	55.8000
55.2000	54.6000	54.0000	53.4000	52.8000	52.2000	51.6000	51.0000
50.4000	49.8000	49.2000	48.6000	48.0000	47.4000	46.8000	46.2000
45.6000	45.0000	44.4000	43.8000	43.2000	42.6000	42.0000	41.4000
40.8000	40.2000	39.6000	39.0000	38.4000	37.8000	37.2000	36.6000
36.0000	35.4000	34.8000	34.2000	33.6000	33.0000	32.4000	31.8000
31.2000	30.6000	30.0000	29.4000	28.8000	28.2000	27.6000	27.0000
26.4000	25.8000	25.2000	24.6000	24.0000	23.4000	22.8000	22.2000
21.6000	21.0000	20.4000	19.8000	19.2000	18.6000	18.0000	17.7000
17.4000	17.1000	16.8000	16.5000	16.2000	15.9000	15.6000	15.3000
15.0000	14.7000	14.4000	14.1000	13.8000	13.5000	13.2000	12.9000
12.6000	12.3000	12.0000	11.7000	11.4000	11.1000	10.8000	

G = 1.8610 U = 0.0600 C1 = 0.2000 C2 = 0.0000 C3 = 630.0000 C4 = 0.2745

C5 = 0.0000 C6 = 0.0000 C7 = 0.0000 C8 = 560.3450 C9 = 0.2017 TA = 1.5950

RA = 56.000

RC = 16.000

STG = 0.000

TEST NO.= 1

STAGE NO = 1

PUNCH TRAVEL = 19.78 (MM)
CUP HEIGHT = 18.69 (MM)

I	INNER-RAD (MM)	C-STRAIN	T-STRAIN	CIR-STR (MN/SQ.METRE)	TAN-STR	U-T-FORCE (MN.MM/SQ.METRE)	ANGLE (RAD)	ELE-RAD (MM)	LOAD (KN)	OUTER-RAD (MM)
DIE CONTACT ZONE :										
1	56.00	-.06900	0.02192	-275.38	0.00	0.00	0.4488	60.0000	0.00	56.71
2	55.42	-.06937	0.02151	-273.43	2.84	4.62	0.4795	59.4000	0.75	56.17
3	54.85	-.06957	0.02136	-271.27	5.68	9.24	0.5077	58.8000	1.56	55.64
4	54.29	-.06958	0.02055	-268.91	8.52	13.87	0.5337	58.2000	2.42	55.12
5	53.74	-.06942	0.02000	-266.35	11.36	18.48	0.5580	57.6000	3.33	54.60
6	53.20	-.06938	0.01940	-263.58	14.20	23.09	0.5807	57.0000	4.27	54.09
7	52.66	-.06856	0.01876	-260.60	17.03	27.68	0.6022	56.4000	5.23	53.58
8	52.14	-.06787	0.01807	-257.39	19.85	32.25	0.6226	55.8000	6.22	53.09
9	51.62	-.06731	0.01734	-253.95	22.67	36.79	0.6420	55.2000	7.21	52.59
10	51.11	-.06597	0.01657	-250.26	25.47	41.30	0.6605	54.6000	8.22	52.11
11	50.61	-.06474	0.01577	-246.31	28.25	45.78	0.6783	54.0000	9.23	51.63
12	50.12	-.06334	0.01492	-242.08	31.02	50.22	0.6953	53.4000	10.24	51.16
13	49.64	-.06175	0.01404	-237.55	33.76	54.61	0.7117	52.8000	11.24	50.69
14	49.16	-.05997	0.01313	-232.69	36.47	58.94	0.7275	52.2000	12.24	50.24
15	48.69	-.05799	0.01219	-227.47	39.16	63.22	0.7428	51.6000	13.23	49.78
16	48.03	-.05482	0.01079	-219.25	42.94	69.24	0.7638	50.7385	14.62	49.15

ZONE BETWEEN DIE AND PUNCH :

17	47.79	-.05315	0.01025	-215.94	44.34	71.46	0.7393	50.4000	14.62	48.88
18	47.35	-.05044	0.00938	-210.27	46.89	75.49	0.6997	49.8000	14.62	48.39
19	46.89	-.04803	0.00859	-204.80	49.50	79.63	0.6644	49.2000	14.62	47.88
20	46.42	-.04586	0.00787	-199.52	52.18	83.88	0.6330	48.6000	14.62	47.37
21	45.94	-.04391	0.00721	-194.39	54.91	88.21	0.6048	48.0000	14.62	46.85
22	45.44	-.04214	0.00660	-189.39	57.69	92.63	0.5794	47.4000	14.62	46.32
23	44.94	-.04053	0.00603	-184.51	60.53	97.12	0.5564	46.8000	14.62	45.79
24	44.43	-.03907	0.00550	-179.73	63.40	101.69	0.5356	46.2000	14.62	45.25
25	43.91	-.03773	0.00501	-175.03	66.32	106.32	0.5167	45.6000	14.62	44.70
26	43.39	-.03649	0.00454	-170.40	69.29	111.01	0.4994	45.0000	14.62	44.15
27	42.86	-.03536	0.00410	-165.82	72.29	115.78	0.4836	44.4000	14.62	43.60
28	42.32	-.03431	0.00369	-161.28	75.33	120.60	0.4691	43.8000	14.62	43.05
29	41.78	-.03334	0.00329	-156.78	78.42	125.49	0.4557	43.2000	14.62	42.49
30	41.24	-.03244	0.00291	-152.30	81.54	130.44	0.4434	42.6000	14.62	41.93
31	40.69	-.03159	0.00254	-147.84	84.70	135.45	0.4320	42.0000	14.62	41.36
32	40.14	-.03081	0.00219	-143.37	87.91	140.52	0.4216	41.4000	14.62	40.80
33	39.59	-.03008	0.00186	-138.91	91.15	145.66	0.4118	40.8000	14.62	40.23
34	39.04	-.02939	0.00153	-134.43	94.44	150.86	0.4028	40.2000	14.62	39.66
35	38.48	-.02874	0.00121	-129.93	97.76	156.12	0.3945	39.6000	14.62	39.09
36	37.92	-.02813	0.00090	-125.40	101.13	161.45	0.3867	39.0000	14.62	38.52
37	37.36	-.02755	0.00059	-120.84	104.54	166.84	0.3795	38.4000	14.62	37.95
38	36.79	-.02701	0.00030	-116.24	107.99	172.30	0.3728	37.8000	14.62	37.37
39	36.23	-.02649	0.00000	-111.58	111.49	177.83	0.3665	37.2000	14.62	36.80
40	35.66	-.02600	-.00029	-106.87	115.03	183.43	0.3607	36.6000	14.62	36.22
41	35.09	-.02554	-.00057	-102.09	118.62	189.09	0.3554	36.0000	14.62	35.65
42	34.52	-.02509	-.00085	-97.23	122.25	194.82	0.3504	35.4000	14.62	35.07
43	33.95	-.02467	-.00113	-92.29	125.93	200.63	0.3458	34.8000	14.62	34.49
44	33.38	-.02426	-.00141	-87.27	129.65	206.50	0.3415	34.2000	14.62	33.91
45	32.81	-.02387	-.00168	-82.14	133.42	212.44	0.3376	33.6000	14.62	33.33
46	32.23	-.02349	-.00196	-76.90	137.23	218.46	0.3340	33.0000	14.62	32.76
47	31.66	-.02313	-.00223	-71.54	141.10	224.54	0.3307	32.4000	14.62	32.18
48	31.08	-.02278	-.00251	-66.04	145.00	230.70	0.3277	31.8000	14.62	31.60
49	30.51	-.02243	-.00278	-60.40	148.96	236.93	0.3250	31.2000	14.62	31.02
50	29.93	-.02209	-.00306	-54.60	152.96	243.22	0.3225	30.6000	14.62	30.44
51	29.35	-.02176	-.00333	-48.63	157.00	249.58	0.3204	30.0000	14.62	29.85
52	28.78	-.02143	-.00361	-42.46	161.09	256.01	0.3185	29.4000	14.62	29.27

53	28.20	-.02111	-.00389	-36.07	165.21	262.49	0.3169	28.8000	14.62	28.69
54	27.62	-.02078	-.00417	-29.45	169.38	269.03	0.3156	28.2000	14.62	28.11
55	27.04	-.02045	-.00445	-22.56	173.58	275.62	0.3146	27.6000	14.62	27.53
56	26.46	-.02012	-.00472	-15.38	177.81	282.26	0.3138	27.0000	14.62	26.95
57	25.88	-.01978	-.00500	-7.85	182.06	288.93	0.3134	26.4000	14.62	26.37
58	25.30	-.01943	-.00528	0.06	186.33	295.63	0.3132	25.8000	14.62	25.79
59	24.72	-.01907	-.00555	8.42	190.61	302.33	0.3134	25.2000	14.62	25.21
60	24.14	-.01868	-.00582	17.31	194.88	309.03	0.3139	24.6000	14.62	24.63
61	23.57	-.01828	-.00609	26.82	199.13	315.69	0.3147	24.0000	14.62	24.06
62	22.99	-.01785	-.00635	37.10	203.35	322.28	0.3160	23.4000	14.62	23.48
63	22.41	-.01738	-.00660	48.32	207.50	328.78	0.3177	22.8000	14.62	22.90
64	21.83	-.01688	-.00685	60.75	211.55	335.11	0.3200	22.2000	14.62	22.33
65	21.25	-.01633	-.00710	74.74	215.45	341.21	0.3228	21.6000	14.62	21.75
66	20.67	-.01572	-.00737	90.80	219.16	346.99	0.3262	21.0000	14.62	21.18
67	20.10	-.01504	-.00770	109.50	222.58	352.30	0.3305	20.4000	14.62	20.61
68	19.52	-.01429	-.00820	131.26	225.65	356.97	0.3358	19.8000	14.62	20.04
69	18.94	-.01344	-.00901	155.41	228.28	360.84	0.3424	19.2000	14.62	19.47

PUNCH PROFILE CONTACT ZONE :

70	18.42	-.01260	-.01010	177.55	230.23	363.53	0.3495	18.6576	14.62	18.96
71	17.84	-.00888	-.01091	196.96	227.45	358.84	0.2881	18.0000	11.57	18.29
72	17.57	-.00730	-.01123	203.04	226.38	357.04	0.2600	17.7000	10.25	17.98
73	17.30	-.00578	-.01150	207.77	225.39	355.38	0.2320	17.4000	8.98	17.66
74	17.03	-.00431	-.01171	211.37	224.46	353.84	0.2041	17.1000	7.74	17.35
75	16.75	-.00289	-.01185	214.04	223.57	352.39	0.1761	16.8000	6.55	17.03
76	16.48	-.00150	-.01194	215.95	222.72	351.01	0.1481	16.5000	5.40	16.71
77	16.20	-.00013	-.01197	217.22	221.88	349.69	0.1201	16.2000	4.29	16.39
78	15.92	0.00124	-.01196	217.98	221.06	348.39	0.0921	15.9000	3.22	16.06
79	15.64	0.00261	-.01191	218.35	220.24	347.12	0.0641	15.6000	2.19	15.74
80	15.36	0.00400	-.01184	218.43	219.42	345.86	0.0361	15.3000	1.21	15.42
81	15.08	0.00543	-.01175	218.36	218.61	344.60	0.0082	15.0000	0.27	15.09
82	15.00	0.00586	-.01173	218.33	218.37	344.24	0.0000	14.9124	0.00	15.00

APPENDIX C

HILL'S NEW YIELD CRITERION

It can be seen in Figures (6.14) to (6.18) that using Hill's theory [3] the correlation between the tensile and biaxial stess-strain curves is fairly good for mild steel and stainless steel whose γ-values are greater than one. The correlation is poor for aluminium and brass whose γ-values are less than one. This phenomenon agrees with those observed by Bramley and Mellor[18], Pearce* and Dillamore**. It seems that further improvement on Hill's theory is necessary.

According to Mellor and Parmar (1978) and Parmar and Mellor[25] a new yield criterion has been proposed by Hill. For deformation under plane stress, the yield criterion has the form,

$$(1 + 2\gamma)\left|\sigma_1 - \sigma_2\right|^m + \left|\sigma_1 + \sigma_2\right|^m = 2(1 + \gamma)Y^m \qquad (C.1)$$

Y is the yield stress in simple tension, γ is the strain ratio measured in simple tension (assuming zero planar anisotropy) and m is a new index which must be determined experimentally. When m=2 the equation reduces to Hill's original yield criterion, see Appendix (A).

---

* Pearce, R. "Some Aspects of Anisotropic Plasticity in Sheet Metals". Int. J. Mech. Sci., Vol. 10, p. 995 (1968)

** Dillamore, I. L. "The Relevance of Tensile Properties to Sheet Formability". J. Phys. D: Appl. Phys., 7 (1974), p. 979.

If τ_m is the yield shear stress in a torsion test, and σ_b is the yield stress in a diaphragm test, then equation (C.1) can be written as:

$$\left(\frac{\sigma_1 + \sigma_2}{2\sigma_b}\right)^m + \left(\frac{\sigma_1 - \sigma_2}{2\tau_m}\right)^m - 1 = 0 .$$

From the yield criterion the equivalent stress $\bar{\sigma}$ is defined by,

$$\bar{\sigma} = \left[\frac{1}{2(1+\gamma)}\left\{(1+2\gamma)\left|\sigma_1 - \sigma_2\right|^m + \left|\sigma_1 + \sigma_2\right|^m\right\}\right]^{1/m} \qquad (C.2)$$

and from the assumption of equivalence of plastic work it follows that the equivalent strain increment,

$$d\bar{\varepsilon} = \frac{\left[2(1+\gamma)\right]^{1/m}}{2}\left\{\frac{1}{(1+2\gamma)^{1/(m-1)}}\left|d\varepsilon_1 - d\varepsilon_2\right|^{m/(m-1)} + \left|d\varepsilon_1 + d\varepsilon_2\right|^{m/(m-1)}\right\}^{(m-1)/m} . \qquad (C.3)$$

The value of m for a particular material can be determined by comparing the experimental work-hardening characteristics for simple tension and balanced biaxial tension. Assuming rotational symmetry about an axis normal to the sheet in the balanced biaxial tension and considering the conditions at the pole, it is possible, assuming an average γ-value and an average stress-strain curve in simple tension, to predict the variation of the polar stress σ_b with polar thickness strain ε in the balanced biaxial tension. Using equations (C.2) and (C.3) it can be shown that,

$$\sigma_b = \frac{\left[2(1+\gamma)\right]^{1/m}}{2}\,\bar{\sigma} \qquad (C.4)$$

and

$$\varepsilon = \frac{2}{\left[2(1+\gamma)\right]^{1/m}}\,\bar{\varepsilon} . \qquad (C.5)$$

Using the experimental data for soft aluminium and mild

steel(having γ-values less than unity) and applying equations (C.4) and (C.5), Mellor and Parmar (1978) have shown that by choosing certain m-values for these two materials, a good correlation can be achieved between theory and experiment.

FIGURES AND PLATES

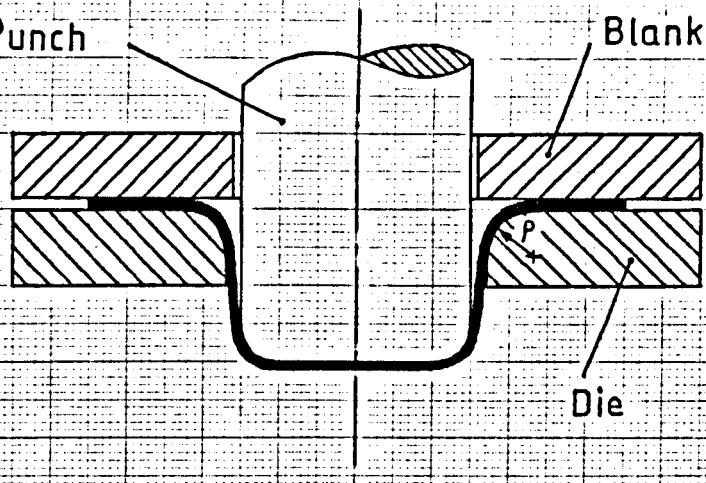

Fig.(2.1)

Conventional deep drawing with a blank-holder

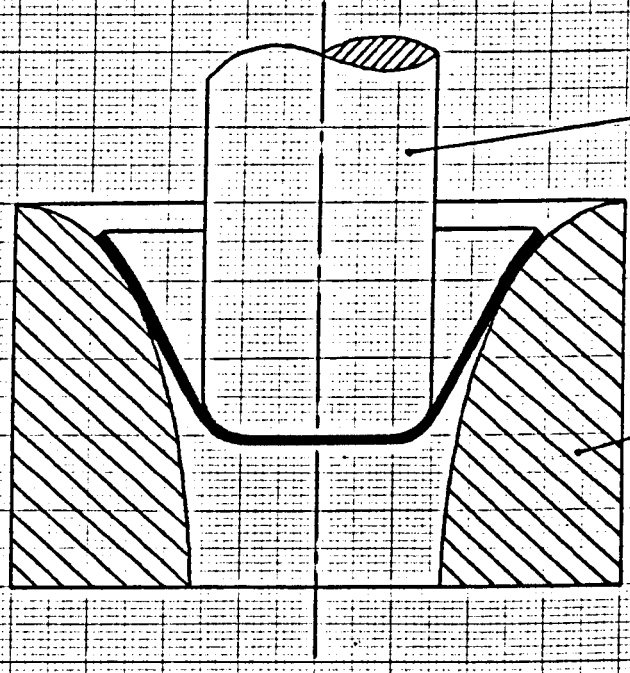

Fig.(2.2)

Deep drawing without a blank-holder

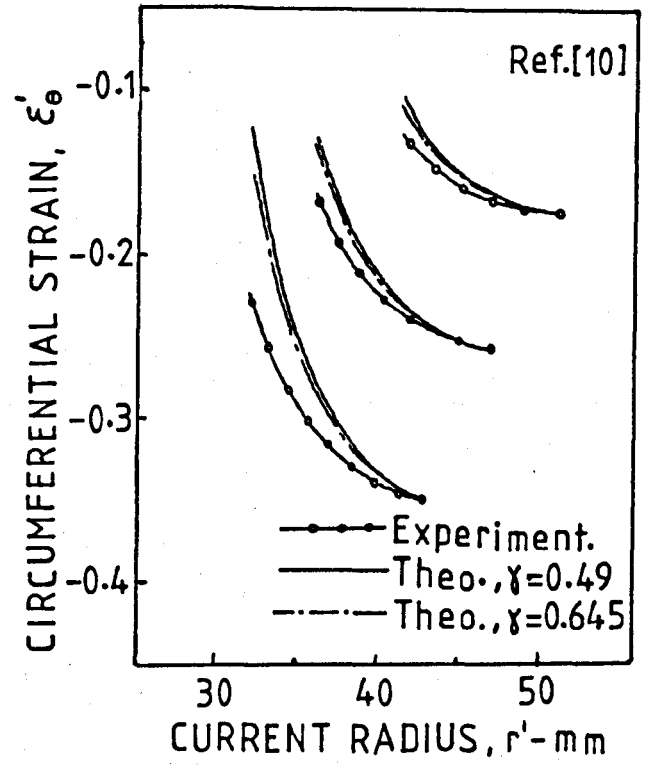

Circumferential Strains

Fig.(2.3)

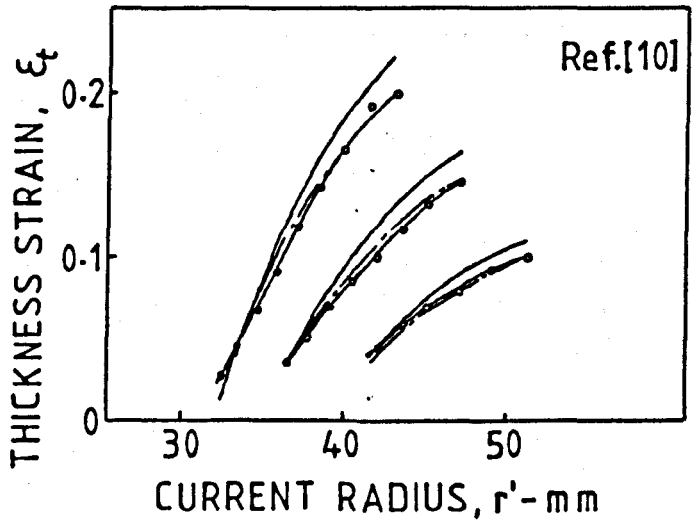

Thickness Strains

Fig.(2.4)

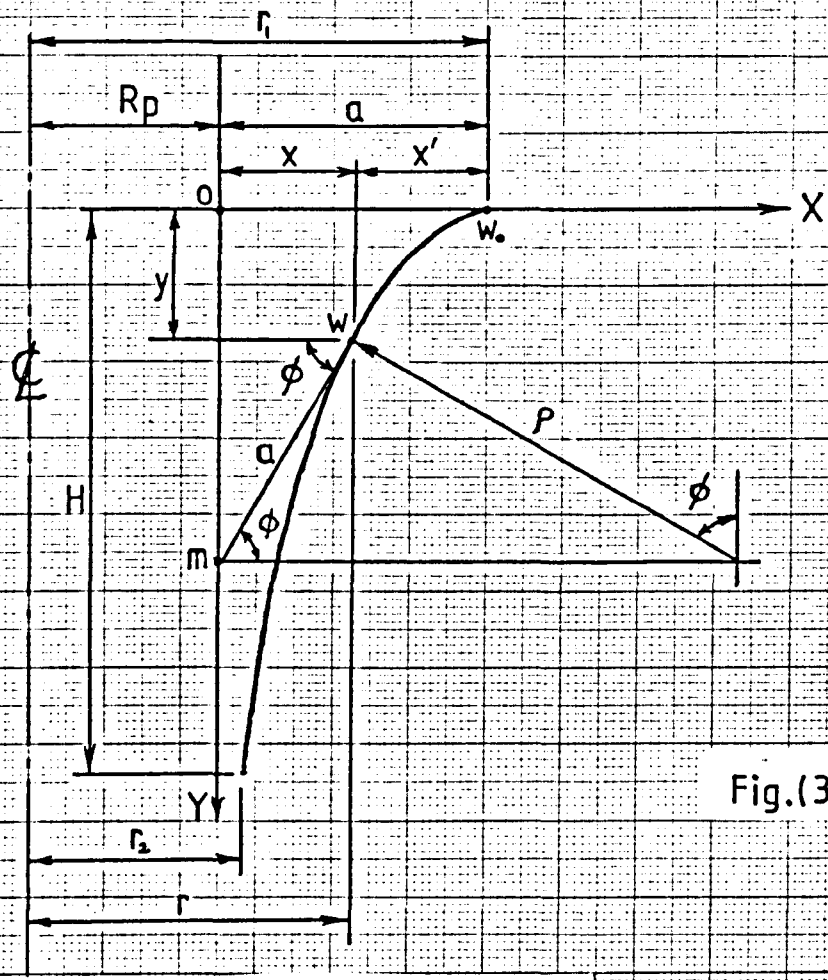

Fig.(3.1)

The tractrix curve geometry

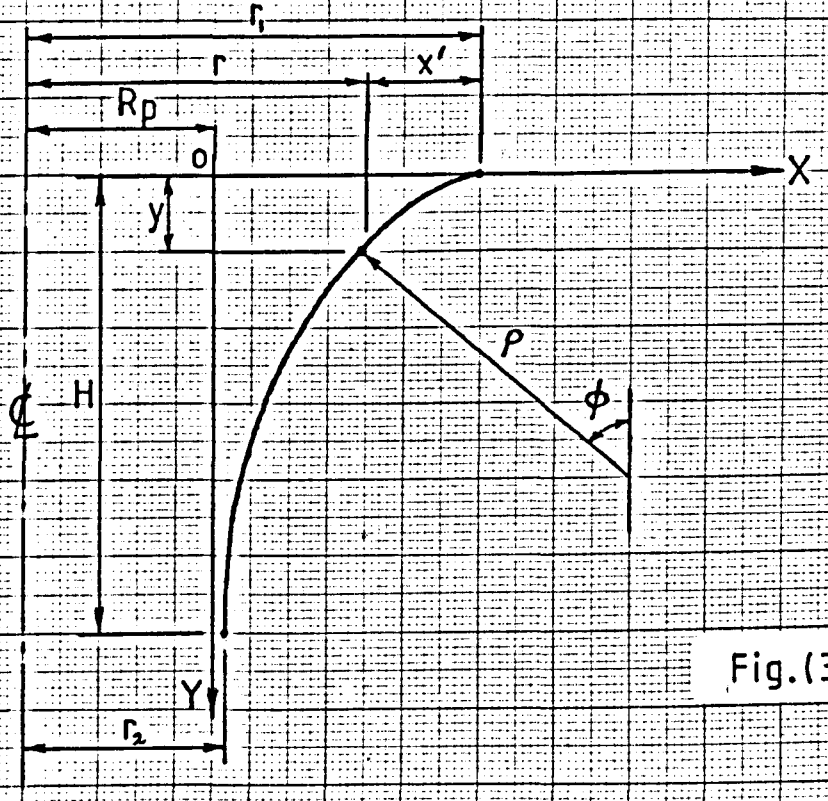

Fig.(3.2)

The second degree and exponential spiral curve geometry

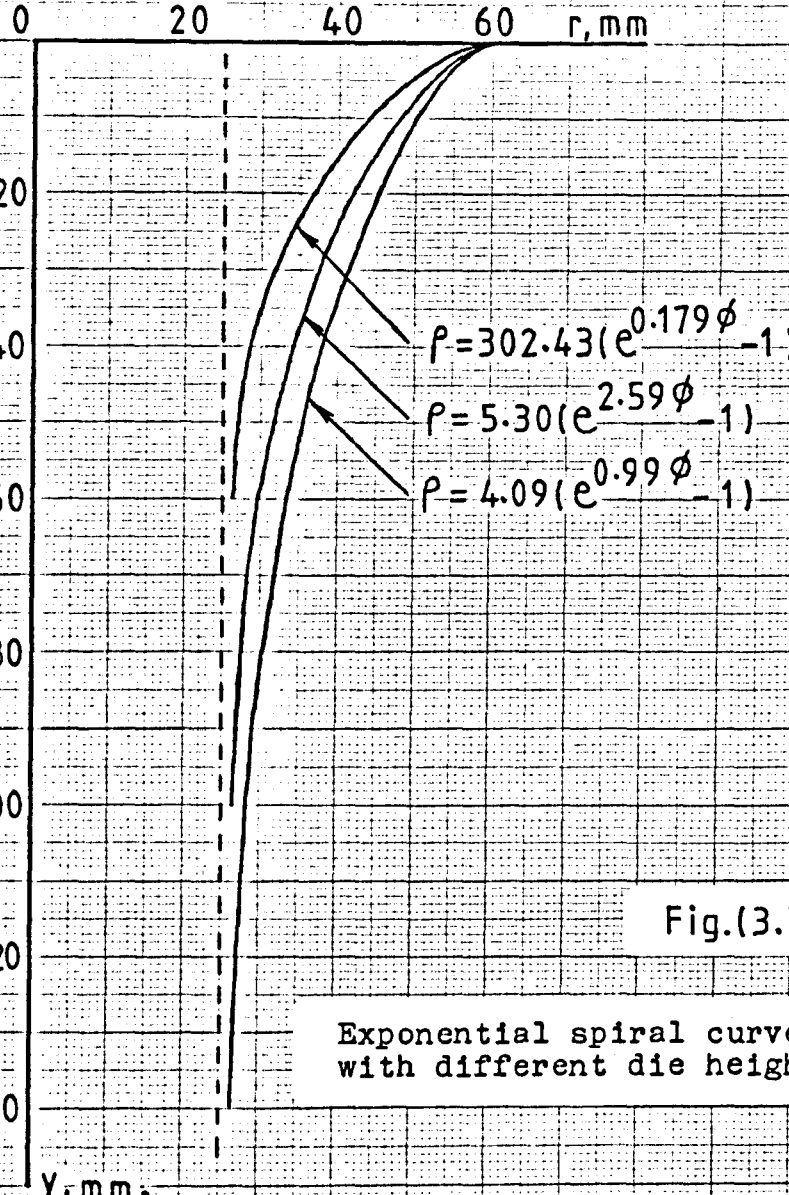

Fig.(3.3)

Exponential spiral curves with different die height

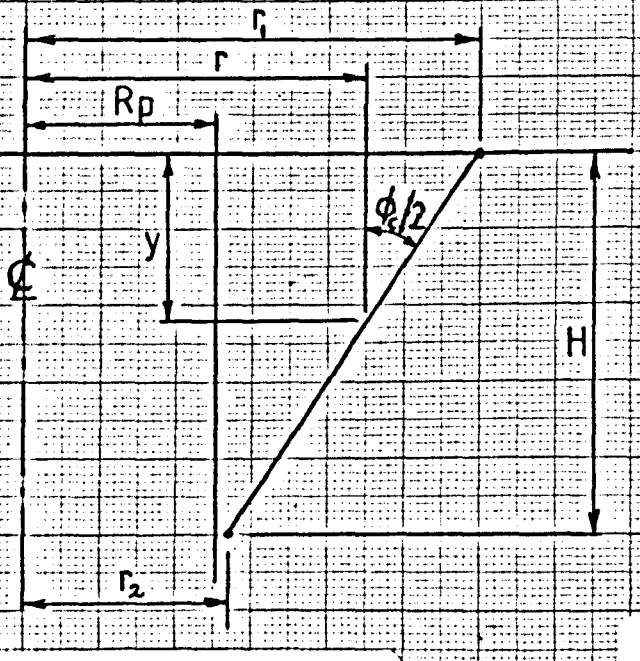

Fig.(3.4)

Conical die geometry

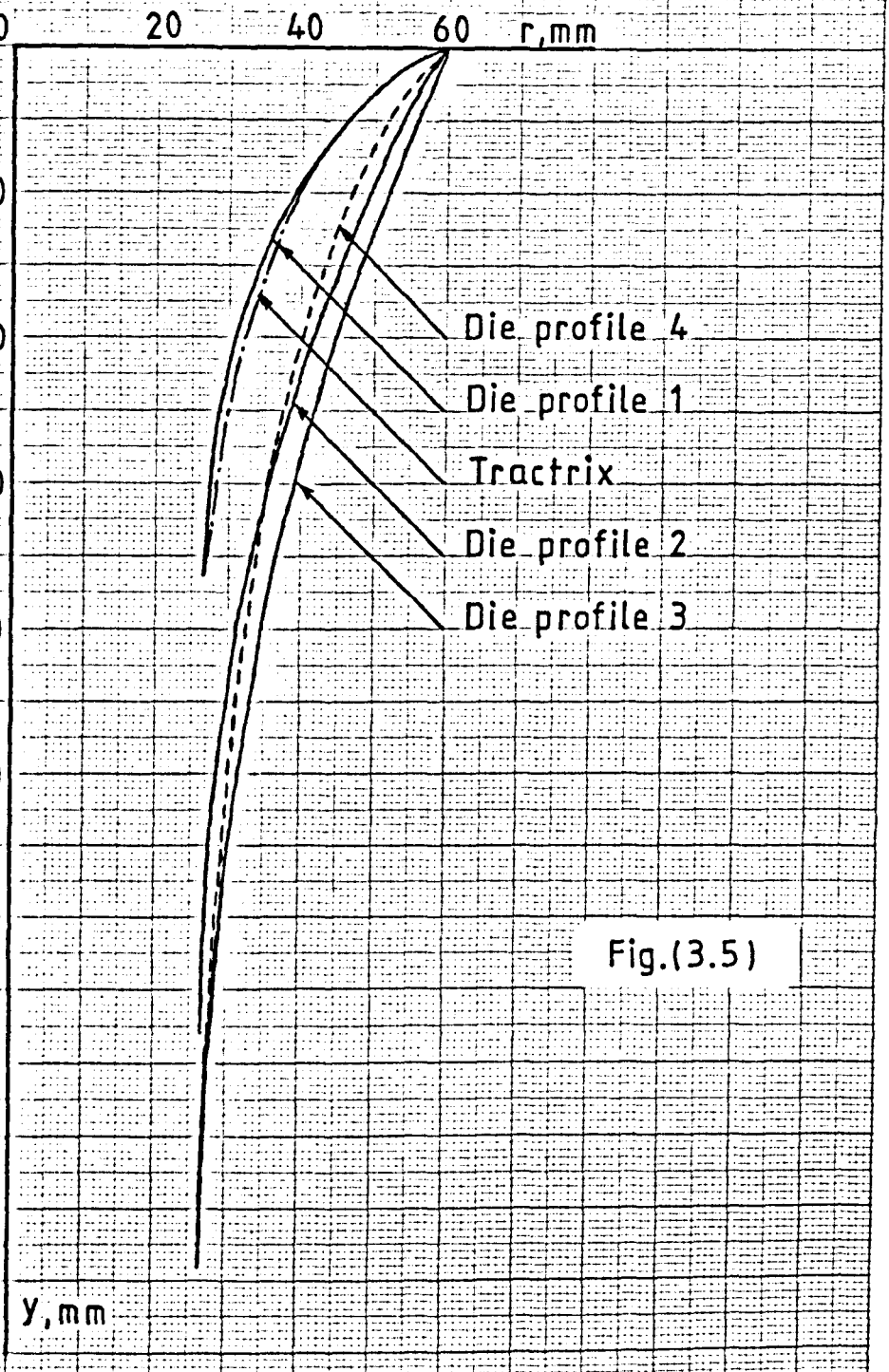

Fig.(3.5)

Die profiles for theoretical and experimental investigations

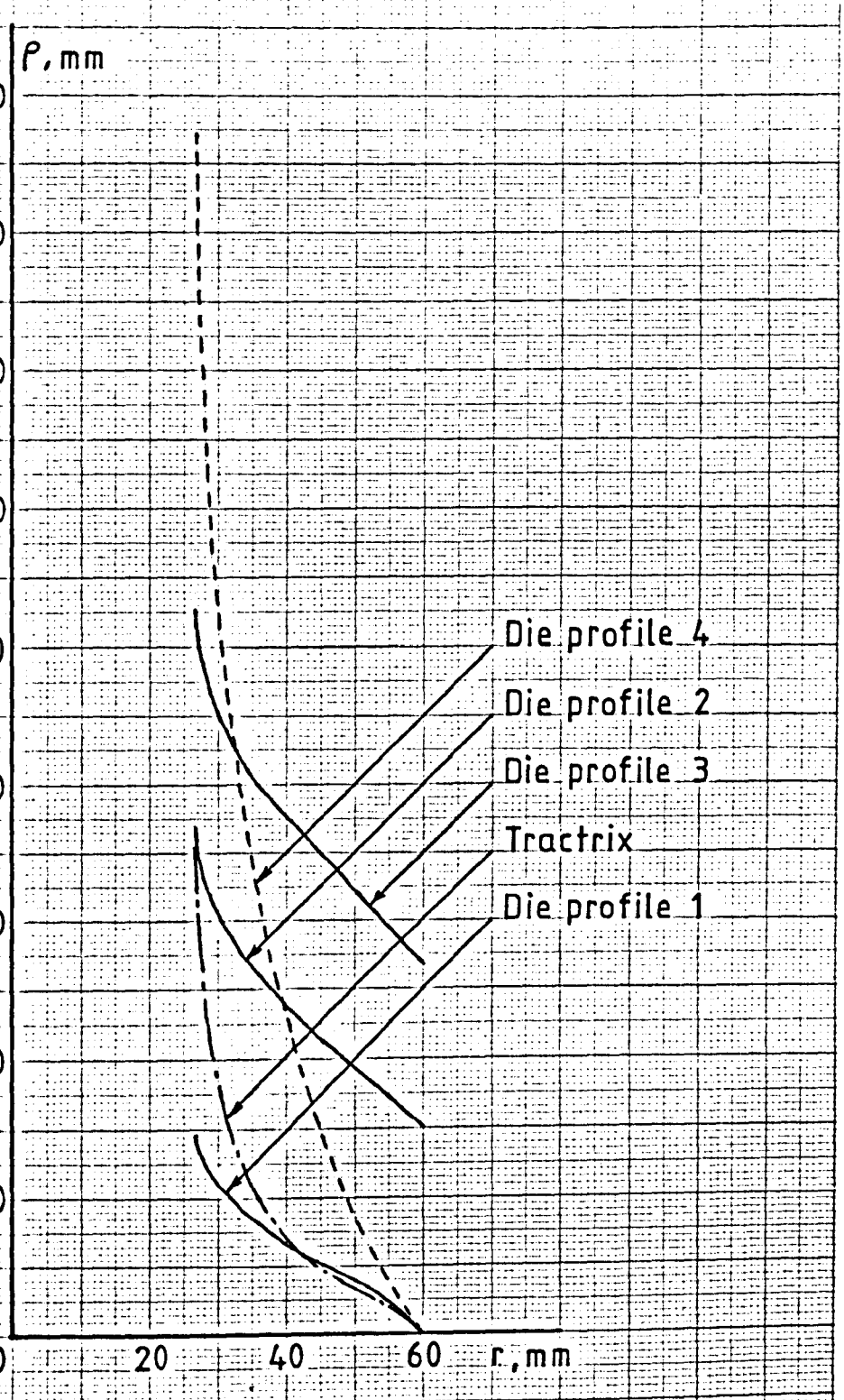

Radius of curvature distribution of different die profiles

Fig.(3.6)

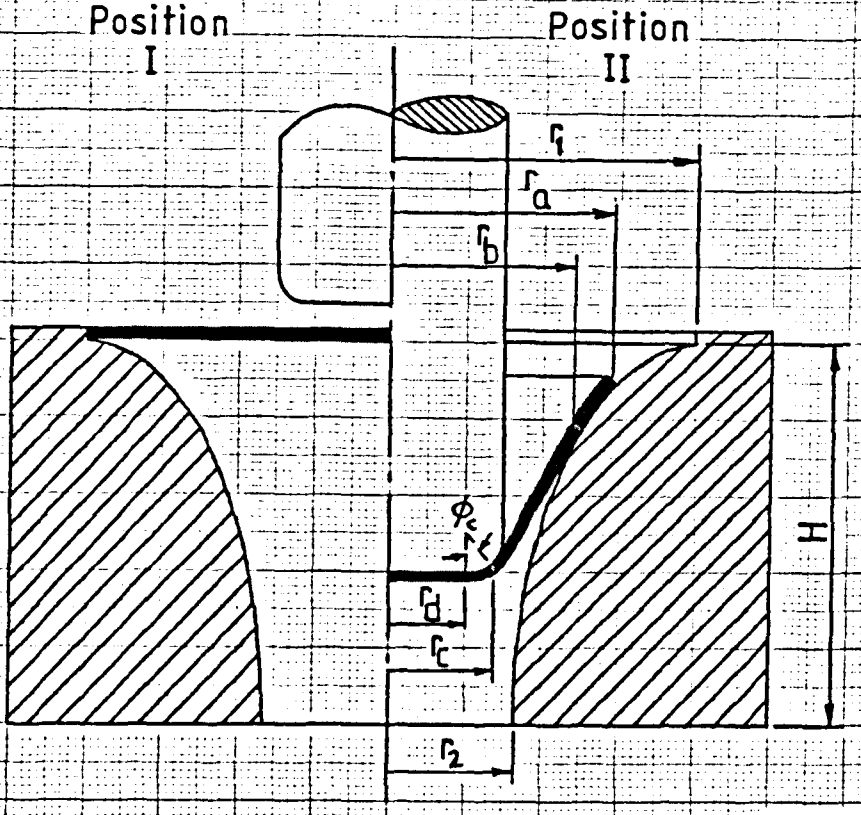

Fig.(4.1)

Deep drawing through a convex type die

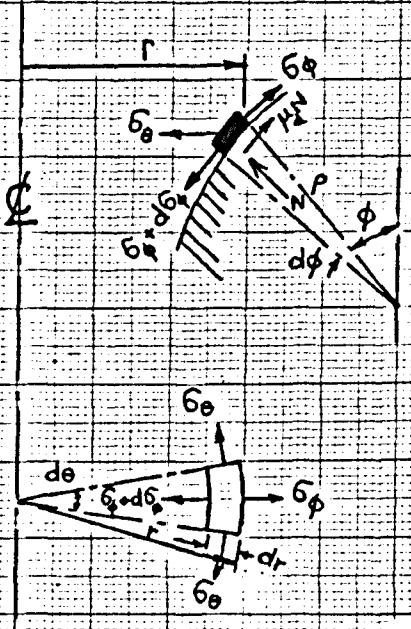

Fig.(4.2)

Stresses on an element of material in contact with die profile

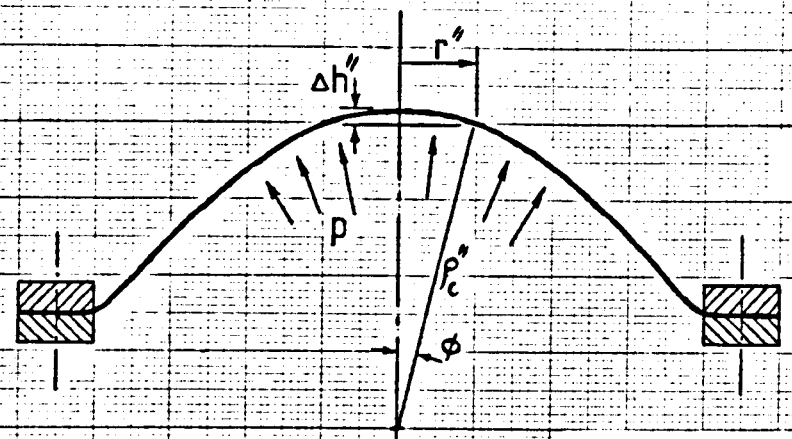

Fig.(4.3a)

Balanced biaxial tension test

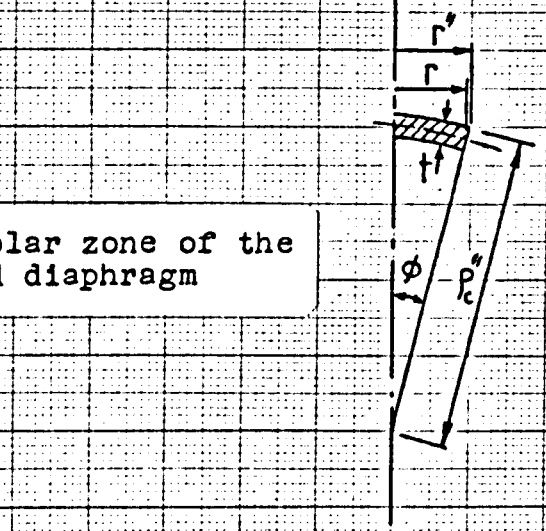

The polar zone of the bulged diaphragm

Fig.(4.3b)

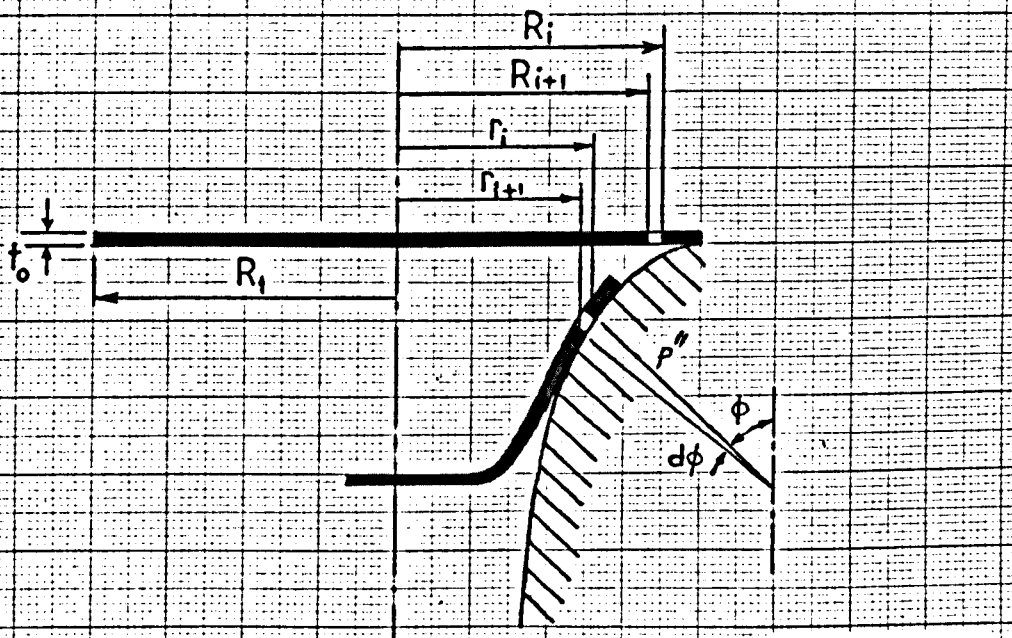

Fig.(4.4)

The volume constancy principle

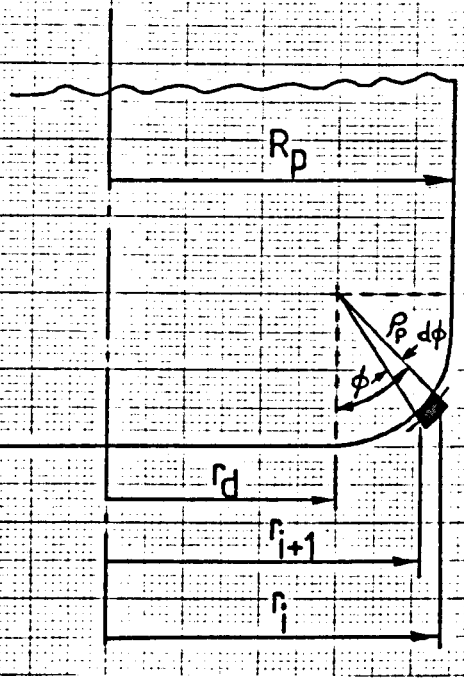

Fig.(4.5)

An element of material in contact with punch profile radius

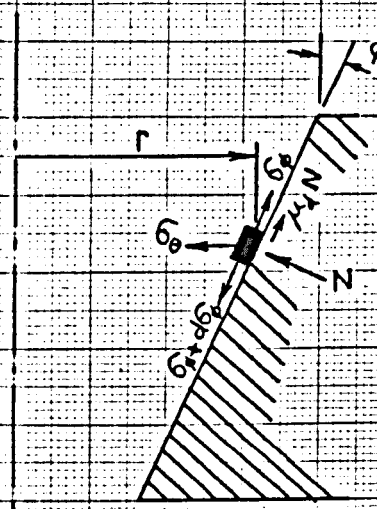

Fig.(4.6)

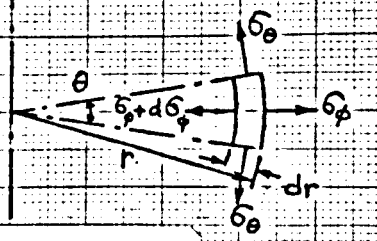

Stresses on an element of material in contact with conical die

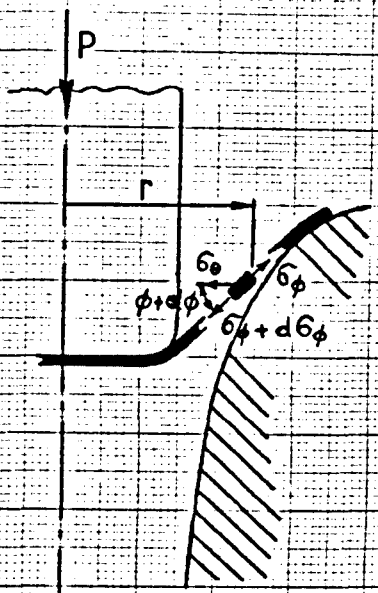

Fig.(4.7)

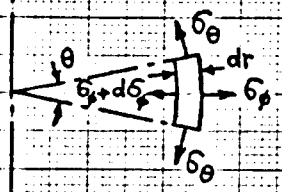

Stresses on an element of matrial in the zone between punch and die

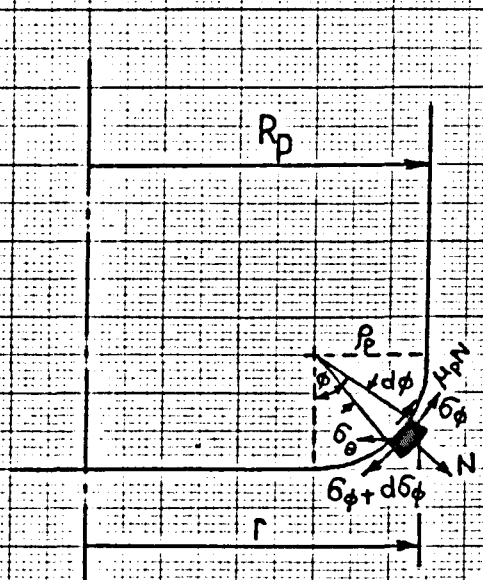

Stresses on an element of material in contact with the punch profile radius

Fig.(4.8)

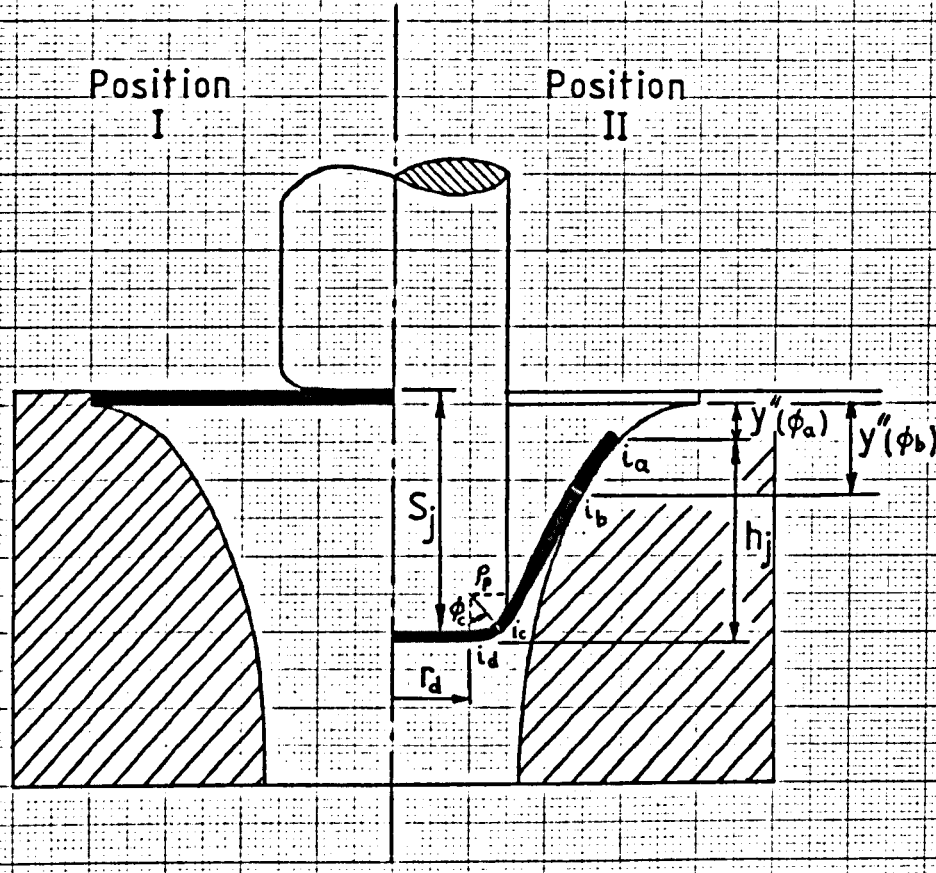

Approximation of punch stroke and cup height

Fig.(4.9)

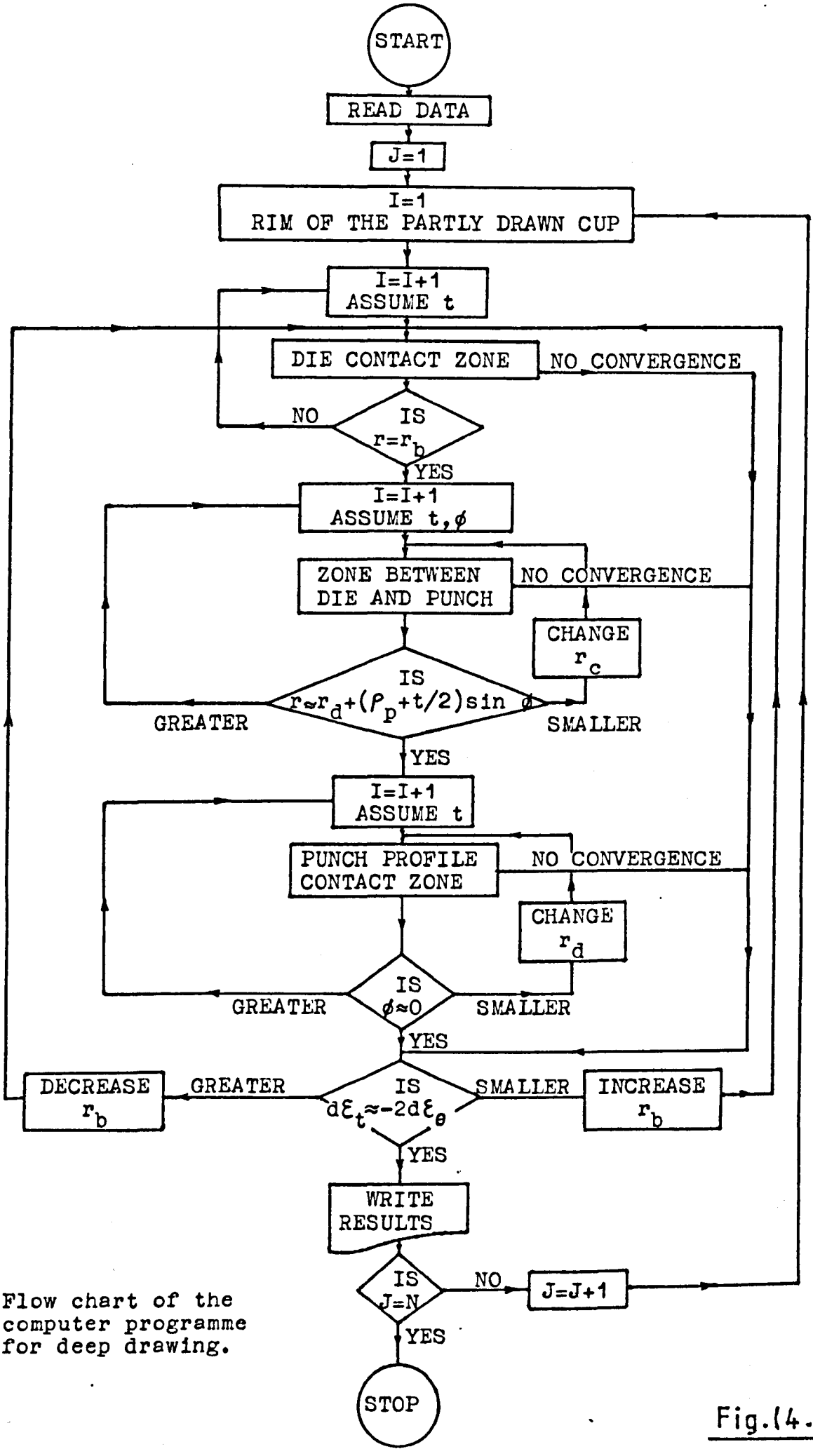

Flow chart of the computer programme for deep drawing.

Fig.(4.10)

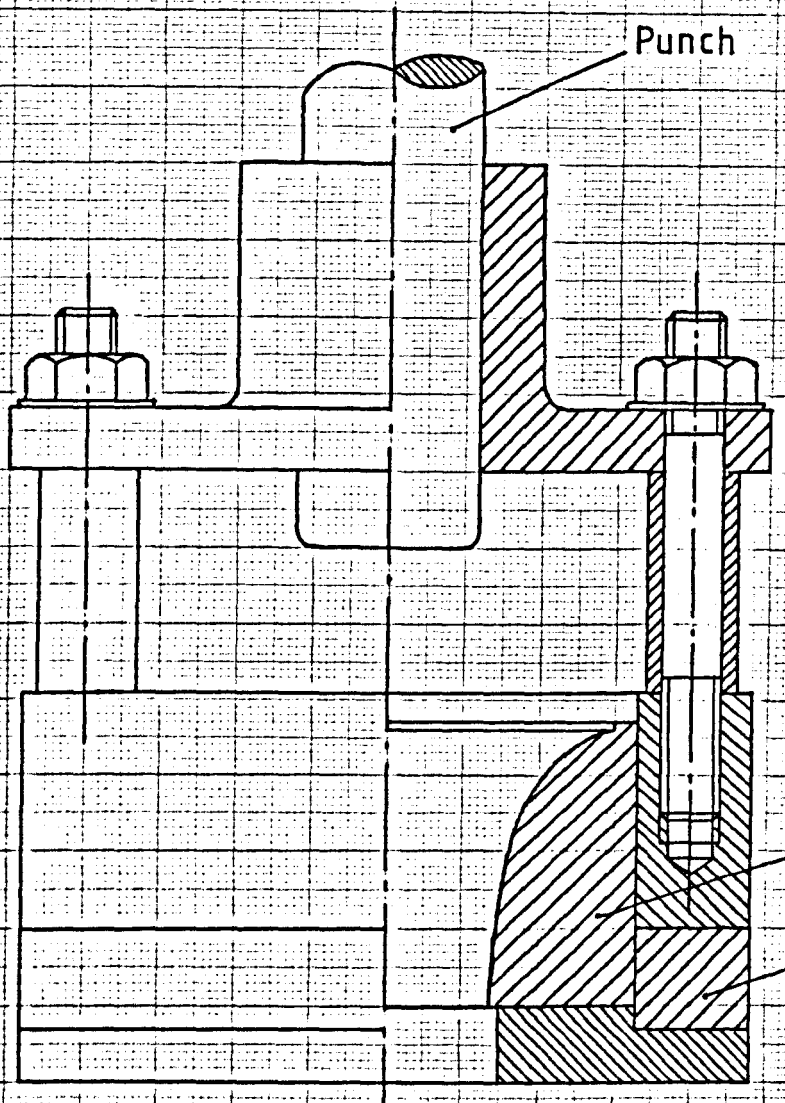

Deep drawing test rig.

Fig.(5.1)

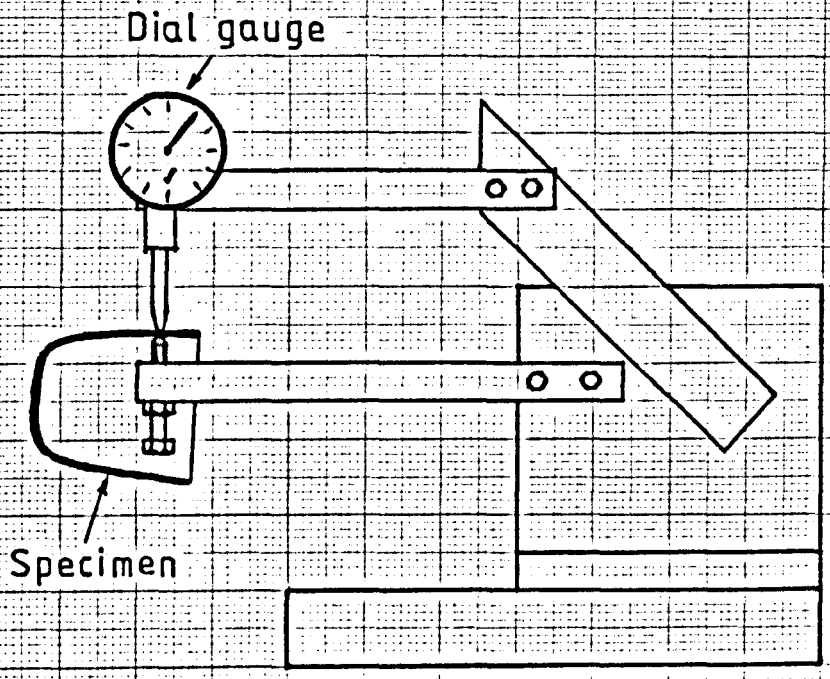

Measurement of thickness.

Fig.(5.2)

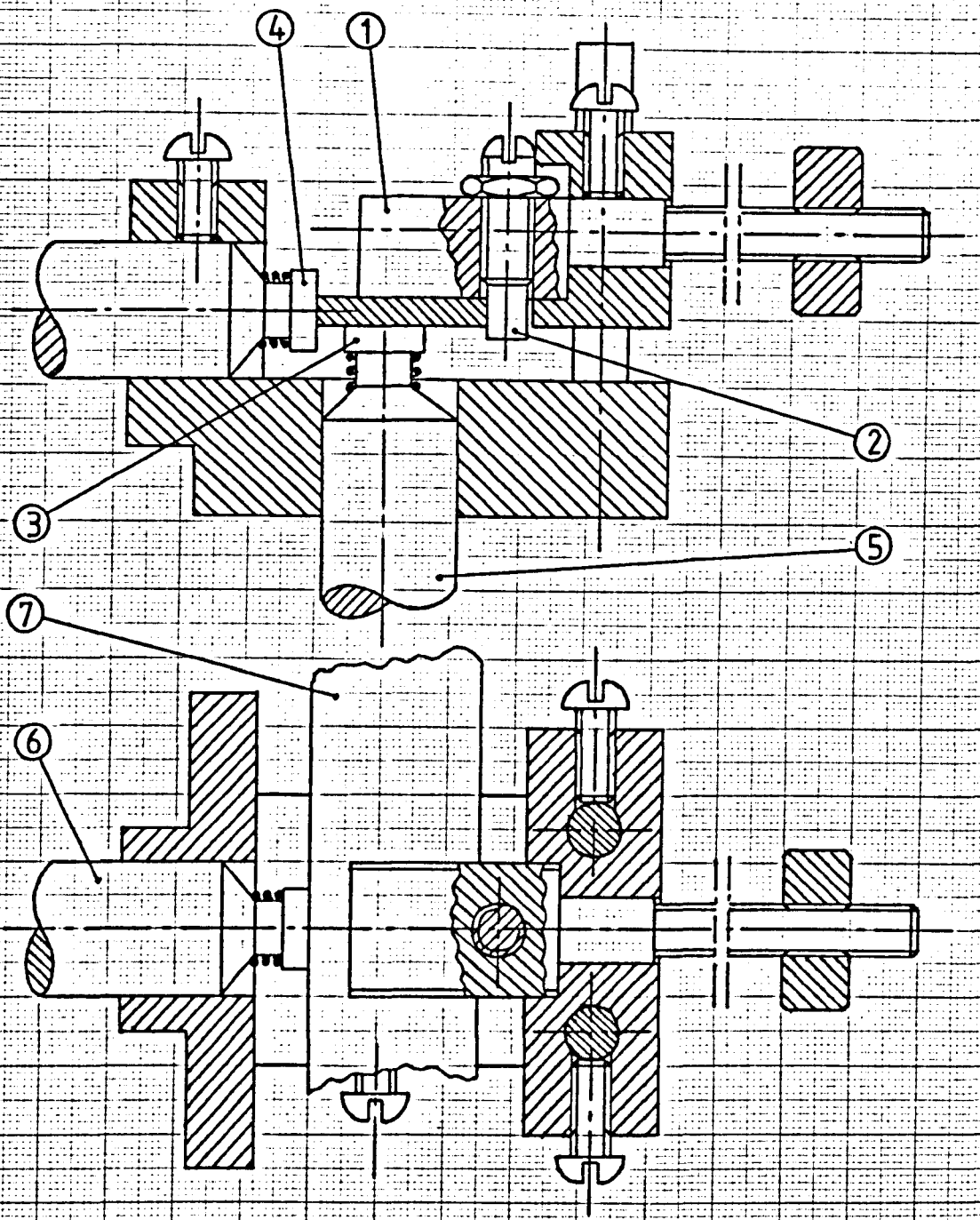

Displacement transducer attachment.

1. Thickness reference pin.
2. Width reference pin.
3. Thickness supporting disc.
4. Width supporting disc.
5. Thickness transducer.
6. Width transducer.
7. Tensile specimen.

Fig.(5.3)

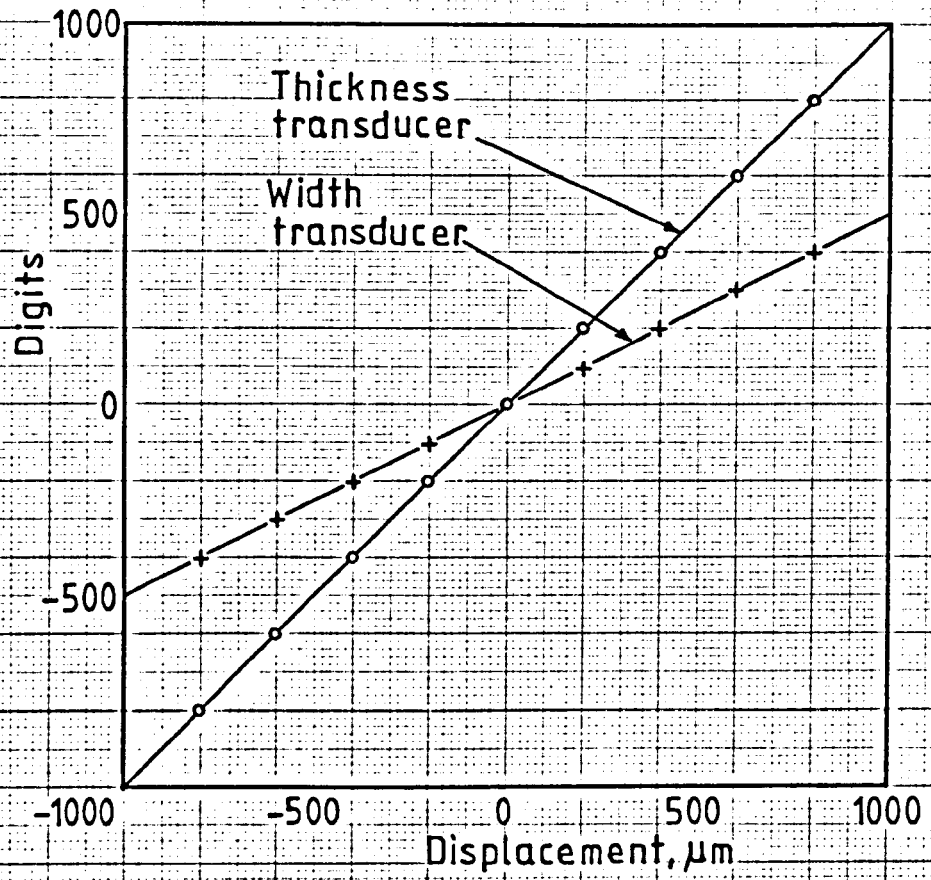

Calibration curves of thickness and width displacement transducers.

Fig.(5.4)

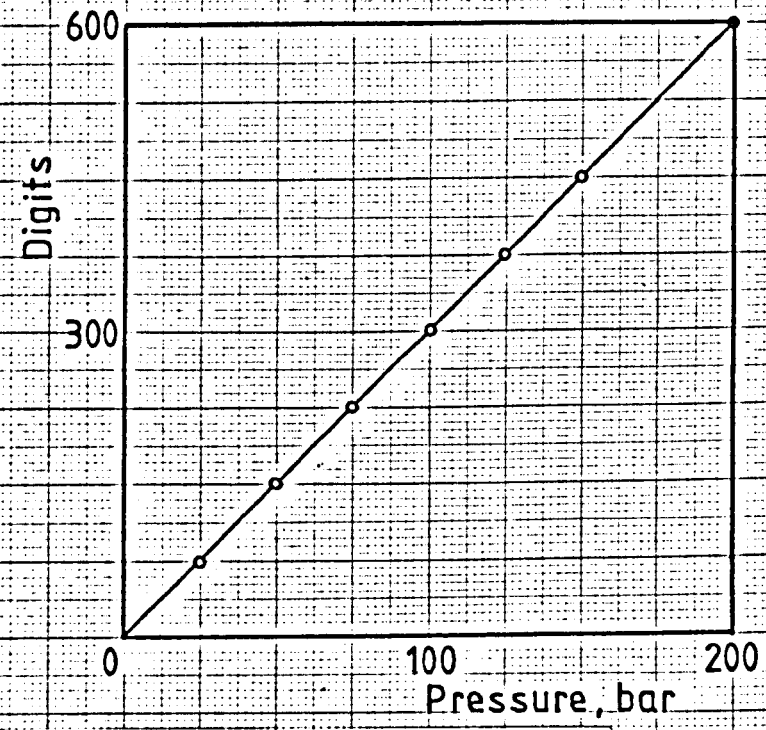

Calibration curve of the pressure transducer.

Fig.(5.5)

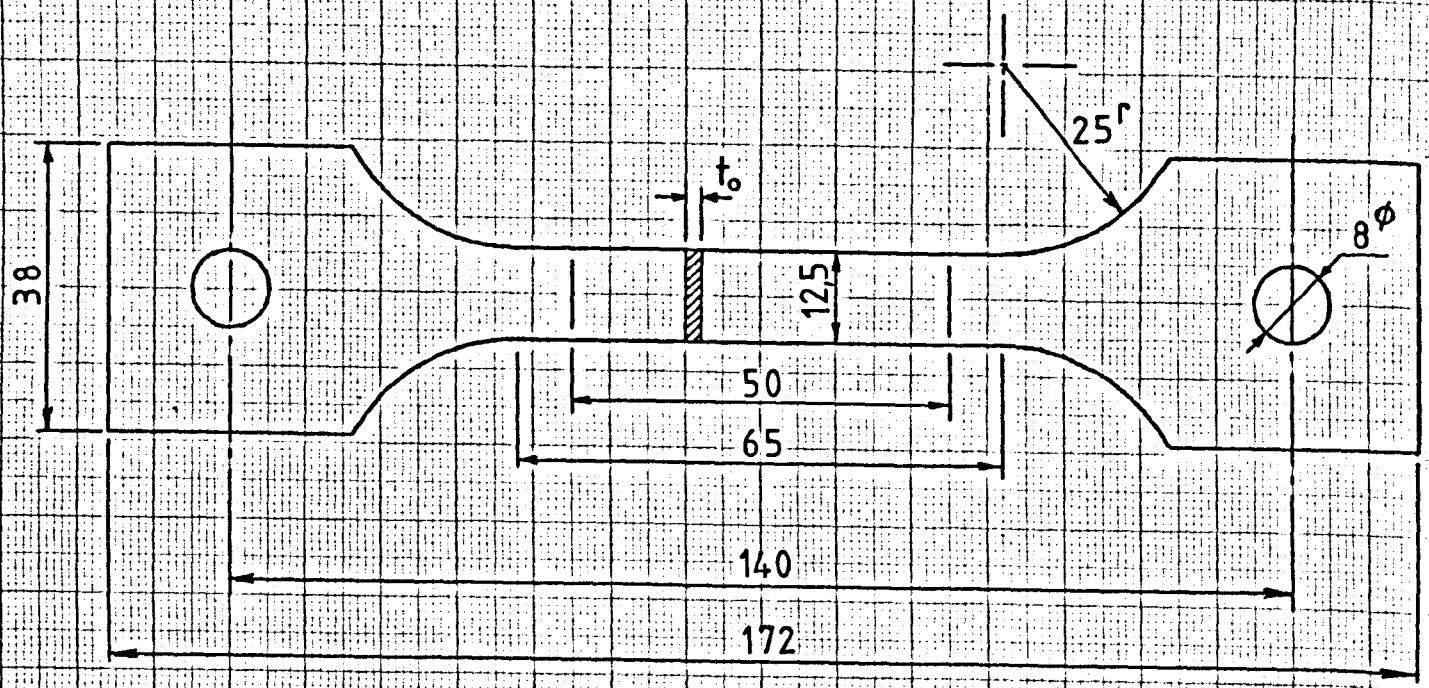

Tensile specimen dimensions.

Fig.(6.1)

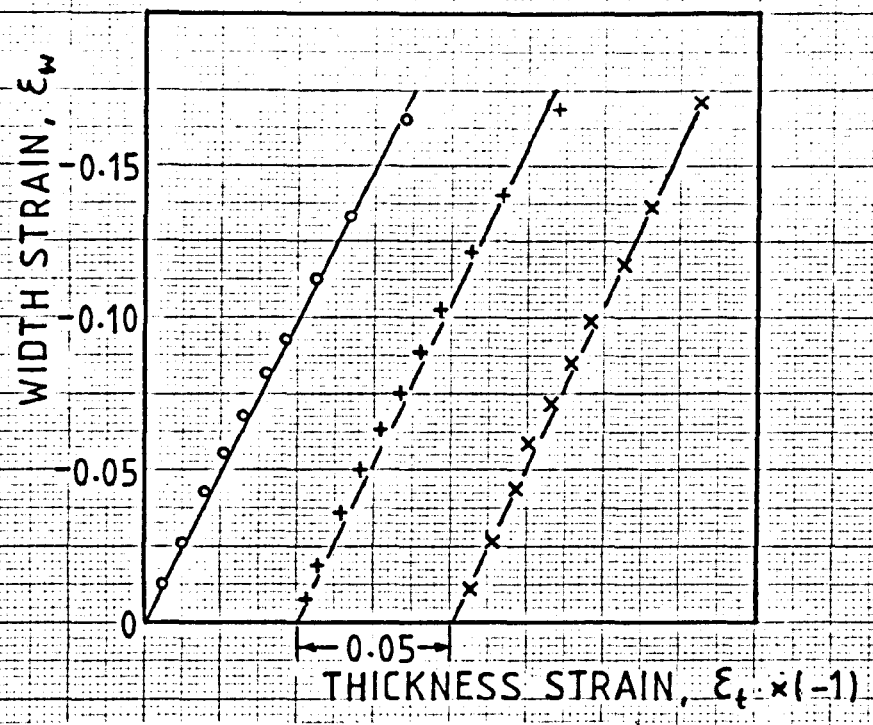

Width/thickness strain relation in tension test. Mild steel. At 0° to the rolling direction.

—o—o—o— Specimen 1, -+-+-+- Specimen 2 and -x—x—x- Specimen 3.

Fig.(6.2)

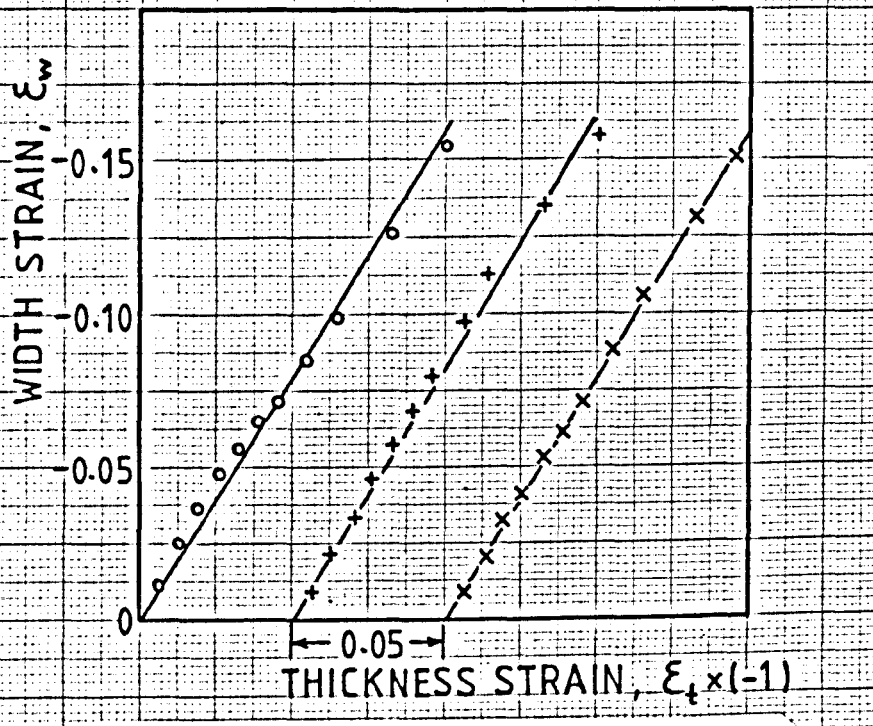

Width/thickness strain relation in tension test. Mild steel. At 45° to the rolling direction.

Fig.(6.3)

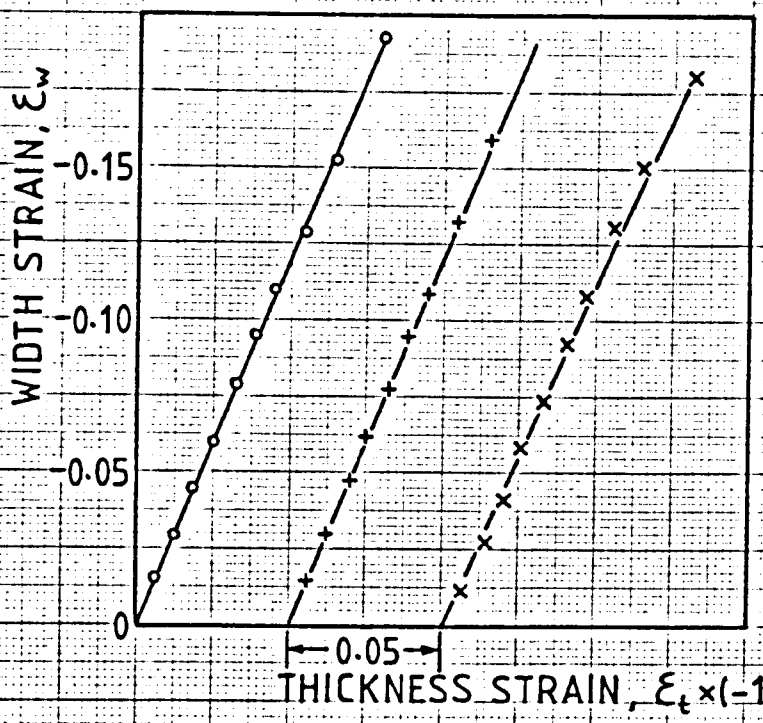

Width/thickness strain relation in tension test. Mild steel. At 90° to the rolling direction.

Fig.(6.4)

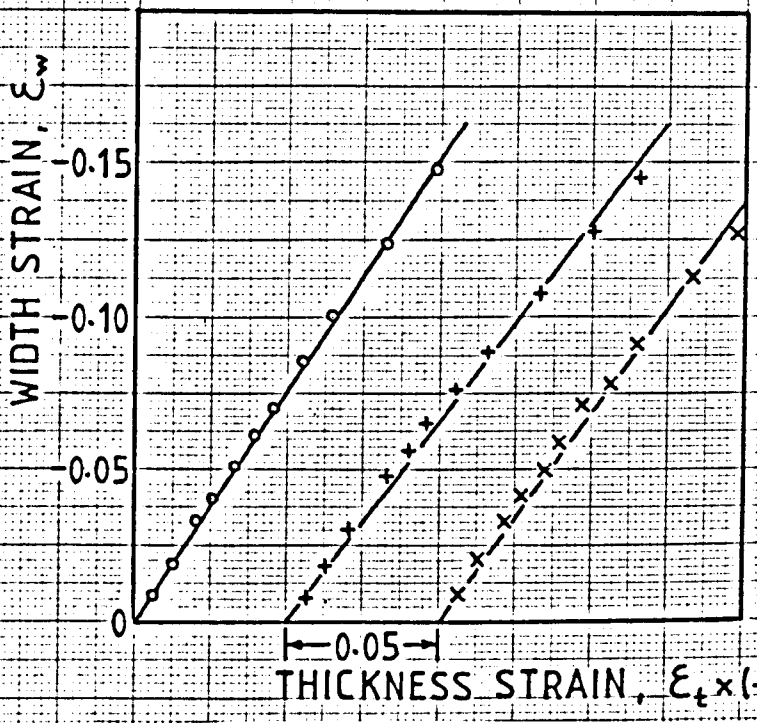

Width/thickness strain relation in tension test. Mild steel. At -45° to the rolling direction.

Fig.(6.5)

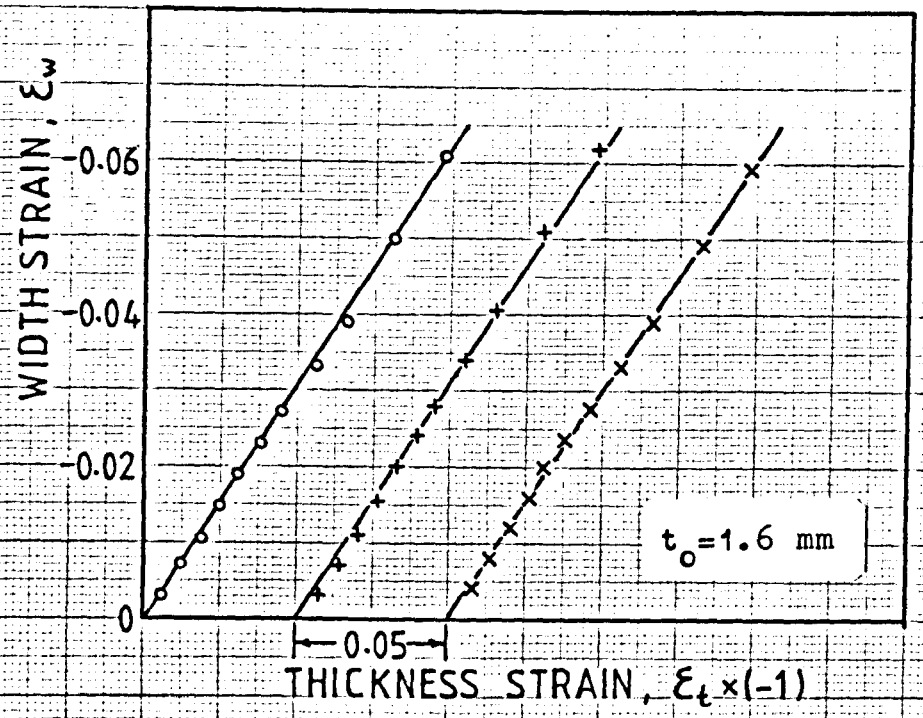

Width/thickness strain relation in tension test. Soft aluminium. At 0° to the rolling direction.

Fig.(6.6)

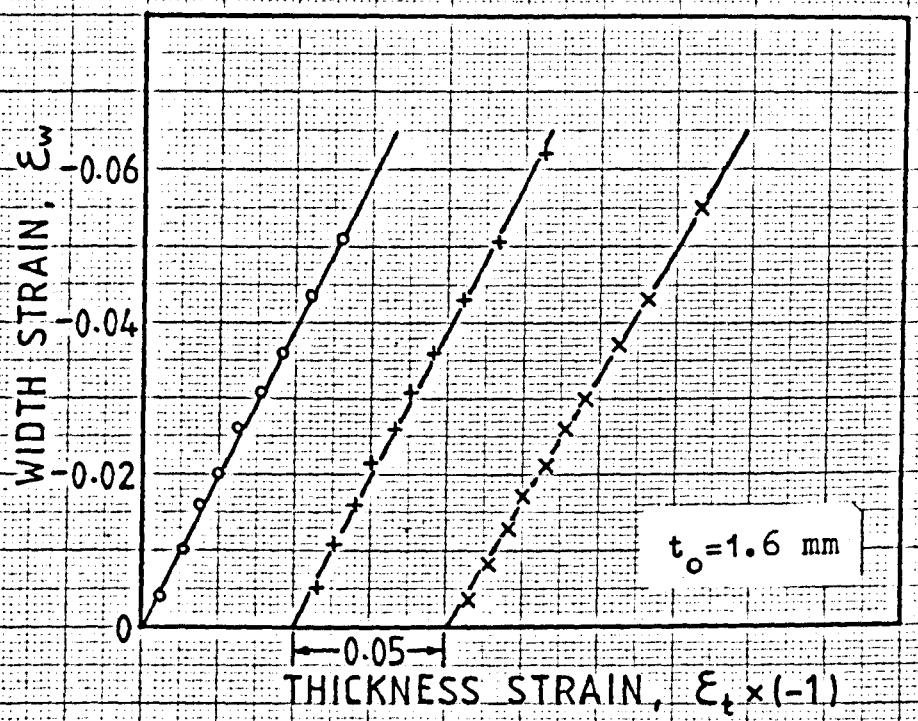

Width/thickness strain relation in tension test. Soft aluminium. At 45° to the rolling direction.

Fig.(6.7)

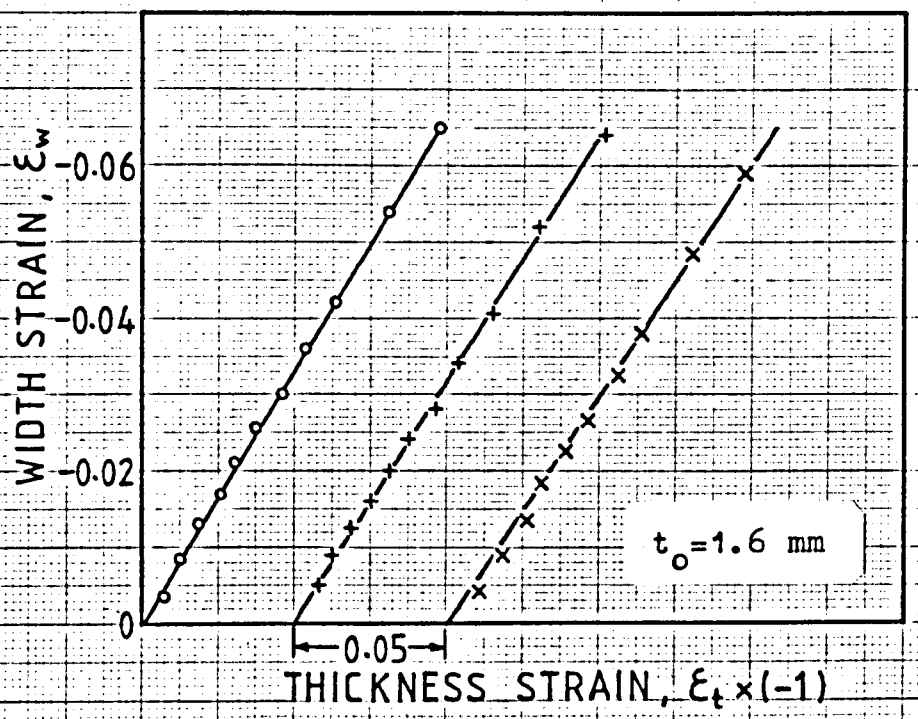

Width/thickness strain relation in tension test. Soft aluminium. At 90° to the rolling direction.

Fig.(6.8)

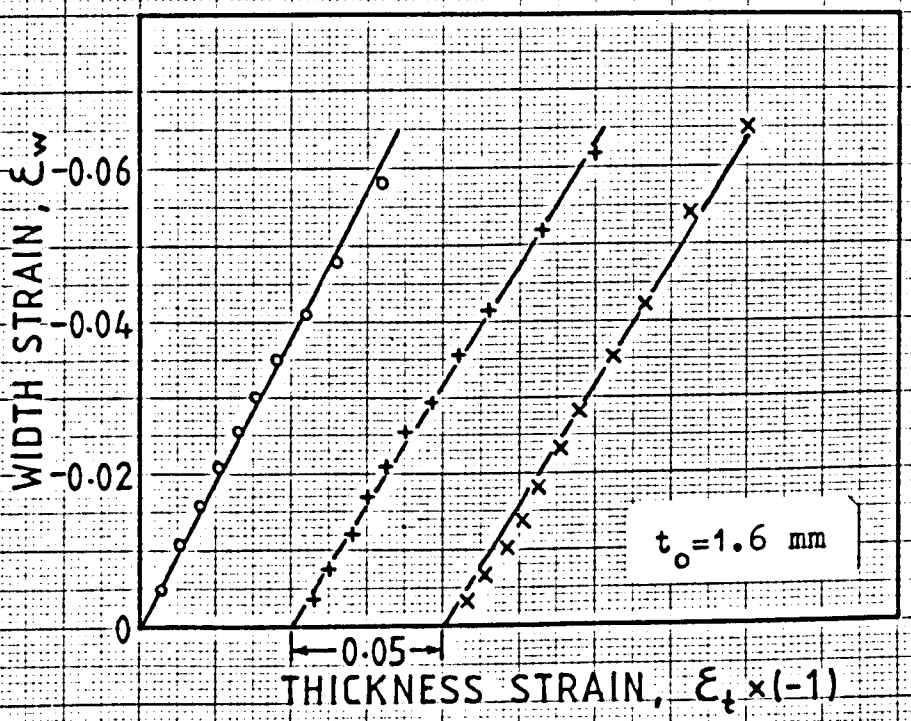

Width/thickness strain relation in tension test. Soft aluminium. At -45° to the rolling direction.

Fig.(6.9)

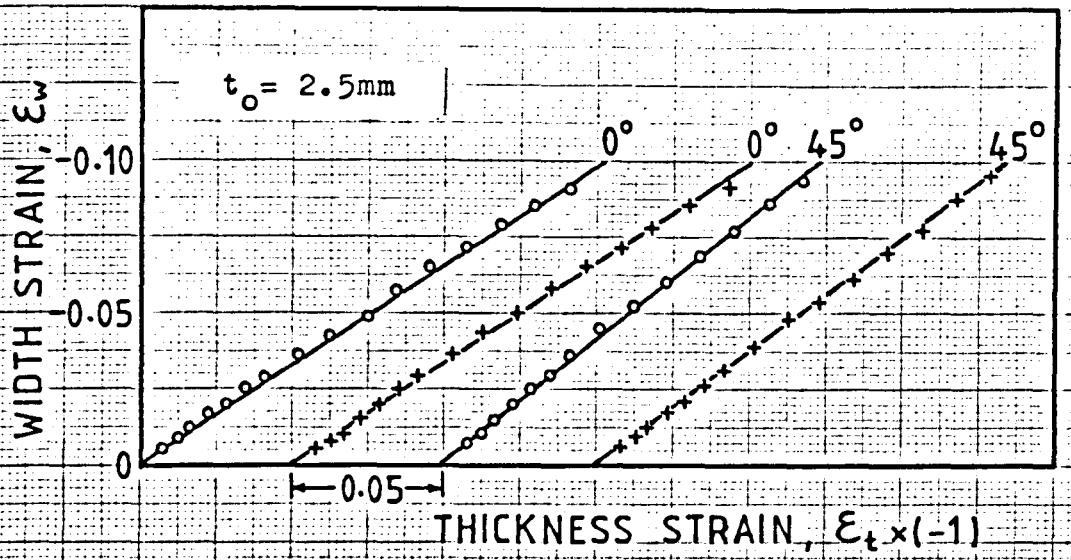

Width/thickness strain relation in tension test. Soft aluminium. At 0° and 45° to the rolling direction.

Fig.(6.10)

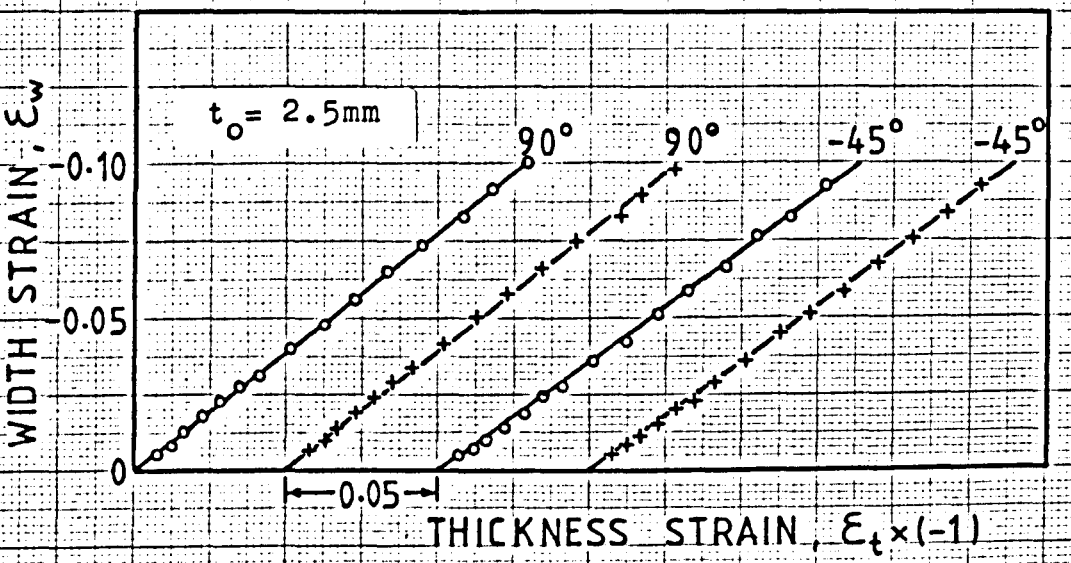

Width/thickness strain relation in tension test. Soft aluminium. At 90° and -45° to the rolling direction.

Fig.(6.11)

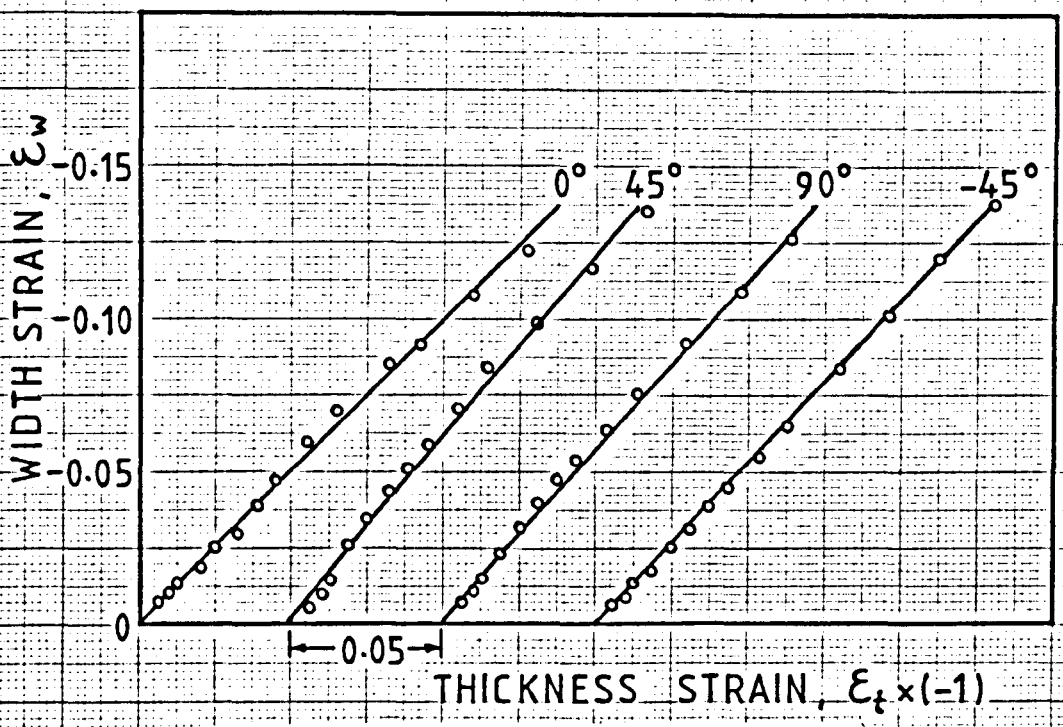

Width/thickness strain relation in tension test. Stainless steel. At 0°, 45°, 90° and -45° to the rolling direction.

Fig.(6.12)

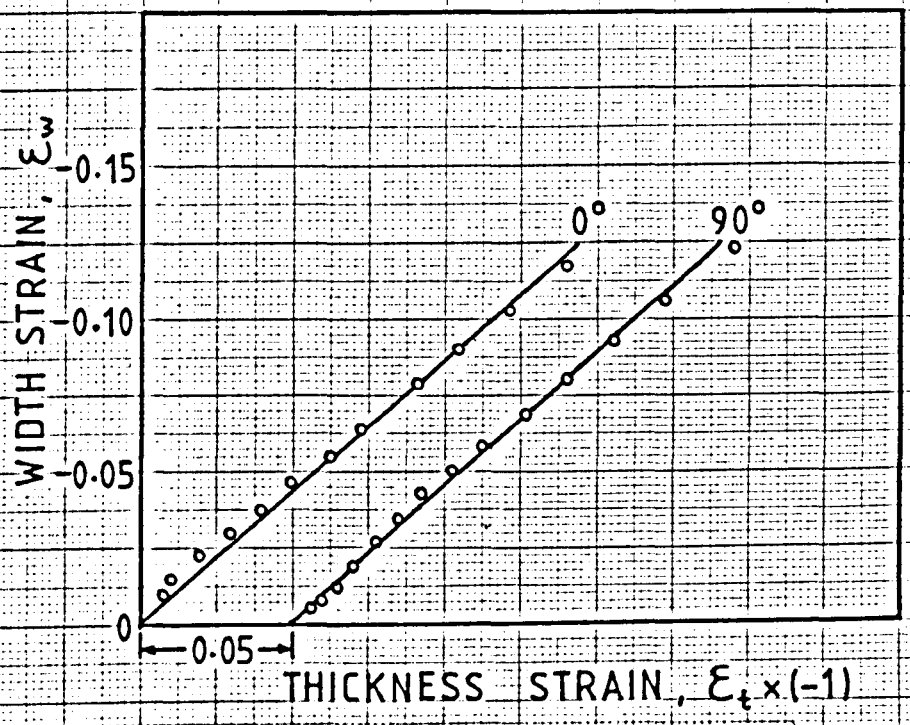

Width/thickness strain relation in tension test. Brass. At 0° and 90° to the rolling direction.

Fig.(6.13)

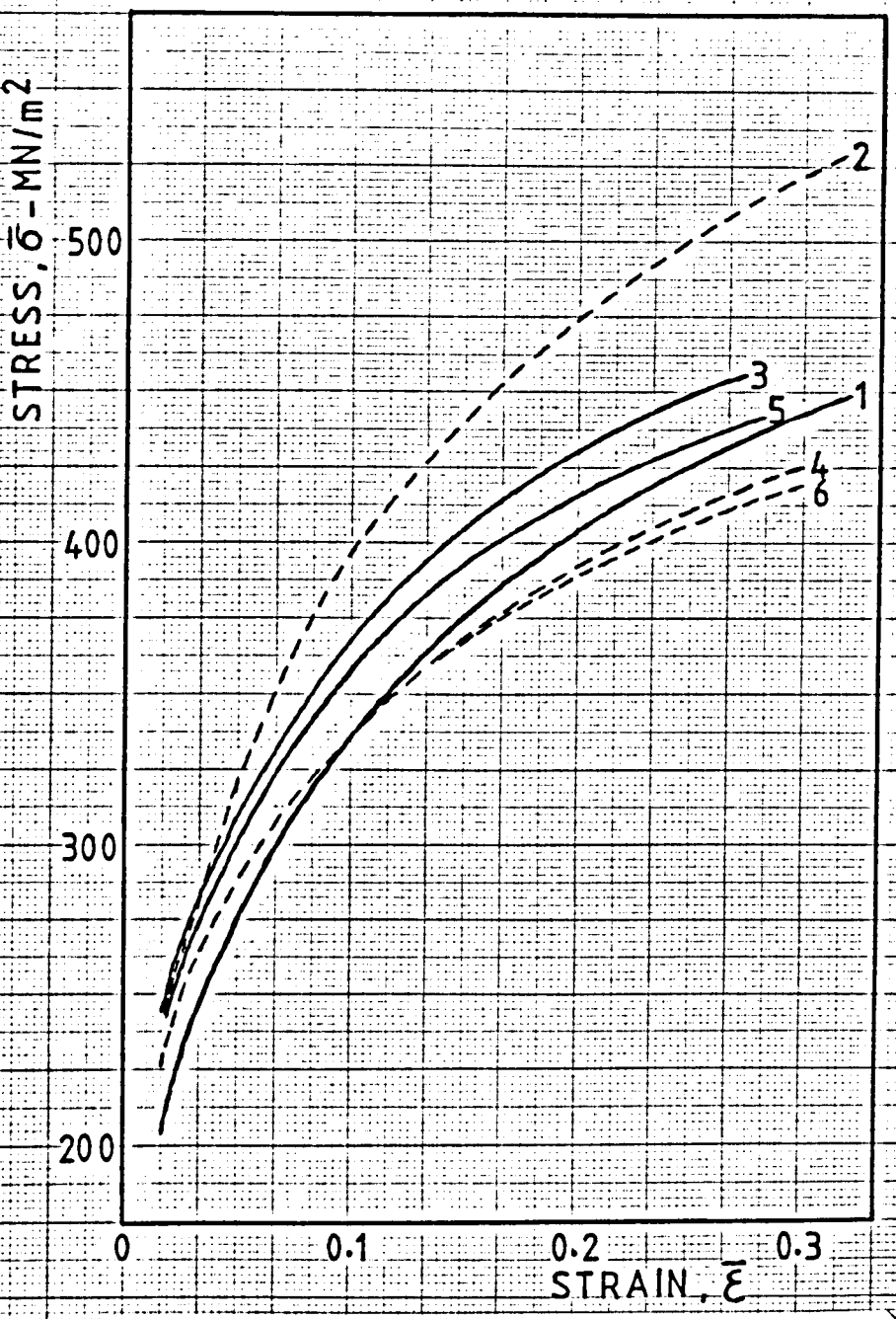

Work-hardening characteristic. Mild steel.

1. Biaxial tension test, anisotropic.
2. Biaxial tension test, isotropic.
3. Simple tension, at 0° to the rolling directon, anisotropic.
4. Simple tension, at 0° to the rolling direction, isotropic.
5. Simple tension, at 90° to the rolling direction, anisotropic.
6. Simple tension, at 90° to the rolling direction, isotropic.

Fig. (6.14)

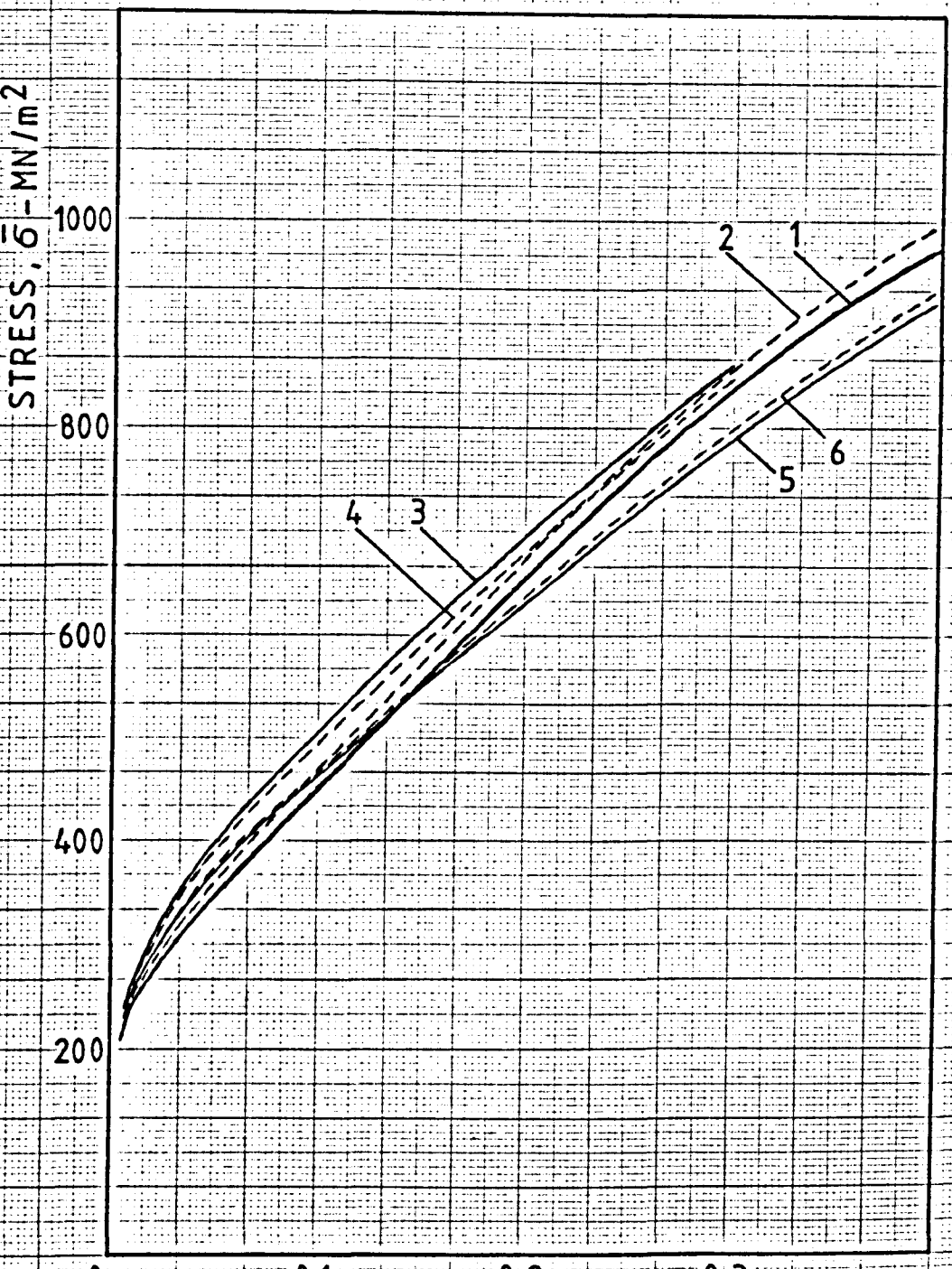

Work-hardening characteristic. Stainless steel.

Key as for Fig.(6.14)

Fig.(6.15)

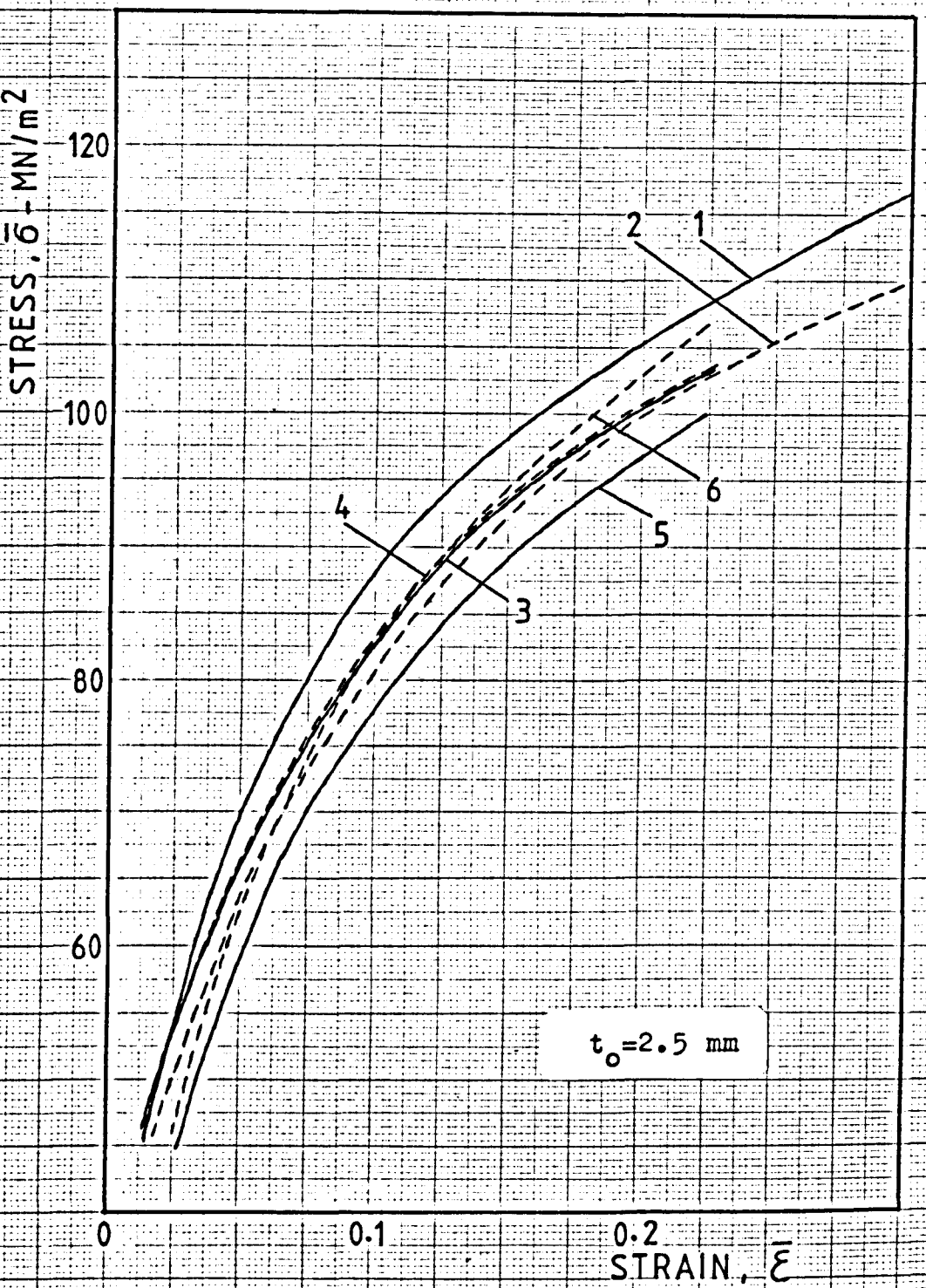

Work-hardening characteristic. Soft aluminium.

Key as for Fig.(6.14)

Fig.(6.16)

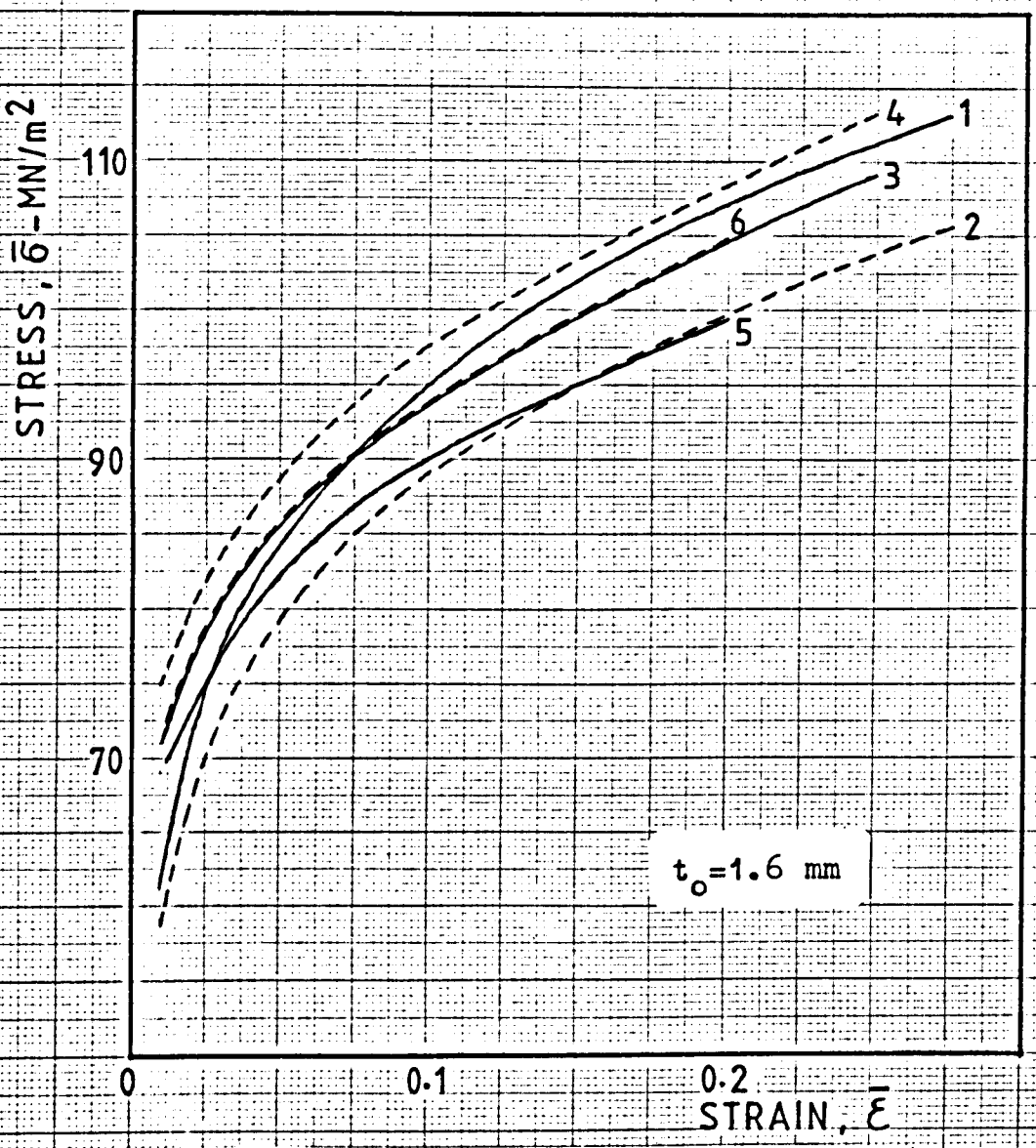

Work-hardening characteristic. Soft aluminium.

Key as for Fig. (6.14)

Fig. (6.17)

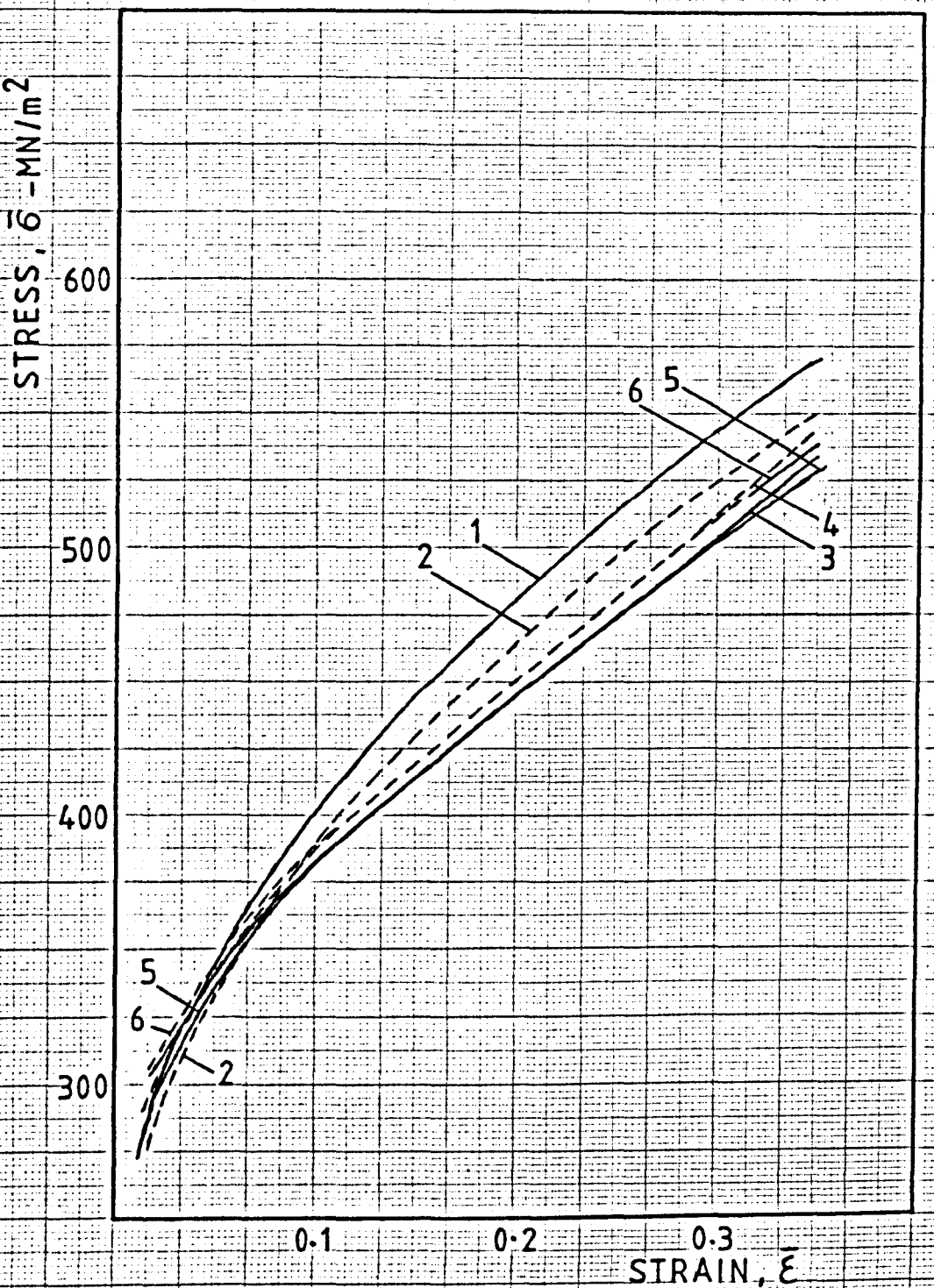

Work-hardening characteristic. Brass.

Key as for Fig. (6.14)

Fig. (6.18)

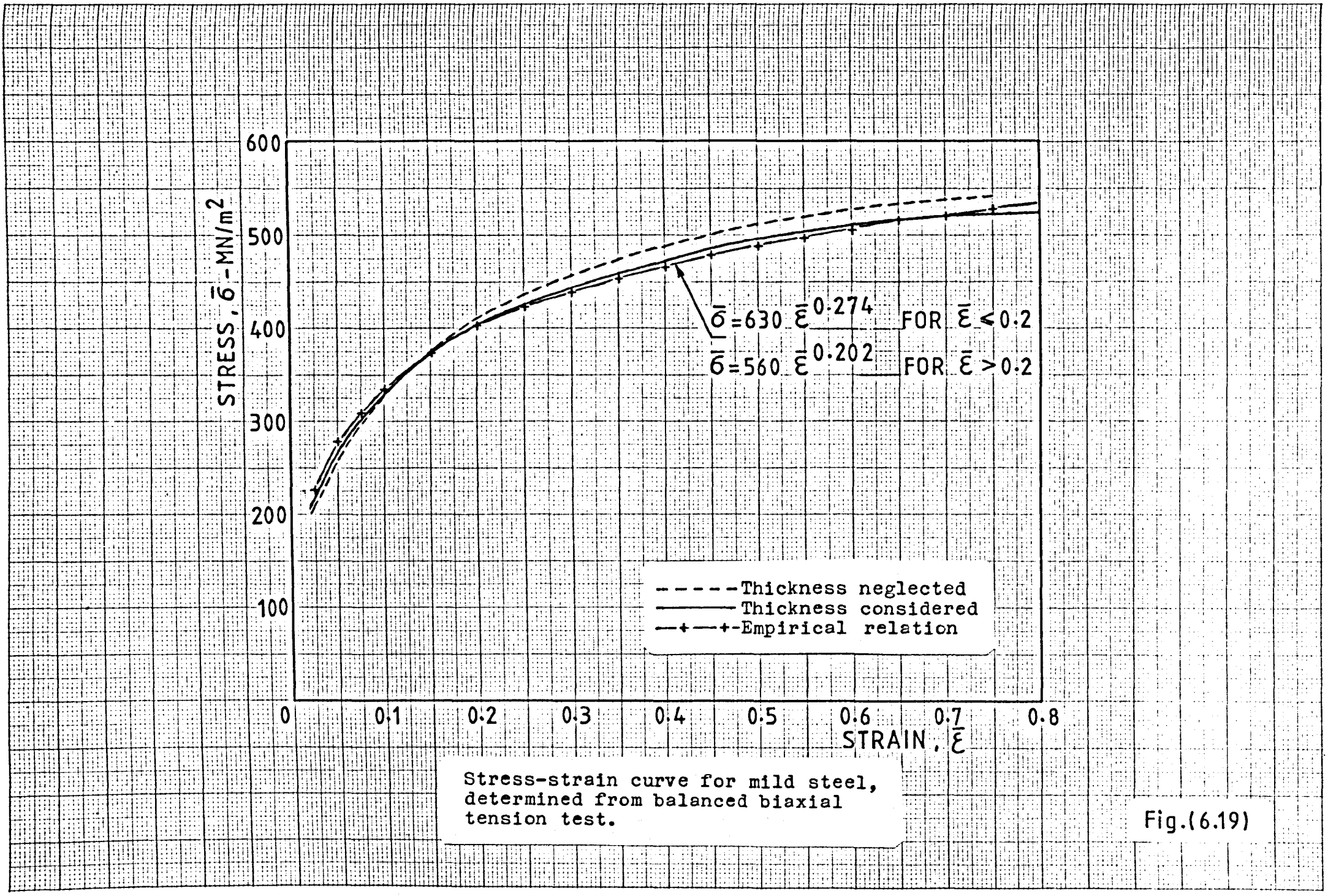

Stress-strain curve for mild steel, determined from balanced biaxial tension test.

Fig.(6.19)

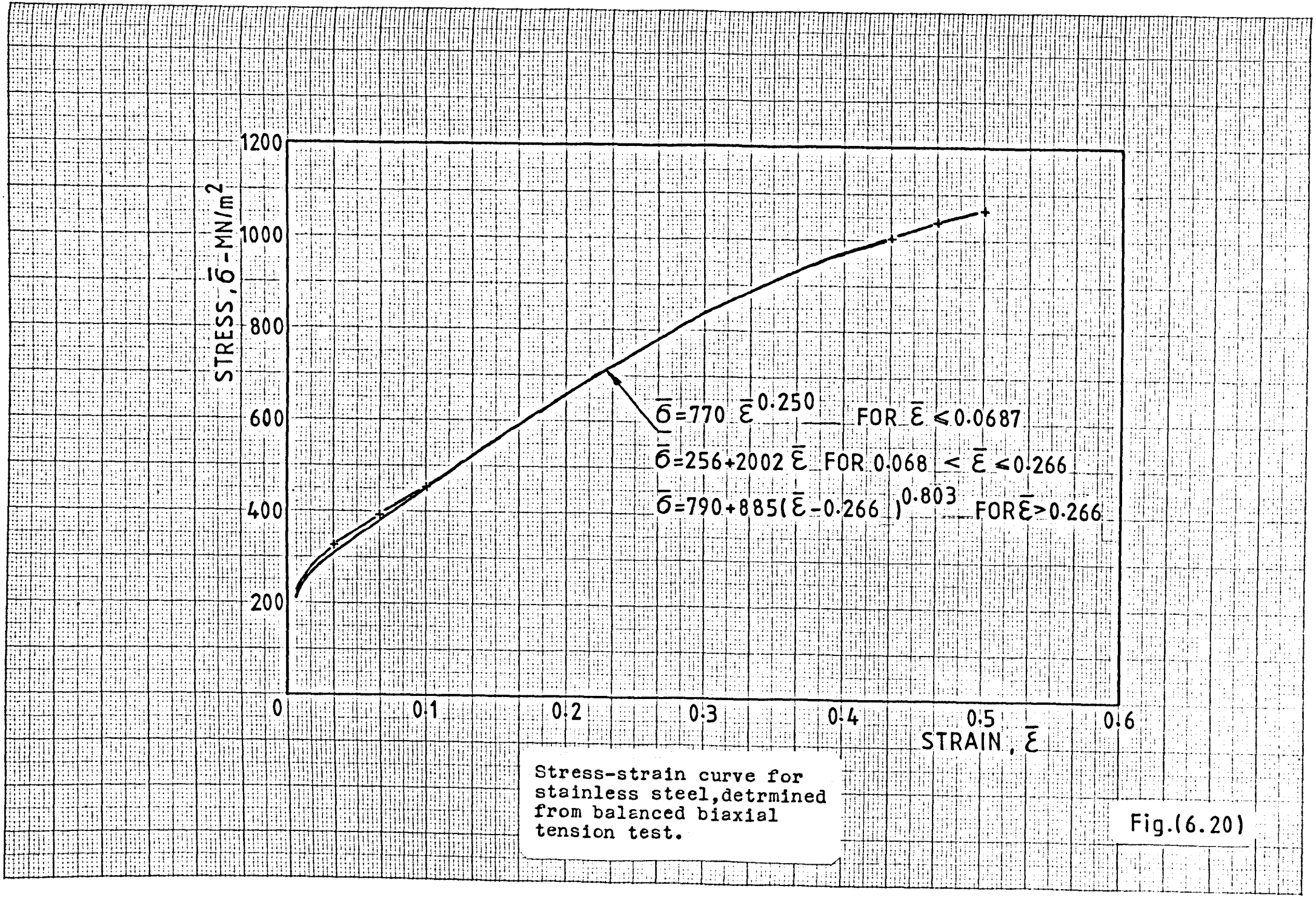

Stress-strain curve for stainless steel, detrmined from balanced biaxial tension test.

Fig.(6.20)

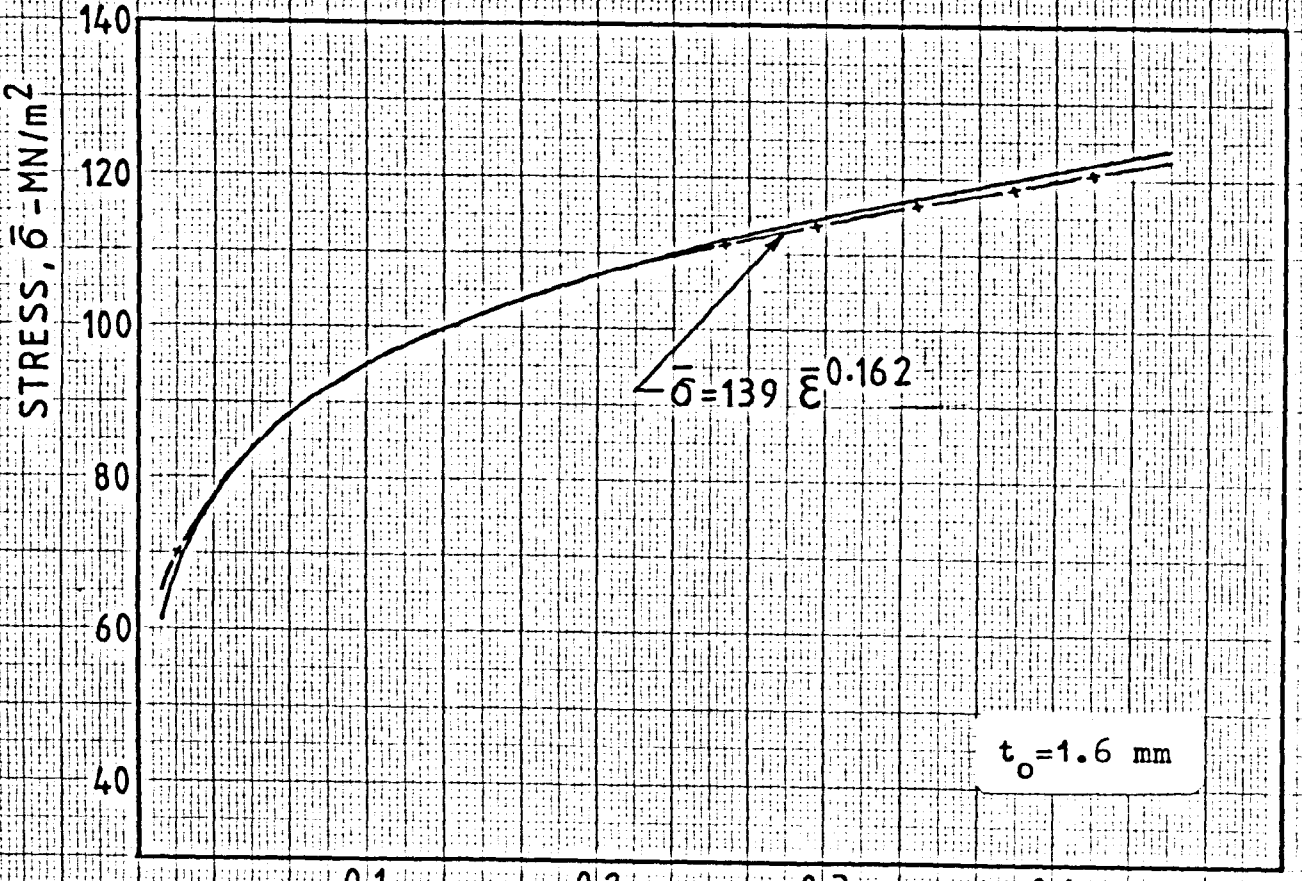

Stress-strain curve for soft aluminium, determined from balanced biaxial tension test.

Fig.(6.21)

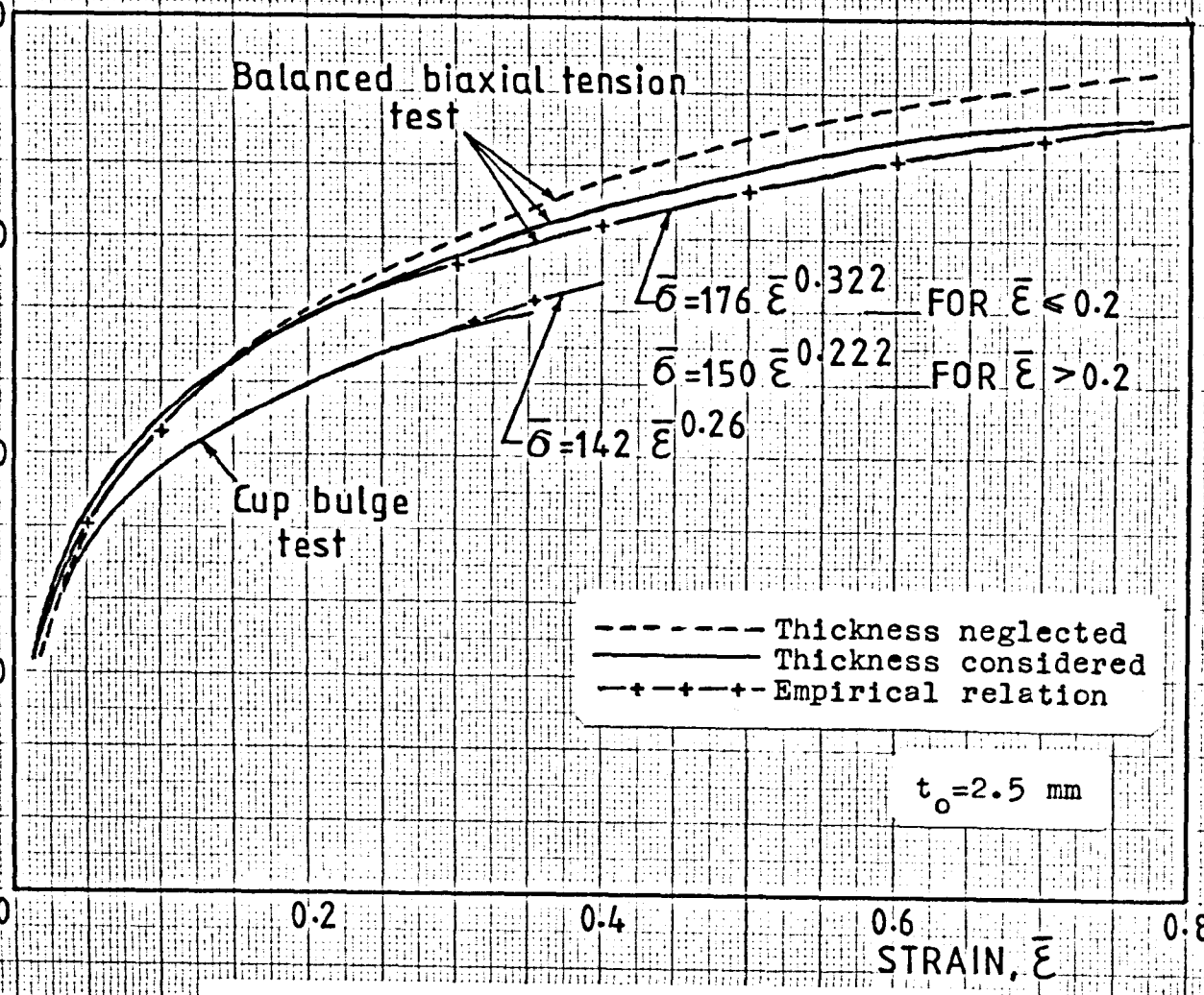

Stress-strain curve for soft aluminium, determined from balanced biaxial tension test and cup bulge test.

Fig.(6.22)

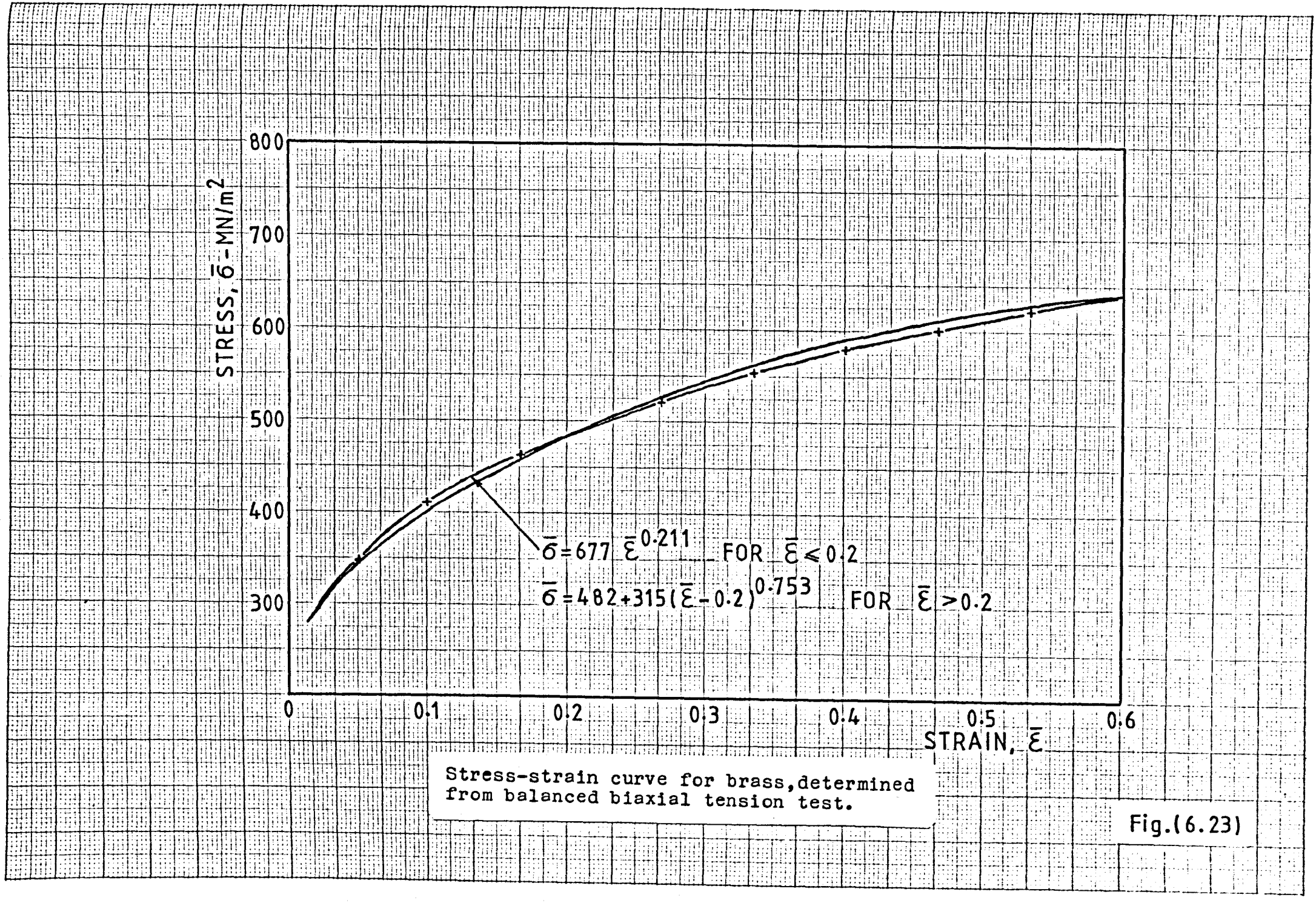

Stress-strain curve for brass, determined from balanced biaxial tension test.

Fig.(6.23)

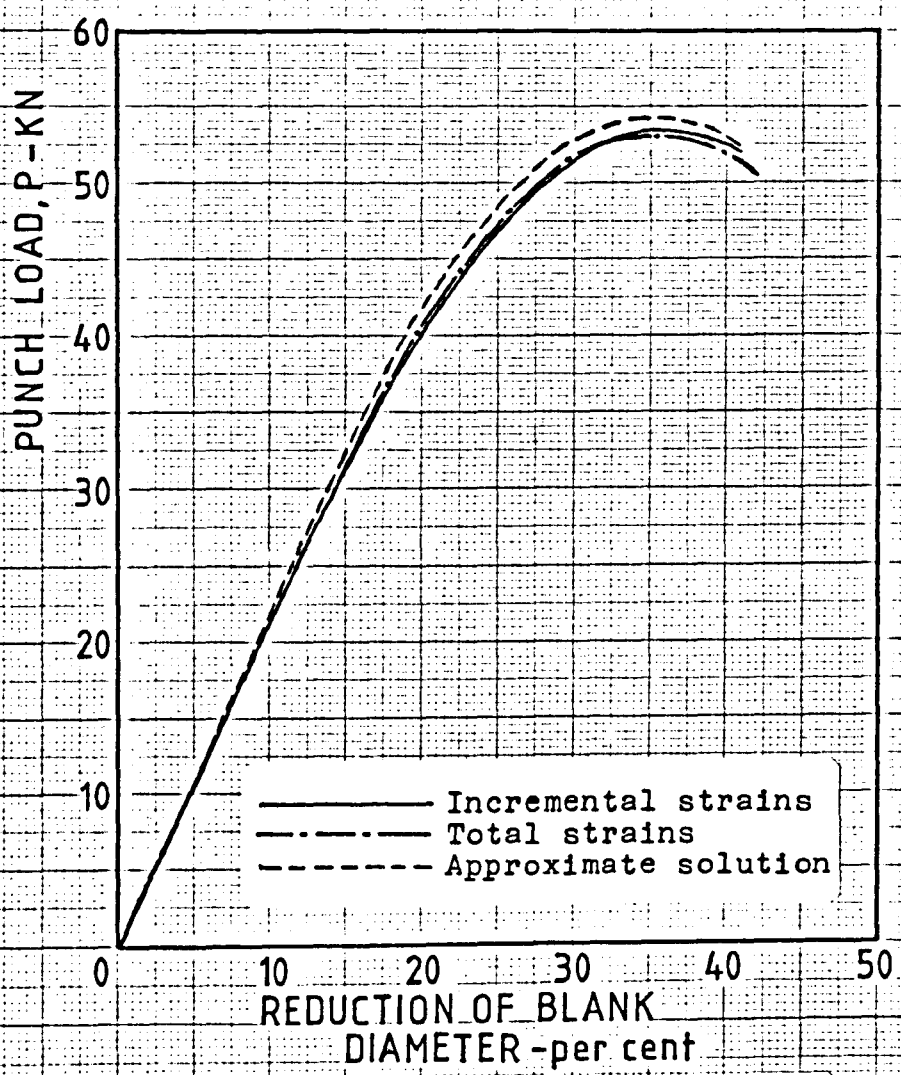

Punch load against reduction of blank diameter determined from theory. Mild steel. Die profile 1.

Fig.(7.1)

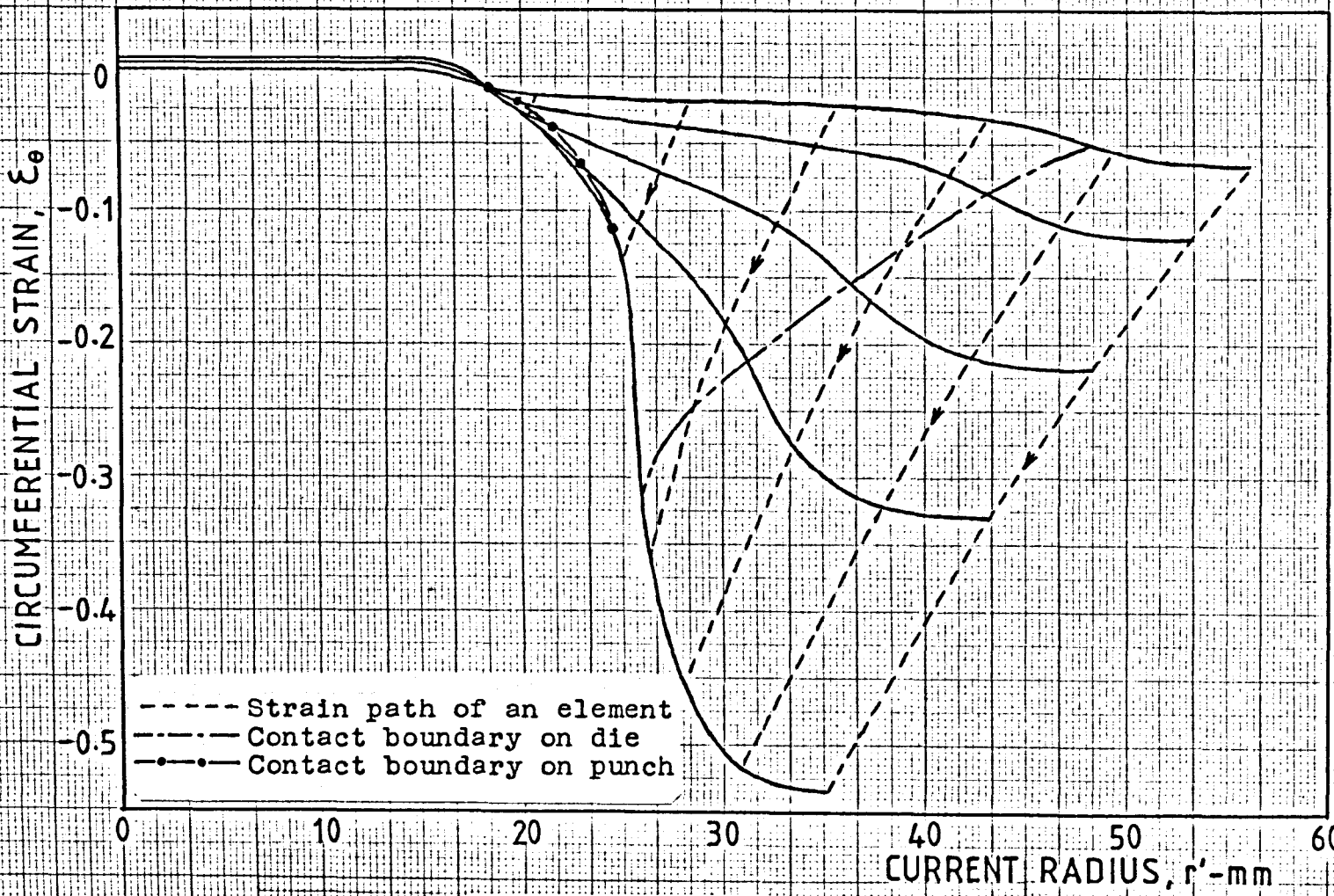

Distribution of circumferential strain .Mild steel.Die profile 1.

Fig.(7.2)

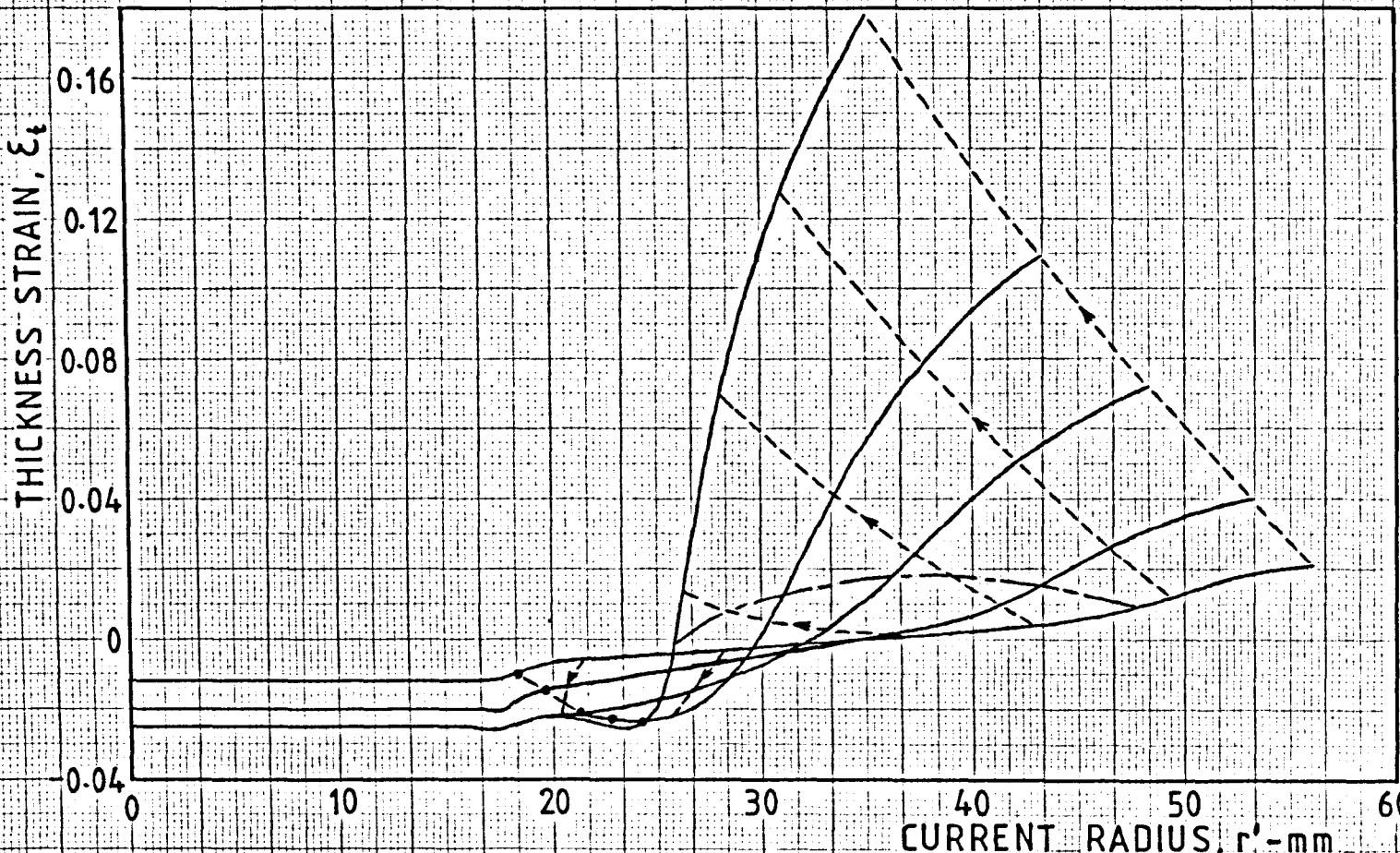

Distribution of thickness strain.
Mild steel.Die profile 1.

Fig.(7.3)

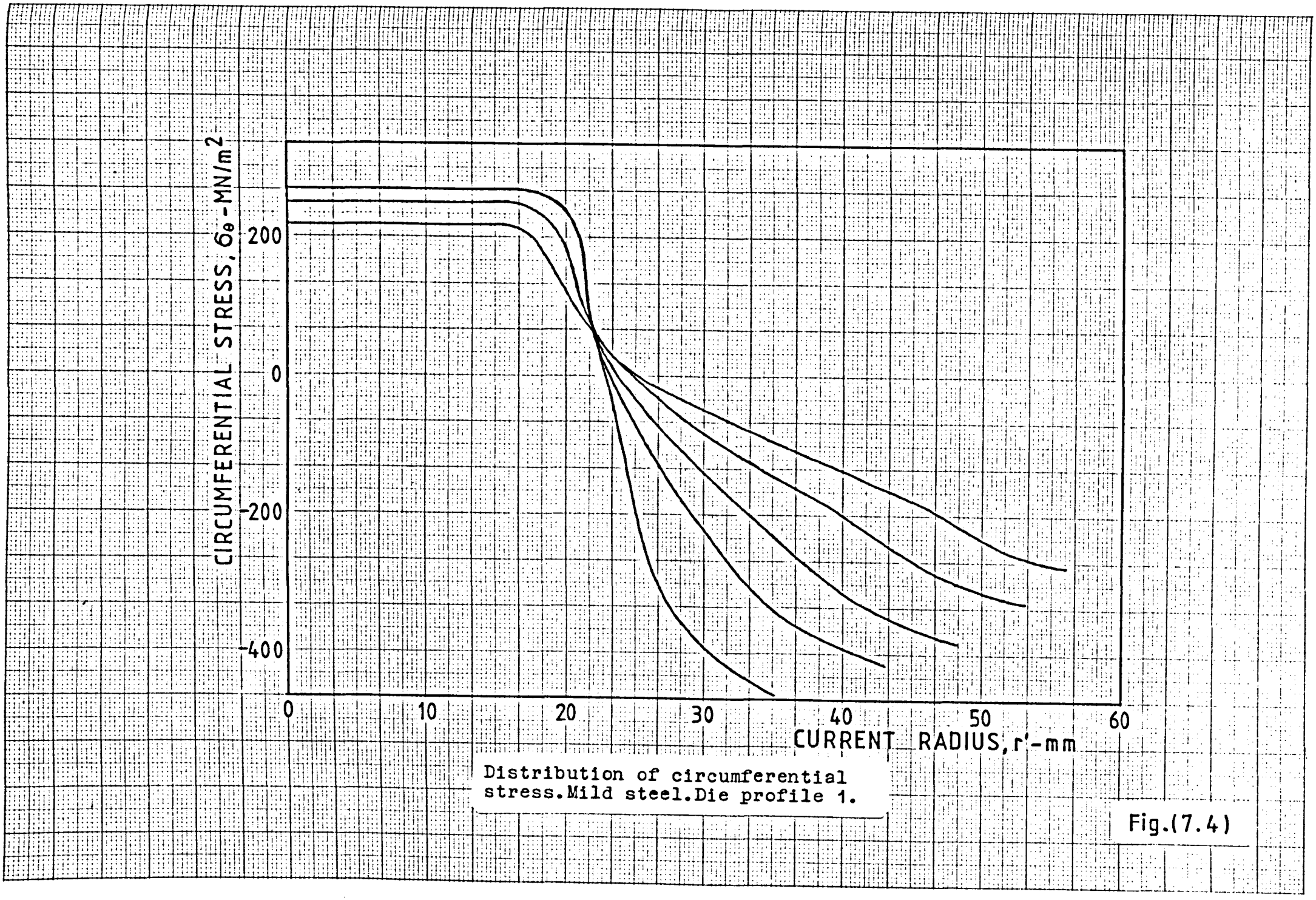

Distribution of circumferential stress. Mild steel. Die profile 1.

Fig.(7.4)

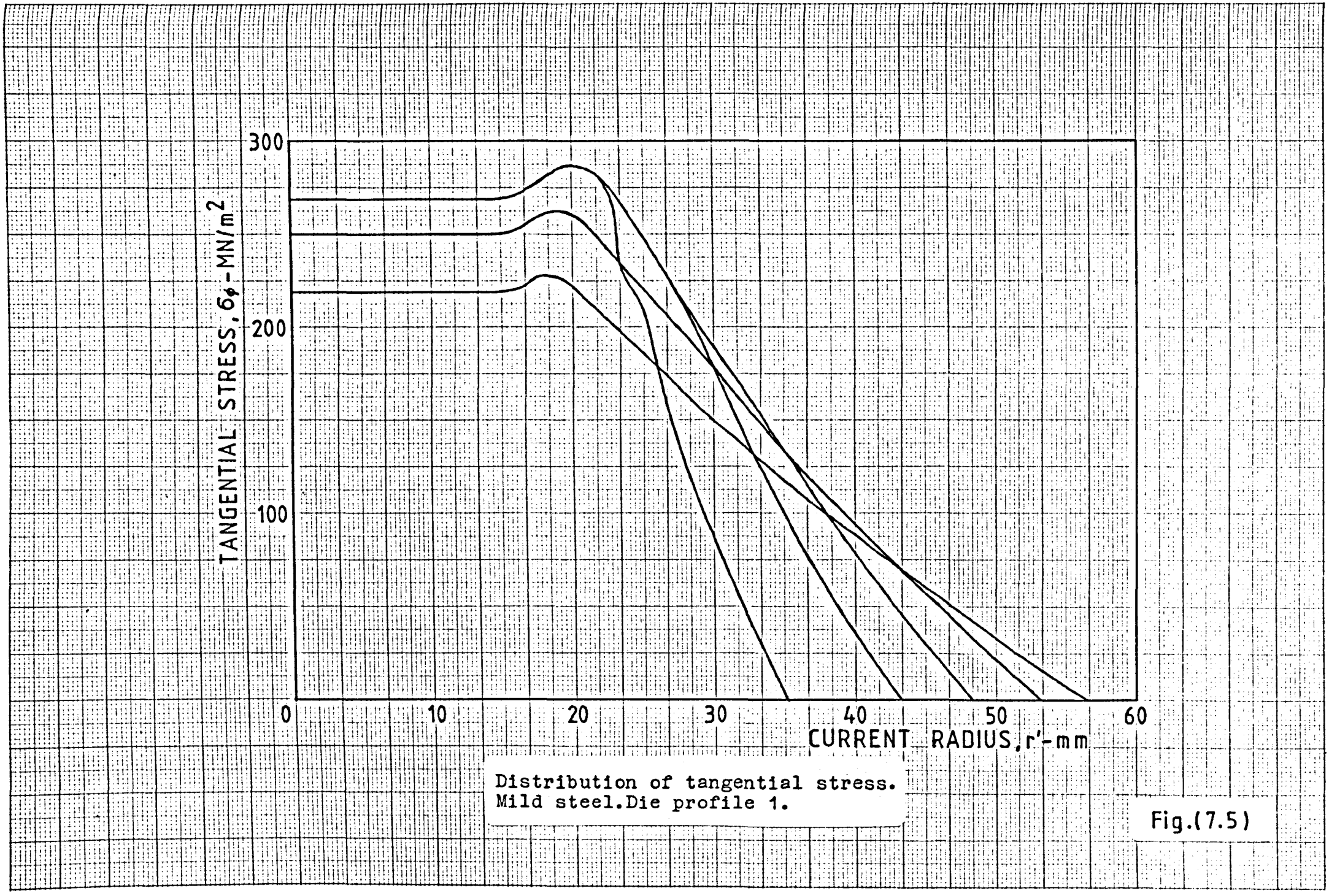

Distribution of tangential stress.
Mild steel. Die profile 1.

Fig.(7.5)

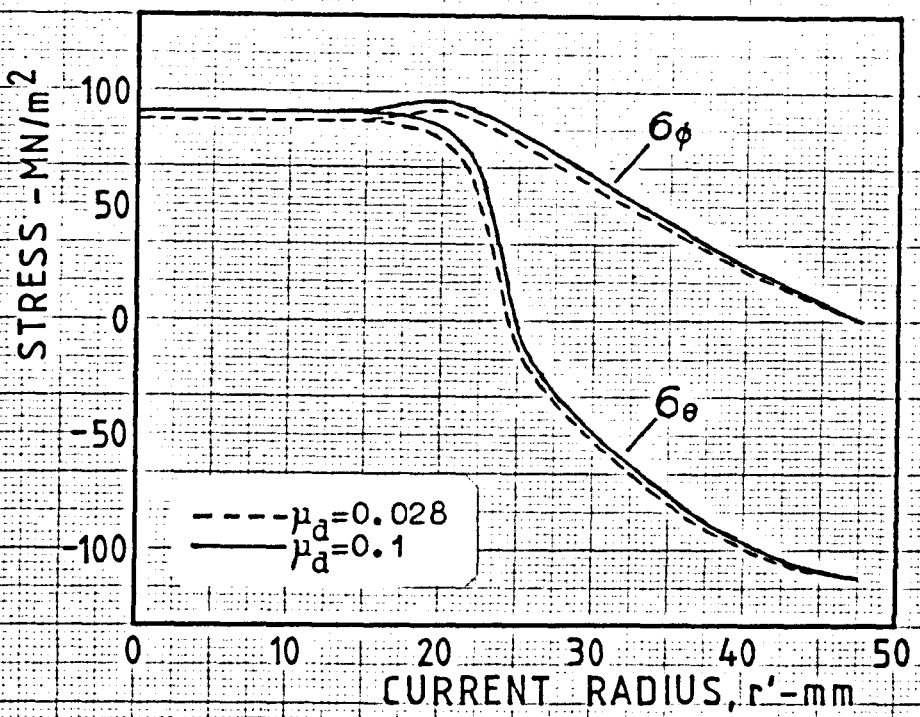

Effect of friction between material and die on stresses.

Fig.(7.6)

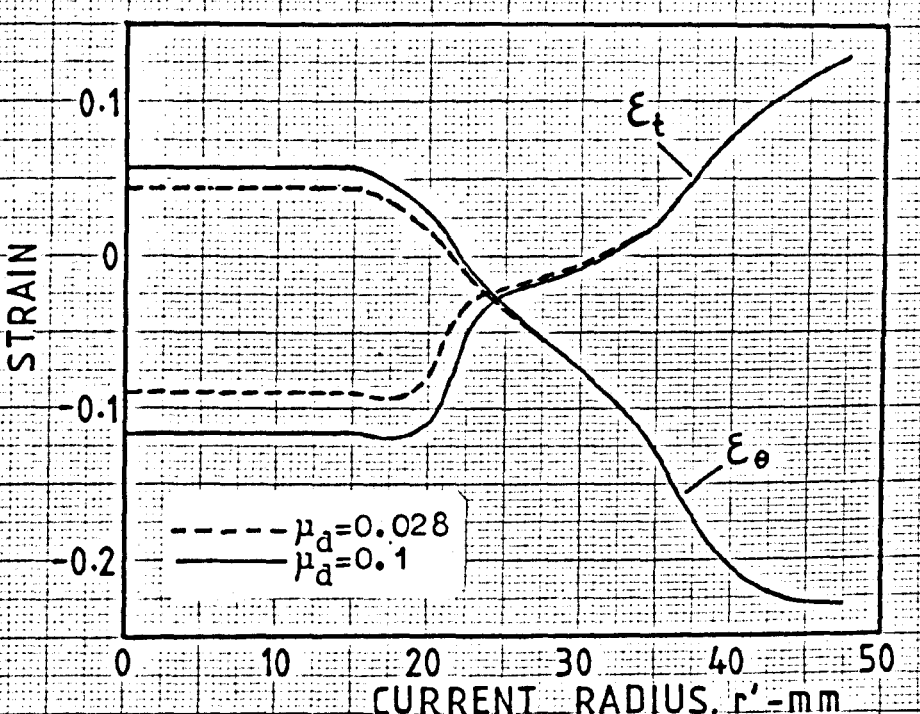

Effect of friction between material and die on strains.

Fig.(7.7)

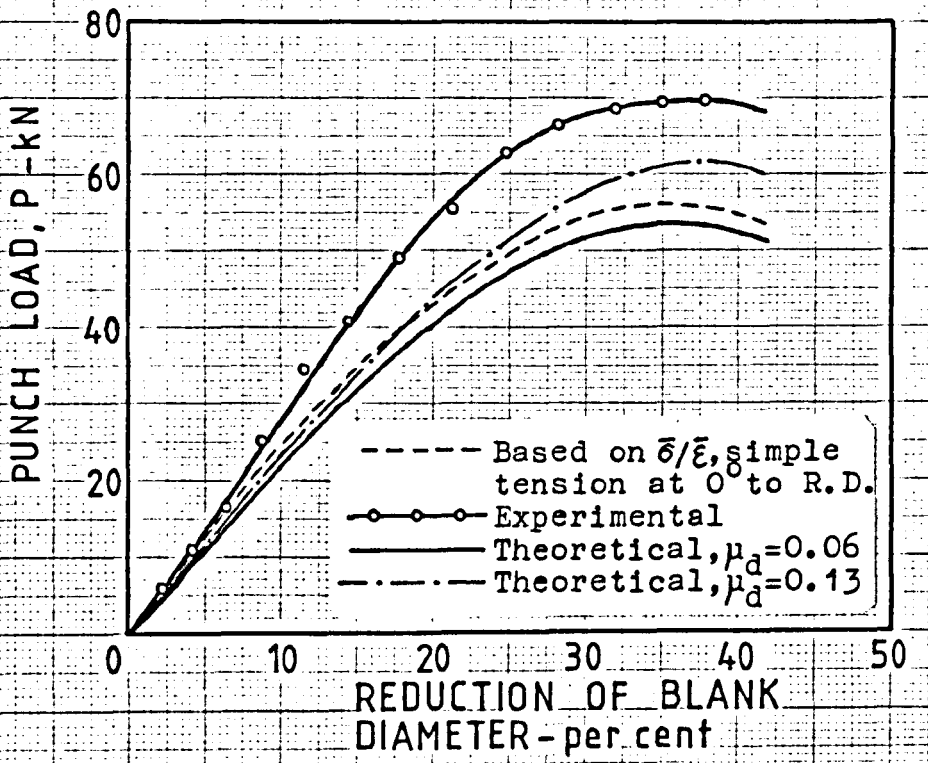

Punch load against reduction of blank diameter. Mild steel. Die profile 1.

Fig.(7.8a)

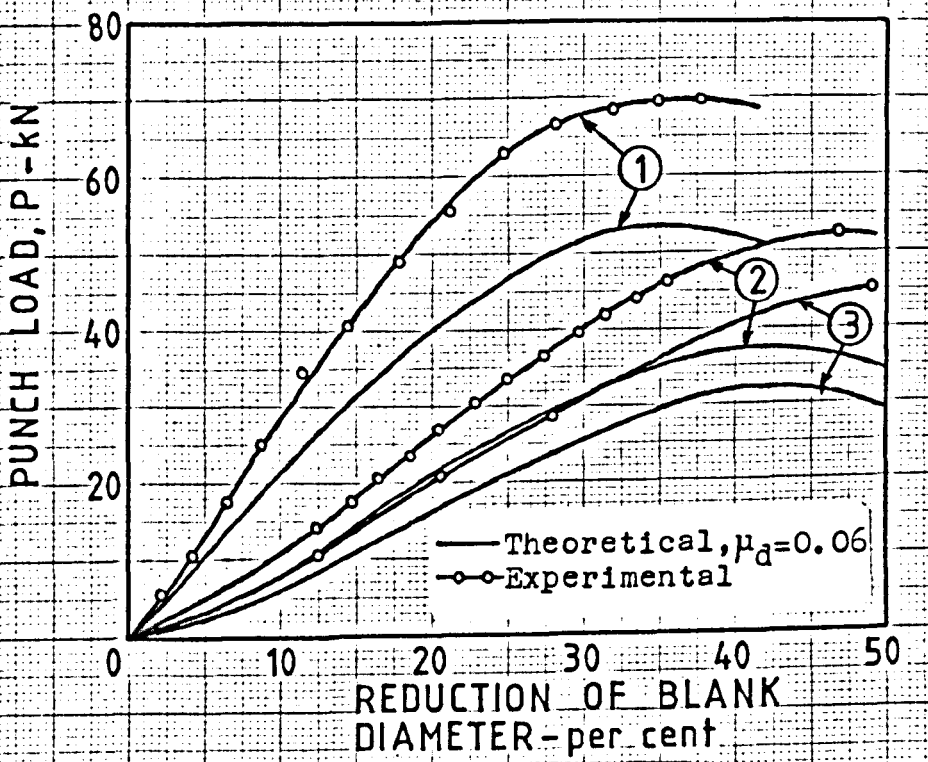

Punch load against reduction of blank diameter. Mild steel. Die profiles 1, 2 and 3.

Fig.(7.8b)

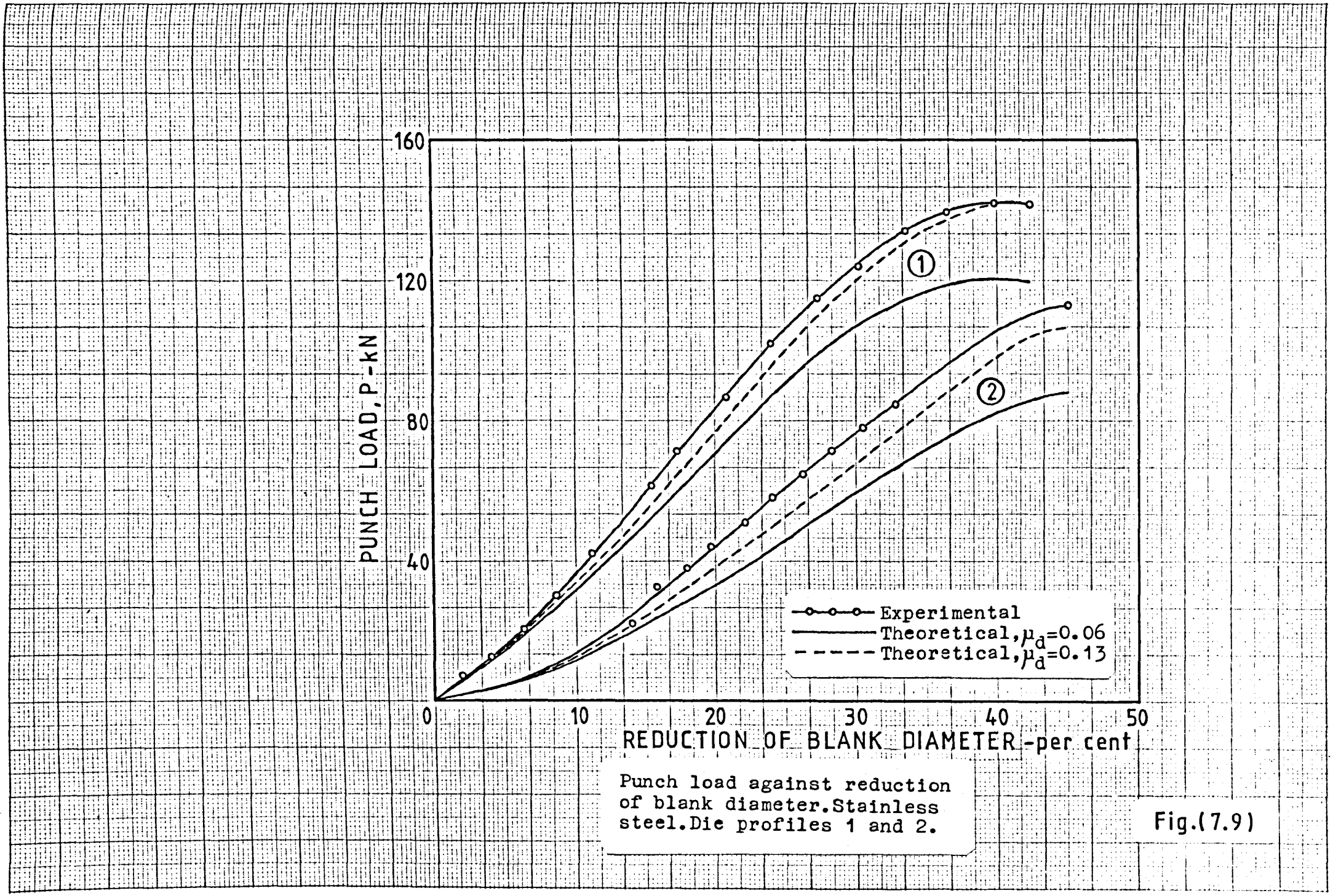

Punch load against reduction of blank diameter. Stainless steel. Die profiles 1 and 2.

Fig.(7.9)

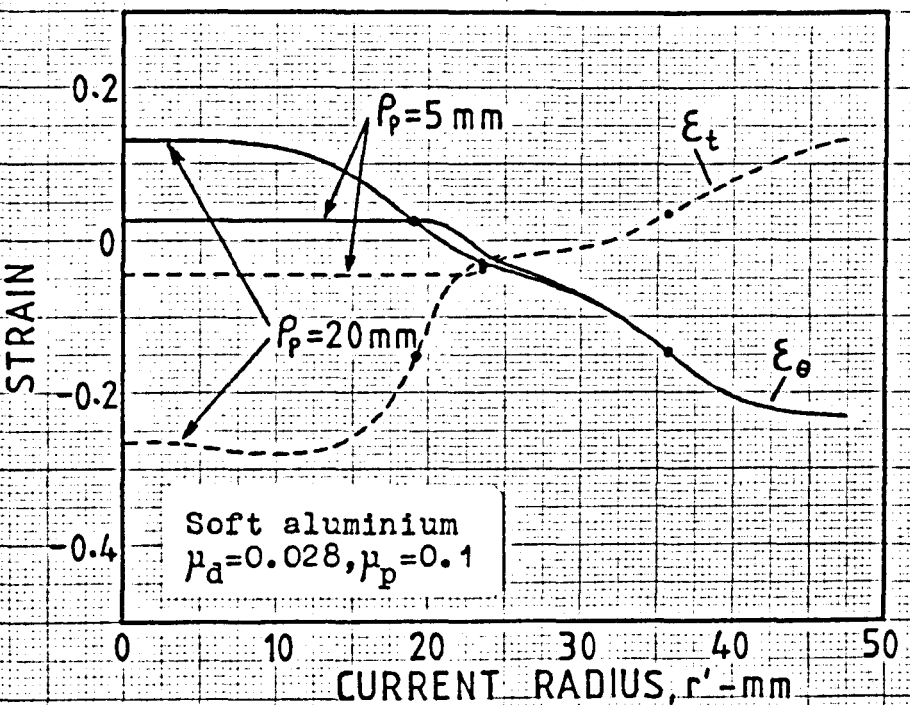

Effect of punch profile radius on strains.

Fig.(7.10)

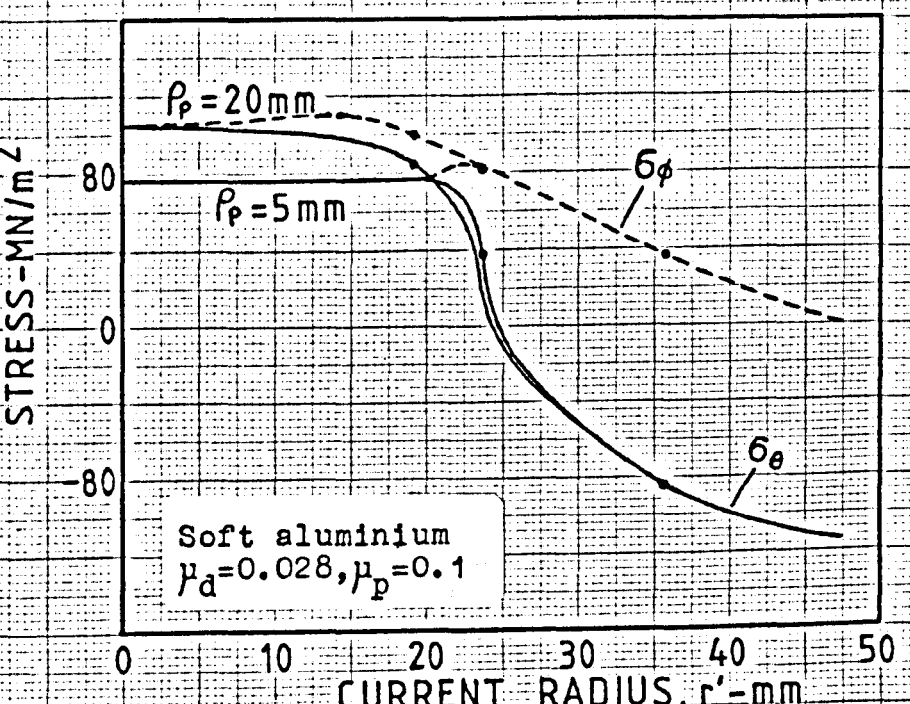

Effect of punch profile radius on stresses.

Fig.(7.11)

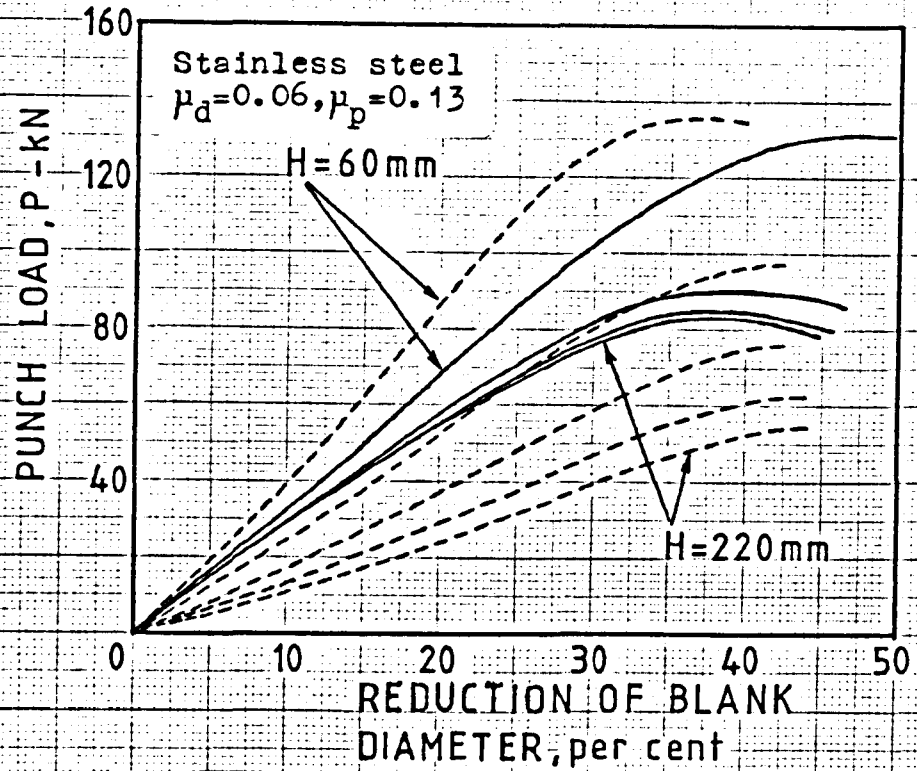

Effect of die height on punch load/reduction of blank diameter relation.
——— Tractrix die profile
- - - - - Exponential spiral die profile

Fig.(7.12)

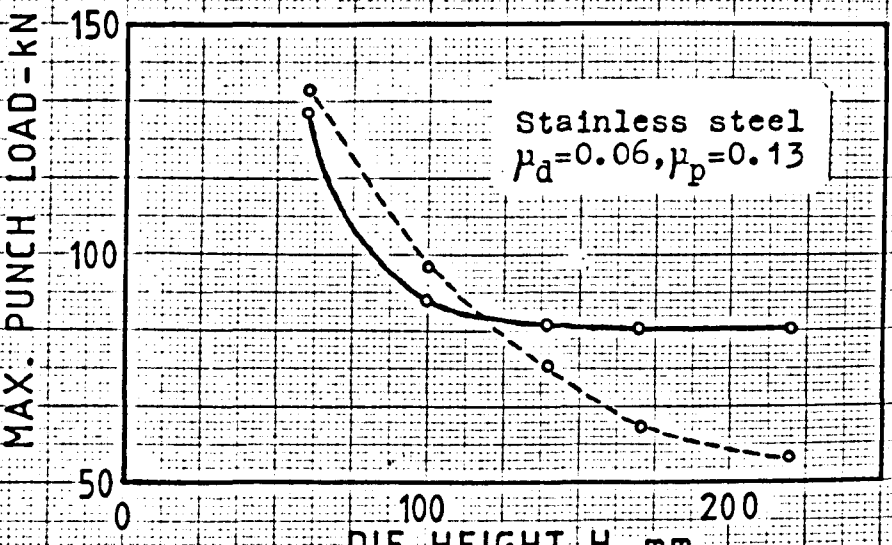

Effect of die height on maximum punch load.
—o—o—o— Tractrix die profile
-o--o--o- Exponential spiral die profile

Fig.(7.13)

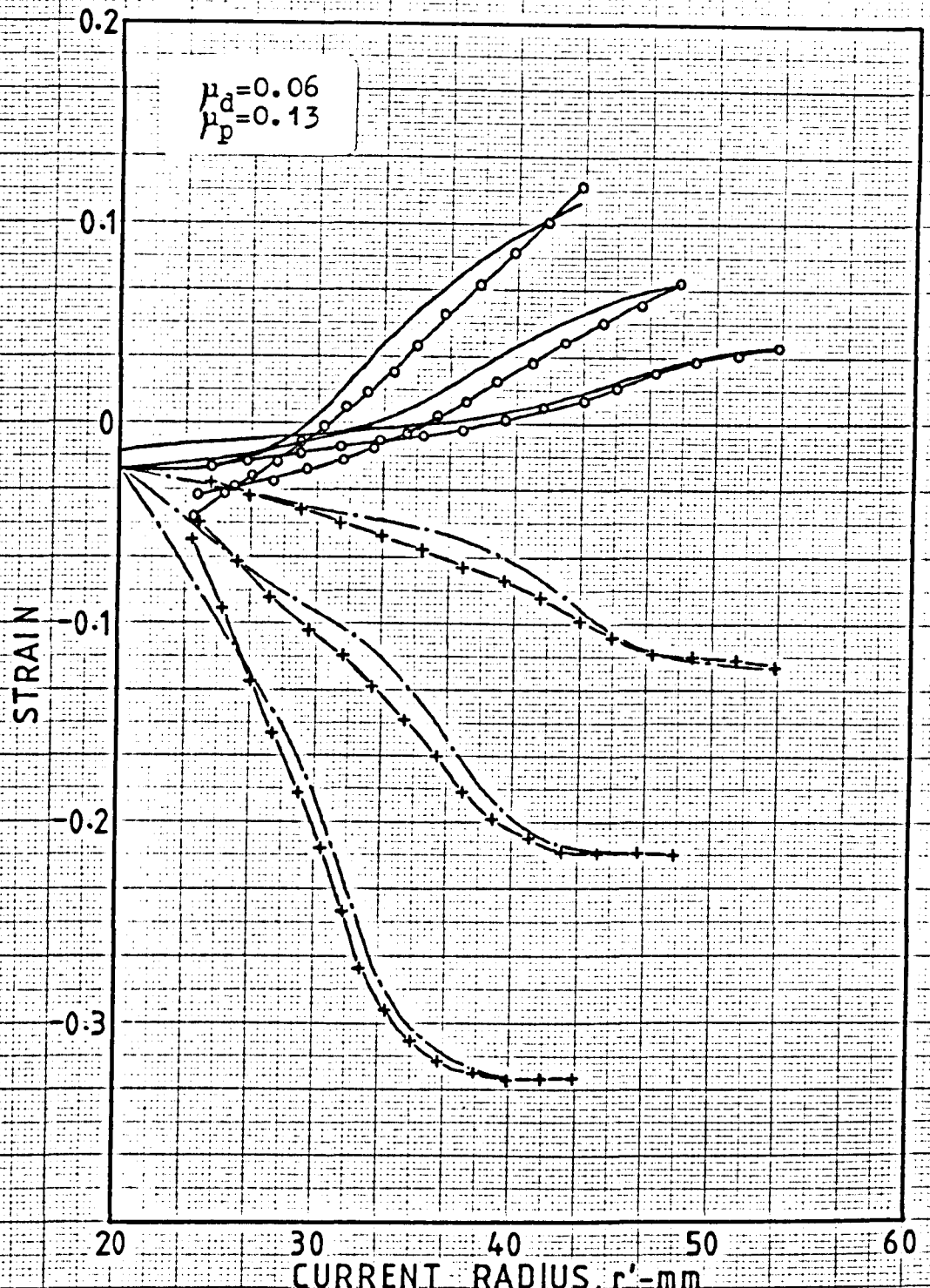

Comparison of theoretical and experimental strains. Mild steel. Die profile 1.

——— Theoretical thickness strain

—o—o—o— Experimental thickness strain

—·—·— Theoretical circumferential strain

—+—+—+— Experimental circumferential strain

Fig.(8.1)

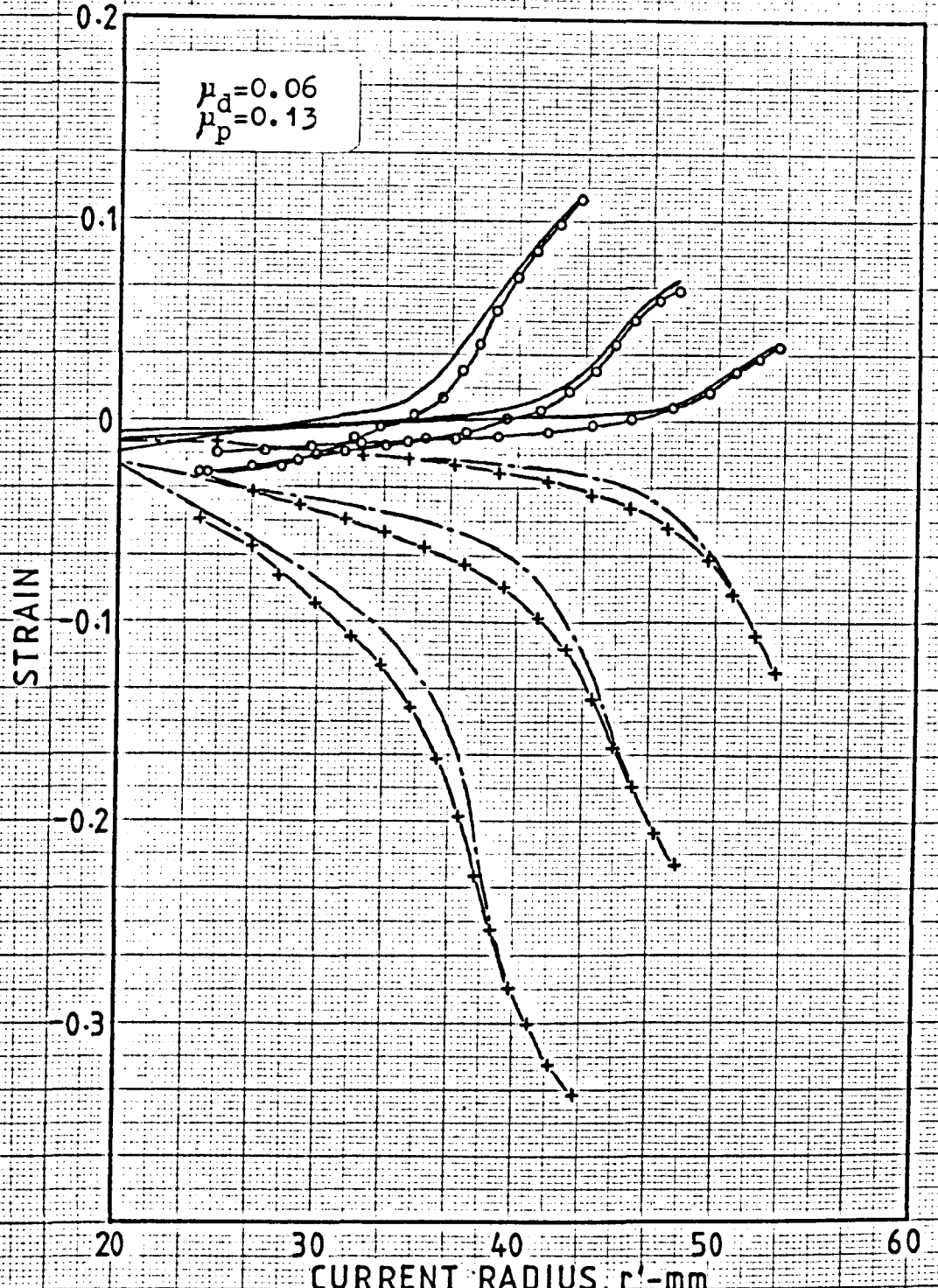

Comparison of theoretical and experimental strains. Mild steel. Die profile 2.

——— Theoretical thickness strain

—o—o—o— Experimental thickness strain

—·—·— Theoretical circumferential strain

—+—+—+— Experimental circumferential strain

Fig.(8.2)

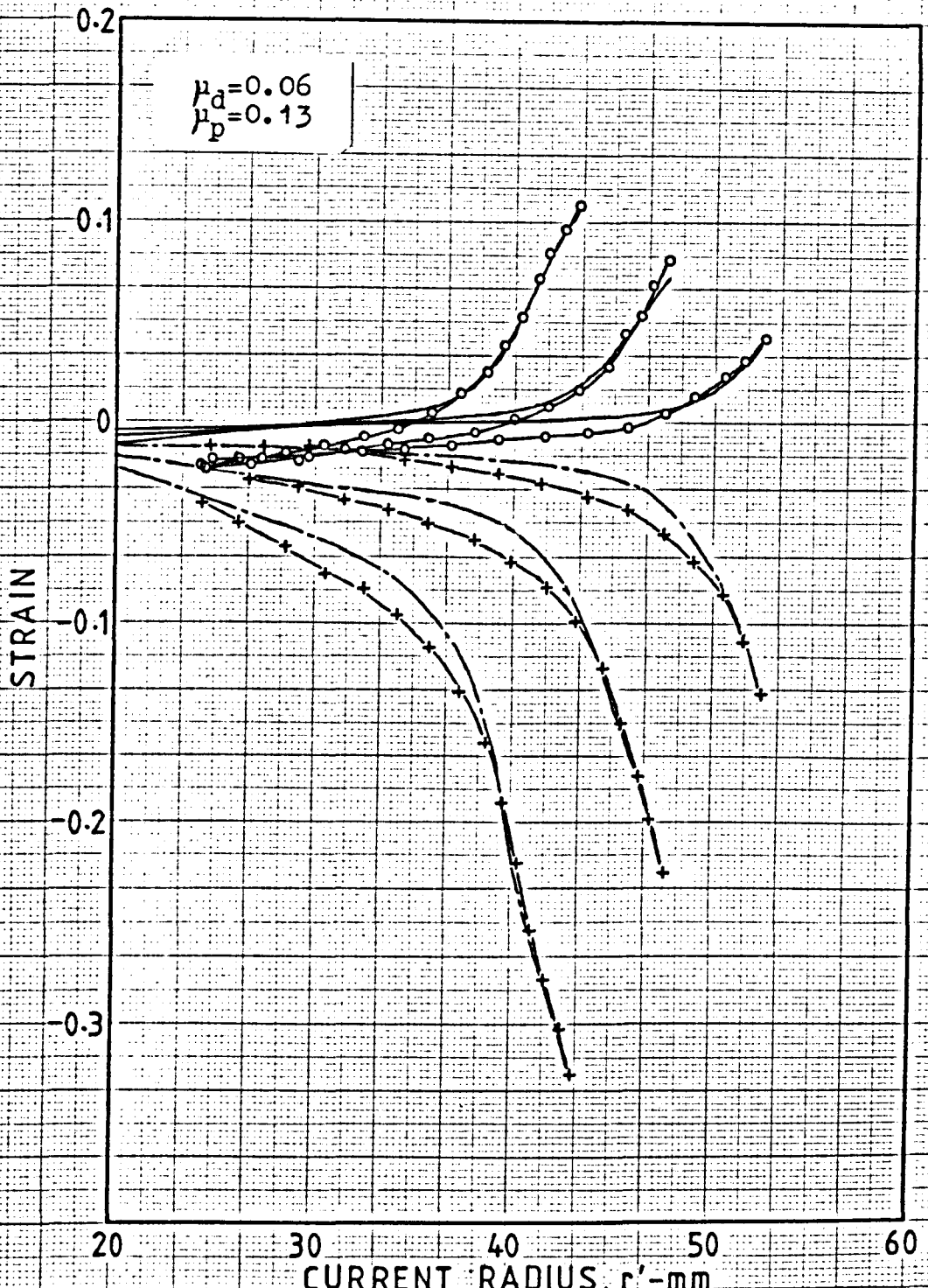

Comparison of theoretical and experimental strains. Mild steel. Die profile 3.

——— Theoretical thickness strain

—o—o—o— Experimental thickness strain

—·—·— Theoretical circumferential strain

—+—+—+— Experimental circumferential strain

Fig.(8.3)

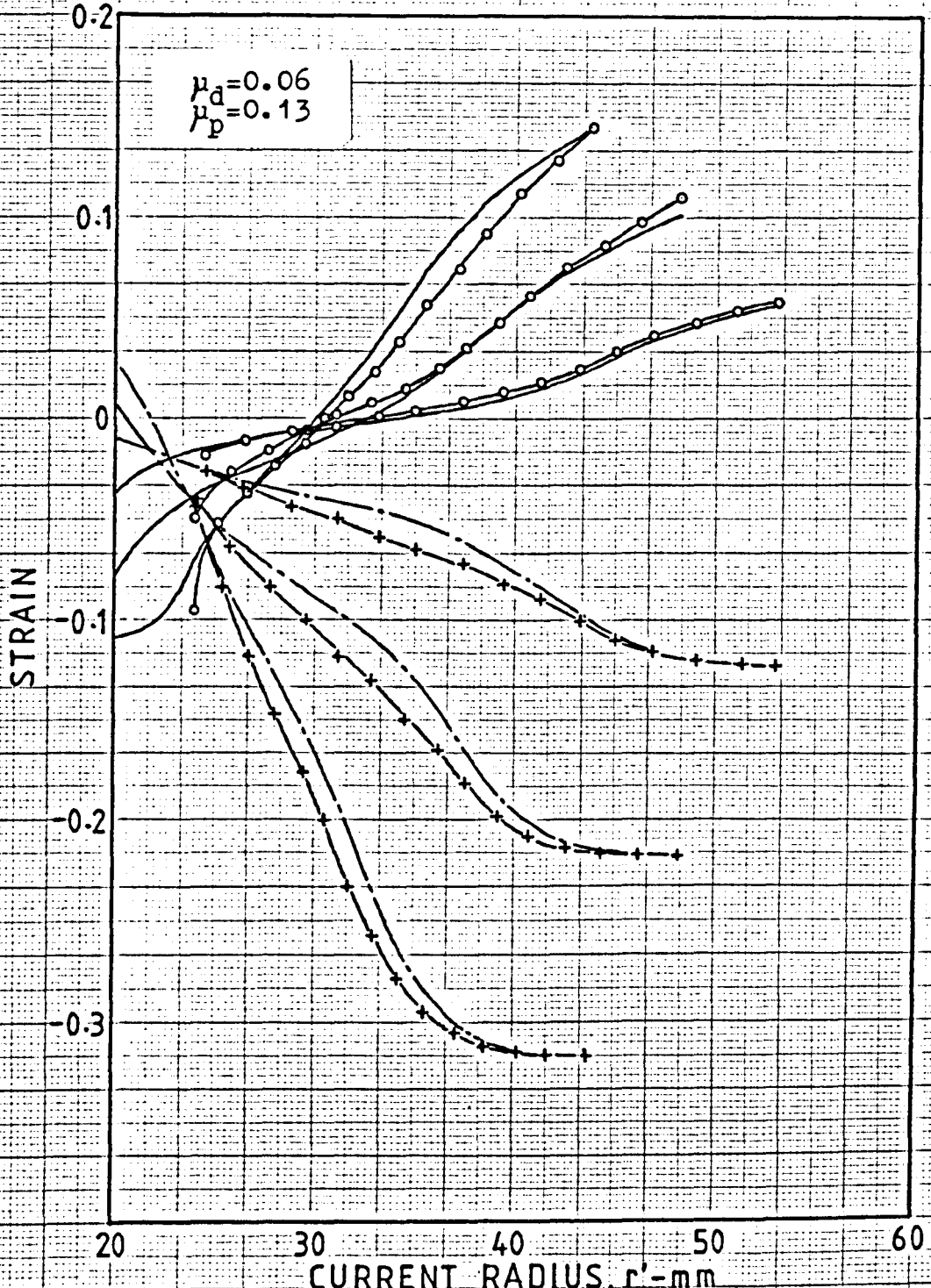

Comparison of theoretical and experimental strains. Stainless steel. Die profile 1.

——— Theoretical thickness strain

—o—o—o— Experimental thickness strain

—·—·— Theoretical circumferential strain

—+—+—+— Experimental circumferential strain

Fig.(8.4)

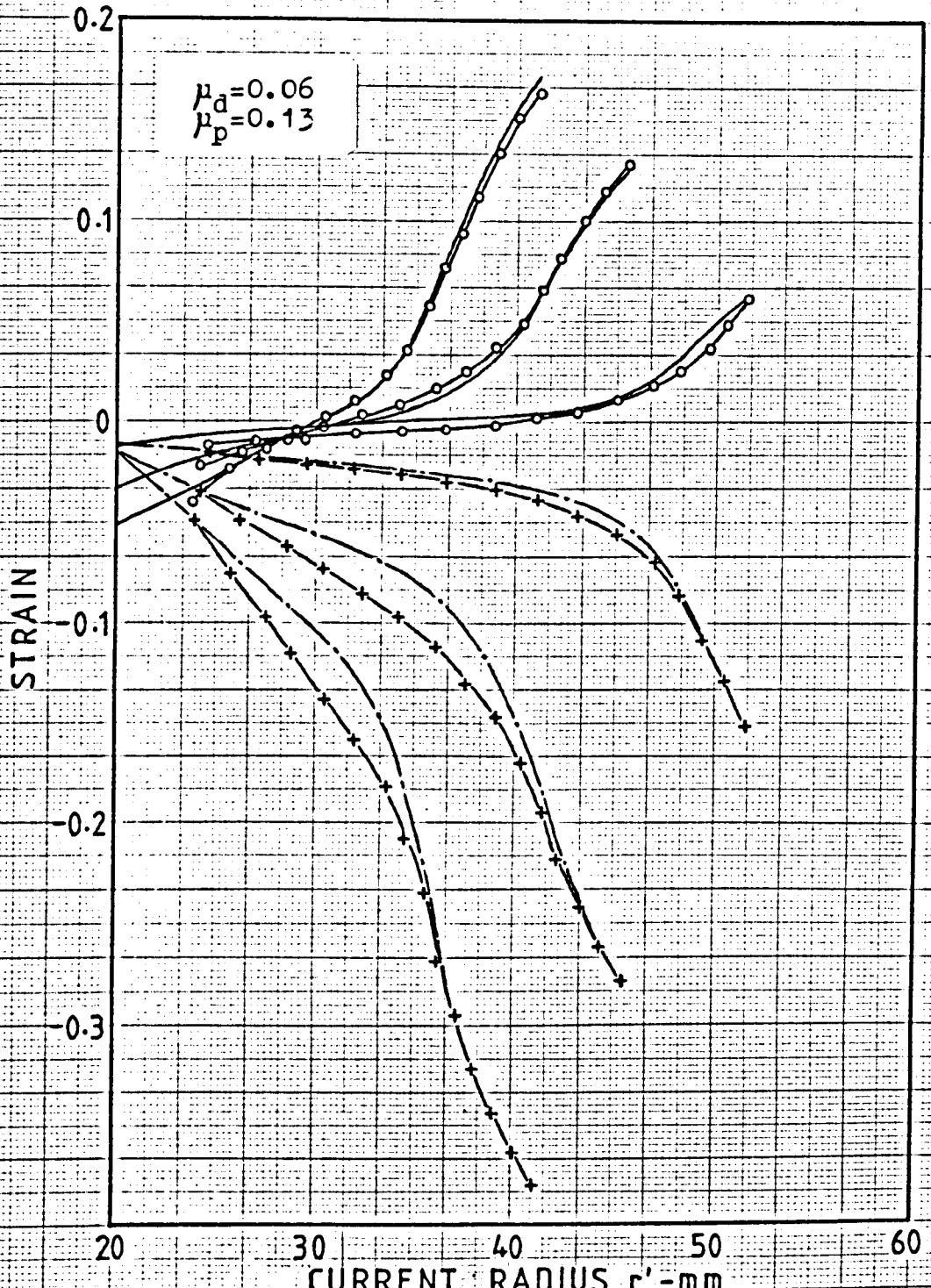

Comparison of theoretical and experimental strains. Stainless steel. Die profile 2.

——— Theoretical thickness strain

—o—o—o— Experimental thickness strain

—·—·— Theoretical circumferential strain

—+—+—+— Experimental circumferential strain

Fig.(8.5)

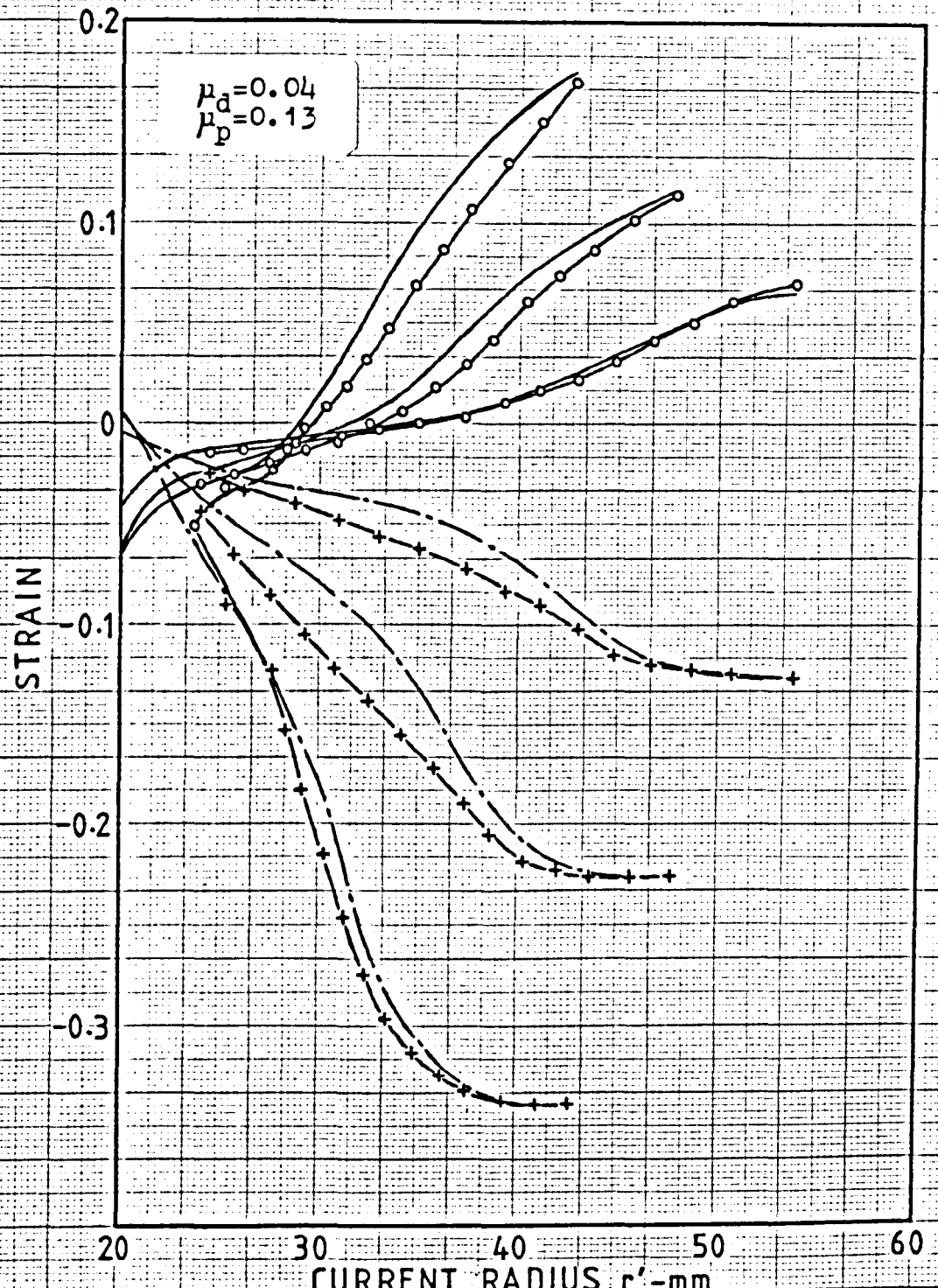

Comparison of theoretical and experimental strains. Brass. Die profile 1.

——— Theoretical thickness strain

—o—o—o— Experimental thickness strain

—·—·— Theoretical circumferential strain

—+—+—+— Experimental circumferential strain

Fig.(8.6)

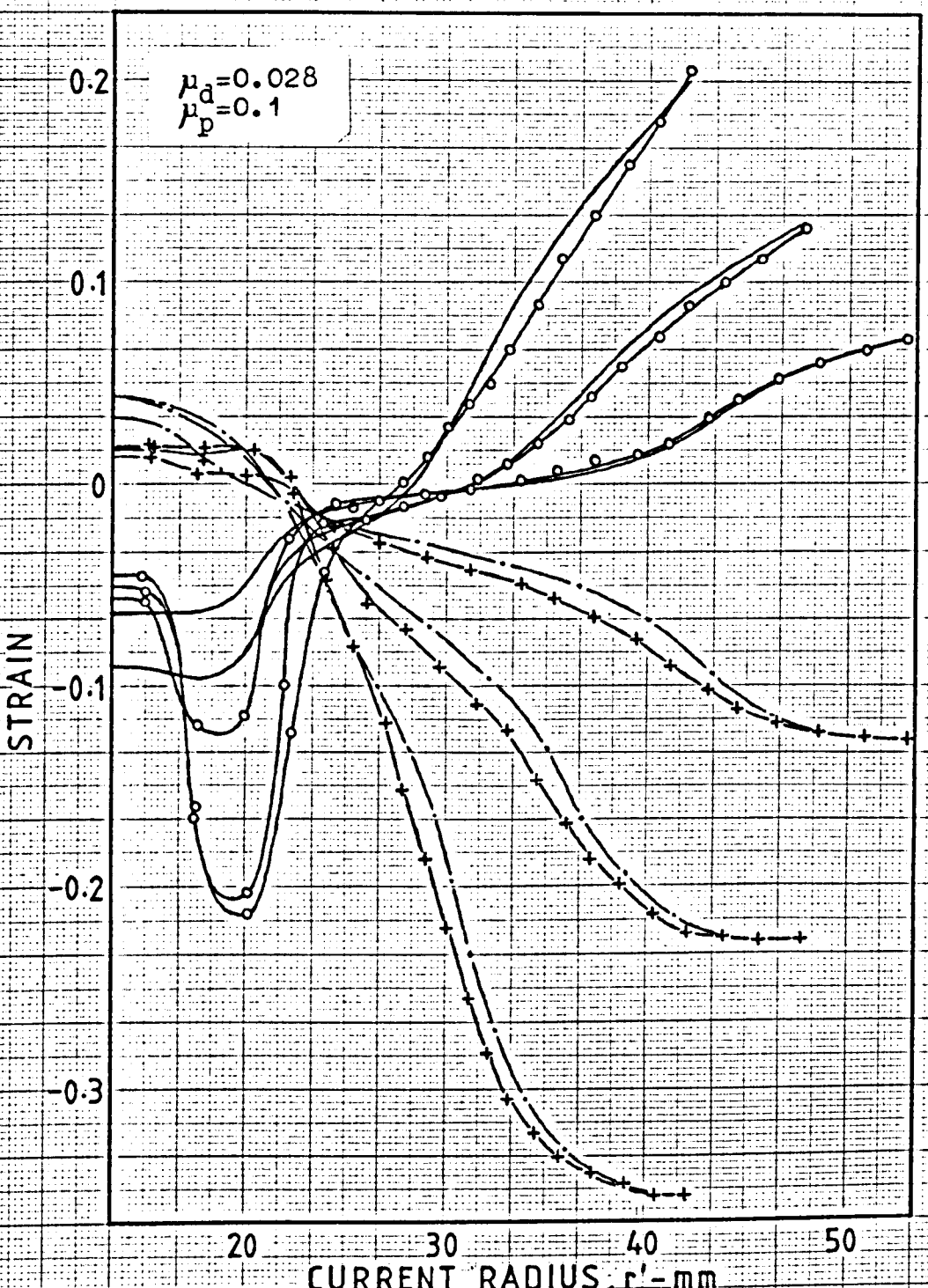

Comparison of theoretical and experimental strains. Soft aluminium. Die profile 1.

——— Theoretical thickness strain

—o—o—o— Experimental thickness strain

—·—·— Theoretical circumferential strain

—+—+—+— Experimental circumferential strain

Fig.(8.7)

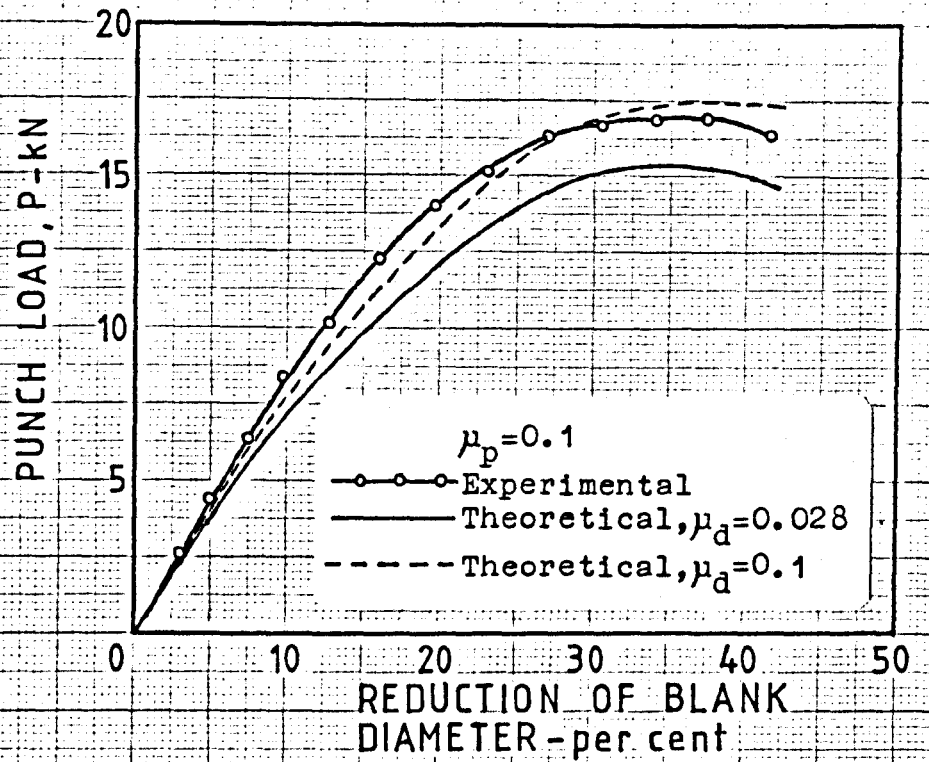

Punch load against reduction of blank diameter. Soft aluminium. Die profile 1.

Fig.(8.8)

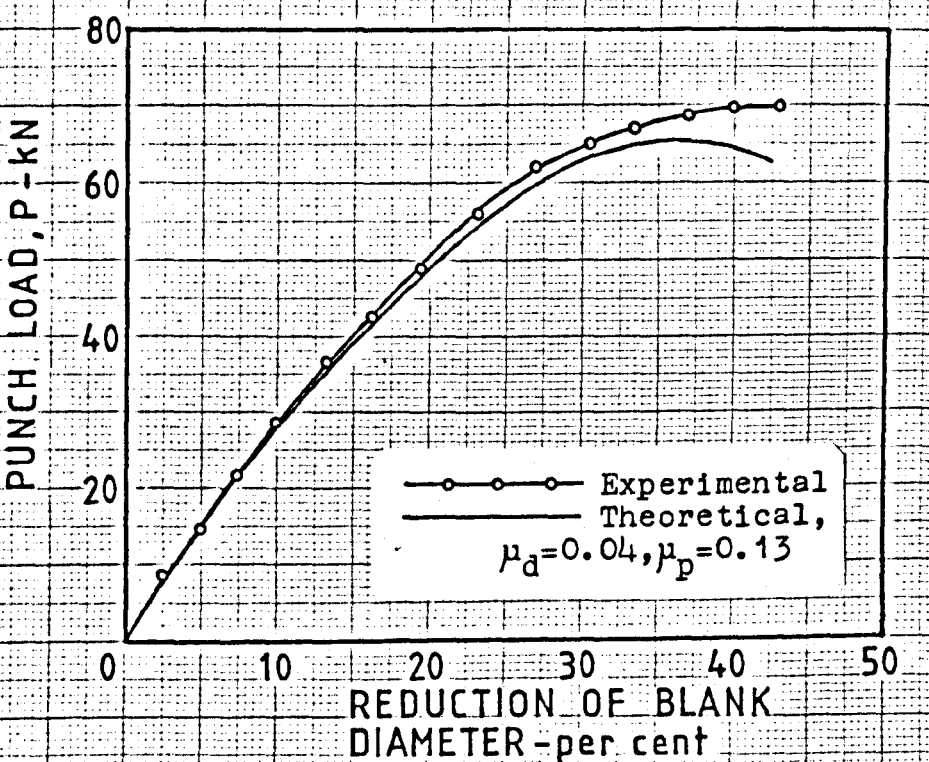

Punch load against reduction of blank diameter. Brass. Die profile 1.

Fig.(8.9)

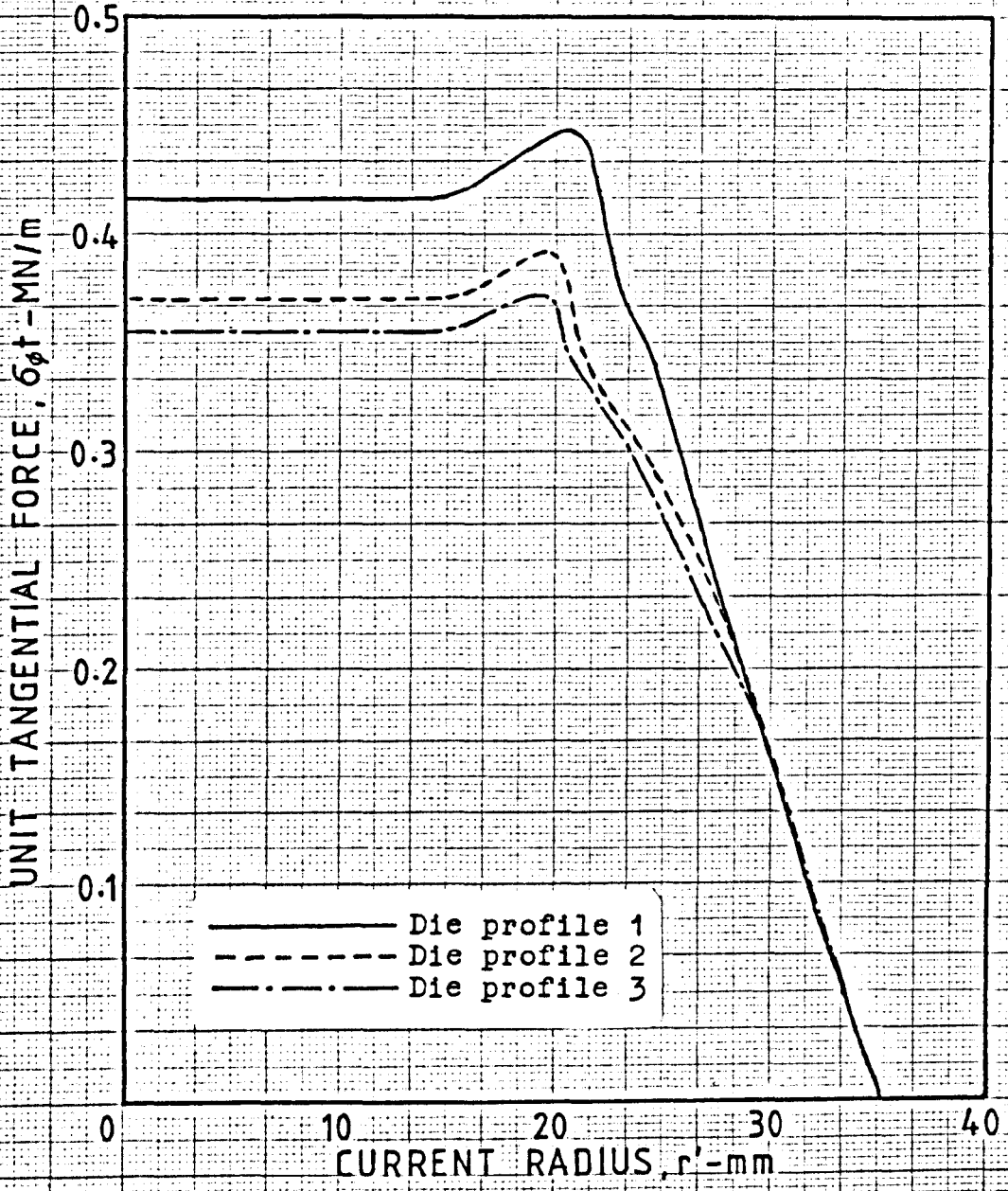

Unit-tangential force distribution.
Mild steel.

Fig.(8.10)

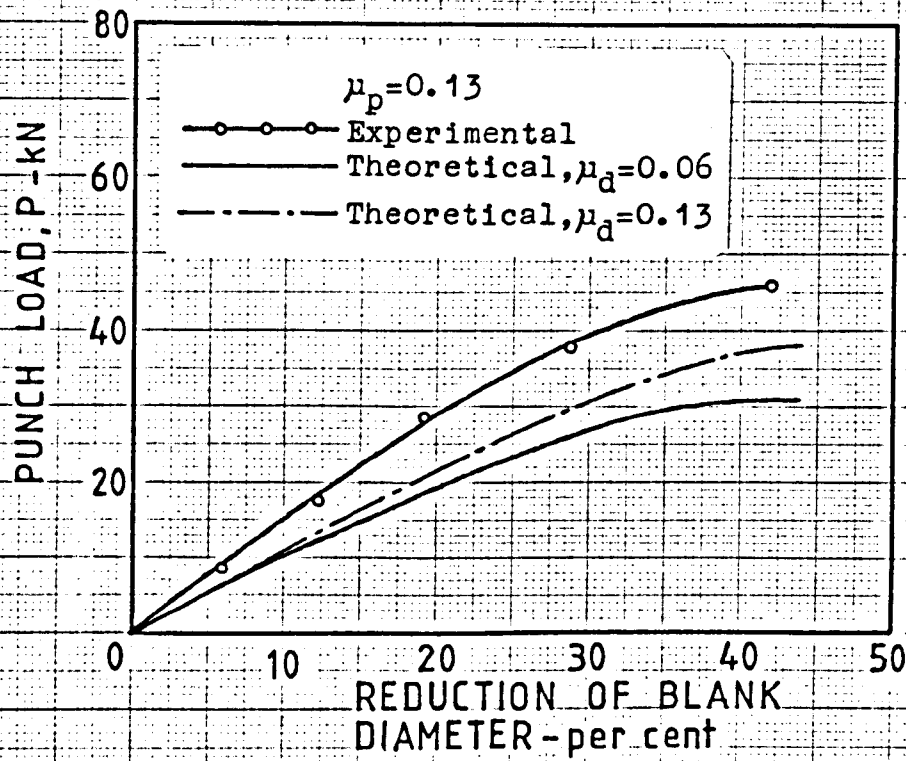

Comparison of theoretical and experimental punch load/reduction of blank diameter relation. Mild steel. Die profile 4.

Fig.(8.11)

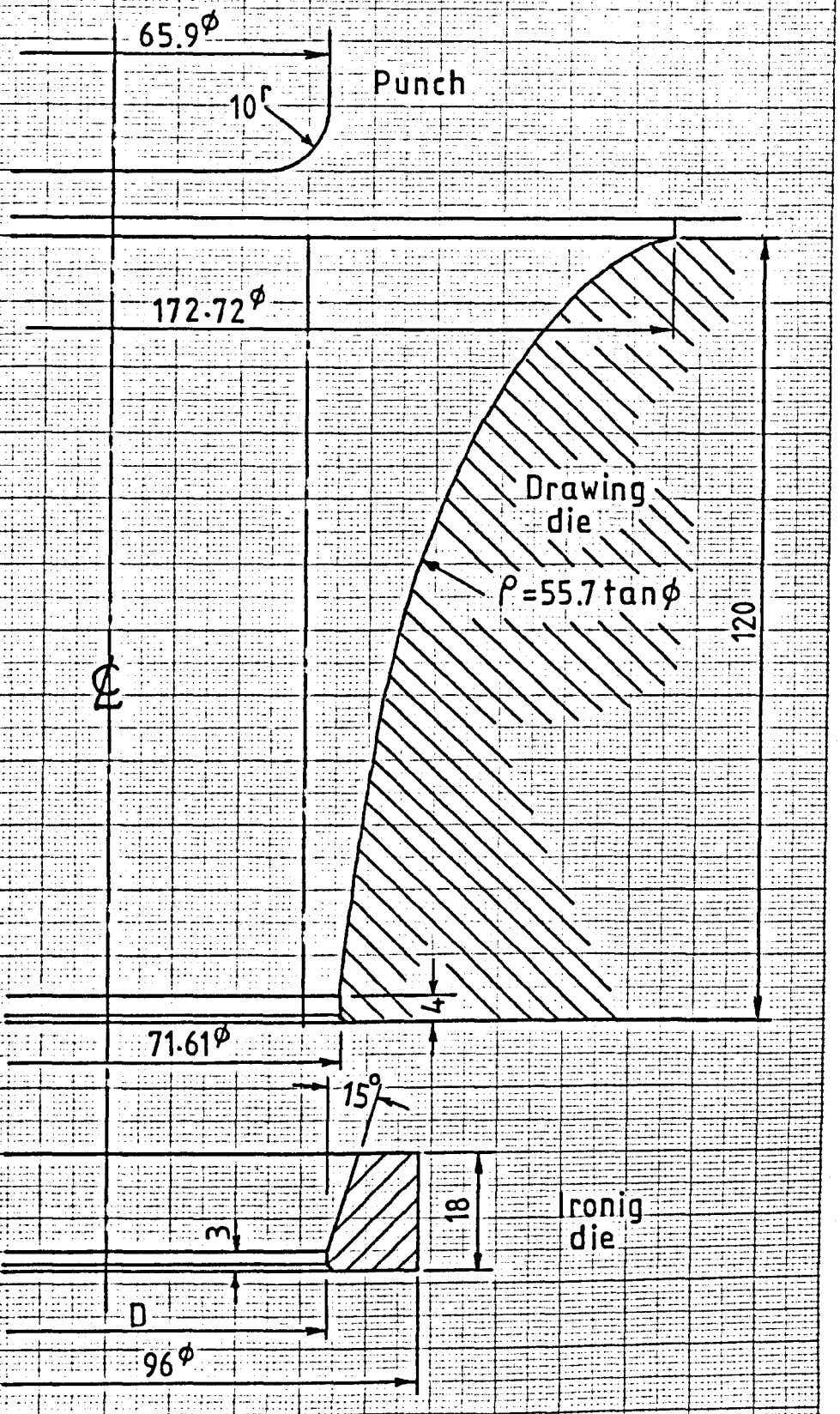

Tooling for deep drawing and ironing.

Fig.(10.1)

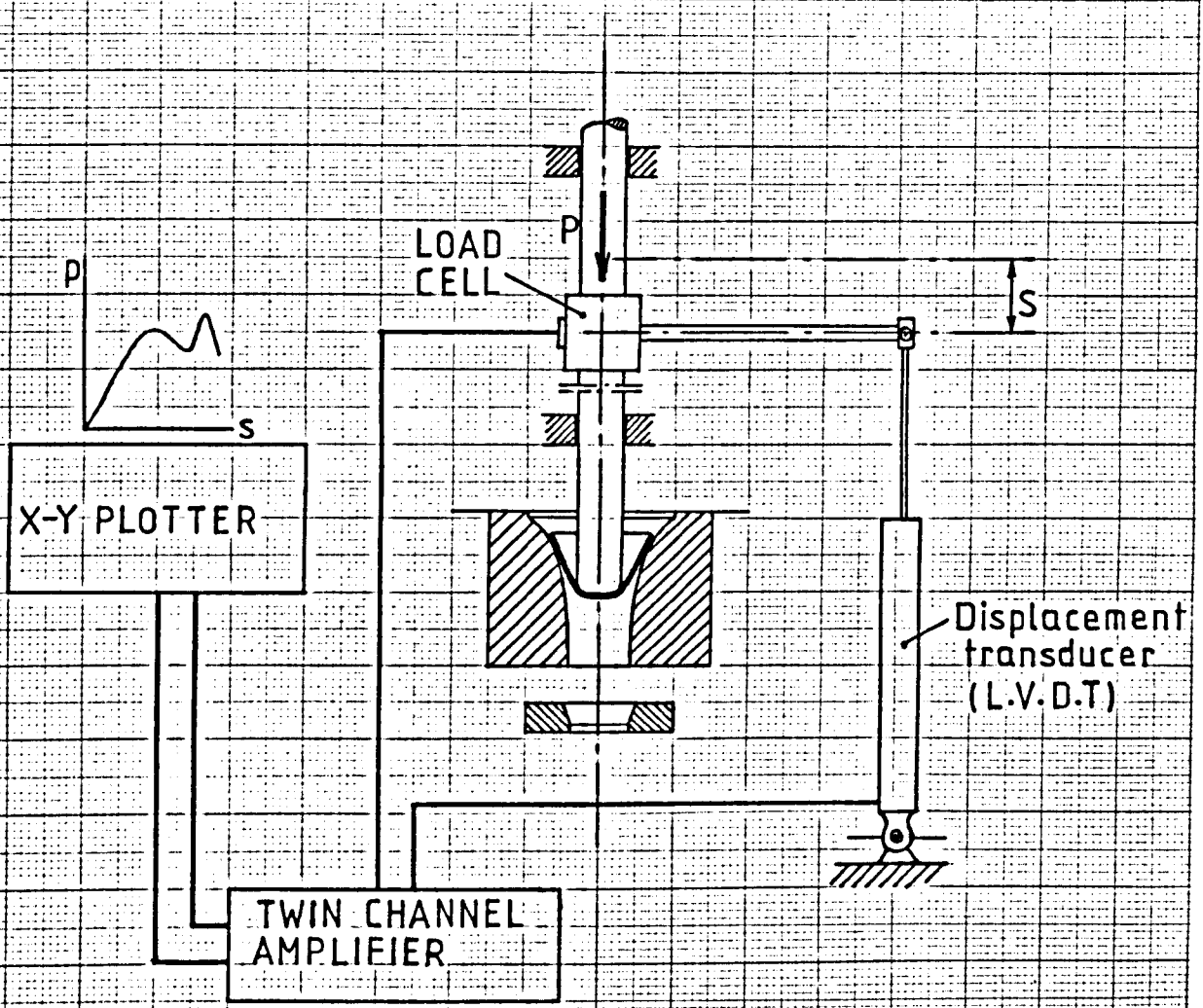

A system for autographic measurement of the punch load/stroke relation in deep drawing and ironing.

Fig.(10.2)

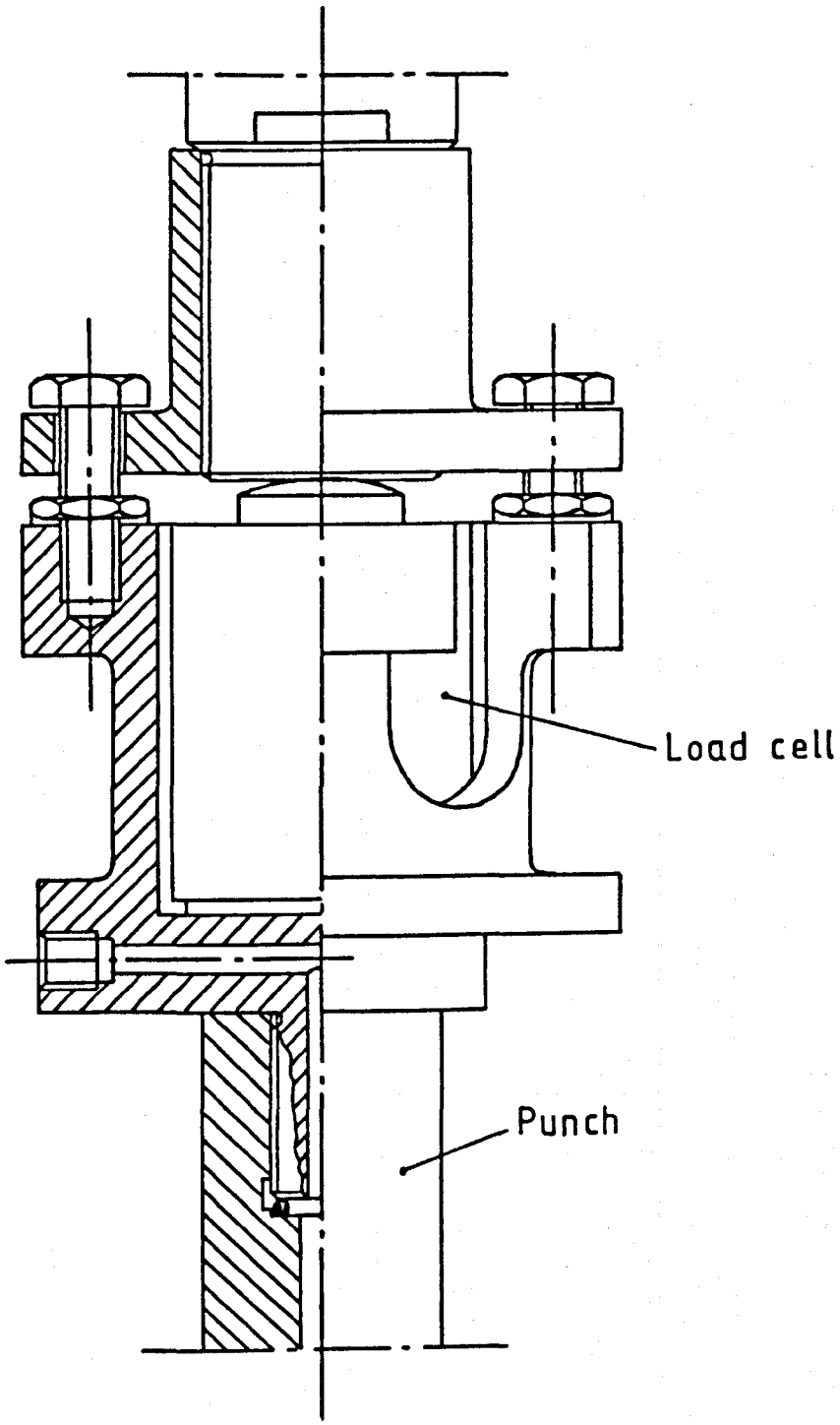

Load cell attachment

Fig.(10.3)

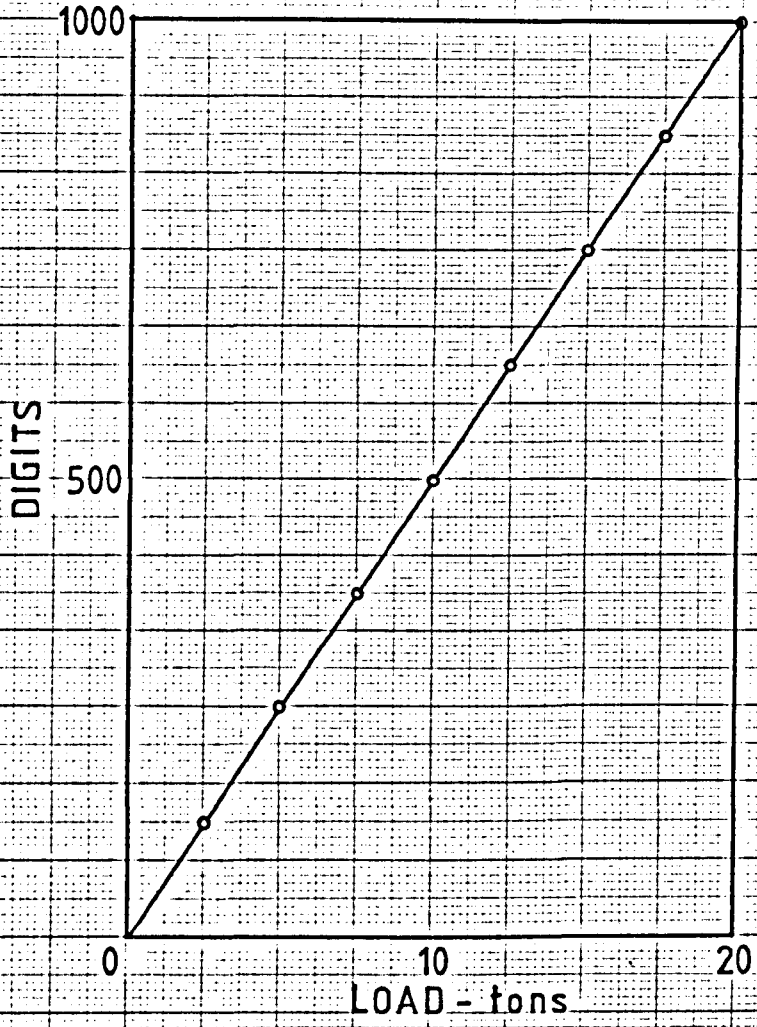

Calibration curve of the load measuring system.

Fig.(10.4)

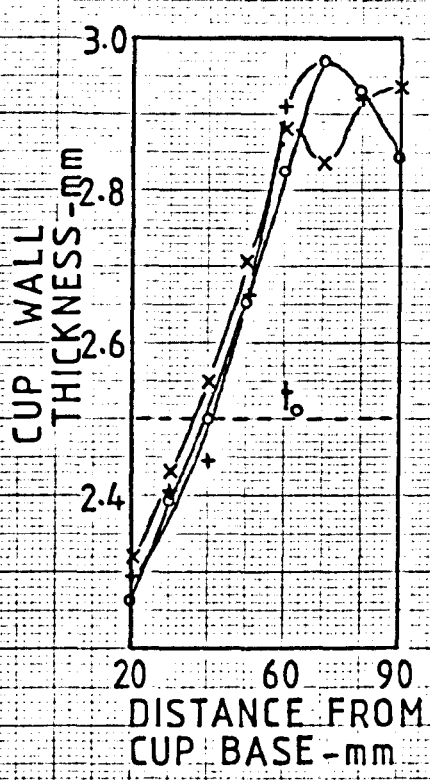

Distribution of wall thickness along the drawn cup.
—o—o—o—, —+—+—+— and —x—x—x— measurements taken along three longitudinal lines of 120° interval drawn on the outer surface of the cup.

Fig.(11.1)

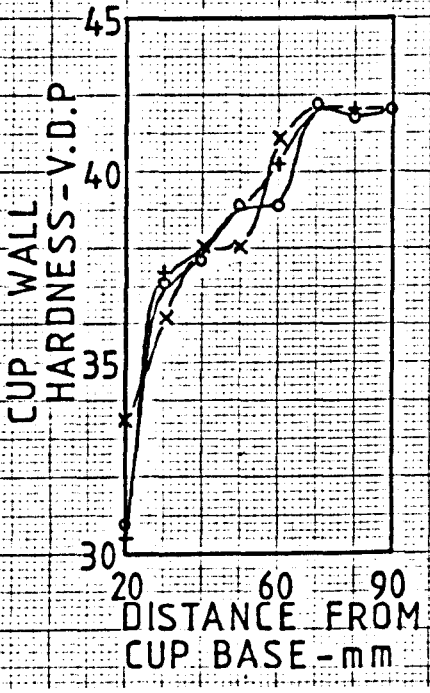

Distribution of wall hardness along the drawn cup.

Fig.(11.2)

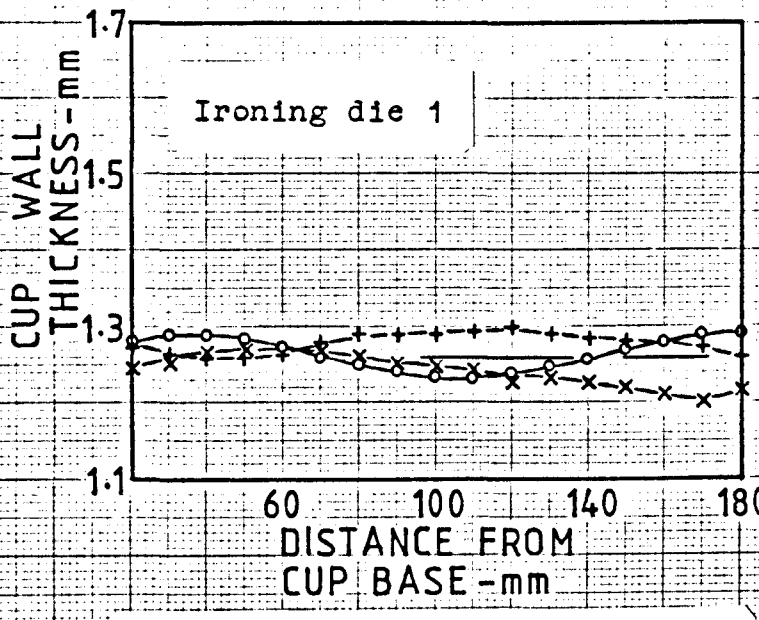

Distribution of wall thickness along the ironed cup.

Fig.(11.3)

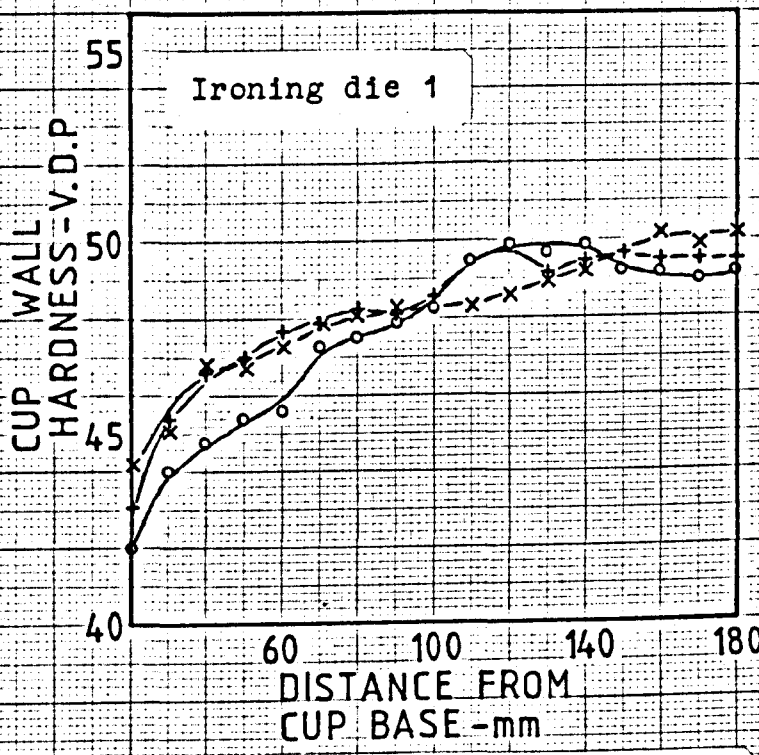

Distribution of wall hardness along the ironed cup.

Fig.(11.4)

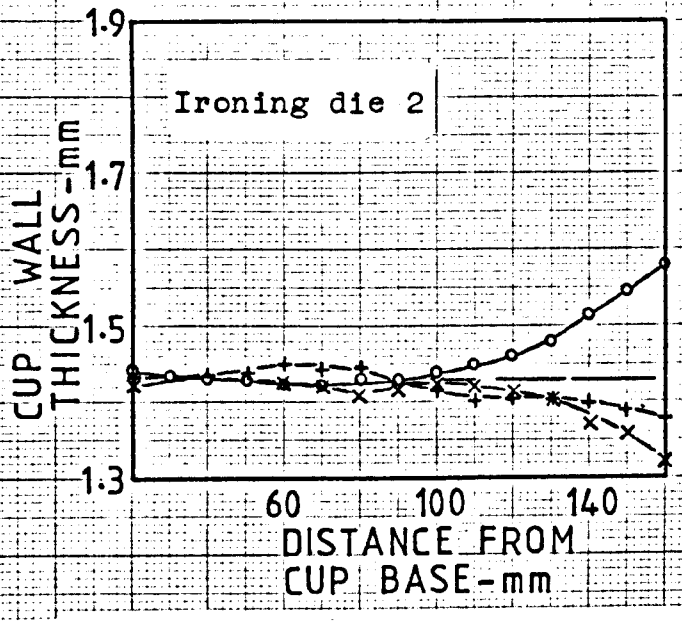

Distribution of wall thickness along the ironed cup.

Fig.(11.5)

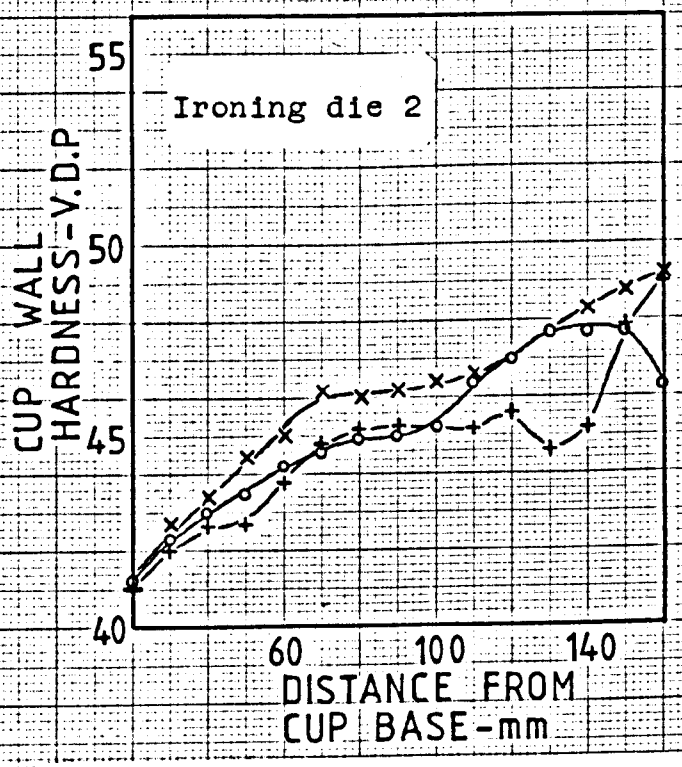

Distribution of wall hardness along the ironed cup.

Fig.(11.6)

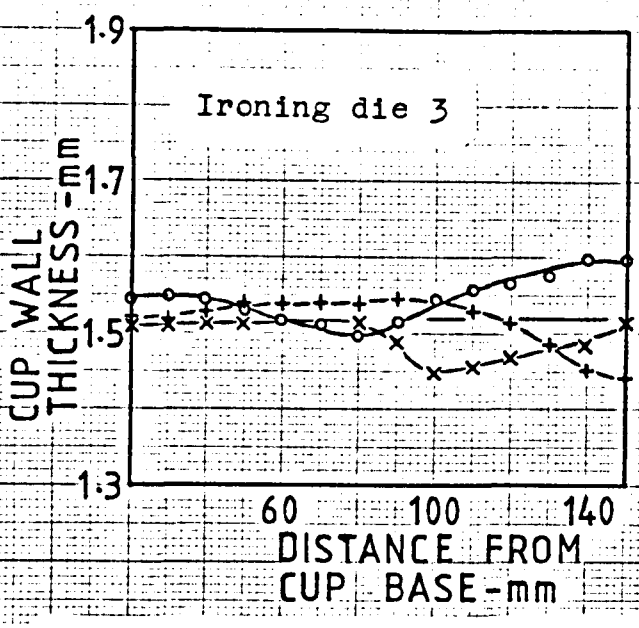

Distribution of wall thickness along the ironed cup.

Fig.(11.7)

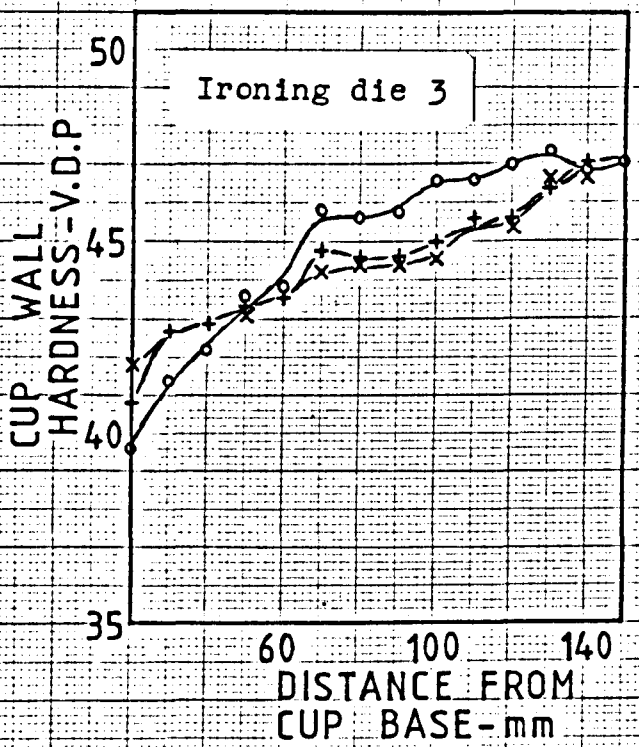

Distribution of wall hardness along the ironed cup.

Fig.(11.8)

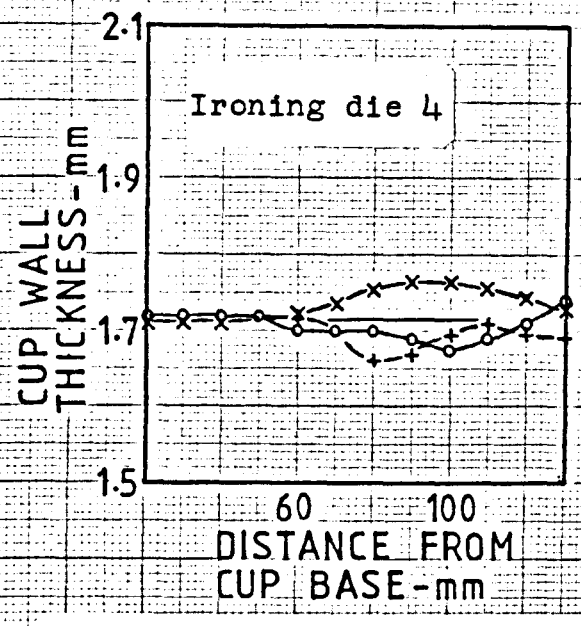

Distribution of wall thickness along the ironed cup.

Fig.(11.9)

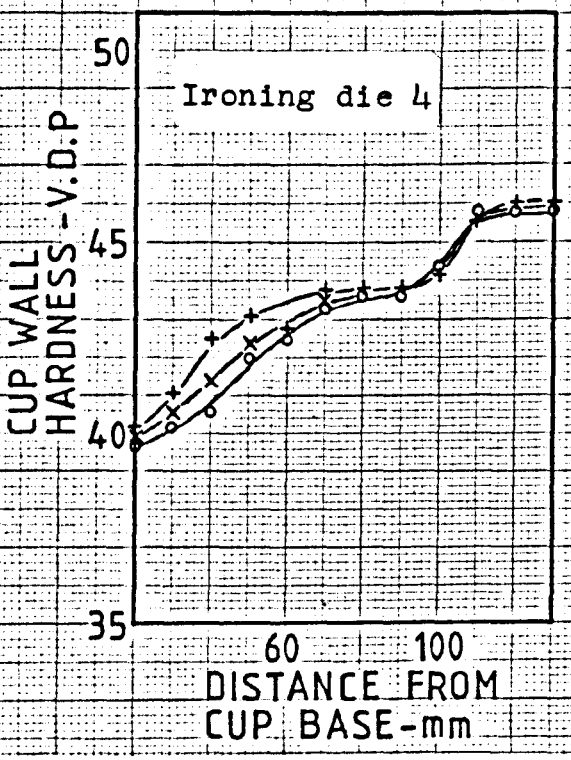

Distribution of wall hardness along the ironed cup.

Fig.(11.10)

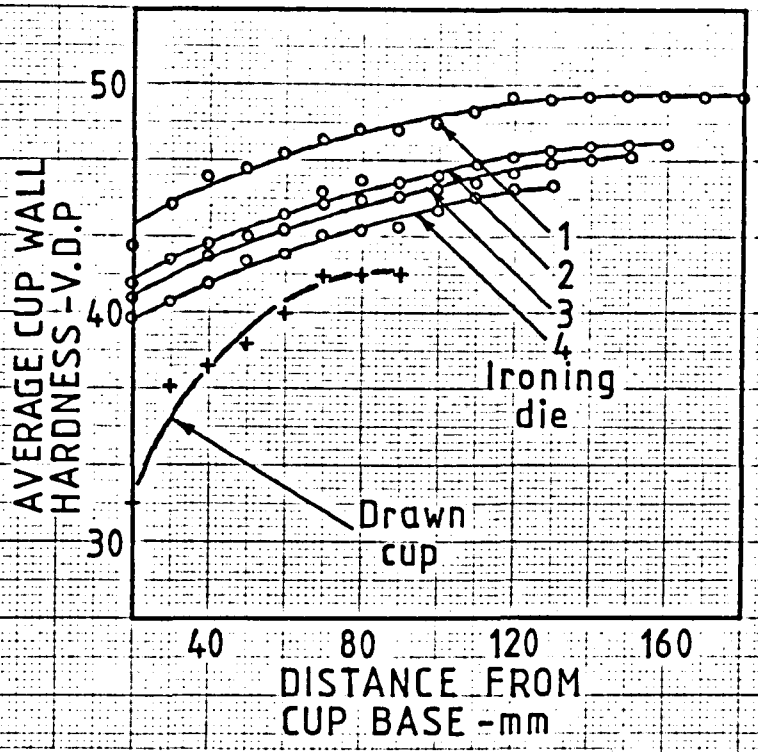

Distribution of average cup wall hardness along the drawn /ironed cup.

Fig.(11.11)

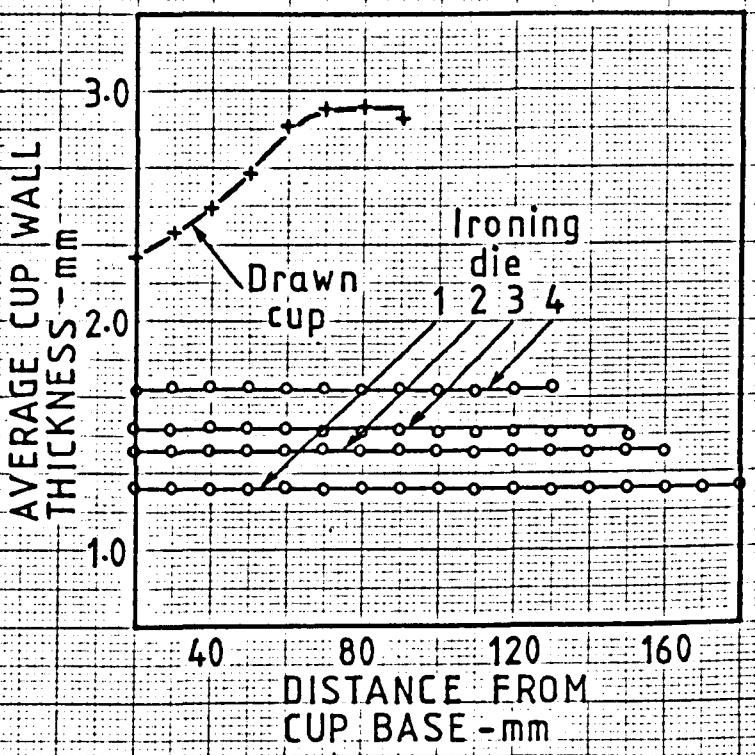

Distribution of average cup wall thickness along the drawn/ironed cup.

Fig.(11.12)

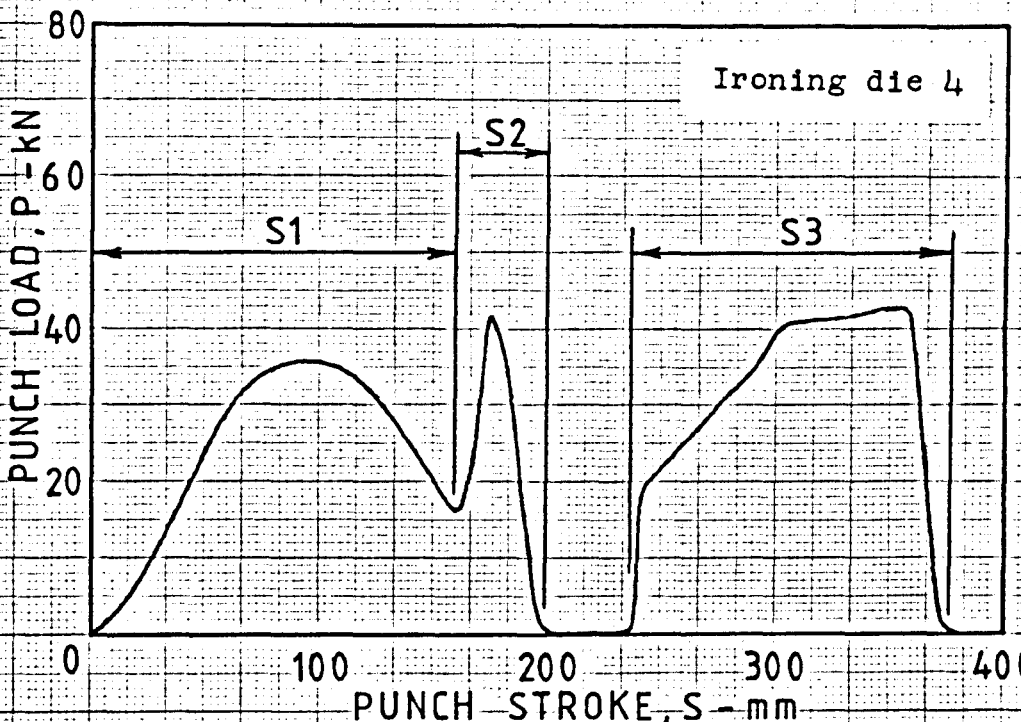

Autographic measurement of punch load/stroke in deep drawing and ironing .

Fig.(11.13)

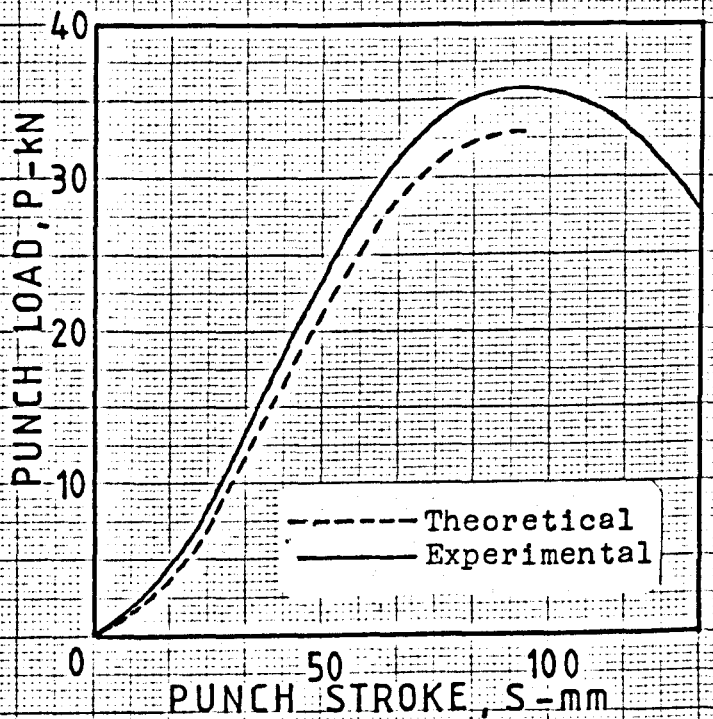

Comparison of theoretical and experimental punch load/stroke in deep drawing.

Fig.(11.14)

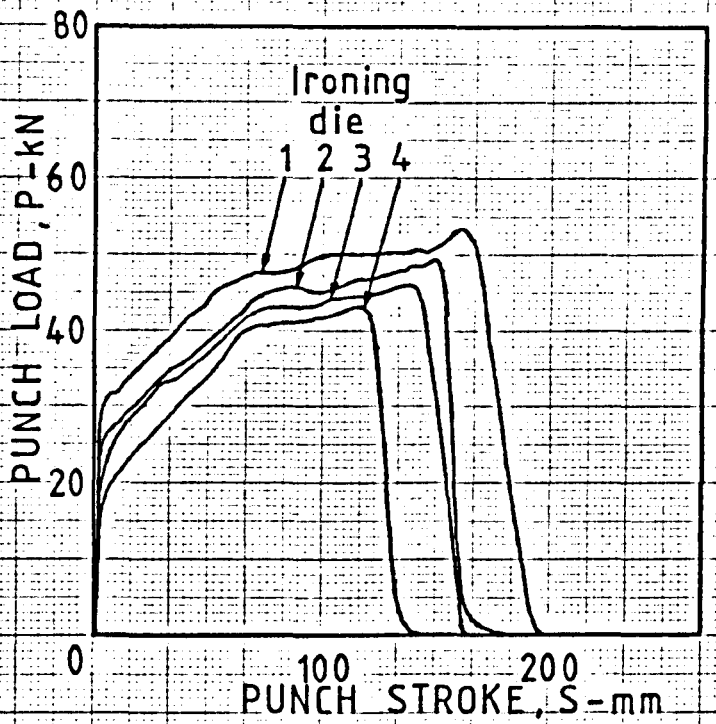

Autographic measurement of punch load/stroke relation for different degrees of ironing .

Fig.(11.15)

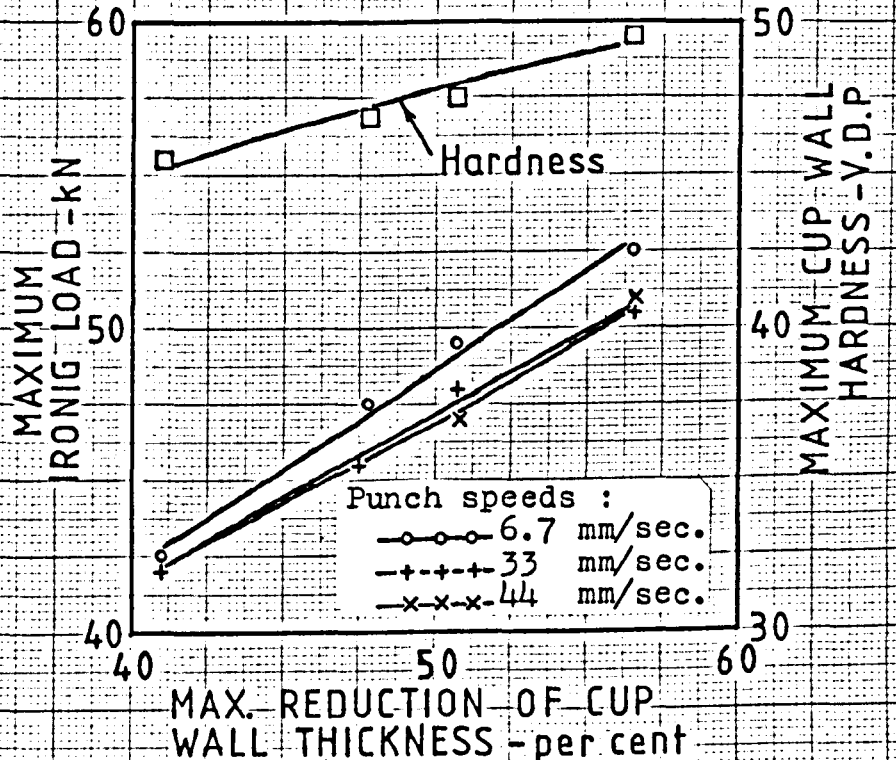

Variation of maximum ironing load and cup wall hardness with the reduction of cup wall thickness .

Fig.(11.16)

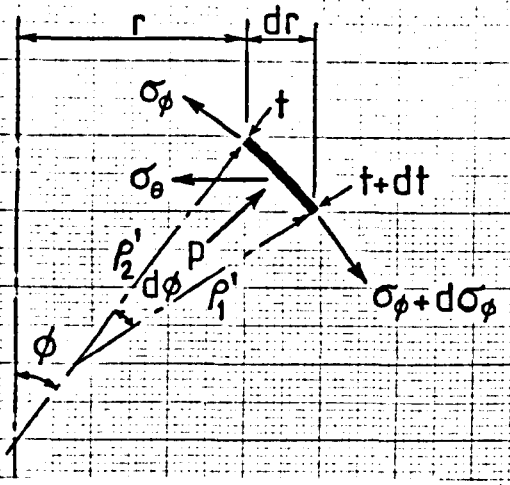

Stresses on an element of material in free bulge forming .

Fig.(13.1)

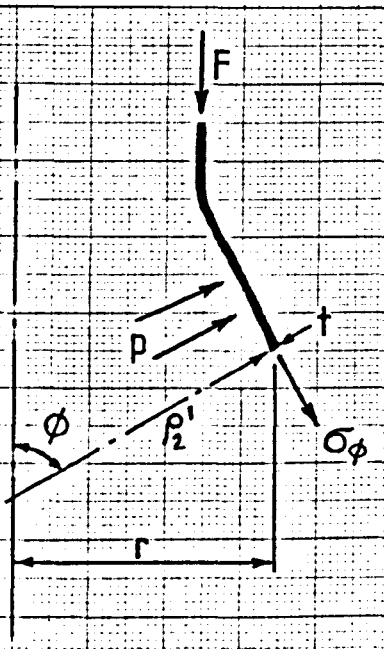

Forces acting on the bulged cup .

Fig.(13.2)

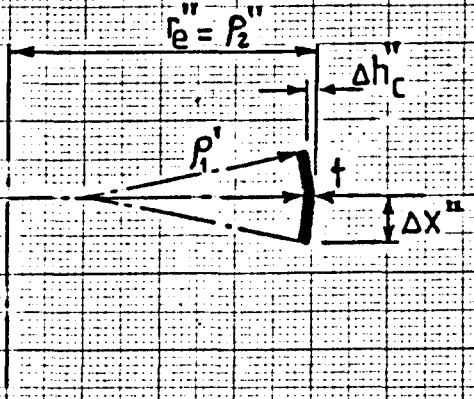

The crown zone of the bulged cup .

Fig.(13.3)

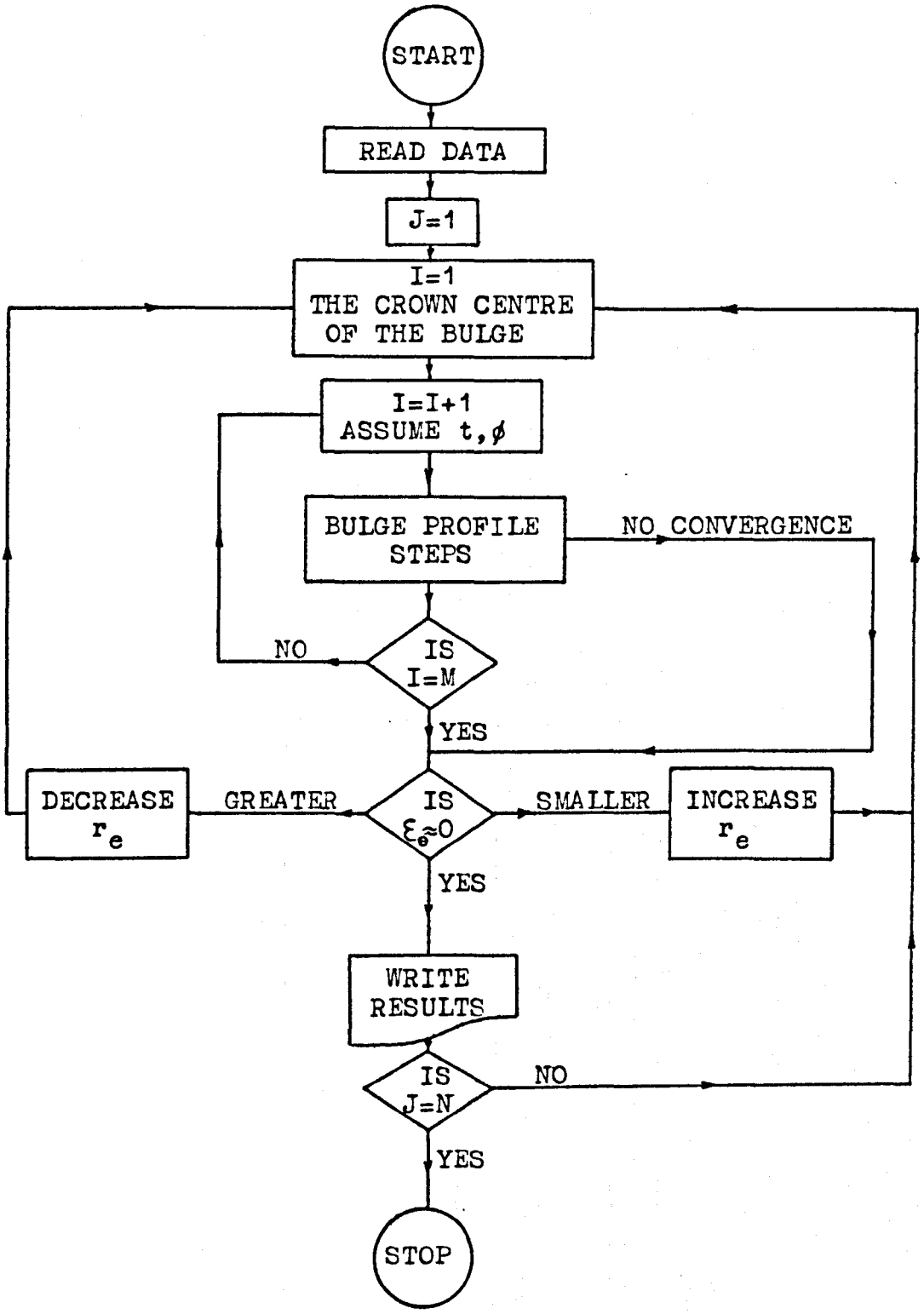

General flow-chart of the computer programme for the analysis of free bulge forming.

Fig.(13.4)

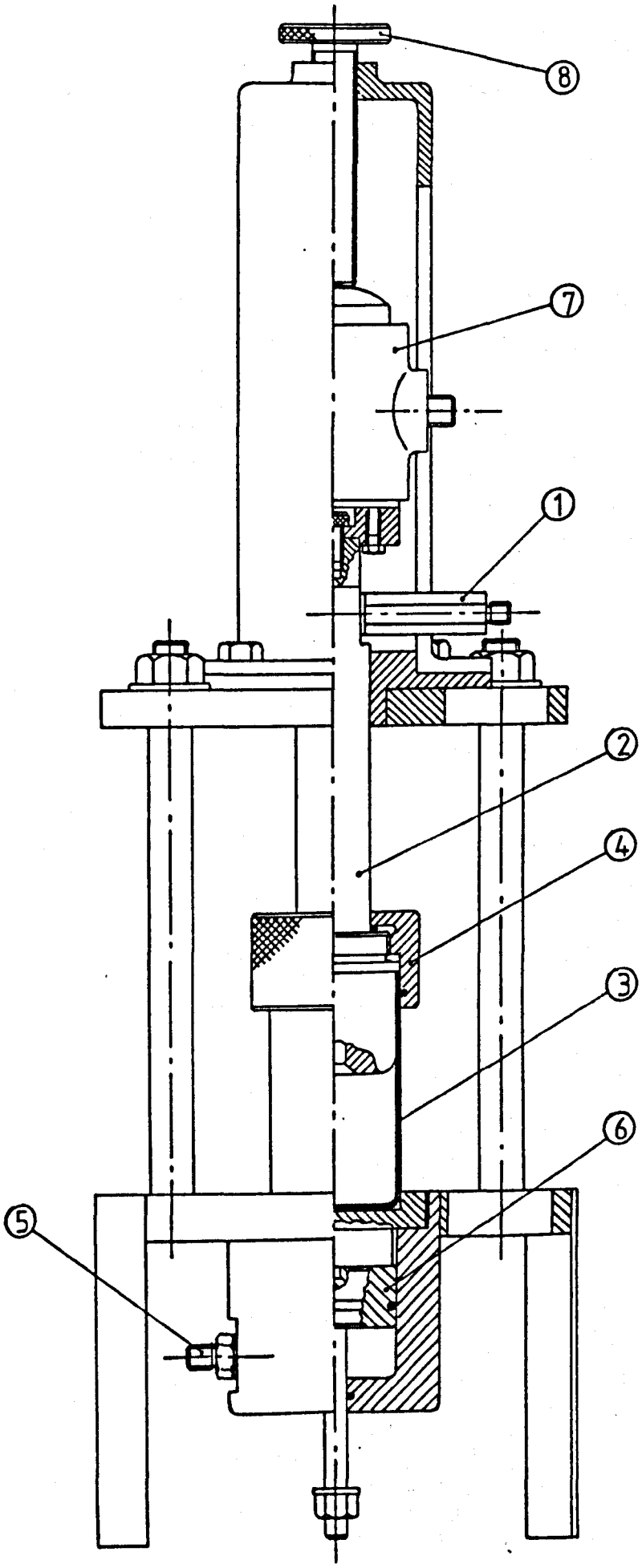

Free bulge formig
test rig

Fig.(14.1)

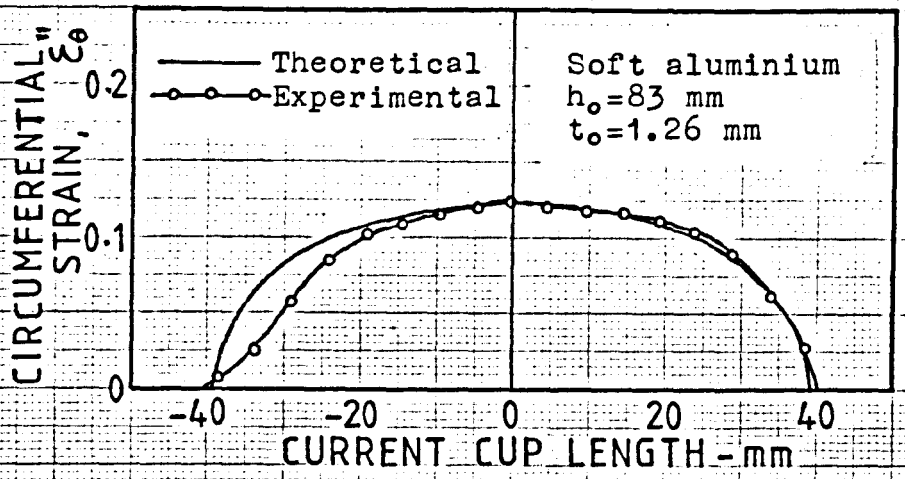

Comparison of theoretical and experimental circumferential strains .

Fig.(16.1)

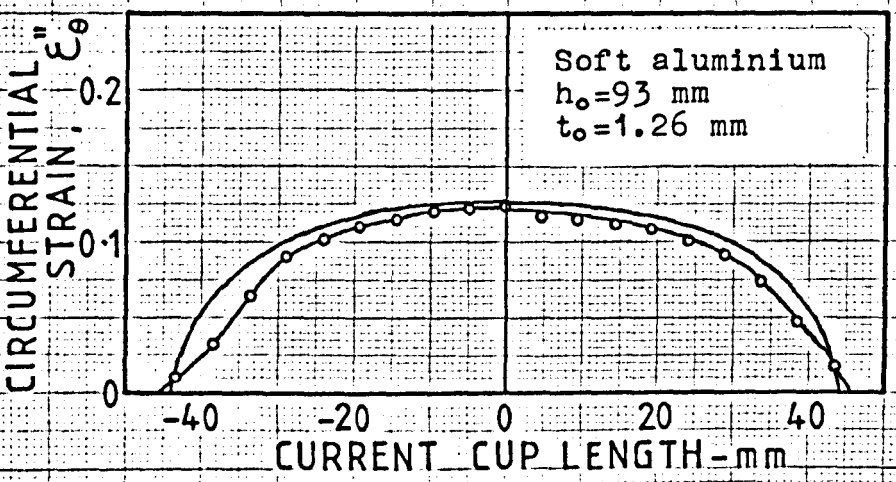

Comparison of theoretical and experimental circumferential strains .

Fig.(16.2)

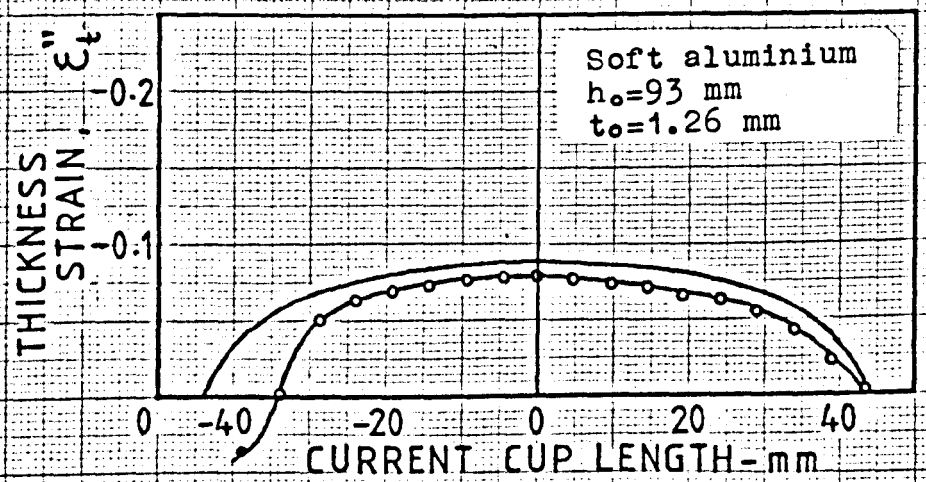

Comparison of theoretical and experimental thickness strains .

Fig.(16.3)

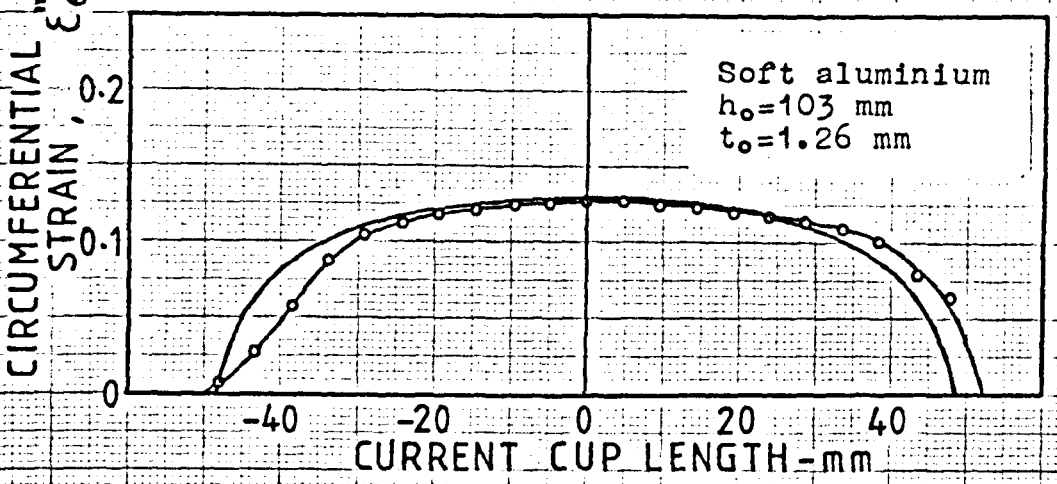

Comparison of theoretical and experimental circumferential strains .

Fig.(16.4)

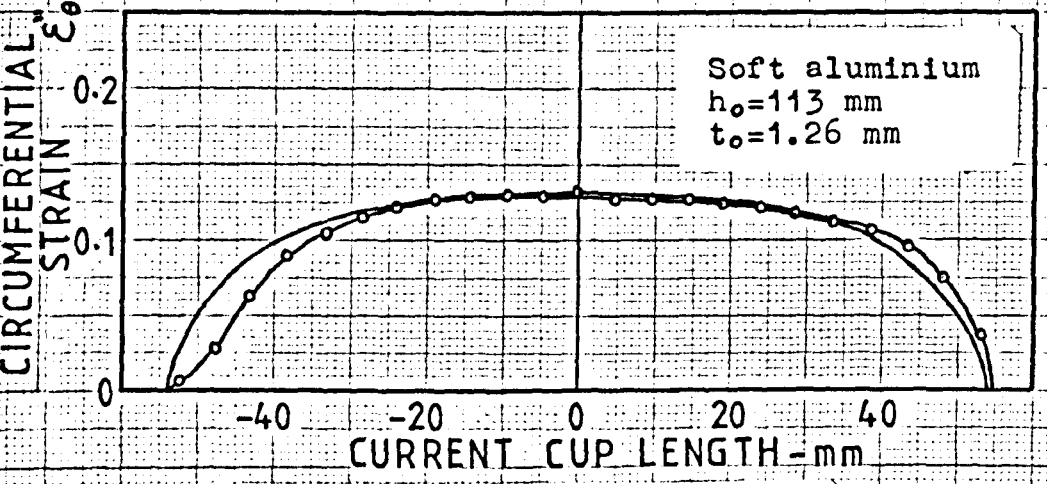

Comparison of theoretical and experimental circumferential strains .

Fig.(16.5)

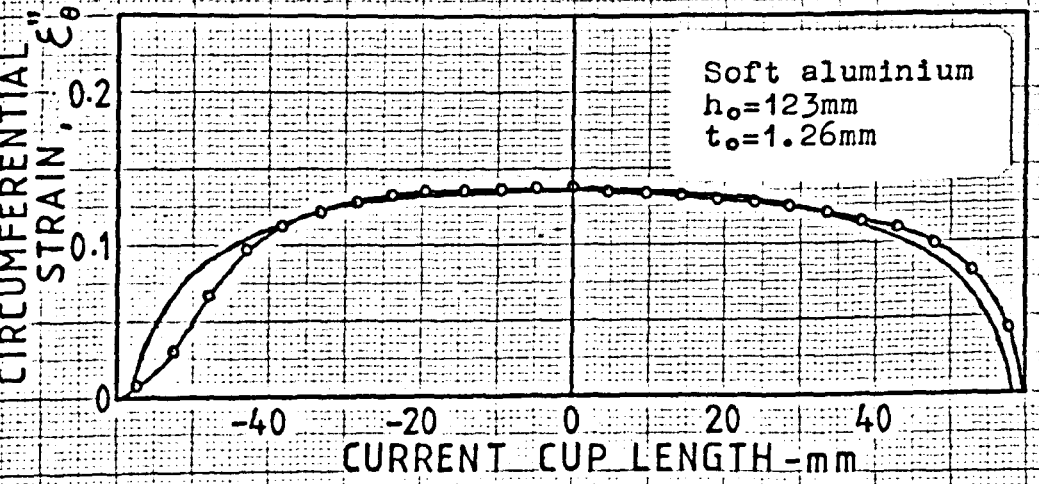

Comparison of theoretical and experimental circumferential strains .

Fig.(16.6)

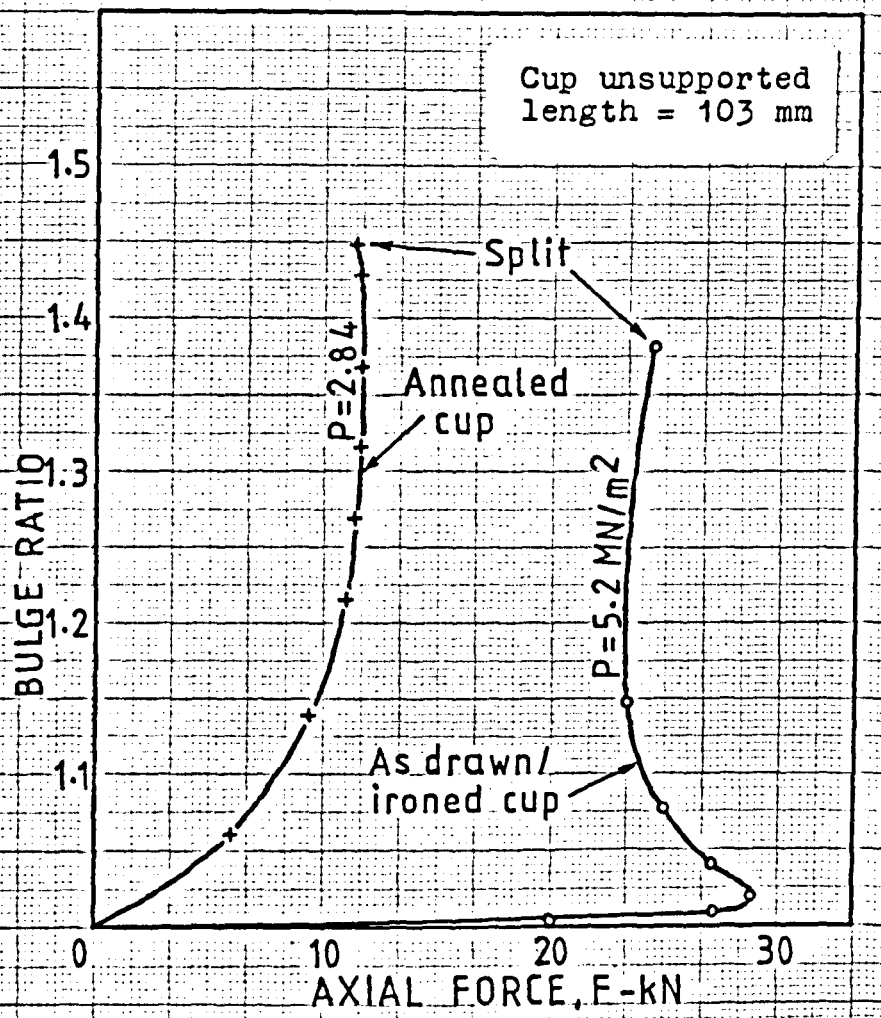

Change of bulge ratio with axial force under constant internal pressure .

Fig.(17.1)

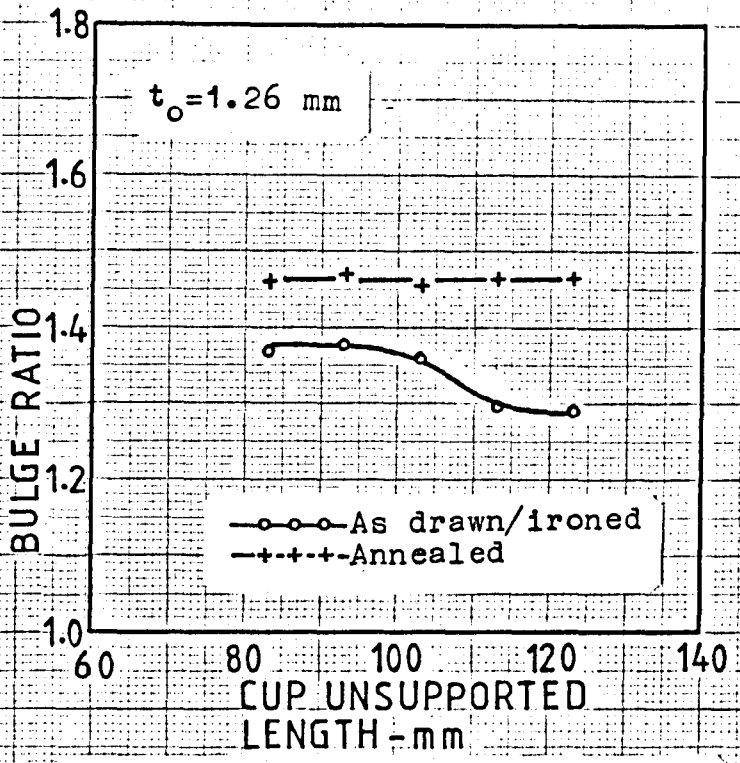

Effect of cup unsupported length on bulge ratio .

Fig.(17.2)

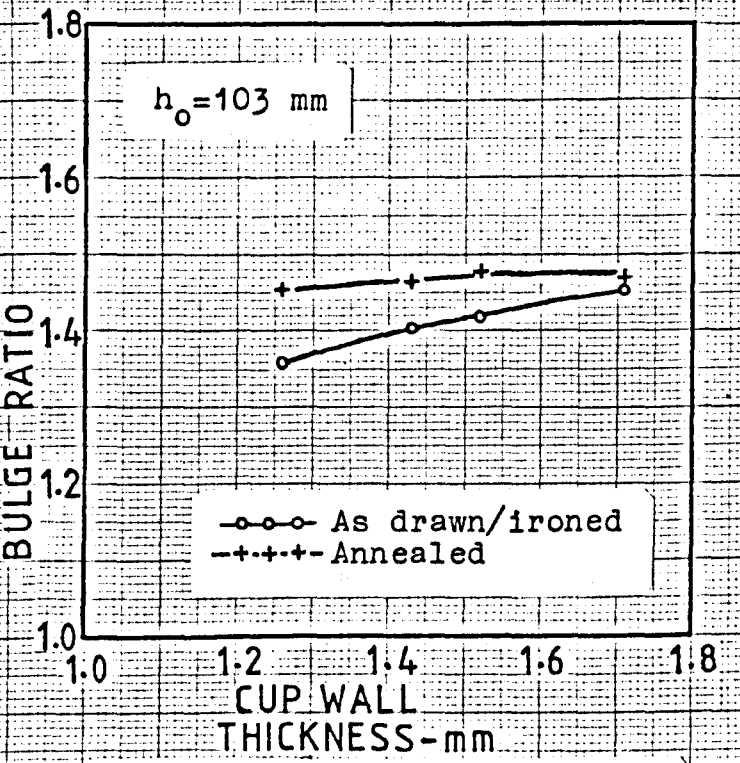

Effect of cup wall thickness on bulge ratio .

Fig.(17.3)

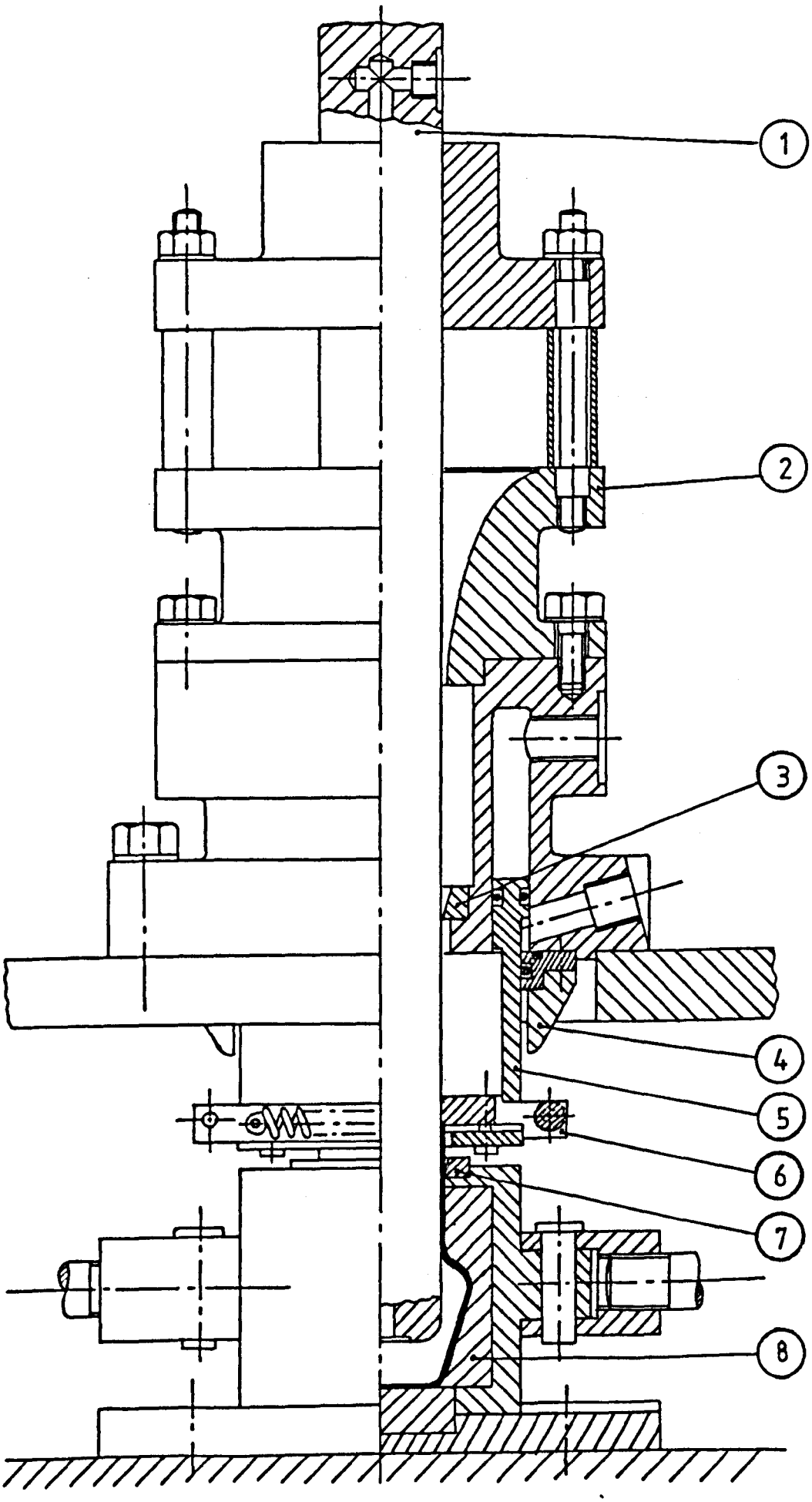

Fig.(20.1)

Bulge forming press assembly

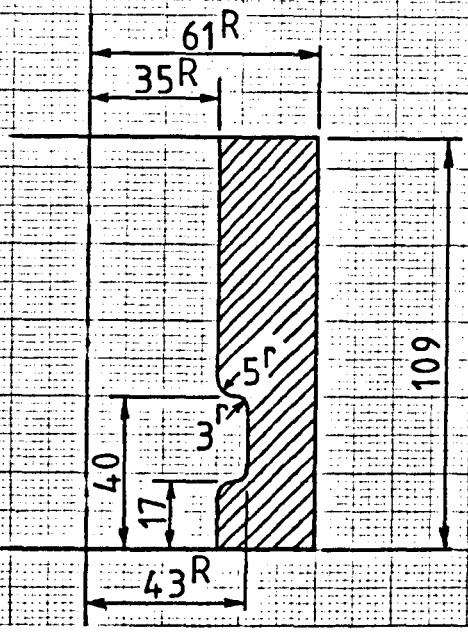

The cylindrical die .

Fig.(20.2)

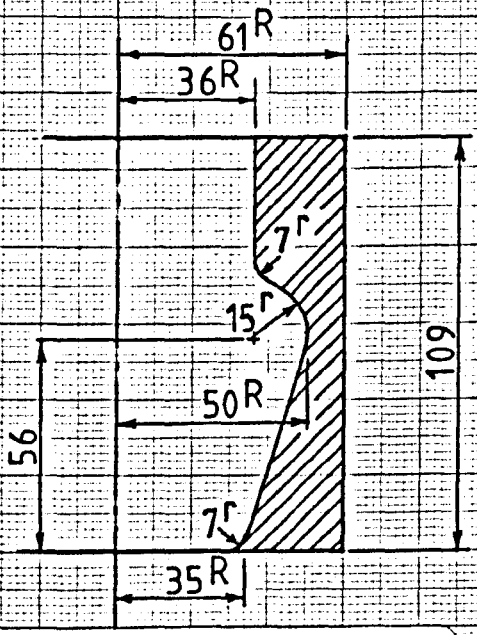

The conical die .

Fig.(20.3)

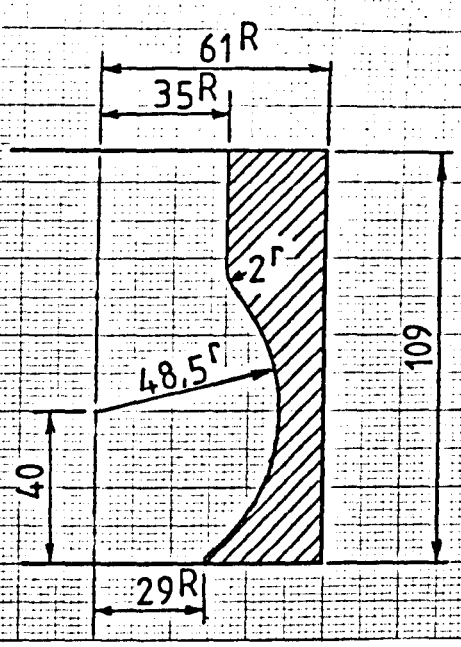

The spherical die .

Fig.(20.4)

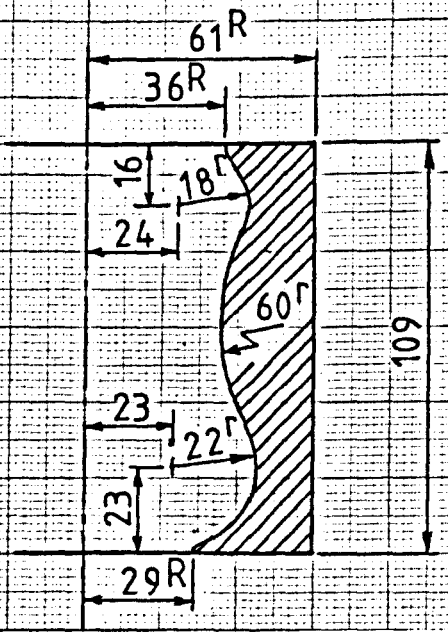

The double bulge shape die.

Fig.(20.5)

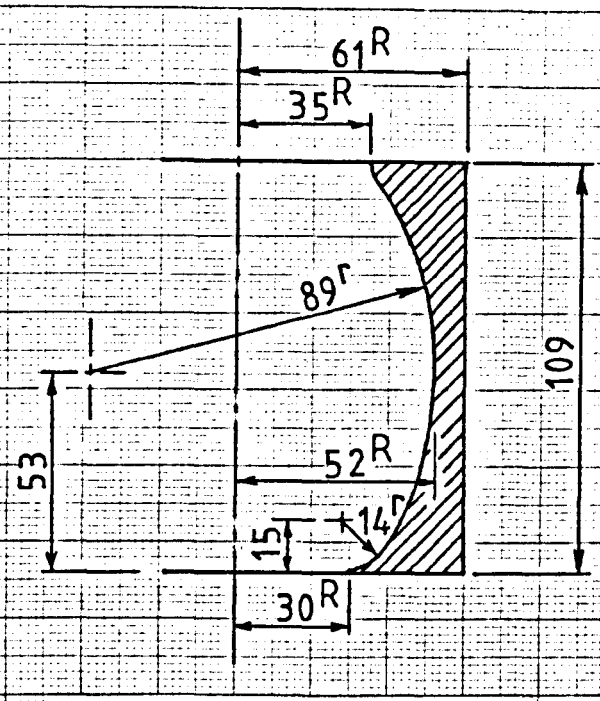

The barrel shape die .

Fig.(20.6)

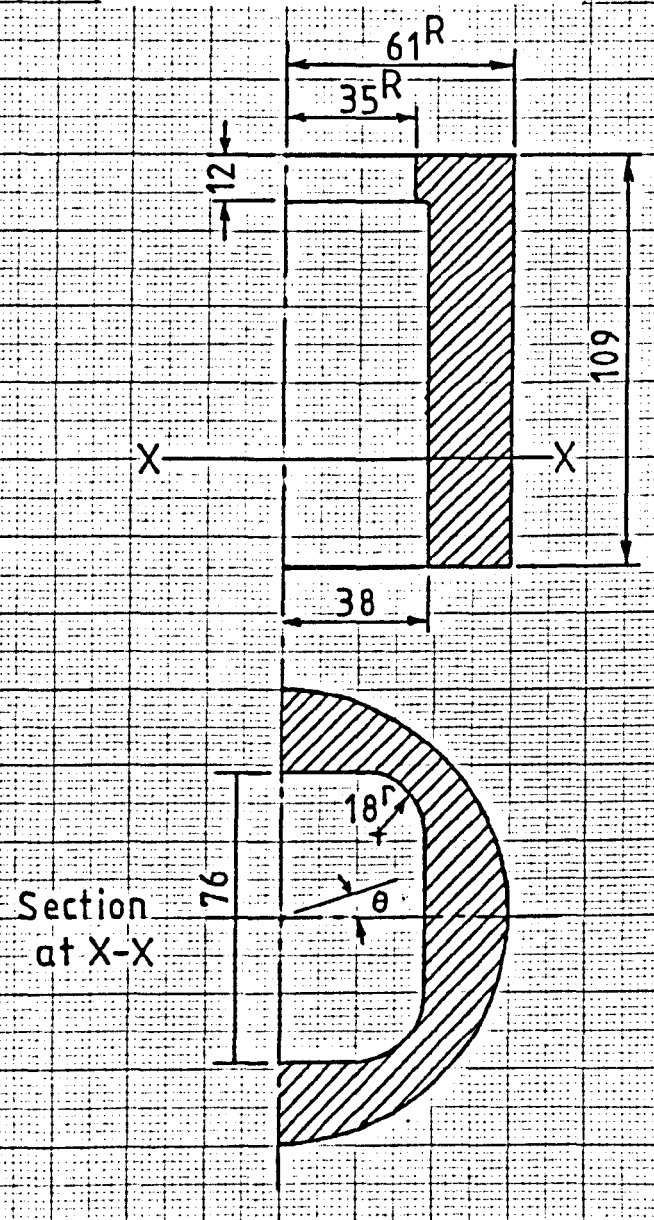

The square shape die.

Fig.(20.7)

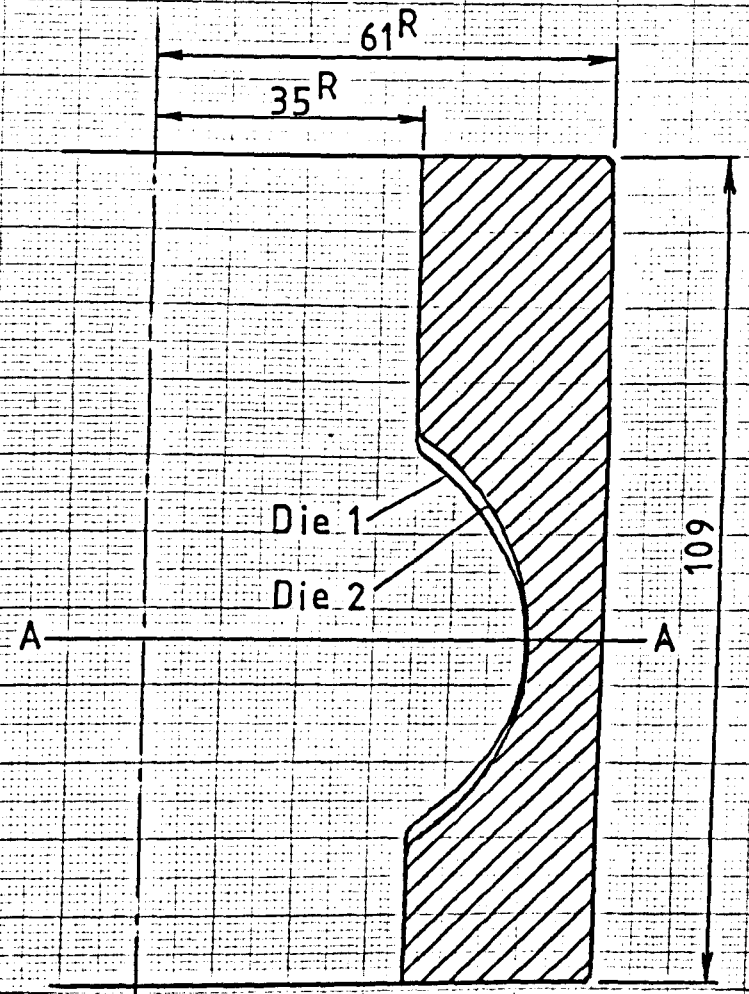

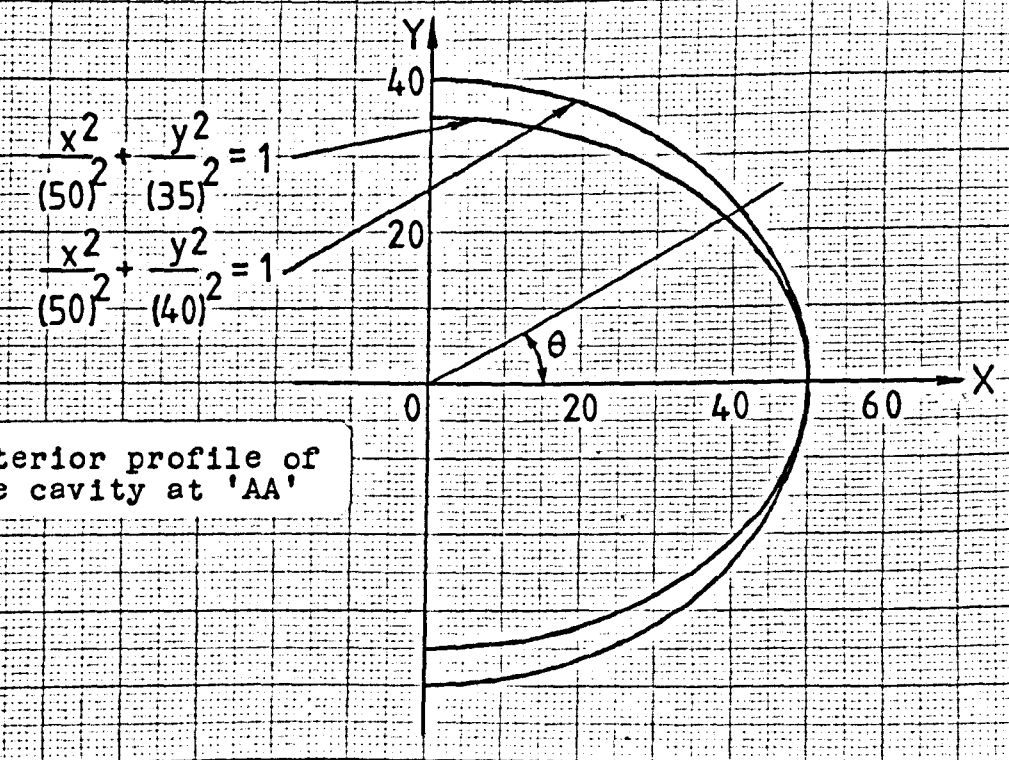

$$\frac{x^2}{(50)^2} + \frac{y^2}{(35)^2} = 1$$

$$\frac{x^2}{(50)^2} + \frac{y^2}{(40)^2} = 1$$

Interior profile of die cavity at 'AA'

Elliptical dies 1 and 2 .

Fig.(20.8)

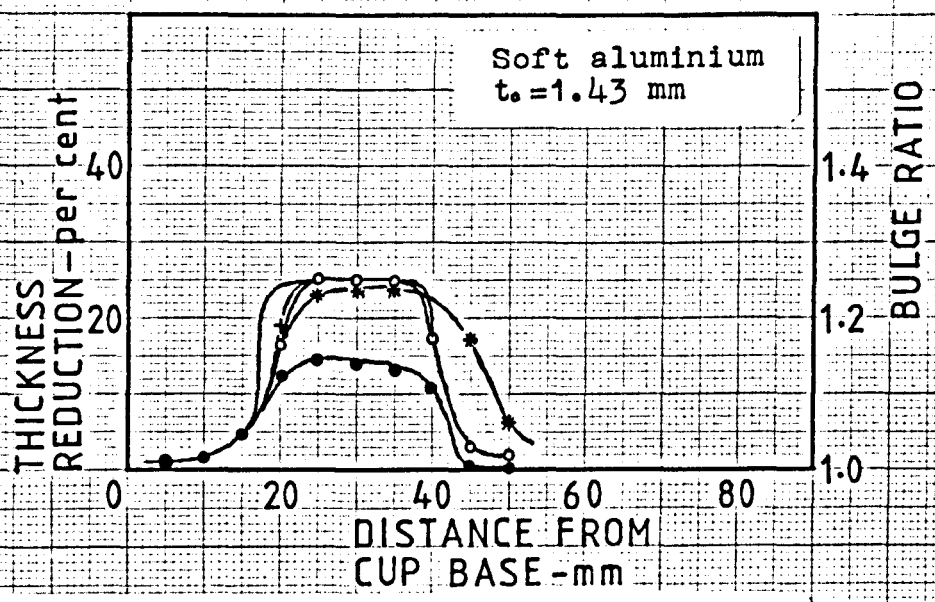

Distribution of bulge ratio and reduction of thickness along the cylindrical shape component .

-*-*-*- Reduction of thickness, annealed.
-+-+-+- Bulge ratio, annealed.
-●-●-●- Reduction of thickness, as drawn/ironed.
-o-o-o- Bulge ratio, as drawn/ironed.

Fig.(21.1)

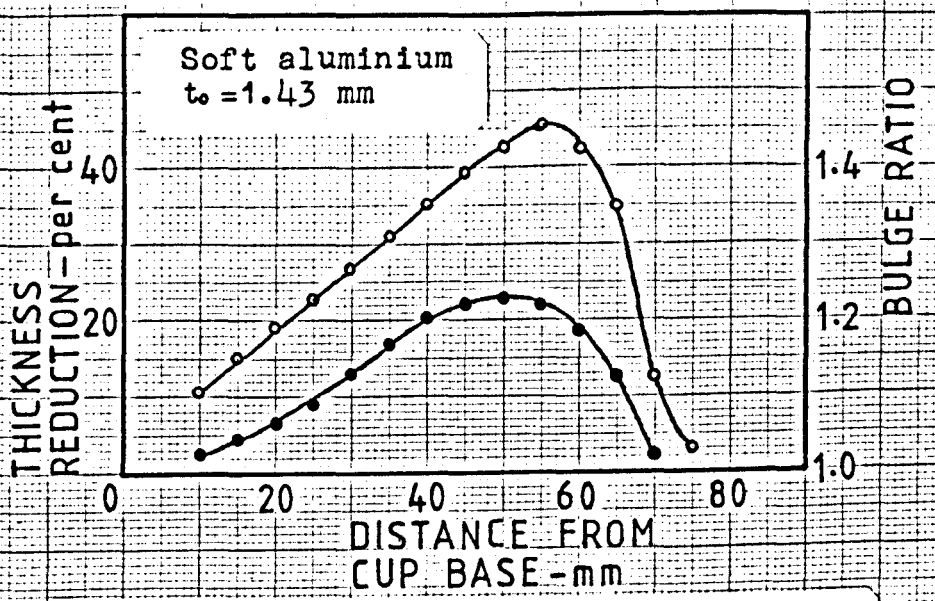

Distribution of bulge ratio and reduction of thickness along the conical shape component .

Fig.(21.2)

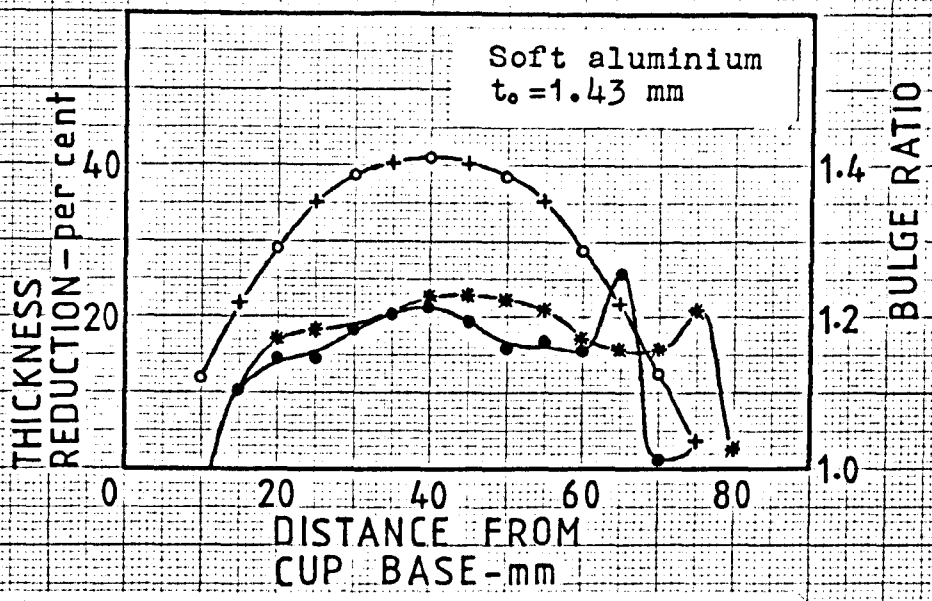

Distribution of bulge ratio and reduction of thickness along the spherical shape component .

Fig.(21.3)

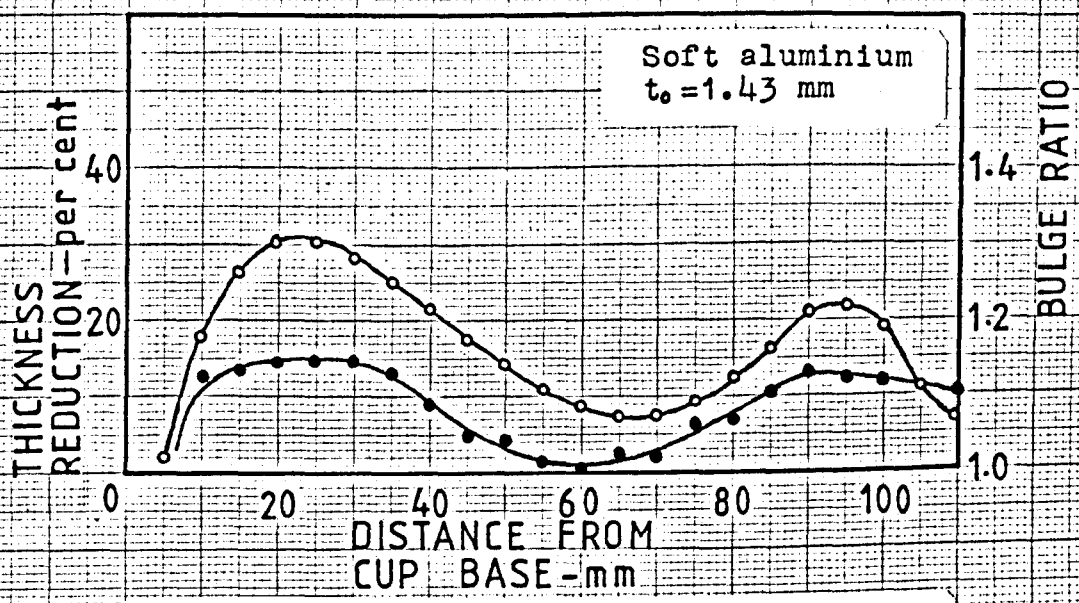

Distribution of bulge ratio and reduction of thickness along the double bulge component .

Fig.(21.4)

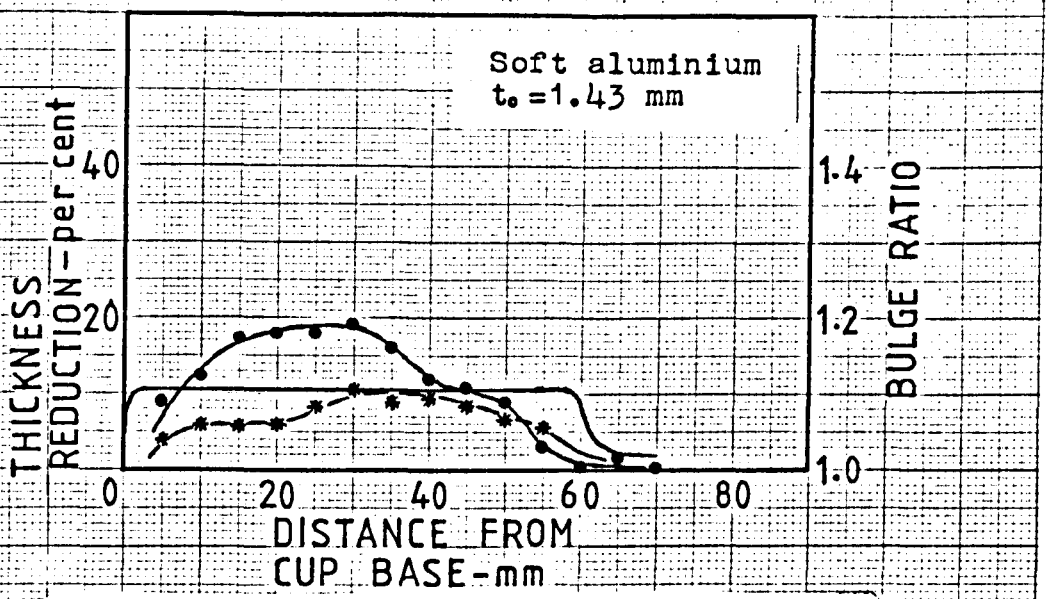

Distribution of bulge ratio and reduction of thickness along the square shaped component.

Fig.(21.5a)

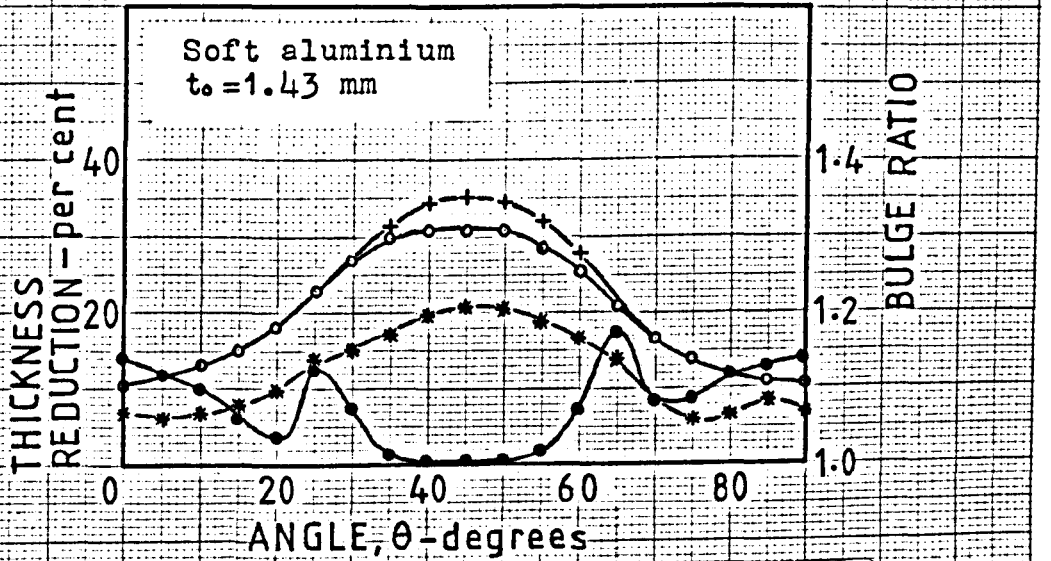

Distributio of bulge ratio and reduction of thickness across the square shaped component ,at 35mm from the base .

Fig.(21.5b)

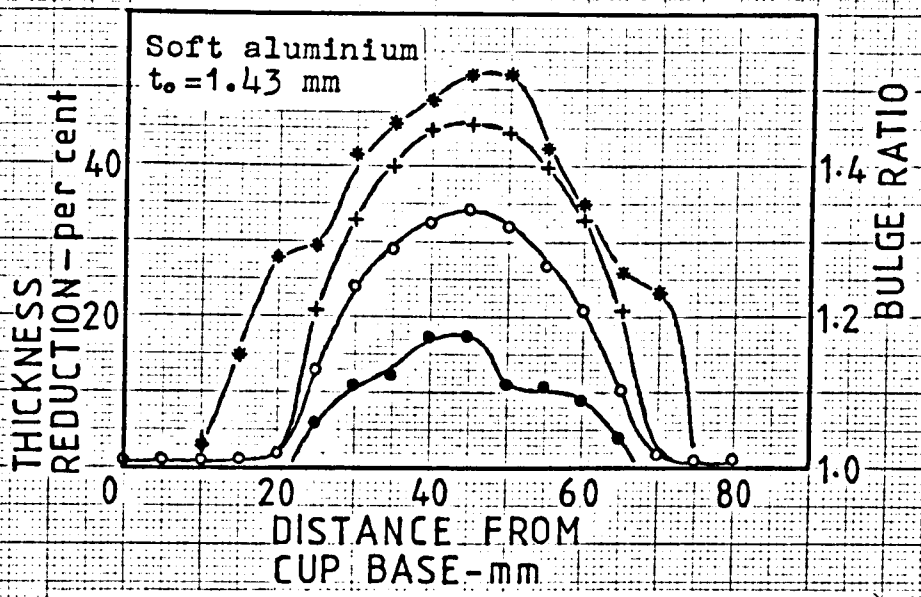

Distribution of bulge ratio and reduction of thickness along the elliptical shaped component. (Die 1)

Fig.(21.6a)

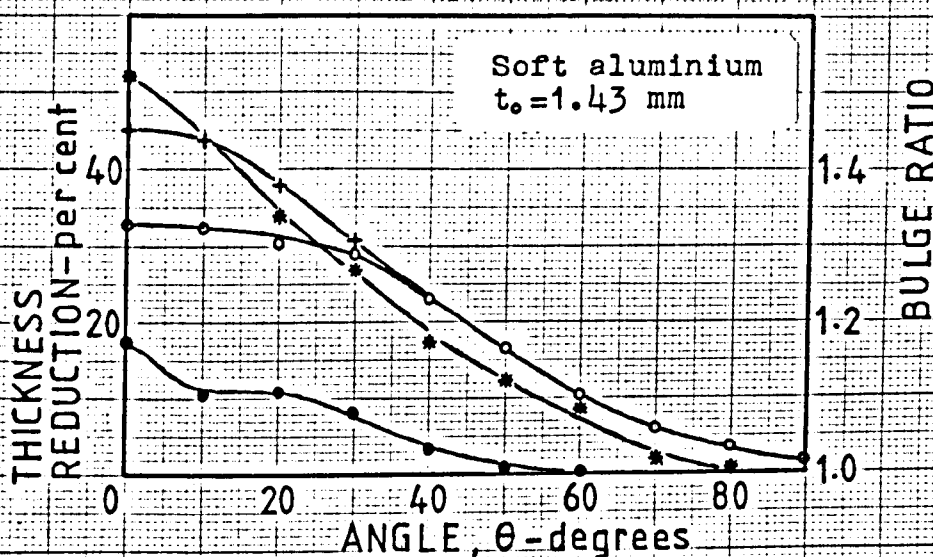

Distribution of bulge ratio and reduction of thickness across the middle of the elliptical shape. (Die 1)

Fig.(21.6b)

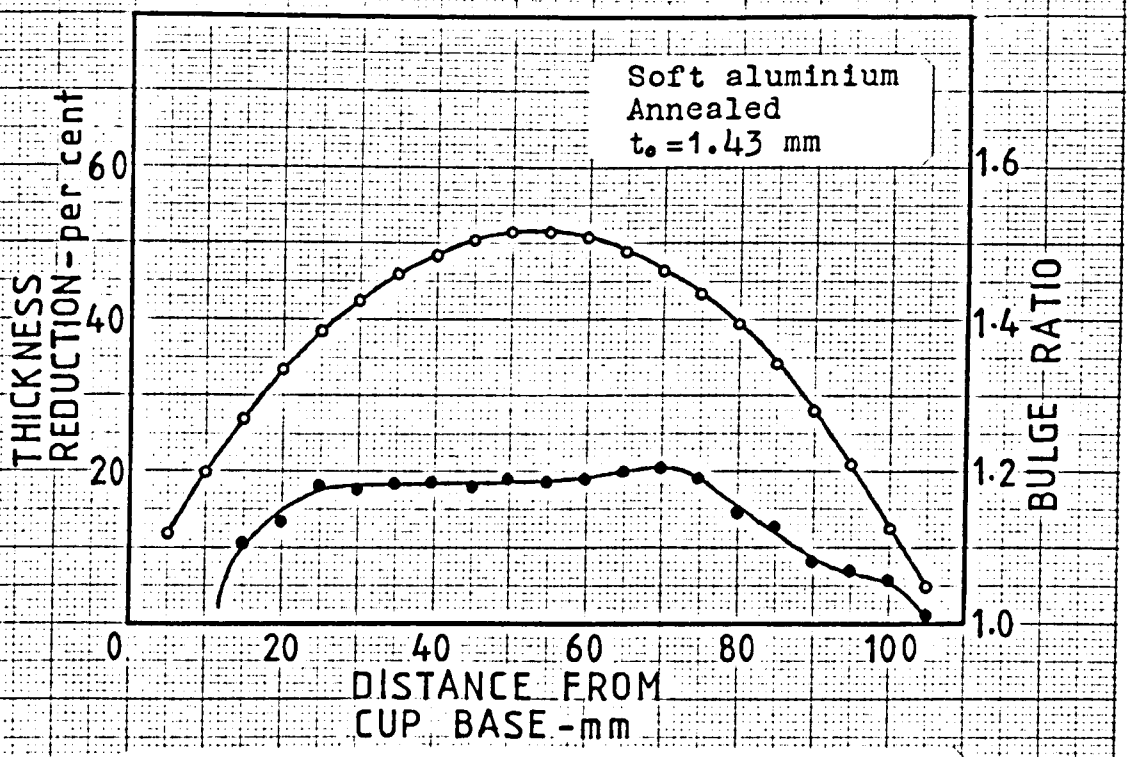

Distibution of bulge ratio and reduction of thickness for barrel shaped component.

Reduction of thicknss
Bulge ratio

Fig.(21.7)

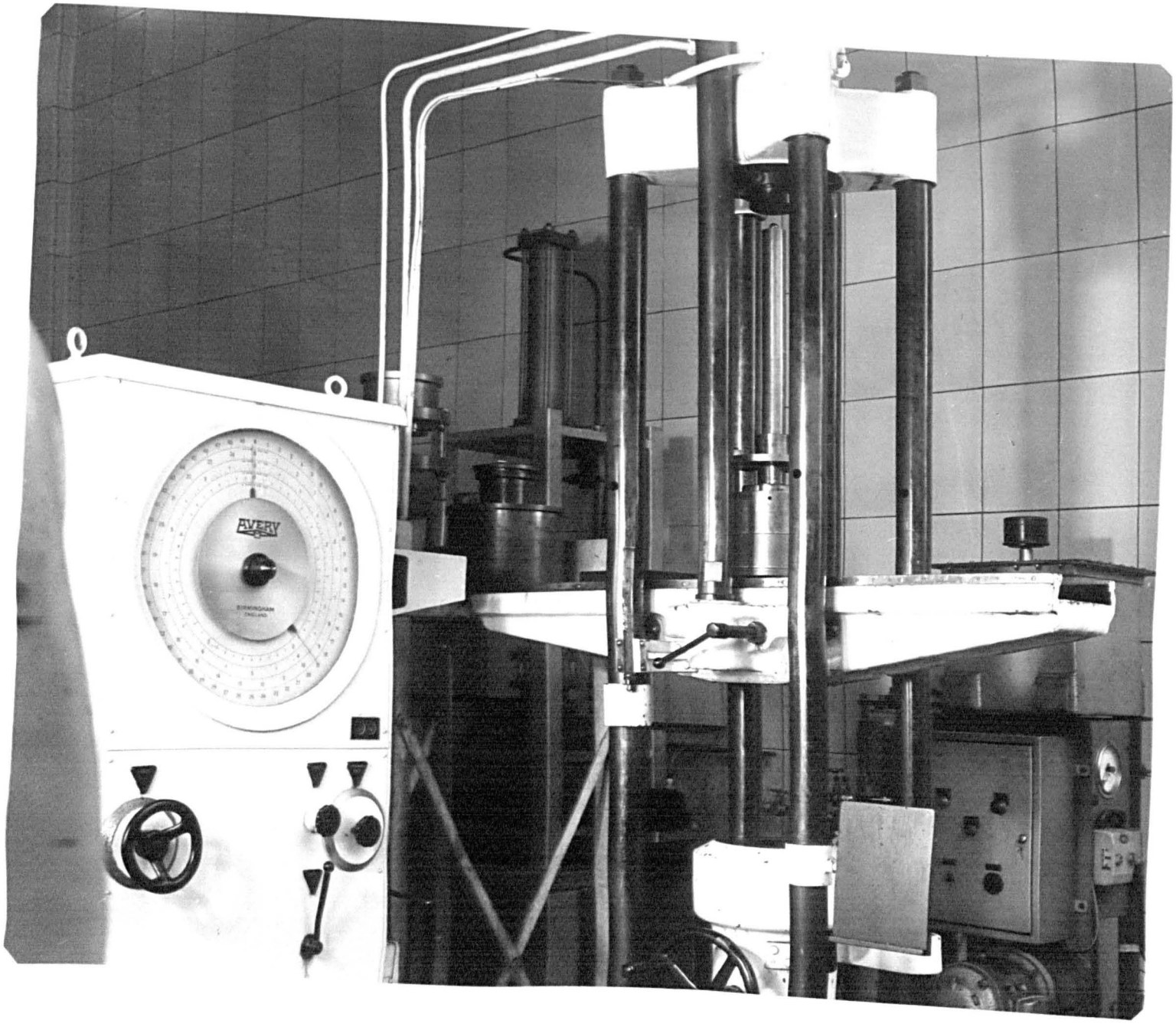

Deep drawing test rig in place on the universal testing machine.

Plate(5.1)

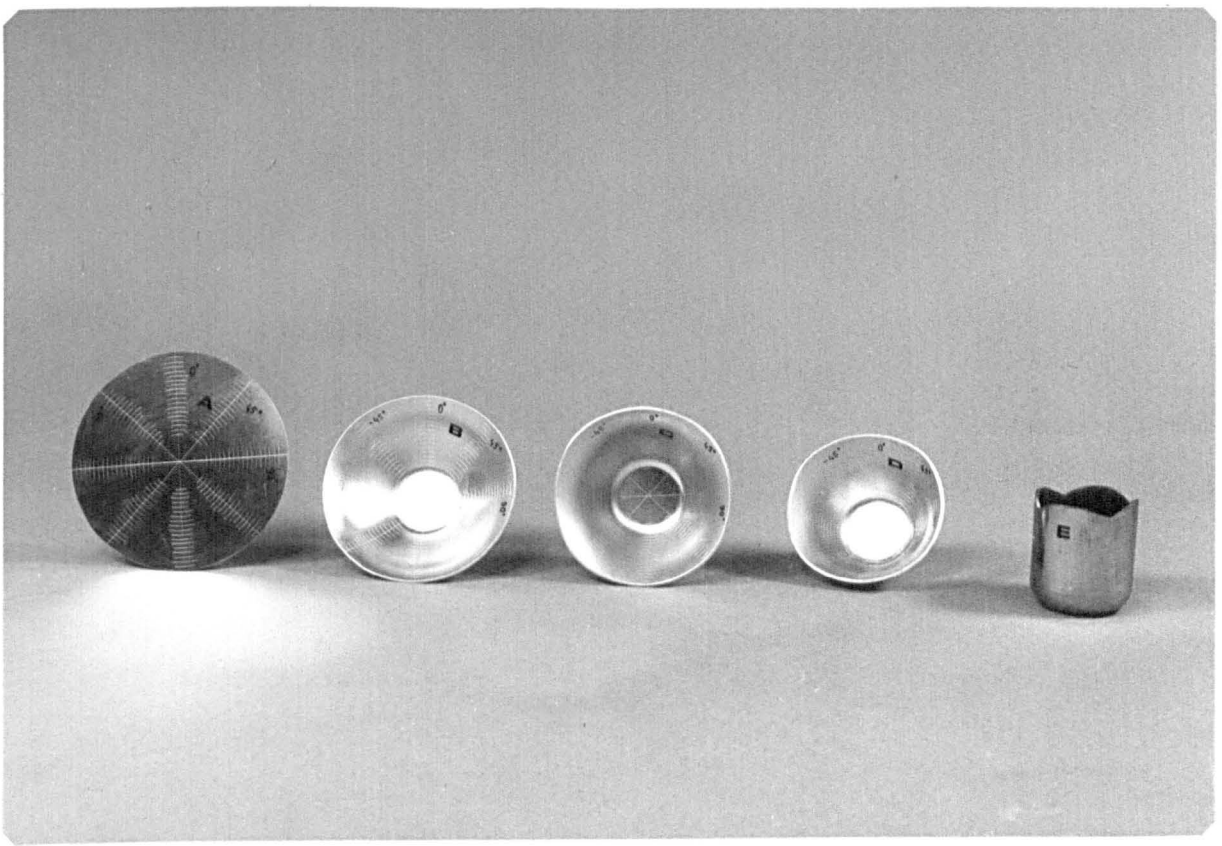

Drawing stages and specimens
for strain measurement.

Plate(5.2)

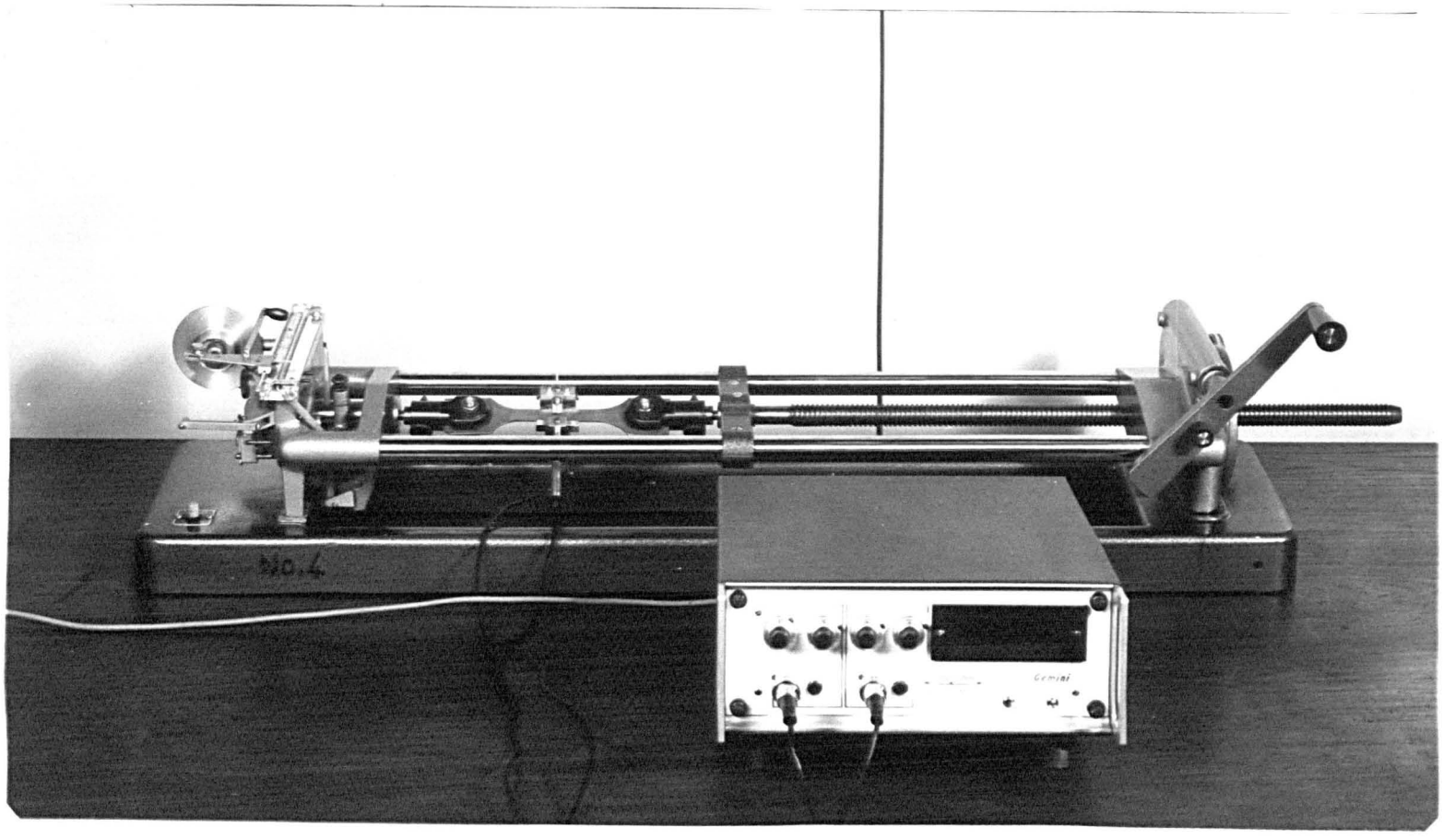

Tension test apparatus.

Plate(5.3)

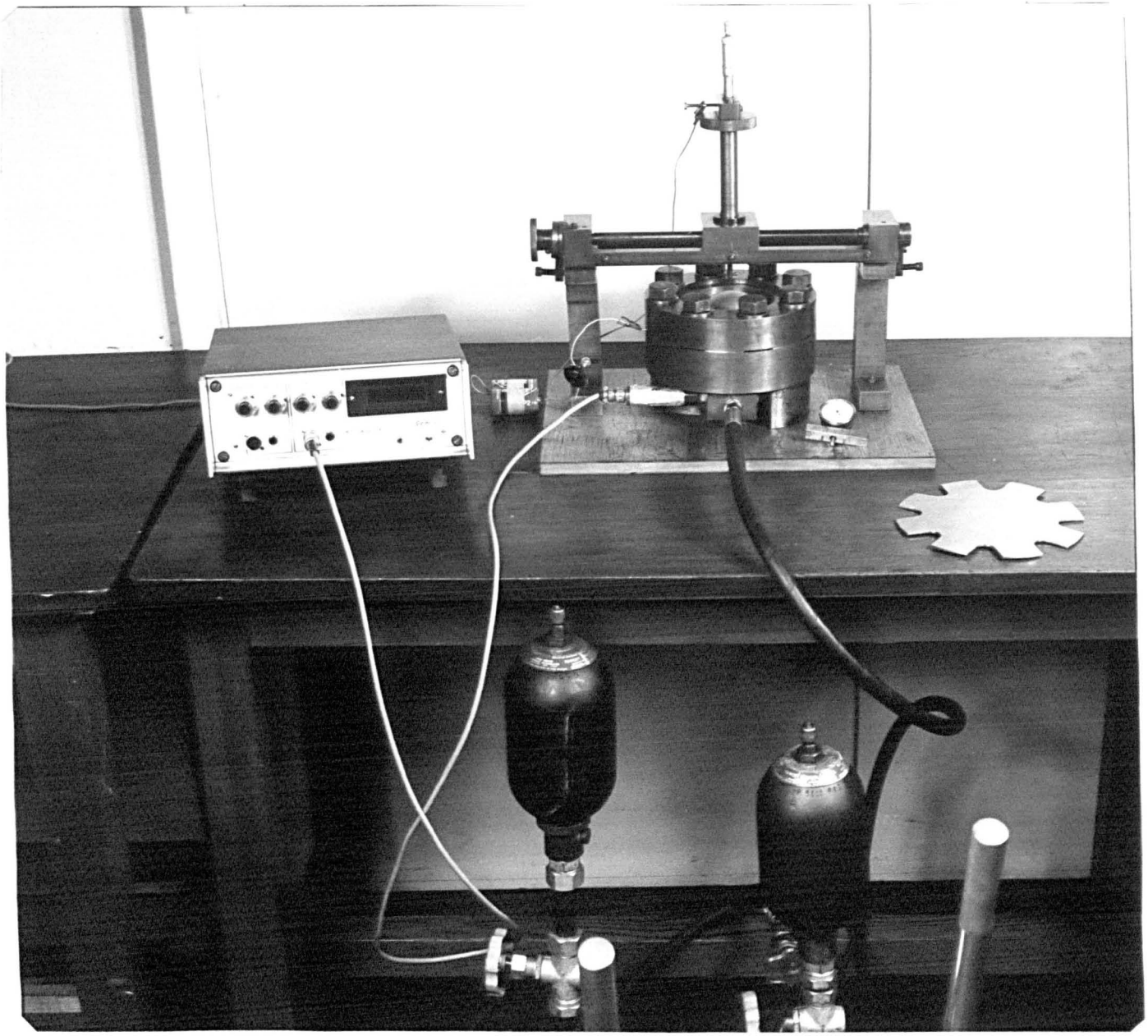

Balanced biaxial tension test apparatus.

Plate(5.4)

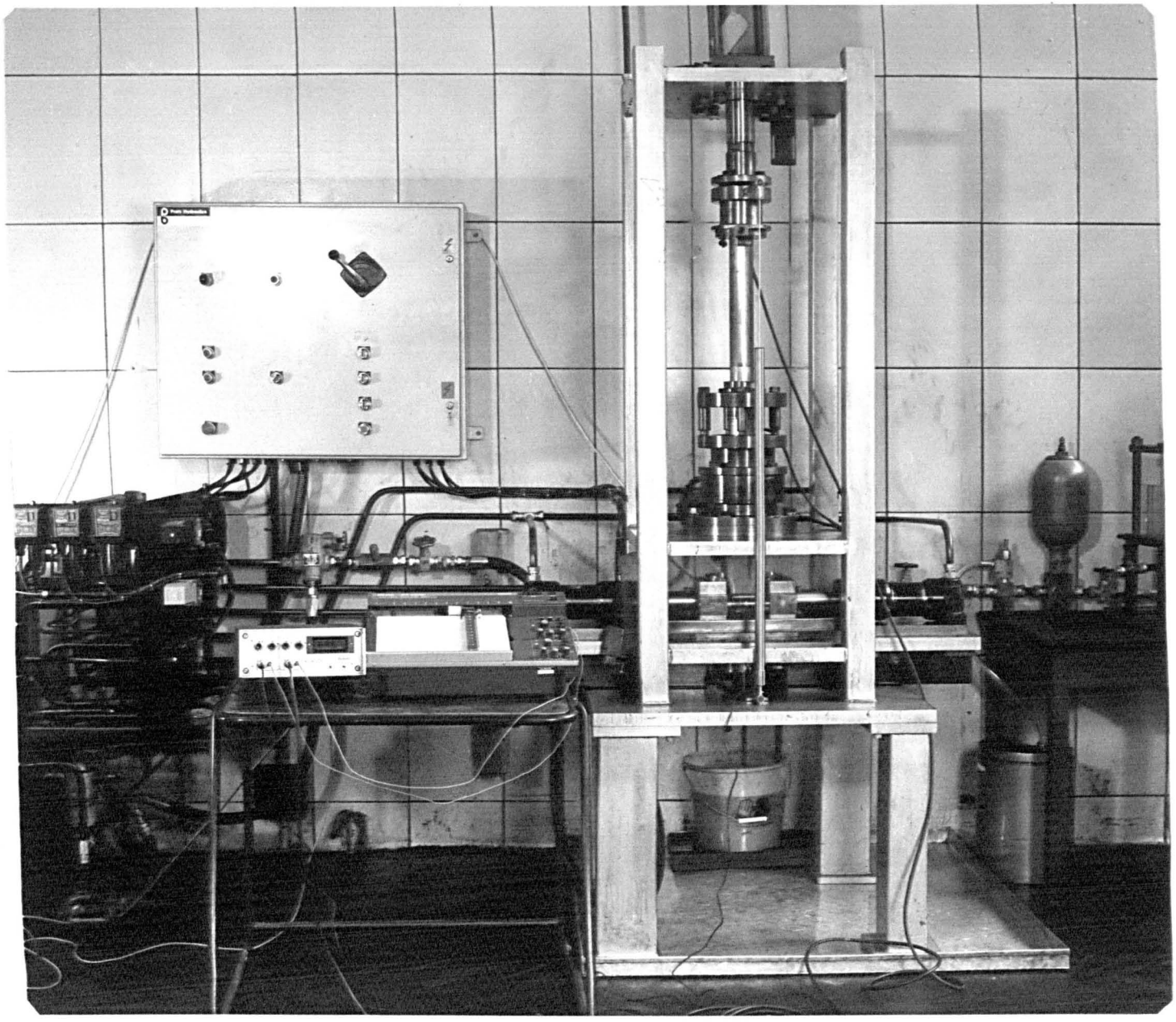

Set-up of the bulge forming machine used for punch load/stroke measurement during drawing and ironing.

Plate(10.1)

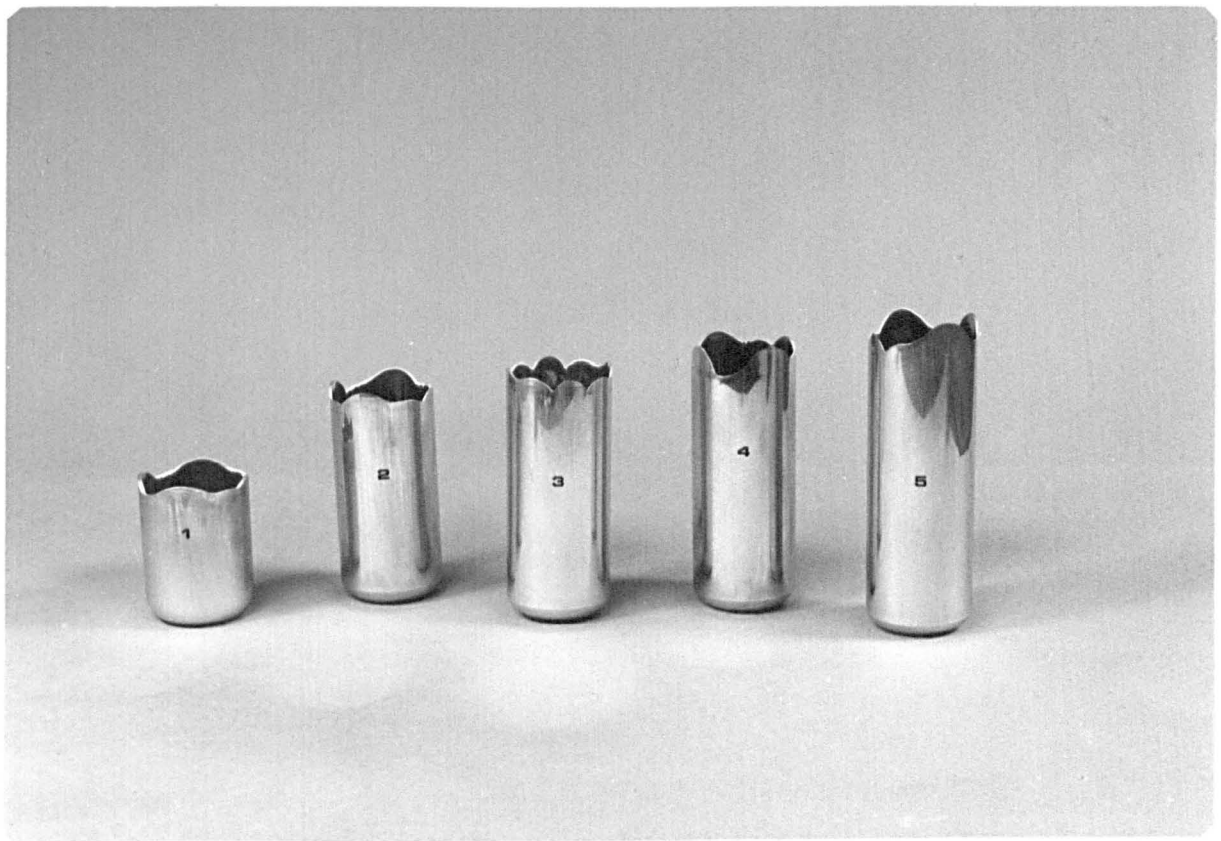

Deep drawn and ironed cups.

Plate(11.1)

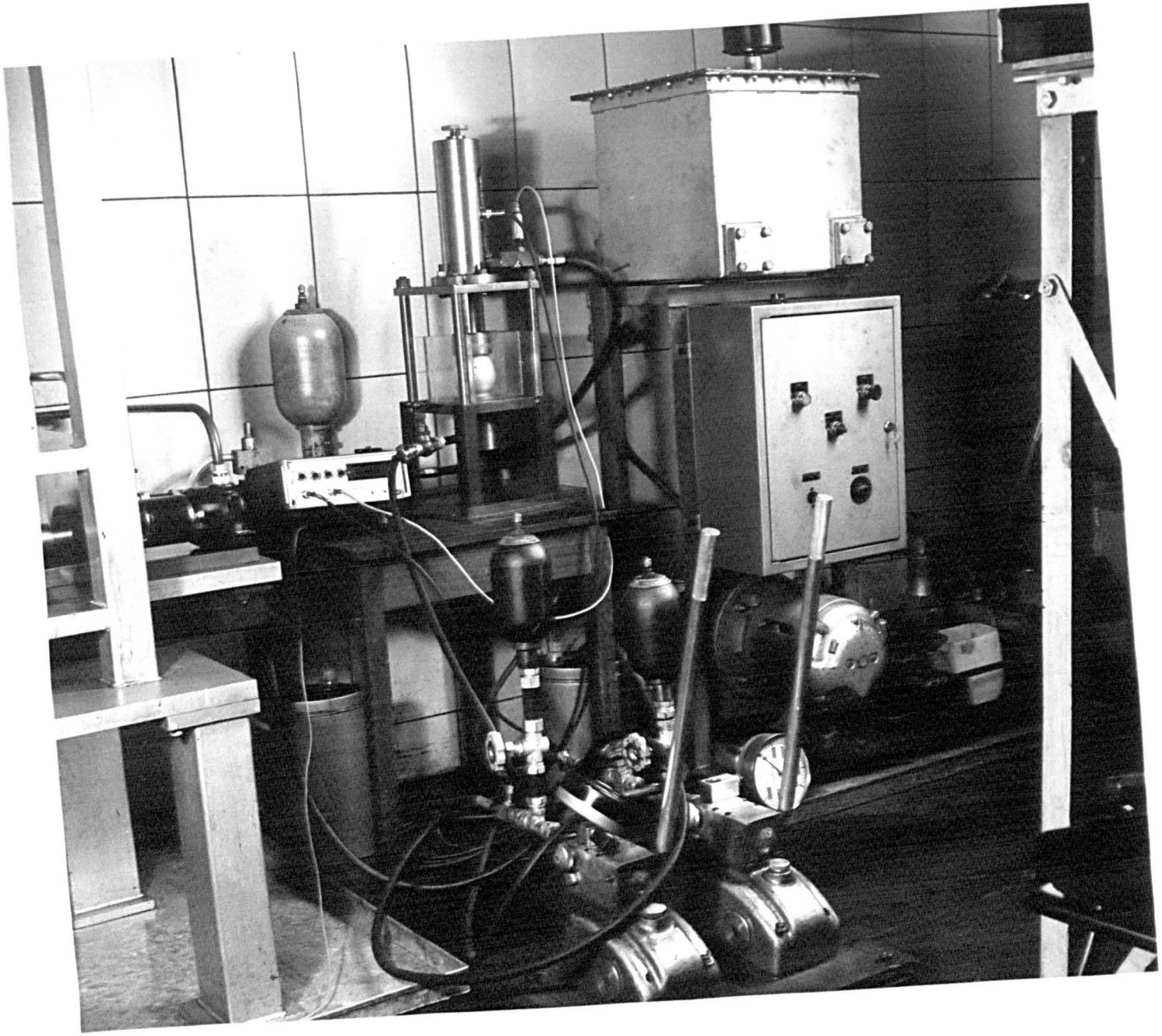

Free bulge forming apparatus.

Plate(14.1)

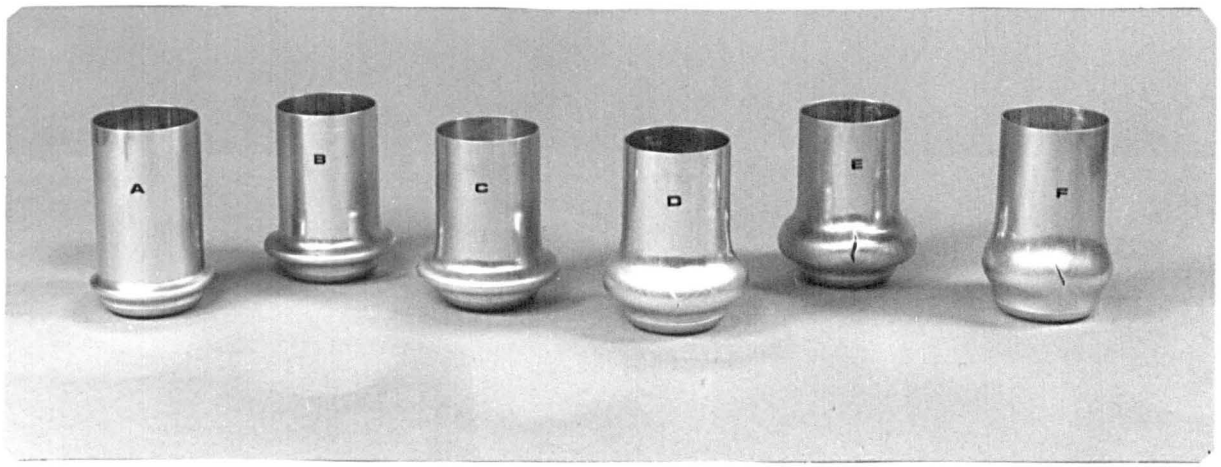

Free bulge forming of as drawn/ ironed cups, typical set of results. Plate(17.1)

Free bulge forming of annealed cups, typical set of results. Plate(17.2)

Effect of cup length on the bulge ratio of annealed cups. Plate(17.3)

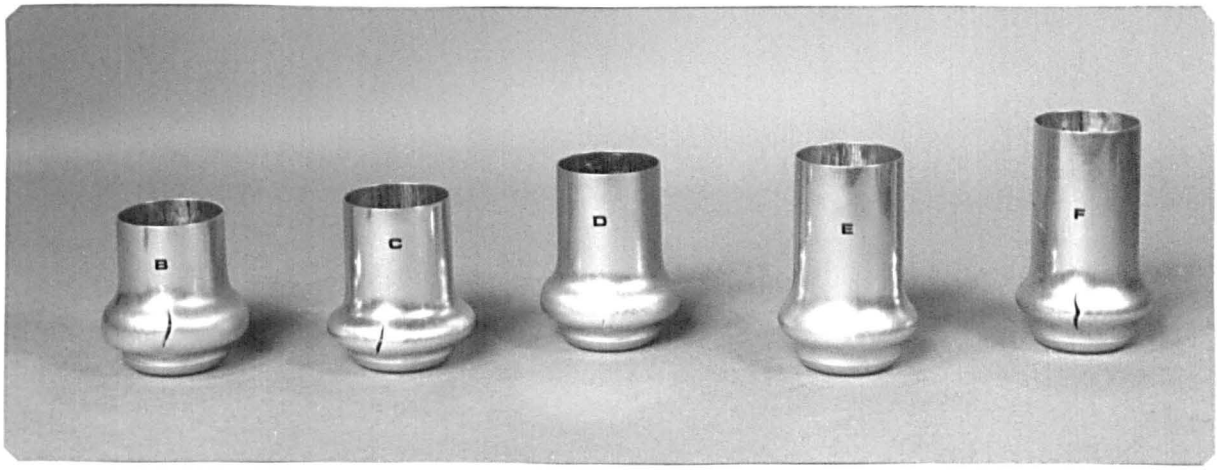

Effect of cup length on the bulge ratio of as drawn/ironed cups. Plate(17.4)

Effect of cup wall thickness on the bulge ratio of annealed cups. Plate(17.5)

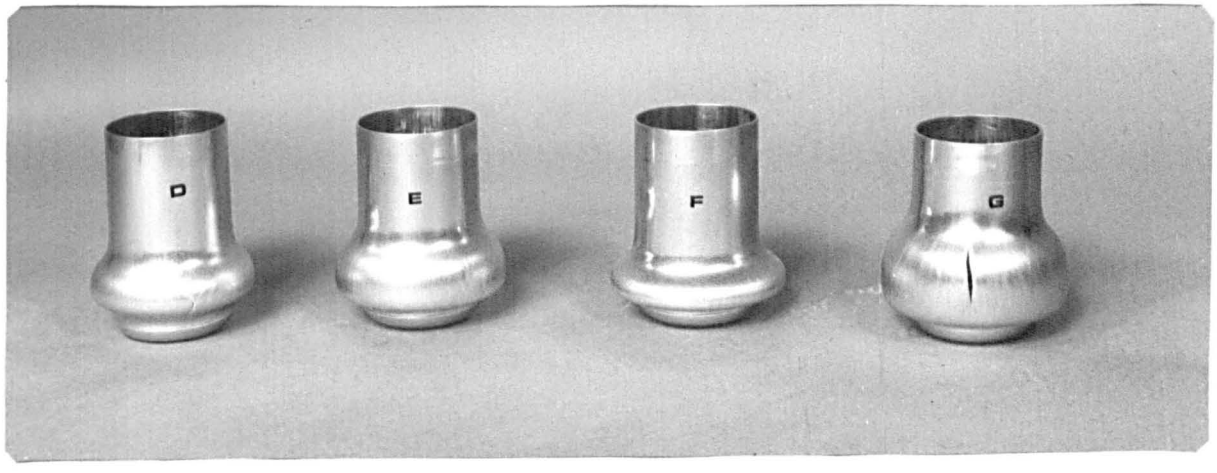

Effect of cup wall thickness on the bulge ratio of as drawn/ironed cups. Plate(17.6)

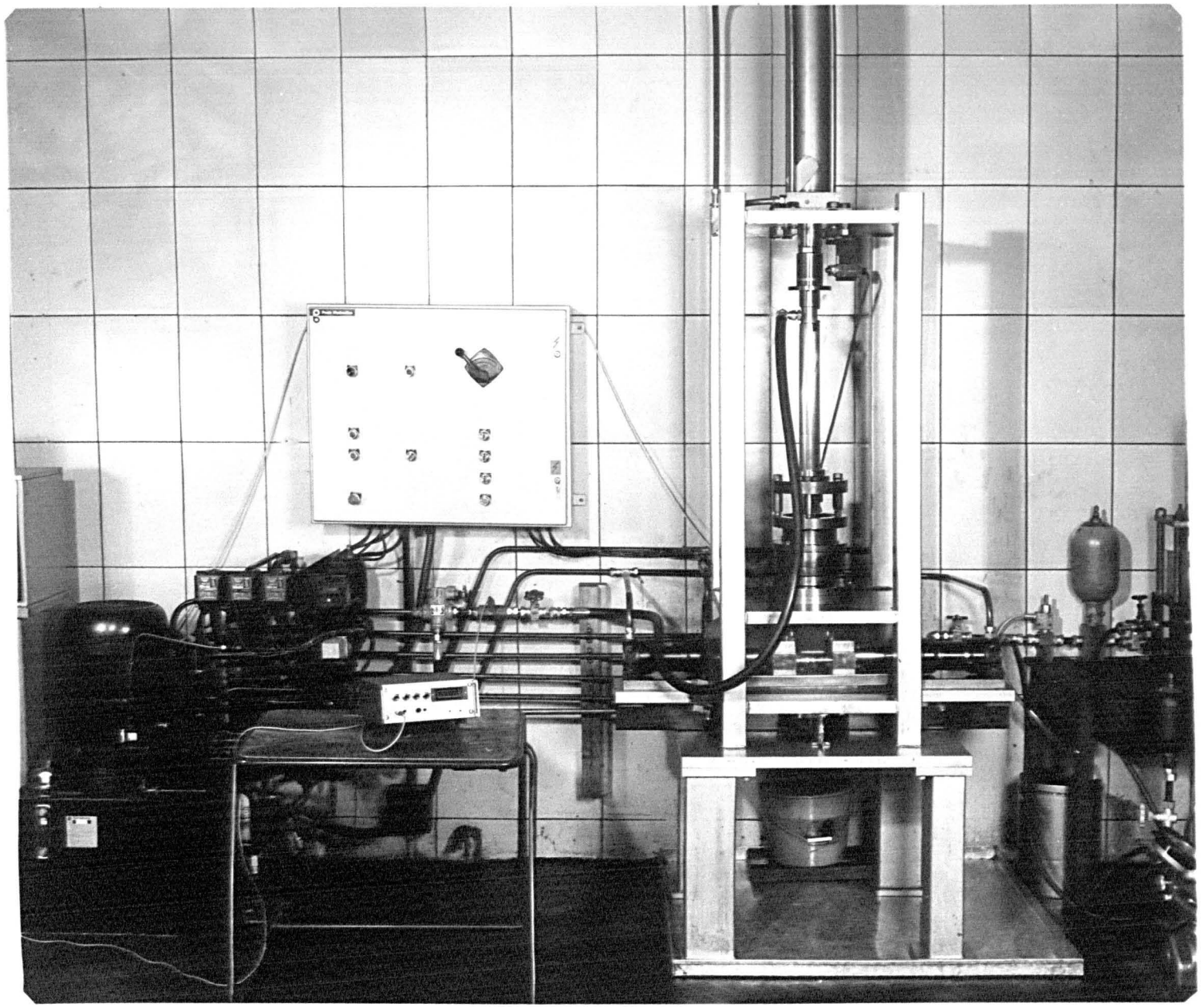

Set-up of the bulge forming machine used for closed die bulge forming.

Plate(20.1)

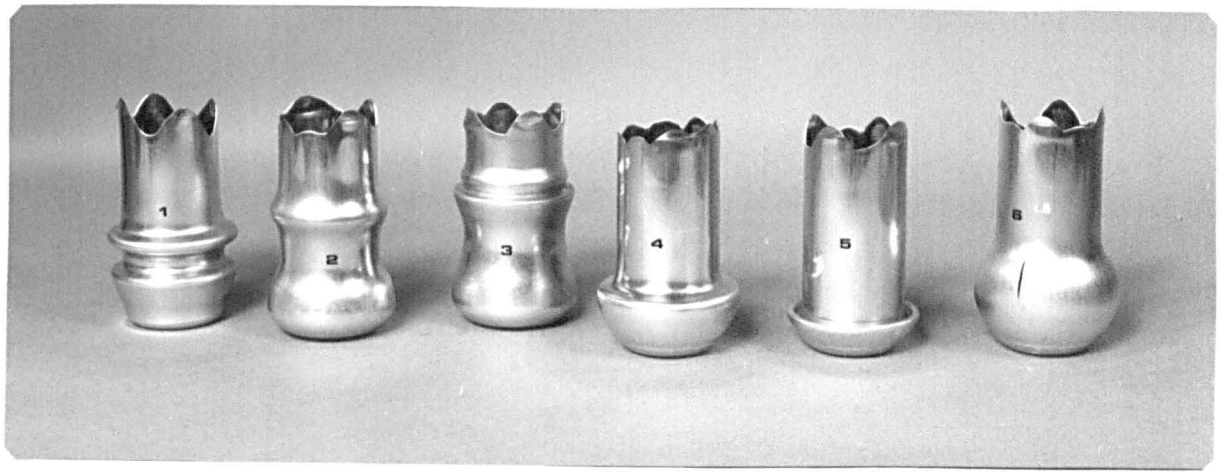

Typical examples of forming technique and failure in closed die forming. Plate(21.1)

Axisymmetric components produced by hydraulic bulge forming. Plate(21.2)

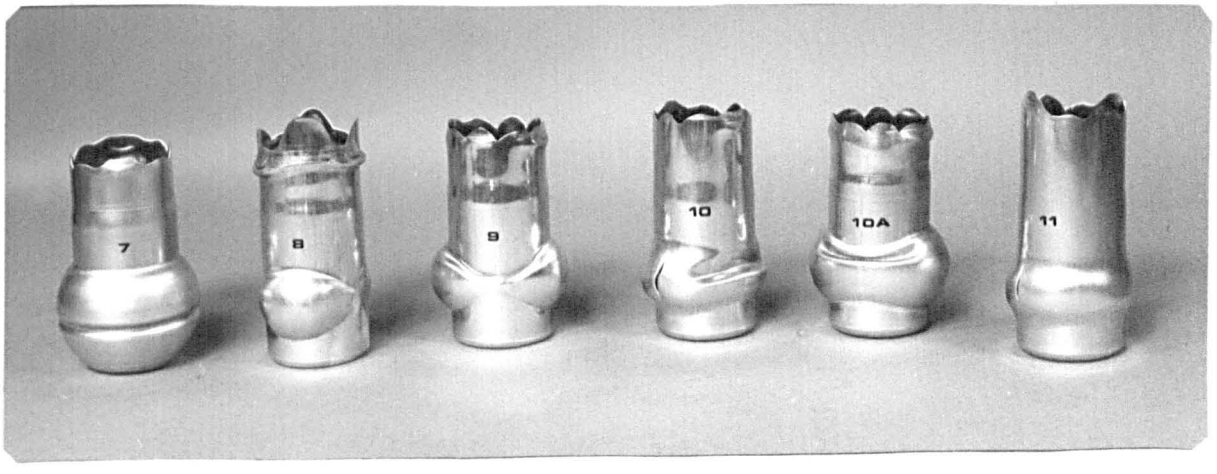

Typical examples of failure in closed die bulge forming. plate(21.3)

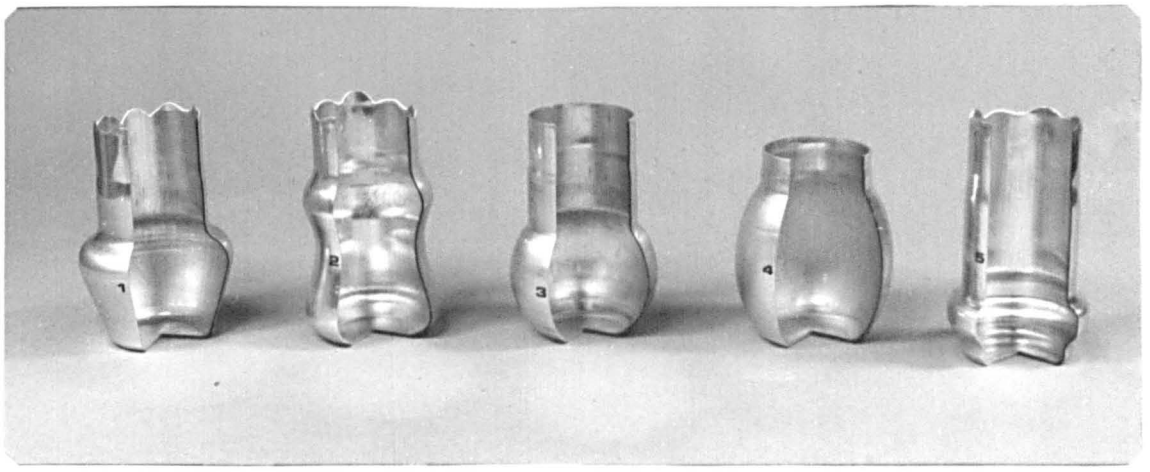

Sections in axisymmetric components. Plate(21.4)

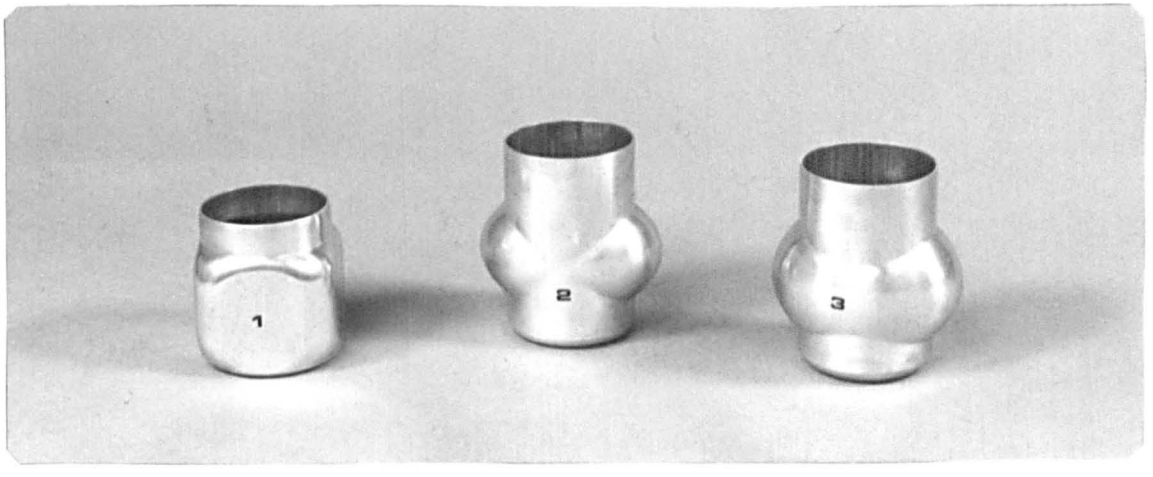

Asymmetric components produced by hydraulic bulge forming. Plate(21.5)

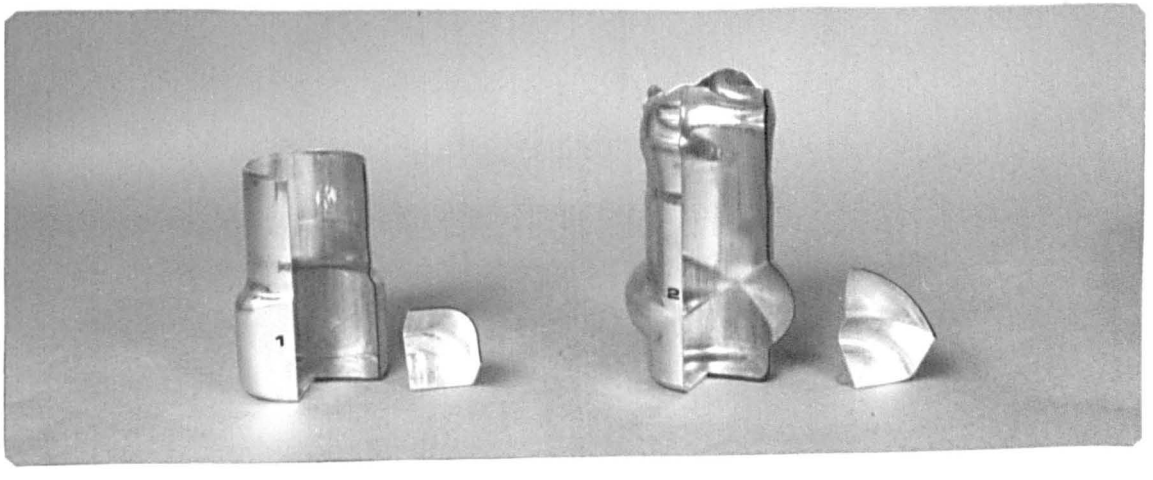

Sections in asymmetric components. Plate(21.6)